Late Transition-Metal Complexes Supported by Pincer Ligands: Applications in Partial Oxidation Catalysis

Wilson D. Bailey

A dissertation submitted in partial fulfillment of
the requirements for the degree of

Doctor of Philosophy

University of Washington

2016

Reading Committee:

Karen I. Goldberg, Chair

D. Michael Heinekey

Brandi M. Cossairt

Program Authorized to Offer Degree:

Department of Chemistry

University of Washington

Abstract

Late Transition-Metal Complexes Supported by Pincer Ligands: Applications in Partial Oxidation Catalysis

Wilson D. Bailey

Chair of the Supervisory Committee:

Prof. Karen I. Goldberg

Department of Chemistry

Late transition-metal pincer complexes of primarily palladium(II) and platinum(II) have been investigated for their application as catalysts in partial oxidation reactions. The epoxidation of higher olefins using molecular oxygen as the oxidant has been targeted, and the individual reaction steps needed to accomplish this overall transformation are described herein, including: (1) hydrogenolysis of a metal hydroxide (M-OH) species to yield a metal hydride (M-H), (2) insertion of O_2 into the M-H bond to form a metal hydroperoxide (M-OOH), and (3) O-atom transfer from the M-OOH to epoxides, yielding a M-OH and completing the catalytic cycle. Previous results from our group on these individual transformations using ($^{t\text{Bu}}$PCP)Pd and ($^{t\text{Bu}}$PCO)Pd fragments are also reviewed.

The requirements for O_2 insertion into Pd^{II} and Pt^{II} hydrides are discussed. An array of cationic, neutral, and anionic Pd-H and Pt-H complexes supported by a $^{t\text{Bu}}$PNP backbone were synthesized and evaluated for O_2 insertion ($^{t\text{Bu}}$PNP = 2,6-bis-(di-^{t}butylphosphinomethyl)pyridine). Metal-ligand cooperation was observed in the activation of

H_2 to form neutral hydride complexes. The effect of ligand protonation/deprotonation on the *trans* influence experienced by the hydride ligand was investigated. No reaction with O_2 was observed with the cationic hydrides, while the neutral and anionic forms reacted with O_2 at the $^{t\text{Bu}}$PNP backbone.

The synthesis and characterization of mono- and dinuclear Pd-OH complexes supported by a PCN^R pincer ligand (PCN^R = (1-(3-((di-*tert*-butylphosphino)methyl)phenyl)-1H-5-R-pyrazole), R = H, Me) is presented. When R = H, ligand pyrazole "rollover" C-H activation was observed, forming a mixed ligand (PCN^H)Pd(μ-OH)Pd(PCC) dinuclear structure. This "rollover" was investigated using DFT computations. The mono- and dinuclear hydroxide species were evaluated for hydrogenolysis. The dinuclear compounds {[(PCN^R)Pd]$_2$(μ-OH)}[OTf] reacted under an H_2 atmosphere to yield the corresponding dinuclear hydrides {[(PCN^R)Pd]$_2$(μ-H)}[OTf]. A mechanistic study on the hydrogenolysis of the μ-bridged hydroxide {[(PCN^{Me})Pd]$_2$(μ-OH)}[OTf] revealed first order kinetics in both [Pd] and [H_2]. Terminal hydrides were not detected, and reduction of the mononuclear hydroxide complexes (PCN^R)Pd-OH to Pd^0 was observed under H_2. The reduction was proposed to proceed through displacement of the pyrazole arm, and was examined by DFT computations.

Lastly, a new strategy to promote O-atom transfer from M-OOH to epoxides, the final step in the targeted catalytic cycle, is proposed. Preliminary studies on NNN^{Pyz}, NNN^{Et}, and NN^{Me} ligated Pd^{II} and Pt^{II} are discussed (NNN^{Pyz} = 2,6-bis(5-^{t}butyl-1H-pyrazol-3-yl)pyridine; NNN^{Et} = 2-(5-^{t}butyl-1H-pyrazol-3-yl)-6-(diethylaminomethyl)pyridine; NN^{Me} = 2-(5-^{t}Bu-1H-pyrazol-3-yl)-6-methylpyridine). The NNN^{Pyz} ligand, containing two acidic sites in proximity to the fourth site in the square plane, was found to protonate M-O_2 complexes, chelate to the

metal center and oxidize phosphine substrates. Similar reactivity was observed with NNN^{Et} and NN^{Me}, however hemilability of these ligands resulted in undesired coordination modes.

TABLE OF CONTENTS

List of Figures

List of Schemes

List of Tables

Glossary

Abbreviation	
PO	propylene oxide
MTBE	methyl-*tert*-butyl ether
^{t}Bu	*tert*-butyl
EO	ethylene oxide
KIE	kinetic isotope effect
CHPO	chlorohydrin propylene oxide
HPPO	hydrogen peroxide propylene oxide
SM	styrene monomer
TBA	*tert*-butyl alcohol
dppe	1,2-bis(diphenylphosphino)ethane
diphoe	*cis*-1,2-bis(diphenylphosphino)ethylene
Me	methyl
Ph	phenyl
OAT	oxygen atom transfer
THF	tetrahydrofuran
Et	ethyl
DME	dimethoxyethane
NMR	nuclear magnetic resonance
TON	turnover number
$^{t\text{Bu}}$PCP	2,6-bis(di^{t}butylphosphino)methylbenzene
$^{t\text{Bu}}$PCO	2-(di^{t}butylphosphino)methyl-6-(methoxy)methylbenzene
IES	internal electrophilic substitution
RE	reductive elimination
^{i}Pr	*iso*-propyl
Cy	cyclohexyl

HAA	hydrogen atom abstraction
BzO	benzoate
IMes	1,3-bis(2,4,6-trimethylphenyl)imidazol-2-ylidene
DFT	density functional theory
^{Imd}PCP	2,6-bis(di-2'-imidazolylphosphino)methylbenzene
$^{t Bu}$PNP	2,6-bis-(di-^{t}butylphosphinomethyl)pyridine
PCN^{H}	1-(3-((di-^{t}butylphosphino)methyl)phenyl)-1H-pyrazole
PCN^{Me}	1-(3-((di-^{t}butylphosphino)methyl)phenyl)-1H-5-methyl-pyrazole
OTf	triflate
NNN^{Pyz}	2,6-bis(5-^{t}butyl-1H-pyrazol-3-yl)pyridine
NNN^{Et}	2-(5-^{t}butyl-1H-pyrazol-3-yl)-6-(diethylaminomethyl)pyridine
NN^{Me}	2-(5-^{t}Bu-1H-pyrazol-3-yl)-6-methylpyridine
$^{t Bu}$PNN	2-[bis(di-^{t}butylphosphinomethyl)]-6-(N,N-diethylaminomethyl)pyridine
^{sec}Bu	1-methylpropyl
LAH	lithium aluminum hydride
^{n}Bu	butyl
COD	cyclooctadiene
CSD	Cambridge Structural Database
TS	transition state
OPh	phenoxide
IS	internal standard
dba	dibenzylideneacetone
TMEDA	tetramethylethylenediamine

Compound Numbering Scheme

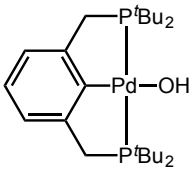

1

($^{t\text{Bu}}$PCP)Pd-OH

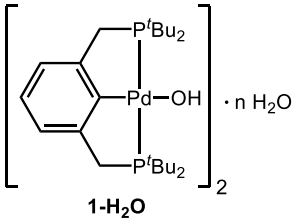

1-H$_2$O

($^{t\text{Bu}}$PCP)Pd-OH n-aqua bridged dimer

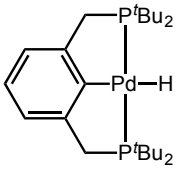

2

($^{t\text{Bu}}$PCP)Pd-H

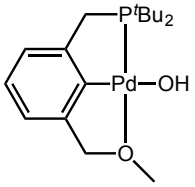

3

($^{t\text{Bu}}$PCO)Pd-OH

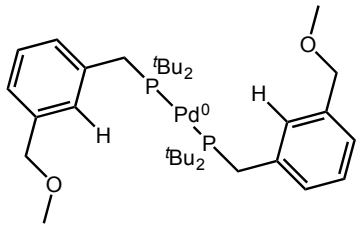

4

($^{t\text{Bu}}$PCO)$_2$Pd^0

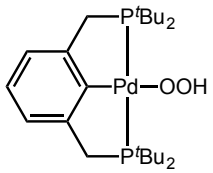

5

($^{t\text{Bu}}$PCP)Pd-OOH

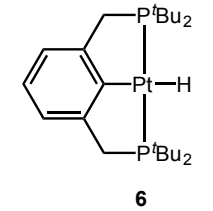

6

($^{t\text{Bu}}$PCP)Pt-OH

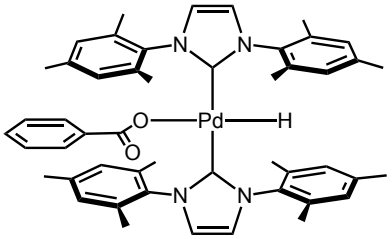

7

(BzO)(IMes)$_2$Pd-H

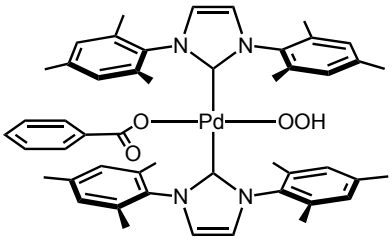

8

(BzO)(IMes)$_2$Pd-OOH

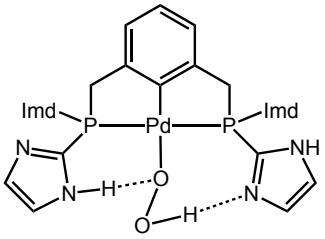

9

(^{imid}PCP)Pd-OOH

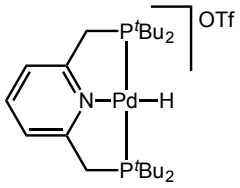

10

[($^{t\text{Bu}}$PNP)Pd-H]OTf

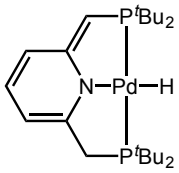

10*

($^{t\text{Bu}}$PNP*)Pd-H

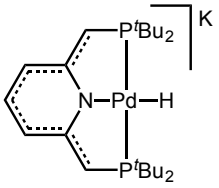

10**

K[($^{t\text{Bu}}$PNP**)Pd-H]

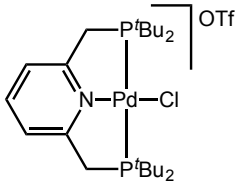

10-Cl

[($^{t\text{Bu}}$PNP)Pd-Cl]OTf

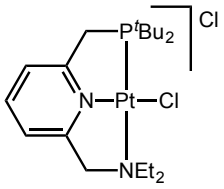

11

[($^{t\text{Bu}}$PNN)Pd-Cl]Cl

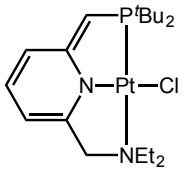

11*

($^{t\text{Bu}}$PNN*)Pt-Cl

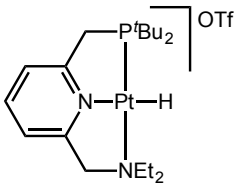

12

[($^{t\text{Bu}}$PNN)Pt-H]OTf

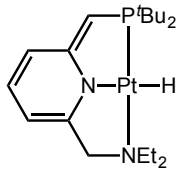

12*

($^{t\text{Bu}}$PNN*)Pt-H

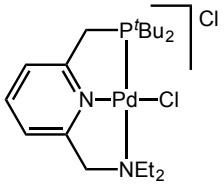

13

[($^{t\text{Bu}}$PNN)Pd-Cl]Cl

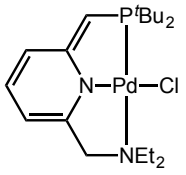

13*

($^{t\text{Bu}}$PNN*)Pd-Cl

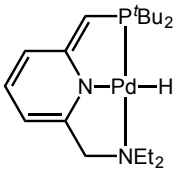

14*

($^{t\text{Bu}}$PNN*)Pd-H

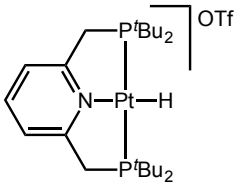

15

[($^{t\text{Bu}}$PNP)Pt-H]OTf

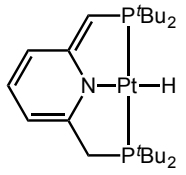

15*

($^{t\text{Bu}}$PNP*)Pt-H

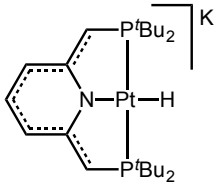

15**

K[($^{t\text{Bu}}$PNP**)Pt-H]

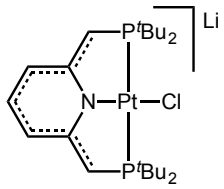

16**

Li[($^{t\text{Bu}}$PNP**)Pt-Cl]

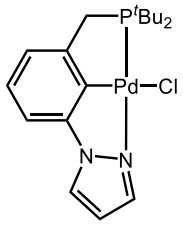

17

(PCN^{H})Pd-Cl

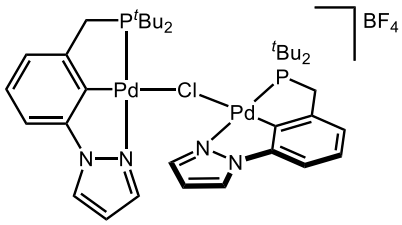

18

{[(PCN^{H})Pd]$_2$(μ-Cl)}[BF$_4$]

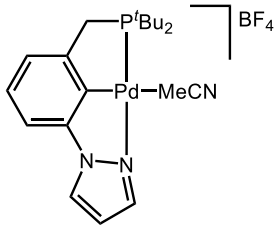

19

[(PCN^{H})Pd-MeCN]BF$_4$

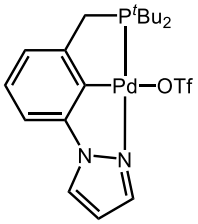

20

(PCN^H)Pd-OTf

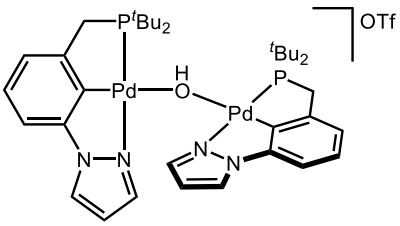

21

{[(PCN^H)Pd]$_2$(μ-OH)}[OTf]

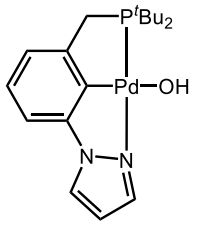

22

(PCN^H)Pd-OH

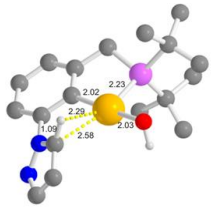

22'

(PCCH)Pd-OH, calculated

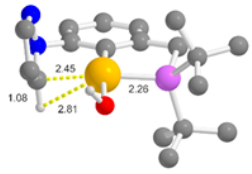

TS$_{rot}$

(PCCH)Pd-OH, calculated transition state

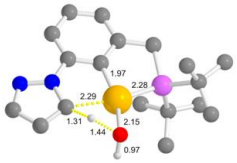

TS$_1$

(PCC)Pd-OH$_2$, calculated transition state

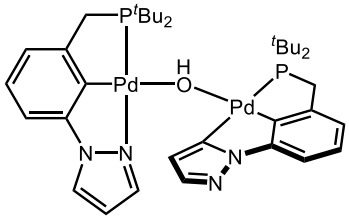

23

(PCN^H)Pd(μ-OH)Pd(PCC)

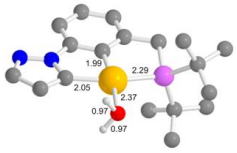

24

(PCC)Pd-OH$_2$, calculated

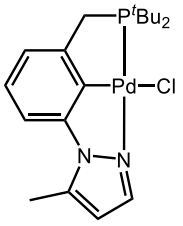

25

(PCN^{Me})Pd-Cl

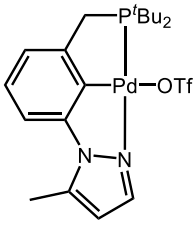

26

(PCN^{Me})Pd-OTf

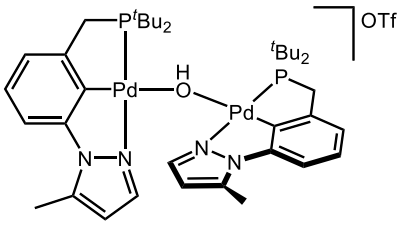

27

{[(PCN^{Me})Pd]$_2$(μ-OH)}[OTf]

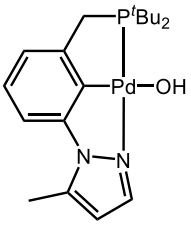

28

(PCN^{Me})Pd-OH

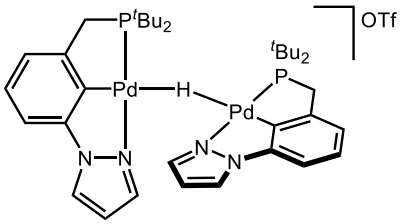

29

{[(PCN^{H})Pd]$_2$(μ-H)}[OTf]

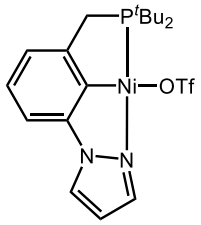

30

(PCN^{H})Ni-OTf

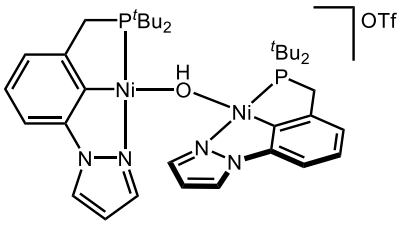

31

{[(PCN^{H})Ni]$_2$(μ-OH)}[OTf]

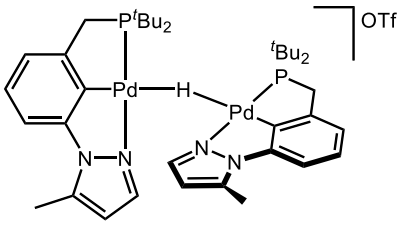

32

{[(PCN^{Me})Pd]$_2$(μ-H)}[OTf]

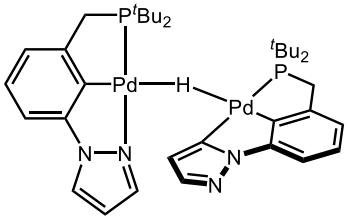

33

(PCN^{H})Pd(μ-H)Pd(PCC)

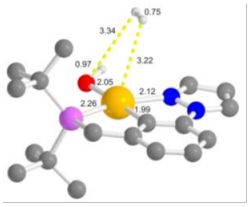

22-H$_2$

(PCN^{H})Pd-OH H$_2$ adduct, calculated

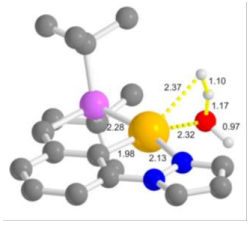

TS$_2$

(PCN^{H})Pd-OH-H$_2$, calculated TS

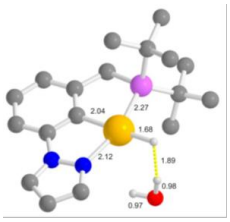

34-H_2O

(PCN^H)Pd-H H_2O adduct, calculated

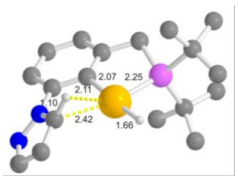

34'

(PCCH)Pd-H, calculated

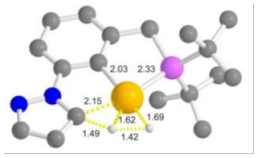

TS_3

(PCC)Pd-H_2, calculated transition state

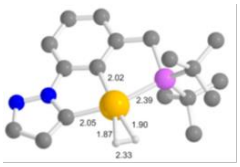

35

(PCC)Pd-H_2, calculated

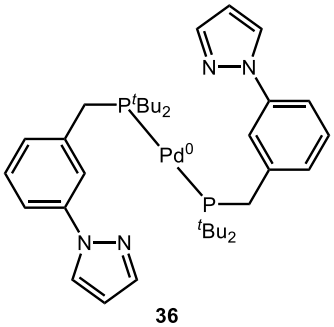

36

(PCN^H)$_2$Pd^0

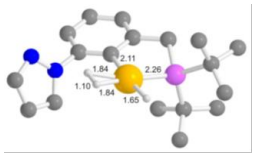

37

(PC)Pd(H_2)(H), calculated

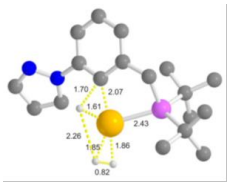

TS_4

(η^1-PCN)Pd-H_2, calculated transition state

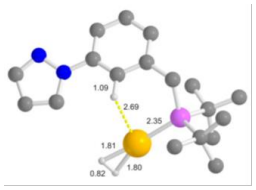

38

(η^1-PCN)Pd^0-H_2, calculated

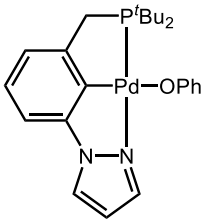

39

(PCN^H)Pd-OPh

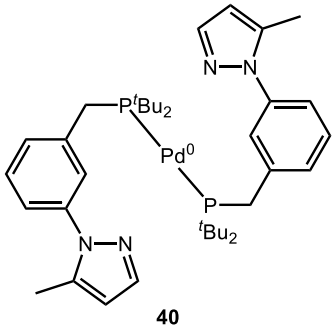

40

(PCN^{Me})$_2$Pd^0

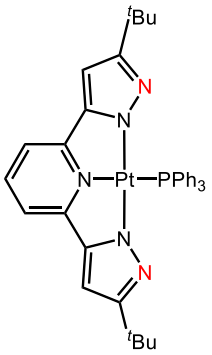

41

(NNN^{pyz})Pt-PPh$_3$

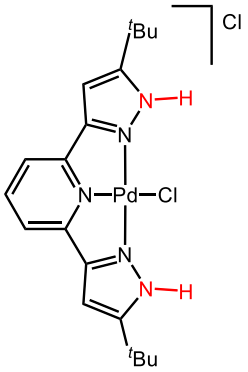

44

[(NNN^{pyz})Pd-Cl]Cl

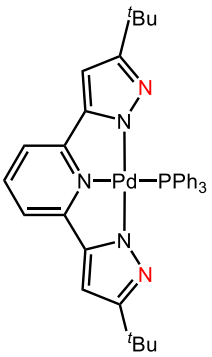

42

(NNN^{pyz})Pd-PPh$_3$

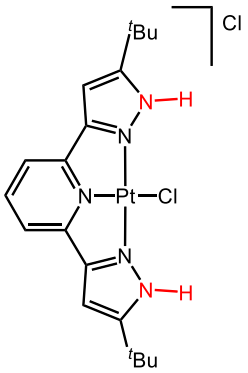

45

[(NNN^{pyz})Pt-Cl]Cl

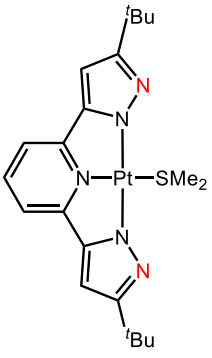

43

(NNN^{pyz})Pt-SMe$_2$

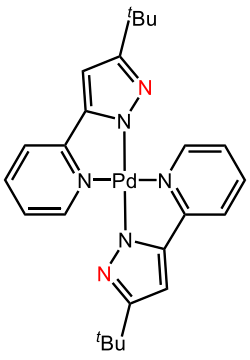

46

(NN)$_2$Pd

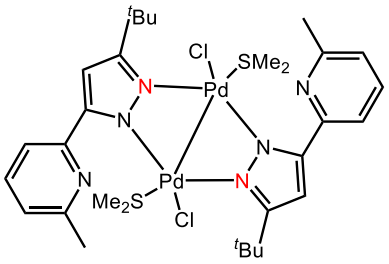

47

$[(NN^{Me})Pd(SMe_2)Cl]_2$

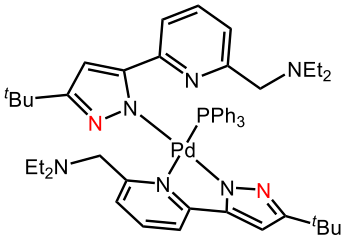

48

$(NNN^{Et})_2Pd\text{-}PPh_3$

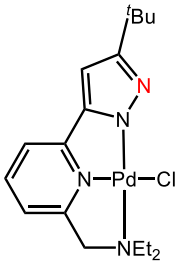

49

$(NNN^{Et})Pd\text{-}Cl$

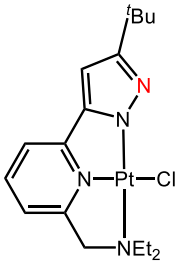

50

$(NNN^{Et})Pt\text{-}Cl$

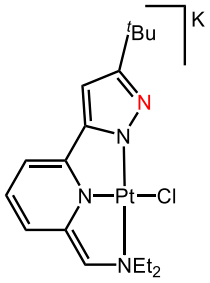

50*

$K[(*NNN^{Et})Pt\text{-}Cl]$

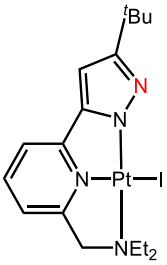

51

$(NNN^{Et})Pt\text{-}I$

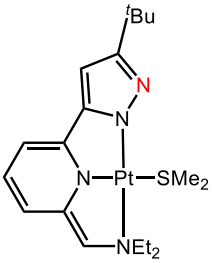

52

$(*NNN^{Et})Pt\text{-}SMe_2$

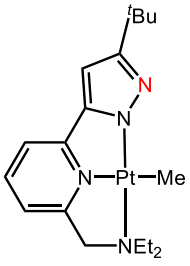

53

$(NNN^{Et})Pt\text{-}Me$

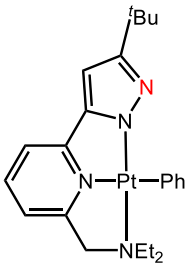

54

(NNN^{Et})Pt-Ph

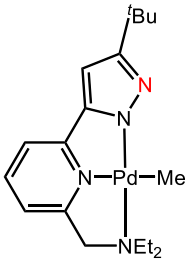

55

(NNN^{Et})Pd-Me

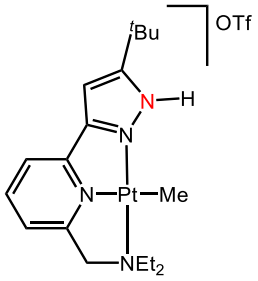

56

[(NNN^{Et})Pt-Me]OTf

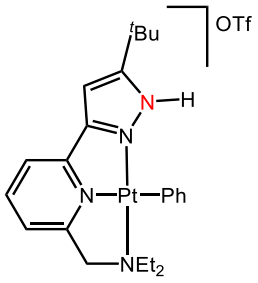

57

[(NNN^{Et})Pt-Ph]OTf

Acknowledgements

I would like to thank all those who have helped me on this incredible journey thus far, and all those who I know will continue to be a positive impact in the future.

I want to thank Mr. Kilkenny at Grant High School, who was the first to show me how fun chemistry can be.

To Jo, Eric, and Dasher at the University of Puget Sound, thank you so much for your mentorship, friendship, and encouragement throughout my undergraduate career. I owe much of my effectiveness in teaching to the characteristics portrayed by you three. The community that you nurtured at UPS allowed me to grow into the scientist that I am today. I can't wait to emulate your style, caring nature, and love of learning in my future career.

Thank you, Karen Goldberg, so very much for your guidance, intellect, and never ending support and caring. You have pushed me to be the best researcher I can be, doing so in a way tailored to my individuality. When I first came to the University of Washington, I knew that you were someone I wanted to work with. At first it was because of the detailed and exceptional chemistry that was published in your lab, as that was all I had to go on. Meeting with you in person solidified my choice to spend my graduate career working in your lab. You met me as I have seen you meet with all students: welcoming, offering a cup of coffee from your highly-used Nespresso machine; present, making it clear that our thoughts, concerns, questions were all relevant and important; inspirational, jumping into discussions of chemistry with both feet, where your excitement about the field and what we will do in our career clearly visible from your language and energy. These traits of yours have carried through for my entire graduate career and are truly an inspiration in what a mentor can be. Thank you, Karen.

Thank you, to my parents Nancy and Scott, and brother Charlie, for giving me every opportunity to blaze my own trail. Your love and support truly allowed me to live the life I want to live. You continue to be an inspiration in how to create a community of friends and family that is centered around acceptance, love, and finding the fun in life.

Speaking of the fun in life, thank you to my fellow graduate students and self-named "Diner Club" Ben, Carolyn, Jon, Karena, Louise, Sophia, Travis and Tyler. I am forever grateful for having you all to joke, travel, adventure, eat, and enjoy life with. Sophia, you are simply an amazing human being. Never stop being you, because you are the best. Thank you for your love, support, and always letting me know that you got my back. I love you.

And finally, thank you Cecily. Not a day goes by without thinking of how lucky I am to have met you so early in life. Thank you for sharing this journey with me. Thank you for your love and support. Thank you for helping me believe in me. You constantly remind me how great life is. I cannot wait to find out where our adventures will take us. I know, with you by my side, we can accomplish anything. I love you, always.

Chapter 1

Introduction

1.1 Partial oxidation of organics, an overview

The mass production of commodity chemicals by partial oxidation is of paramount importance. Our commodity chemical supply is primarily obtained from reduced, unfunctionalized petroleum feedstocks, and as such, selective partial oxidation is a necessary value adding transformation. The partial oxidation of hydrocarbons is carried out at the megaton scale each year, in large part to create monomer units for the polymer industry.[1] Any small inefficiency is inflated at such a large scale and thus it is of critical importance that we strive for highly efficient and clean oxidative technology in order to secure a sustainable future.

For any large scale oxidation process to be environmentally and economically feasible in today's market, the process should adhere to as many of the principles of green chemistry as possible.[2] Atom efficient transformations must be targeted to minimize waste. Catalysis should be incorporated to minimize energy cost. Benign, inexpensive, and readily available

reagents are a requirement. Arguably, the optimal oxidant for large scale oxidations is molecular oxygen, O_2. Molecular oxygen, being inexpensive and readily available, can be considered the "greenest" oxidant as only H_2O is a possible byproduct. Indeed, the majority of industrial oxidative processes to produce organic materials utilize O_2 or air as the reagent of choice (**Table 1.1**). Notably, of the top 16 partial oxidation reactions of organic compounds by production weight, 14 of those use air or O_2 as the oxidant.[1] The two products that are currently lacking in this regard are adipic acid and propylene oxide (PO).

Table 1.1. Mass produced organic compounds from oxidation.[1]

Product	Production rate[a]	Oxidant					
	(Mt/year)	Air	O_2	HNO_3	Cl_2	ROOH	H_2O_2
Terephthalic Acid	44	X					
Formaldehyde	19	X					
Ethylene Oxide	18		X				
1,2-Dichloroethane	18	X	X		X		
Propylene Oxide	8				X	X	X
Cyclohexanone	6	X	X				
Vinyl Acetate	6	X	X				
Acrylonitrile	6	X					
Styrene	5	X	X				
Phenol/acetone	5	X					
Phthalic Anhydride	5	X					
Acrylic Acid	5	X					
MTBE[b]	4		X				
Adipic Acid	3			X			
Maleic Anhydride	2	X					
Hydrogen Cyanide	2	X					

[a] Production rates as of 2008. [b] MTBE = Methyl-^{t}Bu Ether.

Propylene oxide, ranked as the 5th largest mass-produced organic oxidation product as of 2008, currently cannot be produced directly from propylene and O_2 effectively. Instead, PO is made using chlorine, organic hydroperoxides, or hydrogen peroxide as the oxidant.[1] The use of these more expensive and/or hazardous oxidants coupled with considerable waste, by-products, and side reactions results in economic and environmental inefficiency. PO was produced at over 8 billion kg/year in 2008, 9 billion kg/year in 2011, and is estimated to

continue to increase.[3] It is therefore important to develop a more environmentally benign and favorable oxidation process.

1.2 Industrial epoxidation of olefins

Shell has pioneered a highly selective heterogeneous epoxidation catalyst for the production of ethylene oxide (EO) that utilizes O_2 as the direct oxidant.[4-6] The catalyst, consisting of silver particles deposited on α-Al_2O_3 with certain additives, can reach 90-97% selectivity for the formation of EO from ethylene and air (**Scheme 1.1**). It is also highly selective for the epoxidation of butadiene. However, this system is not effective for the epoxidation of propylene and other higher olefins, as the introduction of weak allylic C-H bonds opens up a thermodynamically favored complete oxidation to CO_2 and H_2O.[7-10] This proposal that the overall chemistry is dominated by allylic C-H activation at the silver surface is supported by an observed kinetic isotope effect (KIE). 15% PO was isolated when the sp^3 hydrogens of propylene were replaced with deuterium, whereas only 0-5% conversion to PO was found when the methyl group was not deuterated. Kinetically, the combustion of propylene on the silver oxide surface is estimated to be a factor of 10 faster than that of ethylene.[11] Furthermore, the rate of epoxidation was found to favor EO over PO by a factor of 10. Still, researchers have tried varying conditions and additives in the silver based heterogeneous system in an attempt to reach higher selectivity for PO. However, many of these involve much larger loadings of silver and alkali promoters, and a highly active and selective combination has yet to be realized.[7] A direct partial oxidation of propylene by O_2 would represent a "game changing" or disruptive technology in the chemical industry.[12]

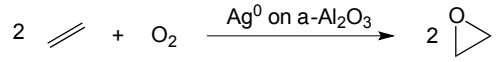

Scheme 1.1. Epoxidation of ethylene to ethylene oxide.

Instead of the direct oxidation of propylene to PO by air or O_2, four less "green" methods are currently employed: the oxidation of propylene by chlorine gas (chlorohydrin, CHPO route **A**), alkyl hydroperoxides (side-product routes **B** and **C,** and cumene-recycling route **D**), and hydrogen peroxide (HPPO route **E**) (**Figure 1.1**).[1] The chlorohydrin route, while selective towards PO (94-96%), is highly wasteful and atom inefficient. Each ton of PO produced requires 1.4 tons of Cl_2 (necessitating special handling) and 1.0 ton of calcium hydroxide, which in turn produces 40 tons of wastewater (requiring proper treatment/disposal) alongside. A main side-product is 1,2-dichloropropane, which can reach up to 10% of the product mixture.[11] The high capital investment to build plants using this method as well as the hazards and waste associated with the chlorohydrin route has dissuaded any new construction.[1] However, this technology, with equipment already in place, is economically competitive in today's market, and PO will continue to be produced by this method if a cleaner, more atom efficient and energetically and economically favorable process is not found.

The co-product routes also suffer from atom inefficiency. In these processes, either ethylbenzene (PO/SM, SM = styrene monomer) or isobutane (PO/TBA, TBA = ^{t}Bu alcohol) are oxidized to a hydroperoxide, which then epoxidizes propylene over a homogeneous Mo^{6+} or heterogeneous Ti-silica catalyst with a selectivity of 95-97% (**B**, **C**, **Figure 1.1**). The co-products, 1-methylbenzyl alcohol or TBA, can be marketed directly, however the majority are dehydrated to styrene or isobutene, respectively.[1,11] This route produces either 2.5 tons of styrene or 2.1 tons of isobutene for each ton of PO formed. As such, the economic value of the co-product highly affects the stability of making PO by this route.

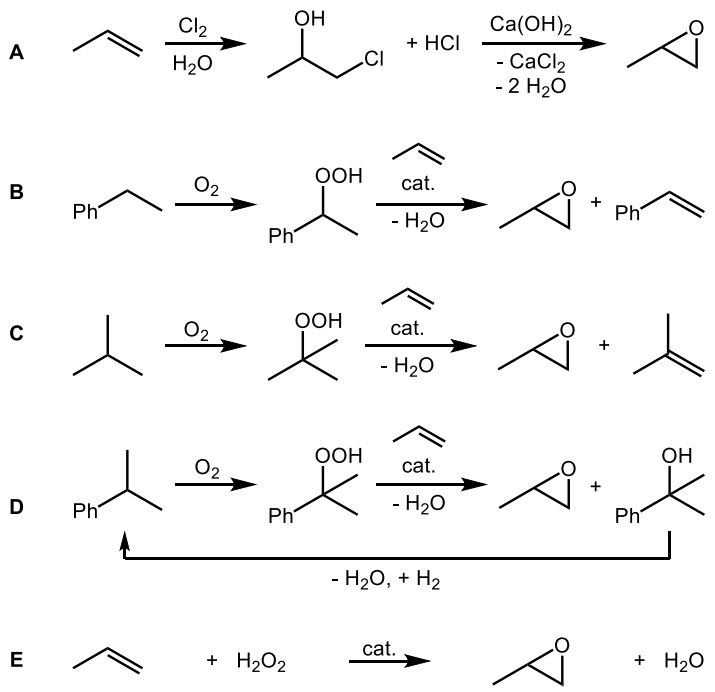

Figure 1.1. Current industrial methods of PO production; CHPO route, A; PO/SM route, B; PO/TBA route, C; Cumene recycling route, D; HPPO route, E.

As of 2005, these three routes (45% **A**, 35% **B**, and 20% **C, Figure 1.1**) were the majority means of producing PO.[11] In order to reduce the amount of co-product produced alongside PO, Sumitomo Chemical invested in a cumene-recycling route.[1,11,13] Similar to the PO/SM and PO/TBA method, PO is produced from propylene and an organic hydroperoxide, cumyl hydroperoxide, over a silylated titanium catalyst. Cumyl hydroperoxide is produced from autoxidation in air, and is relatively more stable than its ethyl benzene analogue. This increased stability leads to a slightly higher selectivity for epoxidation. The surplus cumyl alcohol is then dehydrated and hydrogenated to reform cumene (**D**, **Figure 1.1**). While this method is essentially co-product free, it suffers from low propene conversion and, as such, necessitates the handling of a very large propene recycle stream.[1]

Another method in which PO is produced co-product free is the HPPO route (**E**, **Figure 1.1**). Within the last 10 years, DOW/BASF have teamed together to build side-by-side

hydrogen peroxide and PO plants. This operation, capable of producing 300,000 tons of PO annually, runs efficiently because of the side-by-side nature of the physical plants; the oxidant, H_2O_2 is made in the first plant and does not need to be transported (reducing cost and significant hazard) or purchased (the value of H_2O_2 is comparable to PO).[1] In the second plant, dilute H_2O_2 (10%) in methanol is fed into a propene stream over the TS-1 titanium-silicalite catalyst at 40 °C and 20 atm. PO is formed with a yield of ~85% and a selectivity of 95% based on H_2O_2.[11] This process runs with reduced waste and energy cost compared to the other current methods of PO production. However, the two side-by-side plants require an extremely large capital investment.

Instead of using a H_2O_2 stream, a different and highly attractive route would be the *in situ* formation of H_2O_2 from H_2 and O_2 that can then be used to epoxidize olefins. Generally, *in situ* formation of H_2O_2 results in low concentrations of the oxidant, and TS-1 is able to catalyze the epoxidation of propylene to PO at these low concentrations.[11,14,15] The process, first proposed by EniChem in the 1980's, combines the alkylanthraquinone/alkylanthrahydroquinone method of producing H_2O_2 from air and H_2 over Pd^0, with the epoxidation catalyst TS-1 for PO production (**Scheme 1.2**).[16] Others still have experimented with impregnating TS-1 with late transition metals in an attempt to combine a direct H_2 oxidation/PO production.[11] Conversion and selectivity high enough for industrial production have yet to be realized with these processes, and currently the side-by-side plant system is still the leader in the HPPO method. However, a single plant that utilizes a direct oxidation route has the potential of being far more efficient than using intermediate oxidants, and is still highly desirable.

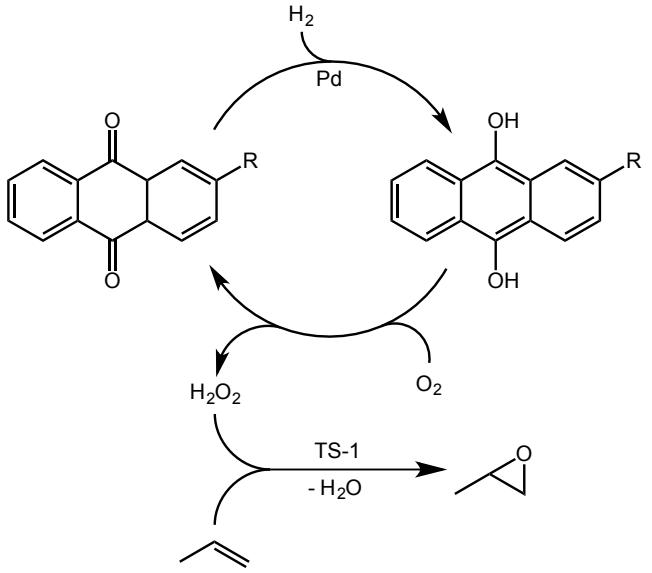

Scheme 1.2. Eni-Chem in situ HPPO epoxidation method.[11]

1.3 Small scale olefin epoxidation catalysis

The use of transition metal catalysts, specifically TS-1, helped to revolutionize the PO industry, as the primary source of PO previously was from the CHPO route.[11] Historically, the catalysts for epoxidation have primarily been homo/heterogeneous early transition metals or heterogeneous Ag/Au surfaces.[7,17-21] Therefore, it was noteworthy when, in 1984, Strukul and Michelin published the first group 10 homogeneous epoxidation catalyst.[22] They found that Pt^{II} hydroxide or hydride species of the type (PP)Pt(CF_3)X (PP = 1,2-bis(diphenylphosphino)ethane (dppe), *cis*-1,2-bis(diphenylphosphino)ethylene (diphoe), 2 PPh_2Me; X = OH, H) reacted with hydrogen peroxide solutions to form the hydroperoxide (PP)Pt(CF_3)OOH. It was this Pt^{II}-OOH complex that was capable of performing O-atom transfer (OAT). This species was able to oxidize substrates such as PPh_3, CO, and NO in tetrahydrofuran (THF). OAT did not occur towards olefins under the same non-aqueous conditions. However, when a mixture of aqueous-organic solvent was used, OAT to propene, 1-hexene and 1-octene was observed.

The complex (diphoe)Pt(CF_3)OH was found to be a catalyst for the epoxidation of a variety of olefins using dilute *aq.* H_2O_2 solutions in organic media. Strukul and Michelin were able to show the complete epoxidation of propene, 1-hexene and 1-octene, with a selectivity for the epoxide >99% (**Scheme 1.3**).[22] Internal alkenes were not oxidized under the same conditions. A solvent dependence on the rate of epoxidation was determined with initial rates being faster in EtOH>THF>DME. This further exemplifies a difference in mechanism compared to the previously established early transition metal catalysts, which are deactivated in the presence of H_2O/alcohol.

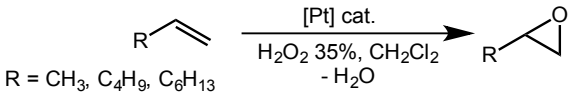

Scheme 1.3. Olefin epoxidation by Strukul's catalyst.[22]

The necessity for aqueous media for epoxidation, as well as the rate enhancement observed in polar protic solvent, led Strukul and Michelin to propose HOO^- dissociation as a critical step.[23] They suggested that Pt^{II} served a bifunctional role: the activation of H_2O_2 to form the nucleophilic HOO^- ion as well as the activation of the olefin by binding to a metal open site. The HOO^- ion could then attack the bound, electron deficient olefin. In-depth kinetic studies were performed on the epoxidation of 1-octene by (diphoe)Pt(CF_3)OH and the solvento species [(diphoe)Pt(CF_3)(CH_2Cl_2)]BF_4. A second order dependence on [Pt] and first order dependence on [olefin] was observed. An initial rate enhancement was also observed when using the solvento species [(diphoe)Pt(CF_3)(CH_2Cl_2)]BF_4 as a precatalyst compared to the hydroxide species. Furthermore, it was found that combining authentic equimolar samples of the olefin complex [(diphoe)Pt(CF_3)(1-octene)]BF_4 and [(diphoe)Pt(CF_3)OOH resulted in the complete formation of 1,2-epoxyoctane, as well as a mix of the solvento and hydroxide Pt^{II}

complexes. Using the above evidence, as well as *in situ* IR and ^{19}F NMR spectral data, the mechanism shown below was proposed (**Scheme 1.4**).[24] It should be noted that this proposed mechanism of epoxidation, invoking an electrophilic bound olefin and a nucleophilic free HOO^- ion, is atypical, as a nucleophilic olefin and an electrophilic hydroperoxide is proposed in early metal[17] and organic peracid epoxidations.[25]

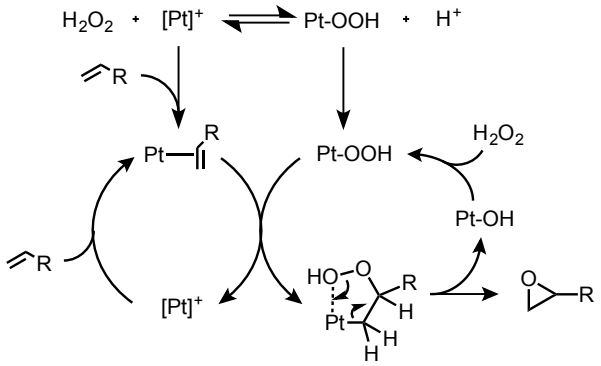

Scheme 1.4. Proposed bifunctional catalytic cycle for olefin epoxidation by $[(diphoe)Pt(CF_3)(CH_2Cl_2)]BF_4$.[24]

Strukul and Michelin designed a second generation catalyst by replacing the $–CF_3$ group on Pt^{II} with perfluorophenyl, $–C_6F_5$.[26] This complex was also capable of the epoxidation of terminal alkenes from *aq*. H_2O_2. However, the activation of the oxidant was instead proposed to occur in the second coordination sphere through H-bonding with the $-C_6F_5$ group (**Figure 1.2**). This activation route was proposed from *in situ* ^{19}F NMR data and steric arguments.[24,27] While this proposal is seemingly abstract, H-bonding assisted OAT has been proposed in oxidation catalysis literature previously.[25,28] The importance of H-bonding to assist in OAT will be discussed in Chapter 5. These examples of late, less-oxophilic transition metal epoxidation catalysts were a remarkable advance, but still the reliance on H_2O_2, and not O_2, ultimately creates inefficiency in this system.

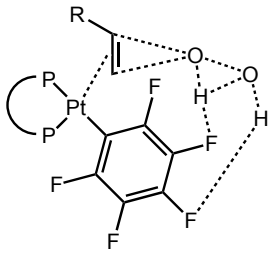

Figure 1.2. Proposed intermolecular H-bonding in O-atom transfer from H_2O_2 to olefins.[24,27]

Soon after Strukul and Michelin published their work on olefin epoxidation with H_2O_2 and [(diphoe)Pt(CF_3)(CH_2Cl_2)]BF_4 as a precatalyst, Wenzel proposed an epoxidation catalytic cycle employing molecular oxygen as the oxidant for a similar Pt^{II} center (**Scheme 1.5**).[29] The cycle begins with OAT to an olefin, forming the epoxide and Pt^{II}-OH products (**Scheme 1.5**, step 1). This step would be analogous to Strukul's work. This Pt^{II}-OH species can then undergo hydrogenolysis to form a Pt^{II} hydride (Pt^{II}-H) and H_2O, or protonation by an alcohol/ß-hydride elimination forming a ketone/aldehyde (**Scheme 1.5**, step 2). Furthermore, the formed H_2O or sacrificial alcohol could enhance the rate of OAT, as was observed by Strukul and Michelin.[22] Lastly, the Pt^{II}-H species could undergo a reaction with O_2 to form a Pt^{II}-OOH species (**Scheme 1.5**, step 3), regenerating the catalyst. Notably, only a handful of examples of O_2 reacting with M-H complexes were known at the time.[30-34] Accordingly, this specific transformation was not observed under ambient conditions with oxygen using (diphoe)Pt(H)CF_3.[29] At elevated temperatures and in the presence of radical initiators, a Pt^{II}-OOH species was finally observed, but only in minor amounts (25%). However, this experiment provided a proof of principle, that under appropriate conditions, O_2 can insert into a Pt^{II}-H bond.

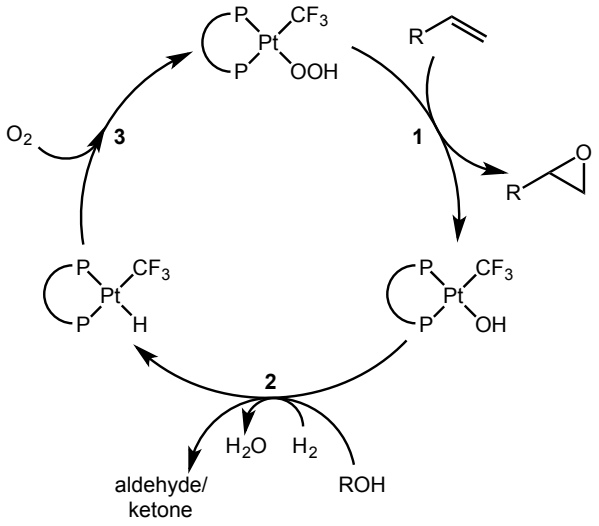

Scheme 1.5. Catalytic cycle proposed by Wenzel for olefin epoxidation using O_2.[29]

Quite recently, Trewyn, Vedernikov, Gunnoe and coworkers published the Pt^{II} catalyzed epoxidation of norbornene using O_2 as the oxidant.[35] Their catalyst, a Pt^{II} scorpionate complex immobilized on mesoporous silica, was capable of epoxidizing the strained olefin with greater than 80% selectivity and TON >40,000 (**Scheme 1.6**). Notably, the unsupported molecular complex under the same conditions deactivated after only 35 turnovers, yielding a dinuclear Pt(μ-OH) species. In depth mechanistic studies were not described. However, previously reported stoichiometric epoxidations with the unsupported molecular analogue suggests oxytane formation, oxidation by O_2 to Pt^{IV} followed by reductive C-O bond formation (**Scheme 1.7**).[36]

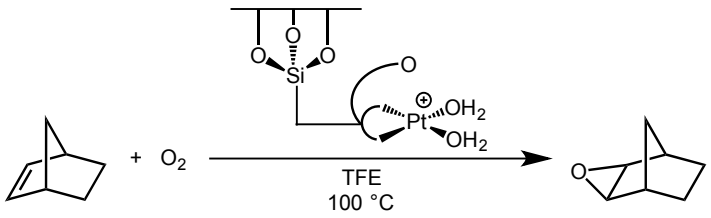

Scheme 1.6. Catalytic epoxidation of norbornene by a cationic Pt^{II}-scorpionate on silica.

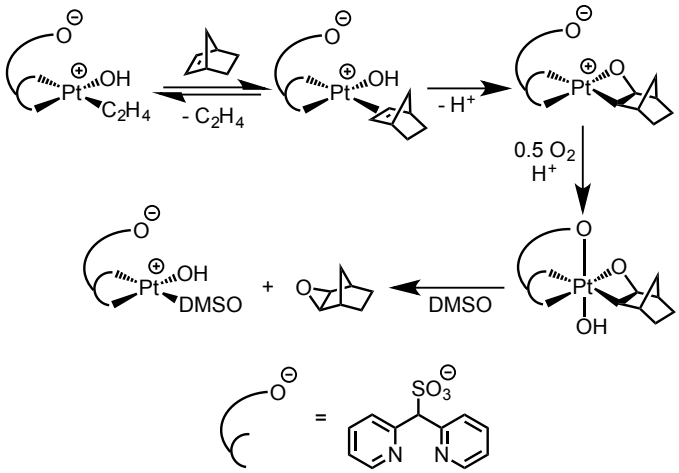

Scheme 1.7. Proposed aerobic epoxidation of norbornene by (dpms)Pt^{II}L(OH).[35]

1.4 Designing new late metal systems for olefin epoxidation

Our group began research on designing late metal catalysts for olefin epoxidation working from a generalized version of the catalytic cycle proposed by Wenzel (**Scheme 1.8**).[37] It was the initial goal of this project to investigate the mechanism by which these individual reaction steps occur, since literature on the aforementioned transformations was lacking. With a greater understanding of the individual steps, a working catalytic cycle could be possible. In order to investigate each transformation in detail, stable, isolable, and catalytically relevant species must be prepared and studied. Pincer ligands could be ideal partners for this application, as they should lend the potential metal catalyst a high degree of robustness while allowing controlled reactivity at one site in the square plane.[38] A notable aspect of the Strukul system is that only one of the sites in the square plane of the metal center is utilized.[24] Therefore, initial studies in catalyst design focused on pincer ligated metal complexes.

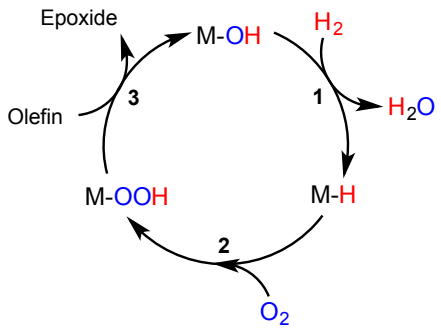

Scheme 1.8. Proposed catalytic cycle for the epoxidation of olefins using molecular oxygen.[37]

Wenzel's investigations highlighted the challenge of insertion of molecular oxygen into a Pt^{II}-H bond, but oxygen insertion into Pd^{II}-H bonds may be an easier reaction as, in general, second row metal-hydride bonds are weaker than the corresponding third row metal. In fact, insertion of molecular oxygen into Pd^{II}-H bonds has been proposed as a key step in a number of Pd-catalyzed oxidations.[39] The lower oxophilicity of this late metal center would allow for facile oxygenation and catalyst regeneration compared to the oxophilic early metal species employed currently. Therefore, Pd^{II} pincer complexes have been the primary focus of this research thus far. The following is a brief summary of the previous mechanistic research conducted with Pd^{II} pincer species for the transformations shown in **Scheme 1.8**.

Hydrogenolysis of Pd^{II}-OH complexes: The first step of the proposed cycle shown in **Scheme 1.8** is an underdeveloped yet powerful transformation that represents the catalyst regeneration step in our cycle. Hydrogenolysis of a Pd^{II} hydroxide species would release H_2O and generate a Pd^{II} hydride complex (**Scheme 1.8**, step 1), while hydrogenolysis of a Pd^{II} alkoxide would release an alcohol. Thus, hydrogenolysis wherein a metal hydride is generated from a metal hydroxide or metal alkoxide could serve as a general catalyst regeneration step for other transformations. However, there are few well-characterized examples of hydrogenolysis of M-O bonds in the literature. This scarcity may be due in part to the paucity of mononuclear

hydroxide and alkoxide complexes of the late metals.[40-42] The tridentate design and the stability of the pincer motif has allowed the isolation and study of such mononuclear complexes of Pd^{II}.

The hydrogenolysis reactions of ($^{t\text{Bu}}$PCP)Pd-OH (**1**) ($^{t\text{Bu}}$PCP = 2,6-bis(di^{t}butylphosphino)methylbenzene) and ($^{t\text{Bu}}$PCO)Pd-OH (**3**) ($^{t\text{Bu}}$PCO = 2-(di^{t}butylphosphino)methyl-6-(methoxy)methylbenzene) have been previously investigated by the Goldberg group.[43-45] Upon pressurization of a solution of **1** in C_6D_6 with 7 atm of H_2 at room temperature, quantitative conversion to the hydride ($^{t\text{Bu}}$PCP)Pd-H (**2**) was observed over 60 hours (**Scheme 1.9**). The mechanisms for these Pd^{II}-OH hydrogenolysis reactions were also studied. Unusual kinetics were observed for the reaction shown in **Scheme 1.9**; the reaction rate was first order in [H_2] but only half-order in [**1**]. Well-behaved kinetic behavior was also only observed when the reaction was carried out in the presence of an excess of H_2O. It was later determined that the half-order term with respect to **1** and the effect of H_2O on the reaction could be explained by the formation of a H_2O-bridged dimer of **1**. X-ray structures of both the monomeric Pd^{II}-OH **1** and a H_2O-bridged dimer **1-*H_2O*** (grown in the presence of H_2O) were also reported. Under the reaction conditions, an equilibrium between the H_2O-bridged dimer and the monomer was established. The kinetic behavior was shown to be consistent with hydrogenolysis occurring by reaction of the monomeric species **1** with hydrogen.

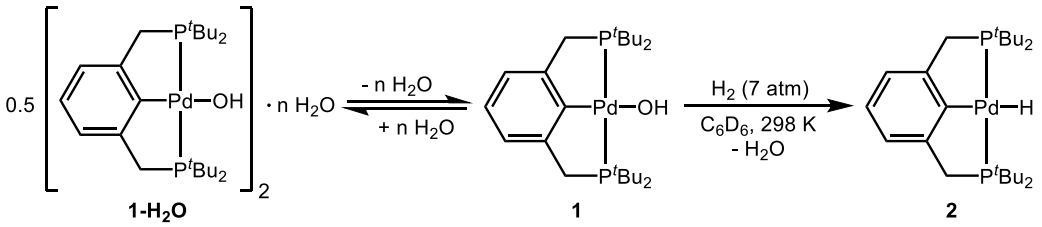

1-H_2O **1** **2**

Scheme 1.9. Hydrogenolysis of ($^{t\text{Bu}}$PCP)Pd-OH (**1**) and preequilibrium of H_2O-bridged dimer **1-H_2O**.[44]

Several mechanisms were proposed for the hydrogenolysis of the monomeric Pd^{II}-OH complex **1**: (**A**) oxidative addition of hydrogen and reductive elimination of H_2O, (**B**) a four-centered transition state with an intramolecular proton transfer (internal electrophilic substitution, IES),[46,47] or (**C**) the deprotonation of a four-coordinate dihydrogen complex by dissociated hydroxide (**Scheme 1.10**). With excess H_2O slowing the rate of hydrogenolysis, a mechanism involving dissociation of hydroxide (**C**) was considered unlikely. No experimental evidence was available to distinguish between paths **A** and **B**. The results of DFT computations at the B3LYP/LACVP** level of theory on this ($^{t\text{Bu}}$PCP)Pd system supported that the reaction proceeds via the four-centered transition state shown in path B ($\Delta G^{\ddagger}$ = 25.7 kcal/mol). Oxidative addition of hydrogen to produce the Pd^{IV} intermediate (ΔG = 40.9 kcal/mol) shown in **Scheme 1.10** was far too high in energy.

The importance of a strongly binding pincer system in these hydrogenolysis reactions became evident when the reaction of H_2 with ($^{t\text{Bu}}$PCO)Pd-OH (**3**), a complex bearing a hemilabile pincer, was studied.[45] In contrast to the reaction of ($^{t\text{Bu}}$PCP)Pd-OH (**1**) with H_2, exposure of **3** to 7 atm of H_2 at room temperature did not yield a Pd^{II} hydride product. Instead a Pd^0 bisphosphine complex (**4**) was formed as shown in **Scheme 1.11**. The difference in reactivity between the two Pd^{II} hydroxide complexes was attributed to the hemilabile ether arm, which can dissociate allowing for the operation of other reaction pathways. Following

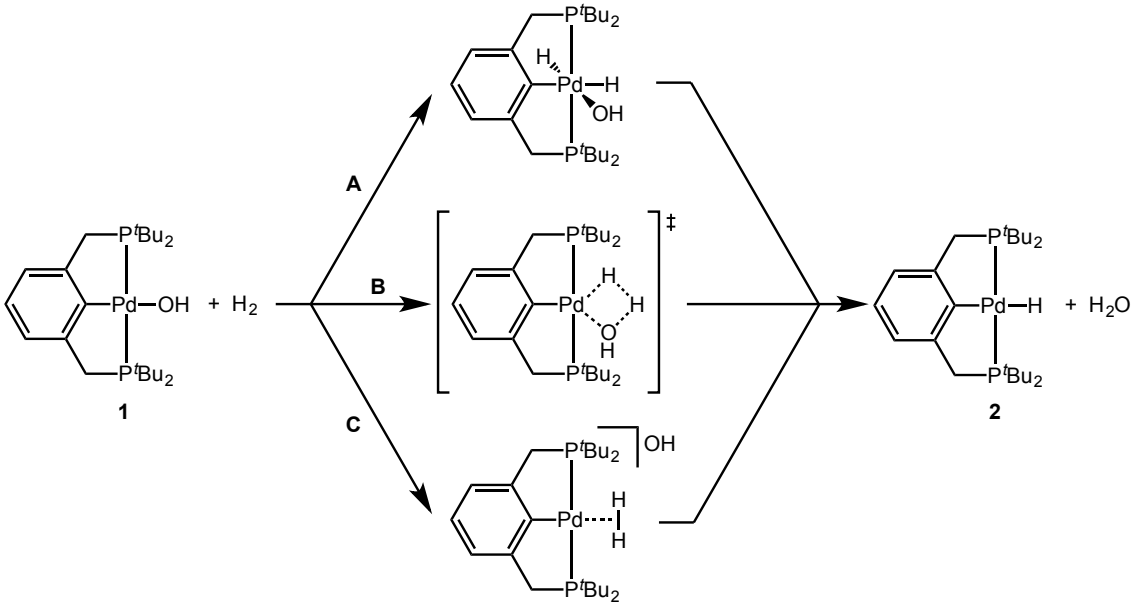

Scheme 1.10. Possible mechanisms for the hydrogenolysis of complex **1**.[44]

deuterium labeling studies, it was proposed that the reaction of **3** with H_2 likely operates by displacement of the ether arm by dihydrogen, followed by IES. Reductive elimination (RE) of the aryl and the hydride ligands lead to Pd^0 (**Scheme 1.11**). As both Pd^0 particles and free ligand are observed in this reaction, it was proposed that the monophosphine Pd^0 species binds an additional $^{t\text{Bu}}$PCO ligand to form the observed product **4**. From these initial investigations of the $^{t\text{Bu}}$PCP and $^{t\text{Bu}}$PCO Pd^{II} hydroxides **1** and **3**, requirements for hydrogenolysis were beginning to present themselves, but further studies would be necessary to confirm general mechanisms.

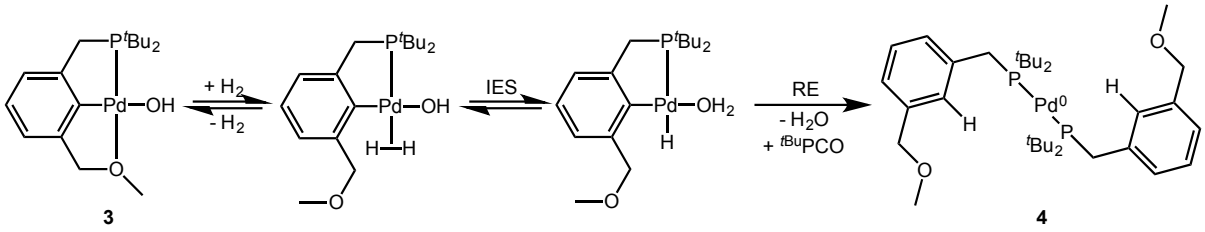

Scheme 1.11. Hydrogenolysis of ($^{t\text{Bu}}$PCO)Pd-OH (**3**) and reduction to a Pd^0-bisphosphine **4**.[45]

O_2 insertion into Pd^{II}-H bonds: In 2006, Goldberg and coworkers utilized a pincer ligand framework and reported the first direct observation of molecular oxygen insertion into a Pd^{II}-H bond.[48] The pincer complex, ($^{t\text{Bu}}$PCP)Pd-H (**2**) underwent insertion of molecular oxygen to generate the Pd^{II} hydroperoxide complex ($^{t\text{Bu}}$PCP)Pd-OOH (**5**) (**Scheme 1.12**). The hydroperoxide was found to be relatively stable, and was structurally characterized. The hydroxide **1** was detected as a minor product in the reaction (with the ratio of **5**:**1** being 25:1 at 10 atm of O_2). Notably, the Pd^{II} hydroperoxide **5** gradually decomposed to the Pd^{II} hydroxide complex **1** over time, suggesting the potential for OAT.

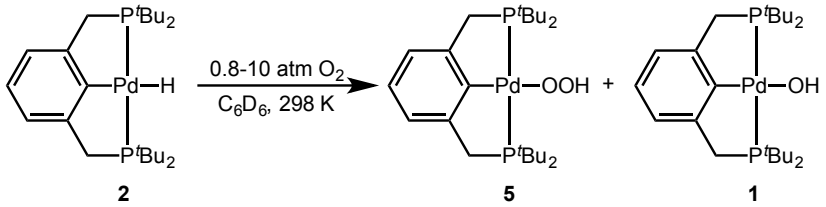

2 **5** **1**

Scheme 1.12. Direct O_2 insertion into the Pd^{II}-H bond of ($^{t\text{Bu}}$PCP)Pd-H (**2**).[48]

This O_2 insertion reaction was found to be general to other modified ^{R}PCP Pd^{II} systems, with varying R groups on the phosphines (^{t}Bu, ^{i}Pr, Cy) as well as bridging groups on the pincer arm (X = CH_2, NH, O) (**Scheme 1.13**).[49,50] However, when replacing Pd^{II} with Pt^{II}, no reaction was observed with oxygen and the hydride ($^{t\text{Bu}}$PCP)Pt-H (**6**), even at high pressures and temperatures.[50] Wenzel similarly had difficulty inserting O_2 into Pt^{II}-H bonds.[29] The Ni^{II} analogues (^{R}PCP)Ni-H were also explored for their O_2 reactivity. While the pincer Ni^{II} hydride complexes were found to react readily with O_2, hydroperoxide species were never isolated and oxidative ligand degradation was observed.[49]

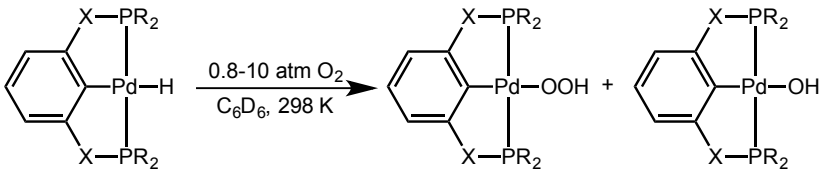

Scheme 1.13. General insertion of O_2 into (^{R}PCP)Pd-H species (X = CH_2, NH, O; R = ^{t}Bu, ^{i}Pr, Cy).

Experimental[48] and computational[51] mechanistic studies for the insertion of O_2 into the Pd^{II}-H **2** were carried out. It was proposed that the insertion occurred through rate-determining H-atom abstraction (HAA) by O_2 (**Figure 1.3**). This was consistent with the experimentally observed KIE (k_H/k_D = 5.8(5)) and first order dependence on **2** and O_2. The calculated pathway indicated that coordination of O_2 followed by insertion (similar to olefin migratory insertion) was not occurring, but instead HAA was the lowest energy route. Furthermore, as the rate-determining step involved homolytic cleavage of the Pd^{II}-H bond, it would follow that the weaker the bond, the more facile insertion should occur. Indeed, computations varying the pincer motif on Pd^{II} indicated an inverse relationship between Pd^{II}-H bond length and the activation barrier for HAA.[52] This indicated that a strong *trans* donor to the hydride should assist in HAA.

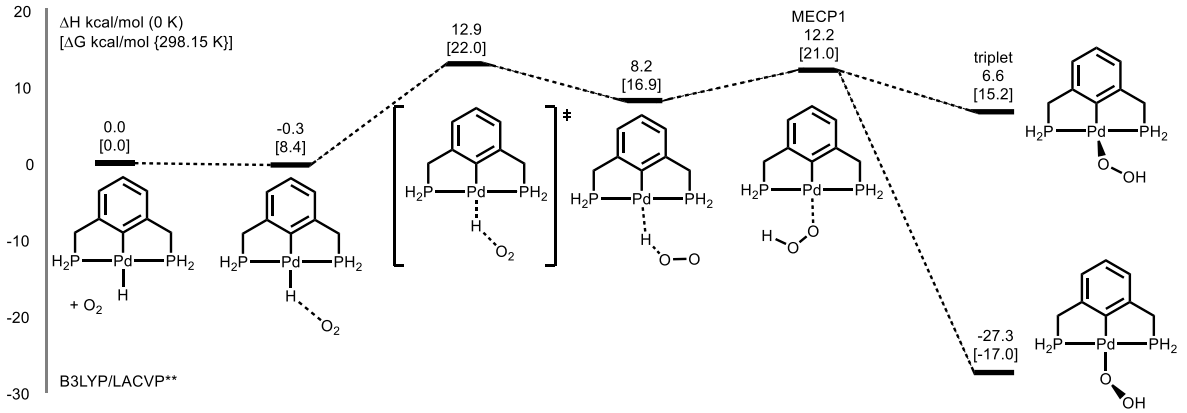

Figure 1.3. Calculated mechanism for the direct insertion of O_2 into (^{H}PCP)Pd-H.[51]

Remarkably, Stahl and coworkers published a different example of O_2 insertion into a

Pd^{II}-H bond at a similar time that operated by a different mechanism.[53-56] Starting from the complex (BzO)$(IMes)_2$Pd-H (**7**) (BzO = benzoate; IMes = 1,3-bis(2,4,6-trimethylphenyl)imidazol-2-ylidene), they showed that upon exposure to O_2, **7** reductively eliminated benzoic acid, forming a Pd^0 intermediate. This low valent species then reacted readily with O_2, forming a Pd^{II}-peroxide. The peroxide is then protonated by benzoic acid, forming the final hydroperoxide (BzO)$(IMes)_2$Pd-OOH (**8**) (**Scheme 1.14**). Furthermore, by changing the electronic donation properties of the *trans* benzoate ligand via substitution at the *para*-position, a mechanistic crossover was observed.[56] Notably, increasing the electron donating ability of benzoate, and thus weakening the Pd^{II}-H bond, resulted in facile HAA to occur. However, substituting benzoate with electron-withdrawing groups resulted in easier insertion by the RE/HX mechanism described above. This variation in O_2 insertion mechanism through ligand design will be a key feature in future catalyst design (see chapter 5).

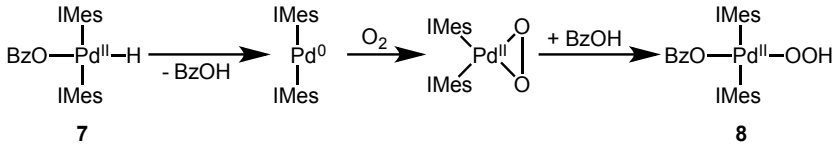

7 **8**

Scheme 1.14. Direct O_2 insertion into (BzO)$(IMes)_2$Pd-H (**7**) by the RE/HX mechanism.[56]

O-atom transfer from Pd^{II}-OOH: As mentioned above, the insertion of O_2 into the hydride of (^{R}PCP)Pd-H yielded an isolable hydroperoxide (^{R}PCP)Pd-OOH (R = ^{t}Bu, ^{i}Pr, Cy).[48] These complexes were found to slowly degrade to the hydroxide (^{R}PCP)Pd-OH, indicating the possibility of OAT to substrates. Indeed, it was found that the Pd^{II}-OOH complex **5** could readily oxidize substrates such as PPh_3 and ^{t}BuNC, forming (O)PPh_3 and ^{t}BuN=C=O respectively.[49] However, no reaction was observed between **5** or other pincer Pd^{II}-OOH complexes and free olefins. Notably, not all ^{R}PCP ligands were inert toward oxidation. When ^{i}Pr or Cy R-groups were used on the phosphine arms, oxidation of these phosphine moieties

by Pd^{II}-OOH occurred, yielding acetone or cyclohexanone, respectively.[49] Interestingly, the Pd^{II} analouges of Strukul's catalyst, (PP)Pd(CF_3)-OOH, were found to react with olefins, but formed primarily the ketone product rather than the epoxide.[24] The change in selectivity was due to the proposed propensity of Pd^{II} to undergo ß-hydride elimination versus oxirane ring closure (**Scheme 1.15**). This ketone selectivity by Pd^{II}-OOH species has been observed in other systems.[57] In order to reason why (^{R}PCP)Pd-OOH showed no reactivity towards olefins, DFT computations were performed.

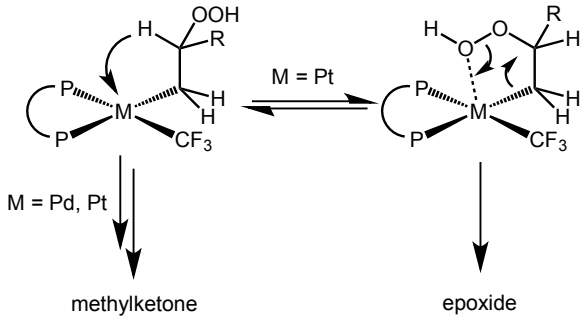

Scheme 1.15. Selectivity determining conformations resulting in either the methylketone or epoxide.[24]

The transition state for OAT from **5** towards olefins was examined by DFT by a previous collaborator, Muller, and compared to a model Ti^{IV} epoxidation catalyst active site (**Figure 1.4**).[58] It was found that an internal proton transfer from the ß-oxygen to the α-oxygen first occurs, followed by ß-OAT toward the olefin. Accordingly, the energy barrier as compared to Ti^{IV} OAT is much higher (~25 kcal/mol). In order to lower the barrier for the Pd^{II} system, it was proposed that H-bonding substituents could be used to assist the internal proton transfer. Indeed, when calculating the transition state for (^{Imd}PCP)Pd-OOH (**9**) (^{Imd}PCP = 2,6-bis(di-2'-imidazolylphosphino)methylbenzene), the barrier was found to be 8-9 kcal/mol lower than the alkyl analogue **5** (**Figure 1.4**). Furthermore, performing the calculations with protonated imidazole groups lowered the barrier even further, from 32 kcal/mol to 19

kcal/mol.[58] These calculations suggested that the inclusion of H-bonding functionality into future catalyst design could greatly assist in OAT.

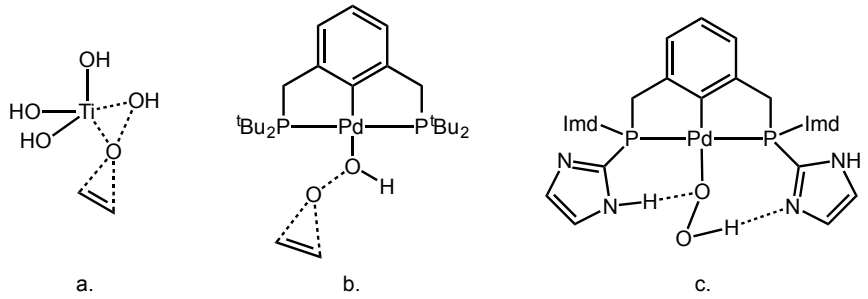

Figure 1.4. Structures of a. the calculated transition state for OAT from model $(HO)_3Ti$-OOH, b. the calculated transition state for OAT from (^{tBu}PCP)Pd-OOH, and c. the calculated intramolecular H-bonding in (^{Imd}PCP)Pd-OOH (**9**).

1.5 Dissertation summary

The following chapters describe the synthesis, characterization, and reactivity studies of model complexes for proposed intermediates in the catalytic cycle shown in **Scheme 1.8**. The focus of this work is on group 10 pincer complexes and their reactivity with H_2 and O_2 gas. Using key past results as inspiration, novel complexes were designed to probe the requirements for each step of catalysis. Chapter 2 discusses the synthesis and characterization of a variety of $^{t\text{Bu}}$PNP ligated Pd^{II} and Pt^{II} hydride complexes ($^{t\text{Bu}}$PNP = 2,6-bis-(di-^{t}butylphosphinomethyl)pyridine). Metal-ligand cooperation was observed in the activation of H_2 to form neutral hydride complexes. The effect of ligand protonation/deprotonation on the *trans* influence experienced by the hydride ligand was investigated.[59] Chapter 3 examines the synthesis and characterization of mono- and dinuclear PCN^R ligated Pd^{II} hydroxide complexes (PCN = 1-(3-((di-^{t}butylphosphino)methyl)phenyl)-1H-pyrazole). "Rollover" activation of the pyrazole arm of the pincer was observed experimentally and examined by DFT computations.[60] Chapter 4 discusses the reactivity of the $(PCN^R)Pd^{II}$ hydroxide species with H_2. Dinuclear

hydrides were isolated, while terminal hydrides were not observed. A mechanistic study on the hydrogenolysis of the μ-bridged hydroxide {[(PCN^{Me})Pd]$_2$(μ-OH)}[OTf] is presented.[61] Lastly, Chapter 5 proposes a novel route for O_2 activation and utilization through metal-ligand cooperation. Preliminary studies on NNN^{Pyz}, NNN^{Et}, and NN^{Me} ligated Pd^{II} and Pt^{II} are discussed (NNN^{Pyz} = 2,6-bis(5-*t*butyl-1H-pyrazol-3-yl)pyridine; NNN^{Et} = 2-(5-*t*butyl-1H-pyrazol-3-yl)-6-(diethylaminomethyl)pyridine; NN^{Me} = 2-(5-*t*Bu-1H-pyrazol-3-yl)-6-methylpyridine. The NNN^{Pyz} ligand, containing two acidic sites in proximity to the fourth site in the square plane, was found to protonate M-O_2 complexes, chelate to the metal center and oxidize phosphine substrates. Similar reactivity was observed with NNN^{Et} and NN^{Me}, however hemilability of these ligands resulted in undesired coordination modes.

1.6 Notes to chapter 1

1. Cavani, F.; Teles, J. H. *ChemSusChem,* **2009**, *2*, 508.
2. Anastas, P. T.; Warner, J. C. *Green Chemistry: Theory and Practice*, Oxford University Press: New York, 1998; pp 30.
3. IHS Chemical, *Propylene Oxide*, 2012 report.
4. SHELL, Ethylene oxide/ethylene glycol (EO/EG) processes, SHELL, **2010**.
5. Campbell, C. *J. Catal.* **1985**, *94*, 436.
6. Özbek, M. O.; van Santen, R. A. *Catal. Lett.* **2013**, *143*, 131.
7. Monnier, J. R. *Appl. Catal. A-Gen.* **2001**, *221*, 73.
8. Osugi, J.; Kubota, H. *Rev. Phys. Chem. Japan* **1964,** *34*, 19.
9. Beran, S.; Jiru, P.; Wichterlova, B.; Zahrandik, R. *React. Kinet. Catal. Lett.* **1976,** *5*, 131.
10. Barteau, M. A.; Madix, R. J. *J. Am. Chem. Soc.* **1983**, *105*, 344.
11. Cavani, F.; Gaffney, A. M. *Synthesis of Propene Oxide: A Successful Example of Sustainable Industrial Chemistry, in Sustainable Industrial Chemistry;* Cavani, F., Ed.; Centi, G., Ed.; Perathoner, S., Ed.; Trifiró, F., Ed.; Wiley-VCH Verlag GmbH & Co. KGaA, Weinheim, Germany, 2009; pp 319.
12. "Technology Roadmap: Energy and GHG Reductions in the Chemical Industry via Catalytic Processes" International Energy Agency, **2013**.
13. Sumitomo Chemical Co., Ltd. *Development of New Propylene Oxide Process*, vol. 2006-I.
14. Clerici, M. G.; Ingallina, P. *J. Catal.* **1993**, *140*, 71.
15. Lane, B. S.; Burgess, K. *Chem. Rev.* **2003**, *103*, 2457.
16. Clerici, M. G.; Bellussi, G.; Romano, U. *J. Catal.* **1991**, *129*, 159.
17. Sheldon, R. A. *J. Mol. Catal.* **1980**, *7*, 107.
18. Katsuki, T.; Sharpless, K. B. *J. Am. Chem. Soc.*, **1980**, *102*, 5974.
19. Zhang, W.; Loebach, J. L.; Wilson, S. R.; Jacobsen, E. N. *J. Am. Chem. Soc.*, **1990**, *112*, 2801.
20. De Vos, D. E.; Sels, B. F.; Jacobs, P. A. *Adv. Synth. Catal.* **2003**, *345*, 457.
21. Mizuno, N.; Yamaguchi, K.; Kamata, K. *Coord. Chem. Rev.* **2005**, *249*, 1944.
22. Strukul, G.; Michelin, R. A. *J. Chem. Soc., Chem. Commun.* **1984**, 1538.
23. Strukul, G.; Michelin, R. A. *J. Am. Chem. Soc.* **1985**, *107*, 7563.
24. Sgarbossa, P.; Scarso, A.; Strukul, G.; Michelin, R. A. *Organometallics* **2012**, *31*, 1257.
25. Hornback, J. M.; *Organic Chemistry*, 2nd ed.; 2006; pp 376-378.
26. Pizzo, E.; Sgarbossa, P.; Scarso, A.; Michelin, R. A.; Strukul, G. *Organometallics* **2006**, *25*, 3056.
27. Colladon, M.; Scarso, A.; Sgarbossa, P.; Michelin, R. A.; Strukul, G. *J. Am. Chem. Soc.* **2007**, *129*, 7680.
28. Musaev, D. G. *Inorg. Chem.* **2006**, *45*, 5703.
29. Wenzel, T. T. *Stud. Surf. Sci. Catal.* **1991**, *66*, 545.
30. Bayson, J. H.; Winfield, M. E. *J. Catal.* **1964**, *3*, 123.
31. Roberts, H. L.; Symes, W. R. *J. Chem. Soc. A* **1968**, 1450.
32. Johnston, L. E.; Page, J. A. *Can. J. Chem.* **1969**, 47, 4241.
33. Gillard, R. D.; Heaton, B. T.; Vaughan, D. H.; *J. Chem. Soc. A* **1970**, 3126.
34. Endicott, J. F.; Wong, C. L.; Inoue, T.; Natarajan, P. *Inorg. Chem.* **1979**, *18*, 450.
35. Munz, D.; Wang, D.; Moyer, M. M.; Webster-Gardiner, M. S.; Kunal, P.; Watts, D.; Trewyn, B. G.; Vedernikov, A. N.; Gunnoe, T. B. *ACS Catal.* **2016**, *6*, 4584.
36. Khusnutdinova, J. R.; Zavalij, P. Y.; Vedernikov, A. N. *Organometallics* **2007**, *26*, 2402.
37. Bailey, W. D.; Parkes, M. V.; Kemp, R. A.; Goldberg, K. I. *Reactions of Square Planar d^8 Pincer Complexes with Oxygen and Hydrogen.* Pincer and Pincer-Type Complexes: Application in

Organic Synthesis and Catalysis*;* Szabo, K. J., Ed.; Wendt, O. F., Ed; Wiley-VCH: Weinheim, Germany, 2014; pp 281-298.
38. For general reviews and books, see: (a) *Pincer and Pincer-Type Complexes: Application in Organic Synthesis and Catalysis;* Szabo, K. J., Ed.; Wendt, O. F., Ed; Wiley-VCH: Weinheim, Germany, 2014. (b) *Organometallic Pincer Chemistry;* Van Koten, G.; Milstein, D., Ed.; Top. Organomet. Chem.; Springer: Heidelberg, 2013; Vol. 40. (c) Niu, J.-L.; Hao, X.-Q.; Gong, J.-F.; Song, M.-P. *Dalton Trans.* **2011**, *40*, 5135. (d) Benito-Garagorri, D.; Kirchner, K. *Acc. Chem. Res.* **2008**, *41*, 201 (e) van der Boom, M. E.; Milstein, D. *Chem. Rev.* **2003**, *103*, 1759. (f) Singleton, J. T. *Tetrahedron* **2003**, *59*, 1837.
39. Stahl, S. S. *Angew. Chem. Int. Ed.* **2004**, *43*, 3400.
40. Bryndza, H. E.; Tam, W. *Chem. Rev.* **1988**, *88*, 1163.
41. Fulton, J. R.; Holland, A. W.; Fox, D. J.; Bergman, R. G. *Acc. Chem. Res.* **2002**, *35*, 44.
42. Roesky, H. W.; Singh, S.; Yusuff, K. K. M.; Maguire, J. A.; Hosmane, N. S. *Chem. Rev.* **2006**, *106*, 3813.
43. Fulmer, G. R.; Muller, R. P.; Kemp, R. A.; Goldberg, K. I. *J. Am. Chem. Soc.* **2009**, *131*, 1346.
44. Fulmer, G. R.; Herndon, A. N.; Kaminsky, W.; Kemp, R. A.; Goldberg, K. I. *J. Am. Chem. Soc.* **2011**, *133*, 17713.
45. Fulmer, G. R.; Kaminsky, W.; Kemp, R. A.; Goldberg, K. I. *Organometallics* **2011**, *30*, 1627.
46. Cundari, T. R.; Grimes, T. V.; Gunnoe, T. B. *J. Am. Chem. Soc.* **2007**, *129*, 13172.
47. Oxgaard, J.; Tenn, W. J., III; Nielsen, R. J.; Periana, R. A.; Goddard, W. A., III *Organometallics* **2007**, *26*, 1565.
48. Denney, M. C.; Smythe, N. A.; Cetto, K. L.; Kemp, R. A.; Goldberg, K. I.; *J. Am. Chem. Soc.* **2006**, *128*, 2508.
49. Boro, B. J. Ph.D. Dissertation, University of New Mexico, 2009.
50. Fulmer, G. R. Ph.D. Dissertation, University of Washington, 2010.
51. Keith, J. M.; Muller, R. P.; Kemp, R. A.; Goldberg, K. I.; Goddard, W. A., III; Oxgaard, J. *Inorg. Chem.* **2006**, *45*, 9631.
52. Parkes, M. V. Ph.D. Dissertation, University of New Mexico, 2012.
53. Konnick, M. M.; Gandhi, B. A.; Guzei, I. A.; Stahl, S. S. *Angew. Chem. Int. Ed.* **2006**, *45*, 2904.
54. Popp, B. V.; Stahl, S. S. *J. Am. Chem. Soc.* **2007**, *129*, 4410.
55. Konnick, M. M.; Stahl, S. S. *J. Am. Chem. Soc.* **2008**, *130*, 5753.
56. Konnick, M. M.; Decharin, N.; Popp, B. V.; Stahl, S. S. *Chem. Sci.* **2011**, *2*, 326.
57. Myaji, T.; Kujime, M.; Hikichi, S.; Moro-oka, Y.; Akita, M. *Inorg. Chem.* **2002**, *41*, 5286.
58. Muller, R. P.; Kemp, R. A.; Goldberg, K. I. Unpublished results.
59. Bailey, W. D.; Kaminsky, W.; Kemp, R. A.; Goldberg, K. I. *Organometallics* **2014**, *33*, 2503.
60. Bailey, W. D.; Luconi, L.; Rossin, A.; Yakhvarov, D.; Flowers, S. E.; Kaminsky, W.; Kemp, R. A.; Giambastiani, G.; Goldberg, K. I. *Organometallics* **2015**, *34*, 3998.
61. Bailey, W. D.; Luconi, L.; Rossin, A.; Yakhvarov, D.; Flowers, S. E.; Kaminsky, W.; Kemp, R. A.; Giambastiani, G.; Goldberg, K. I. Manuscript in preparation, 2016.

Chapter 2*

Cationic, Neutral, and Anionic Hydrides of $^{t\text{Bu}}$PNP -Pd^{II} and -Pt^{II}

2.1 Introduction

Pincer complexes of late transition metals have been heavily utilized in catalysis.[1-12] The tridentate design of the ligands favors strong binding to the metal and allows for stabilization of the catalyst even at high reaction temperatures. The use of $^{t\text{Bu}}$PCP to stabilize M-OR and M-H species relevant to oxidation catalysis has shown that a pincer framework is a valuable tool in catalyst design, and should continue to be employed in this chemistry. The modular structure of the ligands enables tuning of the catalyst activity and selectivity through systematic variation of the donor atoms, their substituents and the ligand backbone framework.[13,14] Interestingly, sites on the ligand framework have been shown in some cases to participate in the reactions of the metal complexes with reactivity ranging from

* The majority of the data presented in this chapter has been previously published: Reprinted with permission from Bailey, W. D.; Kaminsky, W.; Kemp, R. A.; Goldberg, K. I. *Organometallics* **2014**, *33*, 2503-2509. Copyright 2014 American Chemical Society.

deprotonation/protonation to assisting in the binding and activation of small molecules.[7,8,15-20] It was proposed that this type of cooperative reactivity could be useful in H_2 and O_2 activation.

Previous computational results indicated that it may be possible to manipulate the ability of the hydride to insert O_2 by varying the charge and the *trans* donor capacity of the pincer ligand.[21] To further probe this hypothesis, the neutral $^{t\text{Bu}}$PNP ligand, popularized by Milstein,[22-26] was investigated as a competent support for group 10 metal hydrides. Recently, the $^{t\text{Bu}}$PNP ($^{t\text{Bu}}$PNP = 2,6-bis-(di-*t*butylphosphinomethyl)pyridine) ligand has shown a range of cooperative reactivity with metal centers in valuable catalytic and stoichiometric transformations.[22-26] Deprotonation of the methylene carbon in the backbone results in dearomatization of the pyridine ring and yields an isoelectronic species to $^{t\text{Bu}}$PCP. Subsequent deprotonation of the second pincer arm restores and extends the aromatization of the ligand framework. Previously, a series of cationic [($^{t\text{Bu}}$PNP)MX]Cl, neutral ($^{t\text{Bu}}$PNP*)MX and anionic K[($^{t\text{Bu}}$PNP**)MX] (M=Pd^{II}, Pt^{II}; X=Cl, Me) complexes have been reported (* is used to indicate deprotonation of the $^{t\text{Bu}}$PNP ligand).[27] However, a direct comparison of the electronic effects of the neutral, deprotonated and doubly deprotonated ligand had yet to be made. Furthermore, it was shown previously that 0.5 eq. of O_2 reacted cleanly with the Rh species ($^{t\text{Bu}}$PNP)Rh-H to yield the hydroxide ($^{t\text{Bu}}$PNP)Rh-OH.[28] We were thus interested in investigating this ligand on Pd^{II} and Pt^{II} for its ability to labilize the hydride ligand and facilitate O_2 insertion. Discussed below is the synthesis and characterization of $^{t\text{Bu}}$PNP complexes and analogous hemilabile $^{t\text{Bu}}$PNN complexes of Pd^{II} and Pt^{II} and their reactivity with gaseous H_2 and O_2.

2.2 Results and discussion

Synthesis of a Neutral ($^{t\text{Bu}}$PNP*)Pd^{II} Hydride Complex: Upon addition of borohydride salts (K-Selectride® (K[^{sec}Bu$_3$BH]) or Super Hydride® (Li[Et$_3$BH]) solutions) to a THF solution of ($^{t\text{Bu}}$PNP*)PdCl,[27] a new species was observed with a broad hydride signal in the ^{1}H NMR spectrum (-10.4 ppm). Two new doublets were apparent in the ^{31}P{^{1}H} NMR spectrum (73.9 ppm and 76.6 ppm, $^2J_{PP}$ = 319 Hz). These NMR spectral data are consistent with the ($^{t\text{Bu}}$PNP*)PdH (**10***) species shown in **Scheme 2.1**. However, along with the other expected signals for **10*** in the ^{1}H NMR spectrum, signals for a contaminant were also observed (broad peaks at 0.90, 1.21 and 1.67 ppm). The contaminant was possibly a borane species; borane-metal adducts have been observed previously.[29-31] Attempts to purify **10*** and isolate it without the contaminant by using dynamic vacuum under heat, as well as washing the residue with nonpolar solvents, were unsuccessful. Complex **10*** could also be formed by addition of excess lithium aluminum hydride (LAH) to a THF solution of ($^{t\text{Bu}}$PNP*)PdCl at -30 °C; however, this method showed limited reproducibility, and inconsistent yield and product purity.

Alternatively, a high yielding, reproducible method for synthesizing **10*** was found through deprotonation of the $^{t\text{Bu}}$PNP* ligand (to form the doubly deprotonated $^{t\text{Bu}}$PNP**) followed by a cooperative metal-ligand H_2 activation. Thus, a THF-d_8 solution of K[($^{t\text{Bu}}$PNP**)PdCl] was prepared as previously reported,[27] and subsequently pressurized with 3 atm of H_2 (**Scheme 2.1**). Monitoring the reaction by ^{1}H NMR spectroscopy over 72 hours reveals the growth of a broad upfield signal (-10.5 ppm). Concurrently, the growth of two doublets (74.4 and 76.3 ppm, $^2J_{PP}$ = 320 Hz) in the ^{31}P{^{1}H} NMR spectrum is observed. These

signals matched those seen in the preparation of **10*** from ($^{t\text{Bu}}$PNP*)PdCl and the borohydride or LAH reagents.

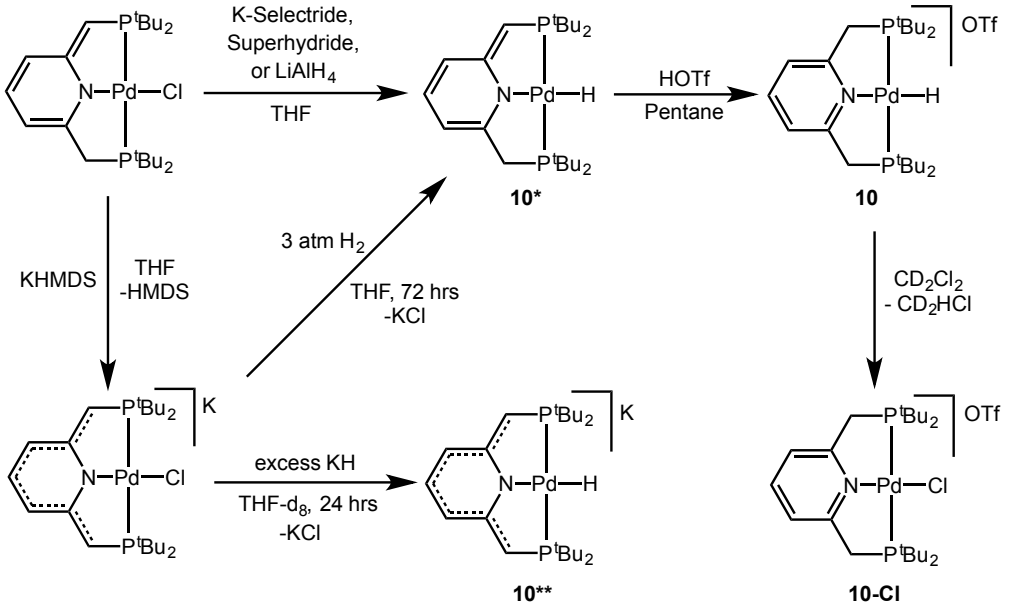

Scheme 2.1. Synthesis of the cationic, neutral and anionic Pd^{II} hydrides **10**, **10***, and **10****.

Complex **10*** was isolated and fully characterized by ^{1}H, $^{31}P\{^{1}H\}$, and $^{13}C\{^{1}H\}$ NMR spectroscopy, IR spectroscopy as well as X-ray crystallography (**Figure 2.1**). Select bond lengths and angles for the square planar hydride complex **10*** are reported in **Table 2.1**. The Pd^{II}-H distance was restrained as no specific electron density was observed for that hydrogen. The C6-C7 bond (1.392(19) Å) appears shorter than the C1-C2 bond (1.46(2) Å), consistent with a saturated C1 resulting from protonation at C1 by H_2. Furthermore, the P1-C1-C2 angle (114.0(12) deg) appears slightly smaller than the P2-C7-C6 angle (115.6(10) deg) also consistent with C7 bearing fewer hydrogen atoms than C1. The Pd1-N1 bond length (2.136(8) Å) is longer than the chloride analog (2.038(4) Å)[27] in agreement with the expected stronger *trans* influence of a hydride ligand.

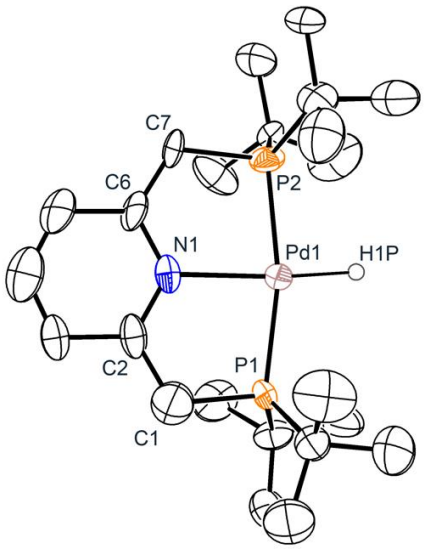

Figure 2.1. Single molecule ORTEP[32] of complex ($^{t\text{Bu}}$PNP*)PdH **(10*)** with ellipsoids shown at 50% probability. Hydrogen atoms bound to carbon atoms are omitted for clarity.

The ^{1}H NMR spectrum of **10*** displays a hydride signal as a broad singlet at -10.5 ppm. After simulating this resonance using gNMR, it was determined that the broad singlet resulted from complicated coupling patterns with the inequivalent P nuclei (**Figure 2.2**). The expected coupling to the two inequivalent phosphorus nuclei appears to be contained within this broad signal. The signals for the ^{t}Bu protons, which are now bound to inequivalent phosphorus nuclei, appear as two separate doublets of doublets. Similarly, the CH and CH_2 moieties in the pincer "arms" appear as separate signals, 2.82 and 3.49 ppm, integrating 2:1 respectively. The proton signals for the pyridine backbone appear upfield and are split into three separate peaks, indicating dearomatization. The dearomatization and broken symmetry of **10*** are further seen in the ^{13}C{^{1}H} NMR spectrum, as the pyridine pincer backbone carbon signals appear as 5 separate peaks in a wide range (97.8-171.4 ppm).

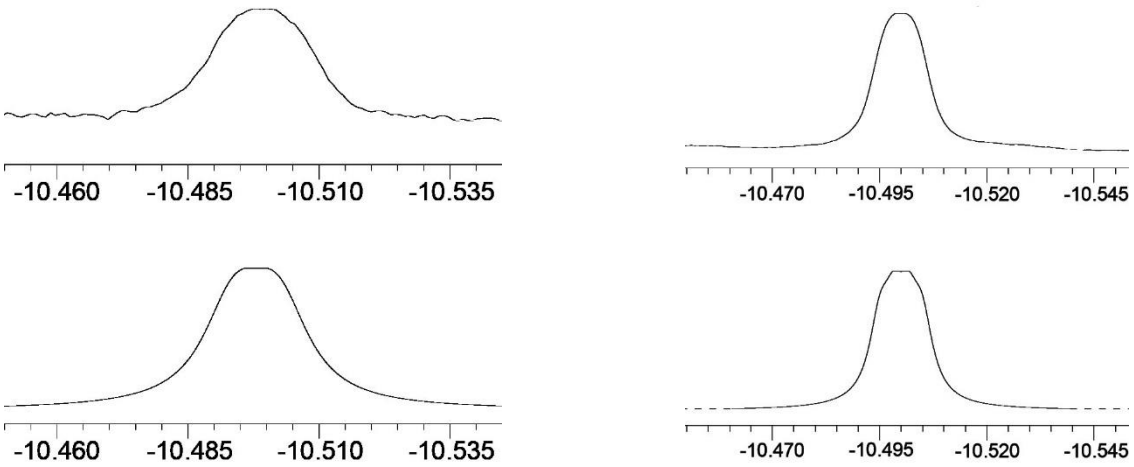

(a). (b).

Figure 2.2. Experimental (top) and simulation (bottom) of the (a) 300 MHz ^{1}H NMR hydride signal and (b) 500 MHz ^{1}H NMR hydride signal of **10***. Signal simulated with gNMR, $^{2}J_{P\text{-}P}$ = 320 Hz, $^{2}J_{P1\text{-}H}$ = 5.5 Hz, $^{2}J_{P2\text{-}H}$ = -3.8 Hz.

Table 2.1. Select bond lengths (Å) and angles (°) for neutral and cationic $^{t\text{Bu}}$PNP Pd/Pt hydrides.

	10*	**10**[a]	**15**[b]	**15*-Pt**[c]
M-N1	2.136(8)	2.1009(26)	2.096(5)	2.099(6)
M-P1	2.262(3)	2.2784(9)	2.2733(16)	2.261(2)
M-P2	2.261(3)	2.2789(9)	2.2730(17)	2.253(2)
P1-C1	1.806(17)	1.847(3)	1.847(7)	1.786(8)
P2-C7	1.862(13)	1.849(3)	1.838(7)	1.810(9)
C1-C2	1.46(2)	1.508(5)	1.503(9)	1.410(10)
C6-C7	1.392(19)	1.506(5)	1.507(9)	1.473(11)
P1-M-P2	167.85(12)	169.69(3)	169.17(7)	168.20(8)
P1-M-N1	84.1(3)	85.33(8)	84.95(15)	84.30(16)
P2-M-N1	84.1(3)	85.29(8)	84.92(15)	84.01(17)

[a] Distances and angles averaged from molecules 1-4 in asymmetric unit, standard deviation of average in parentheses. [b] Distances and angles averaged from molecules 1-3 in asymmetric unit, standard deviation of average in parentheses. [c] Distances and angles averaged from two ($^{t\text{Bu}}$PNP)Pt-H units in linked dimer, standard deviation of average in parentheses.

Synthesis of a Cationic (PNP)Pd^{II} Hydride Complex: Addition of triflic acid (HOTf) to a pentane solution of the neutral Pd^{II} hydride **10*** at -30 °C results in the formation of a new hydride species (**Scheme 2.1**). The ^{1}H NMR spectrum displays a triplet at -11.5 ppm for the hydride, as well as virtual triplets at 1.35 ppm (36 H) and 4.15 ppm (4 H) for the ^{t}Bu protons and methylene "arms", respectively. These signals suggest that the pincer complex has higher

symmetry than the deprotonated **10***, as the "arms" appear equivalent. A singlet at 76.3 ppm in the $^{31}P\{^{1}H\}$ NMR spectrum is consistent with equivalent phosphorus nuclei. In the $^{13}C\{^{1}H\}$ NMR spectrum, the aryl carbons appear as three signals, again consistent with a C_{2v} symmetric molecule. The solution NMR data and an X-ray crystal structure (**Figure 2.3**) are consistent with the characterization of this species as the C_{2v} symmetric cationic hydride complex [($^{t\text{Bu}}$PNP)PdH]OTf (**10**).

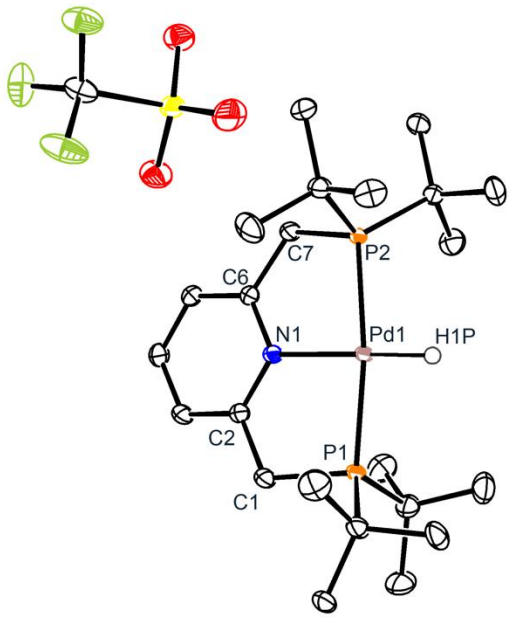

Figure 2.3. Single molecule ORTEP[32] of [($^{t\text{Bu}}$PNP)PdH]OTf (**10**) with ellipsoids shown at 50% probability. Hydrogen atoms bound to carbon atoms are omitted for clarity.

The solid-state structure of **10** displays a square planar species with a triflate counterion in the outer sphere. Select bond lengths and angles are reported in **Table 2.1**. Notably, the C1-C2 (1.508(5) Å) and C6-C7 (1.506(5) Å) bond length are identical, indicating fully saturated pincer "arms". The unit cell contains eight identical Pd-H complexes, one of which is shown in **Figure 2.3**. A trace of chloride, 8.5%, was found to be disordered with the hydride in the solid state structure. As this compound was crystallized from layering pentane on a methylene chloride solution of **10**, it is possible this chloride originated from the solvent. This hypothesis

is further supported as complete conversion of **10** in methylene chloride to the chloride complex [($^{t\text{Bu}}$PNP)PdCl]OTf (**10-Cl**) was observed over time by ^{1}H and ^{31}P{^{1}H} NMR spectroscopy as well as X-ray crystallography (**Figure 2.4**).

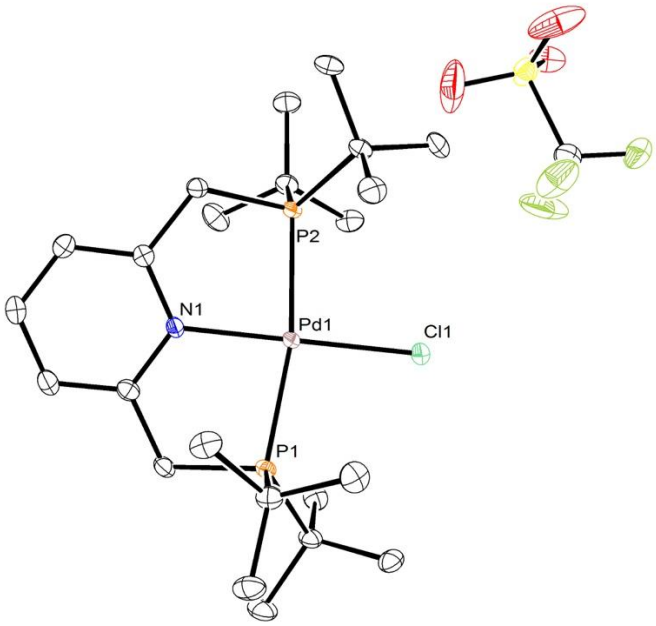

Figure 2.4. Single molecule ORTEP[32] of [($^{t\text{Bu}}$PNP)PdCl]OTf (**10-Cl**) with ellipsoids shown at 50% probability. Hydrogen atoms bound to carbon atoms are omitted for clarity.

Synthesis of an Anionic ($^{t\text{Bu}}$PNP)Pd$^{\text{II}}$ Hydride Complex:** Addition of excess potassium hydride (KH) to a THF-d_8 solution of K[($^{t\text{Bu}}$PNP**)PdCl][27] results in the clean conversion to a new hydride species over 24 hrs (**Scheme 2.1**). The new hydride complex was characterized by a triplet signal at -10.2 ppm ($^{2}J_{\text{PH}}$ = 4.8 Hz) in the ^{1}H NMR spectrum. While this species has a very similar ^{1}H NMR spectroscopic pattern to the cationic species **10**, the ligand backbone signals are shifted upfield by ca. 1-2 ppm for the methylene, *meta* and *para* protons. In addition, the peak assigned to the pincer "arms" displays a smaller coupling constant to phosphorus ($^{2}J_{\text{PH}}$ = 2.0 Hz) when compared to that of the methylene position of **10** ($^{2}J_{\text{PH}}$ = 3.7 Hz). Virtual triplet signals were observed for the C_{2v} symmetric ^{t}Bu protons (18 H) and pincer

"arms" (2 H) at 1.22 and 2.65 ppm respectively. The spectral evidence is consistent with assignment of the new species as K[($^{t\text{Bu}}$PNP**)PdH] (**10****), a rare example of a group 10 anionic hydride complex.[33] The $^{31}P\{^{1}H\}$ NMR spectrum shows a singlet at 72.9 ppm and the $^{13}C\{^{1}H\}$ NMR spectral data are also consistent with a C_{2v} symmetric structure for complex **10****. While it was possible to characterize **10**** by ^{1}H, $^{13}C\{^{1}H\}$ and $^{31}P\{^{1}H\}$ NMR spectroscopy as well as IR spectroscopy, all attempts to isolate the material from solution led to decomposition of the complex. As such, a solid-state structure was not obtained. Similar instability out of solution was previously reported for the related anionic complex K[($^{t\text{Bu}}$PNP**)PdCl].[27]

Synthesis of $^{t\text{Bu}}$PNN complexes of Pd^{II}: The $^{t\text{Bu}}$PNN ligand ($^{t\text{Bu}}$PNN = 2-[bis(di-^{t}butylphosphinomethyl)]-6-(N,N-diethylaminomethyl)pyridine) has been shown to exhibit hemilabile characteristics by the weakly bound diethylamine arm *trans* to phosphorous.[34, 35] It was proposed that a hemilabile arm could allow for olefin coordination and inner-sphere O-atom transfer (OAT) from a hydroperoxide complex. Furthermore, a direct comparison in reactivity could be made with the strongly coordinating $^{t\text{Bu}}$PNP complexes. Therefore, the $^{t\text{Bu}}$PNN ligand was prepared according to a previous literature method in high yield.[36] Platinum complexes of $^{t\text{Bu}}$PNN, including [($^{t\text{Bu}}$PNN)PtCl]Cl **(11)**, ($^{t\text{Bu}}$P*NN)PtCl **(11*)**, ($^{t\text{Bu}}$P*NN)PtH **(12*)**, and [($^{t\text{Bu}}$PNN)PtH]OTf **(12)** have been prepared previously, and will be discussed below.[34] The novel palladium analogues were synthesized in a similar manner (**Scheme 2.2**). It was found that $Pd(PhCN)_2Cl_2$ could be combined with the $^{t\text{Bu}}$PNN ligand in methylene chloride to give the cationic [($^{t\text{Bu}}$PNN)PdCl]Cl **(13)** in good yield (83% isolated). Complex **13** was characterized by ^{1}H, ^{13}C and $^{31}P\{^{1}H\}$ NMR spectroscopy and X-ray crystallography (**Figure 2.5**). Suitable X-ray crystals of **13** were grown from a saturated benzene solution at

room temperature to give orange prisms. The square planar structure crystallizes with a benzene molecule as well as a chloride ion in the outer sphere. The phosphorous and nitrogen of the coordinating arms appear slightly above and below the plane of the pyridine backbone. The Pd-Cl bond (2.2965(5) Å) is only slightly longer than its $^{t\text{Bu}}$PNP analog (2.2927(4) Å), showing a comparable *trans* influence by the pyridine moiety in the backbone.

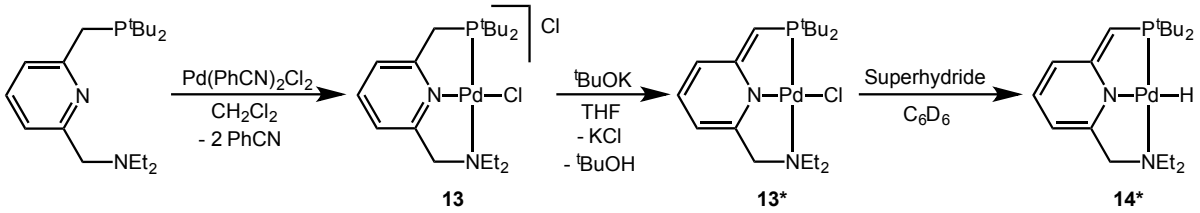

Scheme 2.2. Synthesis of $^{t\text{Bu}}$PNN complexes of Pd^{II}.

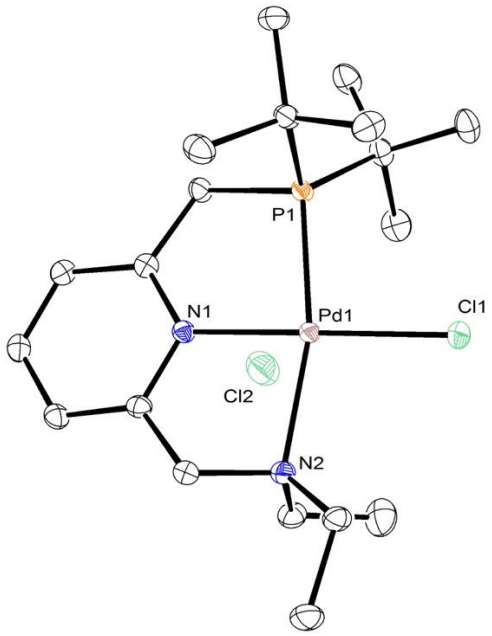

Figure 2.5. Single molecule ORTEP[32] of [($^{t\text{Bu}}$PNN)PdCl]Cl **(13)** with ellipsoids shown at 50% probability. Hydrogen atoms bound to carbon atoms are omitted for clarity.

Complex **13** was selectively deprotonated to ($^{t\text{Bu}}$P*NN)PdCl **(13*)** by addition of one eq. of ^{t}BuOK to a THF suspension of **13** in near quantitative yield (95% isolated), and characterized by ^{1}H, ^{13}C and ^{31}P{^{1}H} NMR spectroscopy. The ^{1}H NMR suggests that the

deprotonation occurs on the phosphorous bearing arm, as the doublet in the methylene region (3.0 ppm) integrates 1:2 to the singlet methylene signal (2.9 ppm) of the nitrogen arm. While the phosphorous signal does not shift significantly upon deprotonation, the proton signals of the ligand backbone shift upfield (5.2-6.5 ppm) as a result of dearomatization.

Complex **13*** exhibited different reactivity than its platinum analog **11***. While **11*** reacts cleanly with ^{n}BuLi in a β-hydride elimination reaction to form **12***, all reactions with **13*** and ^{n}BuLi resulted in multiple unidentified products and decomposition. Superhydride was the only hydride agent that was found to successfully convert **13*** to the neutral hydride ($^{t\text{Bu}}$P*NN)PdH **(14*)** which was characterized by ^{1}H and ^{31}P{^{1}H} NMR spectroscopy. Unfortunately, the borane byproduct could not be removed, and **14*** was never cleanly isolated.

The $^{t\text{Bu}}$PNN ligand was selected for this project because it had been proposed to display hemilabile properties in key intermediate reactions.[34,37] Using alkyllithium agents, it was shown that the amine arm could be displaced in **11*** to form the anionic alkyl species (**Scheme 2.3**).[34] Displacement of the amine arm by olefins could assist in OAT from a metal-hydroperoxo species. To investigate the lability of the amine arm, C_6D_6 solutions of the neutral **12*** and cationic **12** in medium walled J-Young NMR tubes were charged with 10-20 eq. of ethylene or propylene, separately. In all cases, only the free olefin and starting material were observed by ^{1}H NMR spectroscopy; no new complexes were formed.

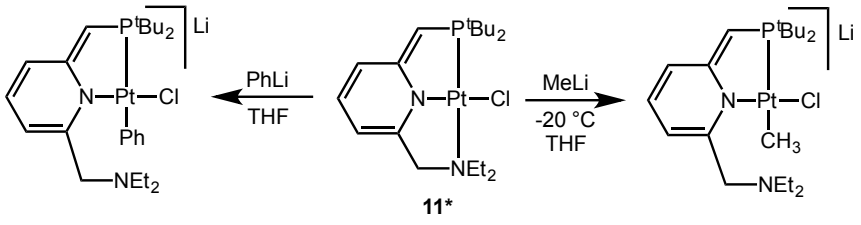

Scheme 2.3. Displacement of the hemilabile diethylamine arm of $^{t\text{Bu}}$PNN by alkyl lithium reagents.[34]

Synthesis of a Neutral ($^{t\text{Bu}}$PNP*)Pt^{II} Hydride Complex: The reaction of ($^{t\text{Bu}}$PNP*)PtCl with LAH in THF-d_8 yields a Pt-H complex, characterized by the triplet ($^2J_{PH}$ = 12.9 Hz) at -12.3 ppm with Pt-satellites ($^1J_{PtH}$ = 1068 Hz) in the ^{1}H NMR spectrum. The ^{1}H NMR signals for the pincer ligand in the new Pt-H species appear very similar to those observed for the neutral Pd^{II} hydride **10***, including separate signals for ^{t}Bu protons (1.06 and 1.39 ppm) and pincer "arms" (2.84 and 3.84 ppm). The ^{31}P{^{1}H} NMR spectrum shows an ABX splitting pattern, consistent with two inequivalent phosphorus nuclei (70.65 and 74.48 ppm) that are coupled to each other ($^2J_{P1P2}$ = 327 Hz), each with Pt satellites ($^1J_{PtP1}$ = 2794 Hz, $^1J_{PtP2}$ = 2640 Hz) (**Figure 2.6**). The signals in the ^{13}C{^{1}H} NMR spectrum also indicate that the two sides of pincer ligand are not equivalent. Two signals are observed for the ^{t}Bu tertiary carbons (28.89, 29.84 ppm) and primary carbons (36.49, 37.03 ppm). The pincer "arm" linker carbons give rise to two signals separated by almost 30 ppm consistent with assignment as a methylene and a methyne carbon (34.09 and 62.03 ppm, respectively). The pyridine carbons appear as

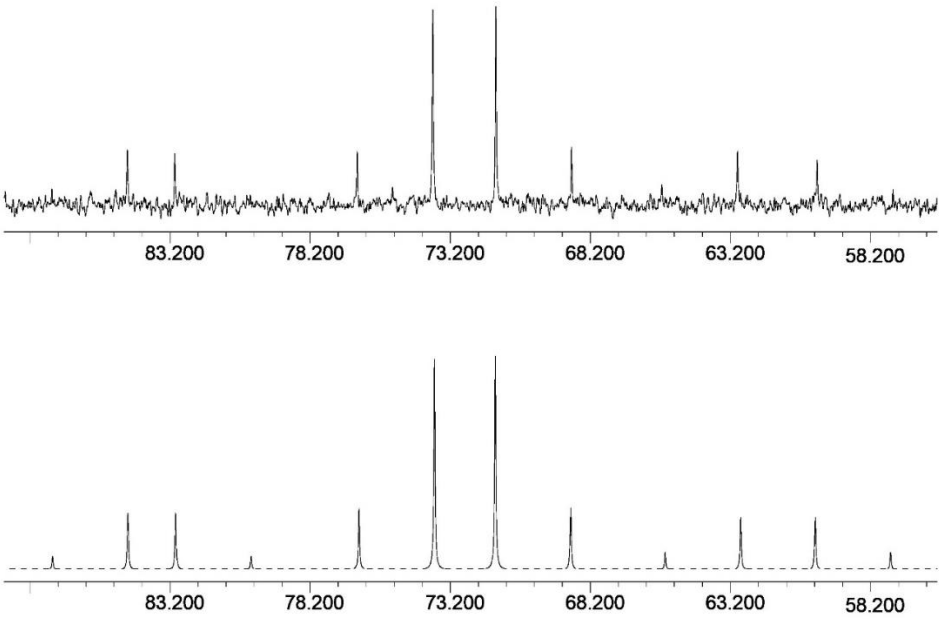

Figure 2.6. Experimental ^{31}P{^{1}H} NMR of **15*** (top) and simulation by gNMR (bottom).

five individual signals in a broad range (97.35-172.42 ppm). All of the spectroscopic data are consistent with assignment of the product of the reaction as ($^{t\text{Bu}}$PNP*)PtH (**15***), the Pt analogue of the neutral ($^{t\text{Bu}}$PNP*)Pd-H complex **10*** (**Scheme 2.4**).

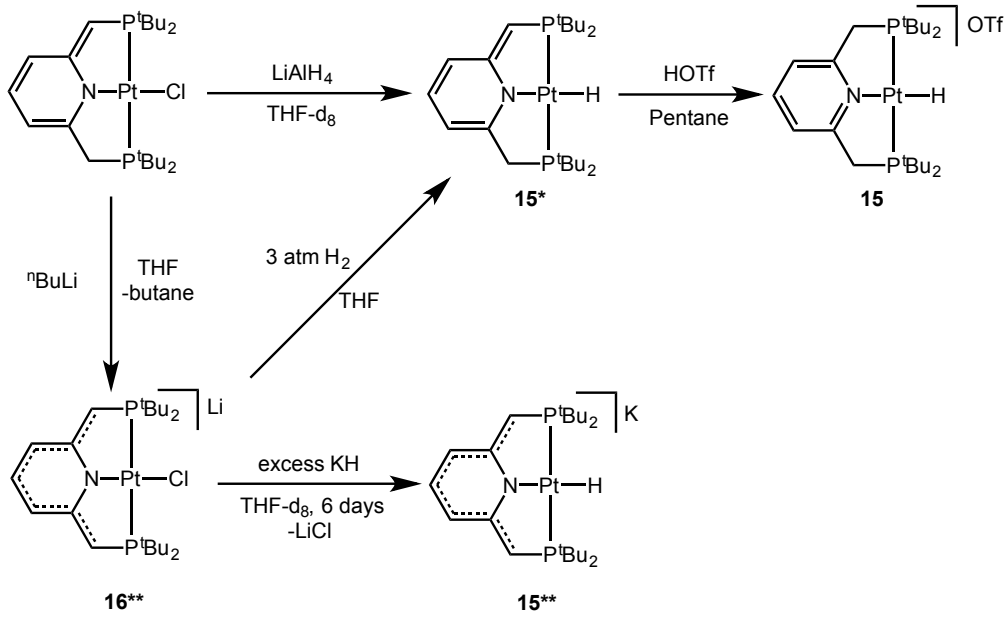

Scheme 2.4. Synthesis of the cationic, neutral and anionic Pt^{II} hydrides **15**, **15*** and **15****.

As the reaction of ($^{t\text{Bu}}$PNP*)PtCl and LAH proceeds, a transient species is observed in the $^{31}P\{^{1}H\}$ NMR spectrum as a singlet at 47.2 ppm with platinum satellites ($^{1}J_{PtP}$ = 2578 Hz). The coupling constant and shift of this singlet is remarkably close to the reported value of the anionic chloride, K[($^{t\text{Bu}}$PNP**)PtCl] (46.53 ppm, $^{1}J_{PtP}$ = 2577 Hz).[27] From this observation, it is proposed that ($^{t\text{Bu}}$PNP*)PtCl first undergoes deprotonation by LAH, forming the anionic Li[($^{t\text{Bu}}$PNP**)PtCl] and H_2, which react leading to **15***. This is supported by the appearance of H_2 in the ^{1}H NMR spectrum (4.53 ppm). The lithium analog, Li[($^{t\text{Bu}}$PNP**)PtCl] (**16****), was independently prepared by the addition of ^{n}BuLi to ($^{t\text{Bu}}$PNP*)PtCl in THF. This complex displays a matching ^{31}P NMR signal (47.3 ppm, $^{1}J_{PtP}$ = 2574 Hz) to the transient species

mentioned above. Furthermore, addition of H_2 to a THF solution of **16**** leads to the production of **15*** (**Scheme 2.4**).

A single crystal was grown from a reaction mixture of ($^{t\text{Bu}}$PNP*)PtCl with ^{n}BuLi. Hydride formation was originally attempted through β-hydride elimination from the ^{n}Bu-complex ($^{t\text{Bu}}$PNP*)Pt-C_4H_9 as reported for a similar ($^{t\text{Bu}}$PNN)Pt^{II} complex.[34] While hydride formation did occur, coupling of two ($^{t\text{Bu}}$PNP*)Pt units at the *meta* position of the pyridine backbone also occurred, resulting in the linked dinuclear species [(*m*-$^{t\text{Bu}}$PNP*)PtH]$_2$ (**15*-Pt**) (**Figure 2.7**). It is unclear how this coupling proceeds, although deprotonation of the backbone by ^{n}BuLi is a viable route.

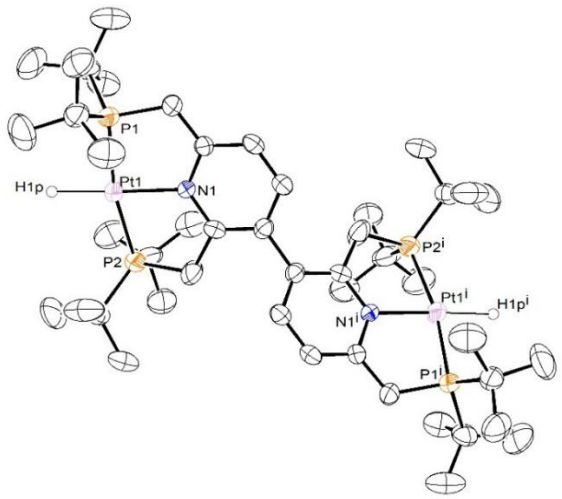

Figure 2.7. Single molecule ORTEP[32] of [(*m*-$^{t\text{Bu}}$PNP*)PtH]$_2$ (**15*-Pt**) with ellipsoids shown at 50% probability. Hydrogen atoms bound to carbon atoms are omitted for clarity.

Synthesis of a Cationic ($^{t\text{Bu}}$PNP)Pt^{II} Hydride Complex: Similar to the chemistry of the Pd analogs, addition of HOTf to a pentane solution of neutral Pt-H **15*** at -30 °C resulted in the formation of a new hydride species. A hydride signal was observed in the ^{1}H NMR spectrum as a triplet at -13.8 ppm ($^2J_{PH}$ = 12.0 Hz) with platinum satellites ($^1J_{PtH}$ = 1179 Hz). The ^{1}H NMR signals attributed to the ligand were also consistent with a C_{2v} symmetric complex.

Virtual triplets were observed for the ^{t}Bu protons and linker methylene groups in the backbone (1.37 and 4.18 ppm, respectively). The $^{31}P\{^1H\}$ NMR spectrum shows a singlet at 75.82 ppm with platinum satellites ($^1J_{PtP}$ = 2677 Hz). The $^{13}C\{^1H\}$ NMR spectrum further supports a symmetric species, as the aryl carbons give rise to three separate signals (123-165 ppm), and virtual triplets are observed for the ^{t}Bu primary, tertiary, and "arm" carbons (28.97, 37.61, 35.75 ppm, respectively). All data are consistent with protonation of the ligand backbone to form the C_{2v} symmetric cationic hydride complex [($^{t\text{Bu}}$PNP)PtH]OTf (**15**) (**Scheme 2.4**).

The solid-state structure of **15** shows a square planar Pt^{II} center with a triflate counterion in the outer sphere. Select bond lengths and angles are reported in **Table 2.1**. Similar to the fully saturated Pd^{II} analog **10**, the C1-C2 (1.503(9) Å) and C6-C7 (1.507(9) Å) bond lengths are identical. There are three Pt^{II} centers in the asymmetric unit, one of which is shown in **Figure 2.8**. The Pt^{II}-H bond distance was restrained at each metal center. Also similar to the cationic Pd^{II} hydride **10**, an 11% chloride impurity was found to be disordered with the hydride. As care was taken to recrystallize **15** under the exclusion of chlorinated solvents, this result was surprising and the origin of this chloride contamination is unclear. This most likely originates from eliminated LiCl from the starting anionic Pt-Cl starting material **16****.

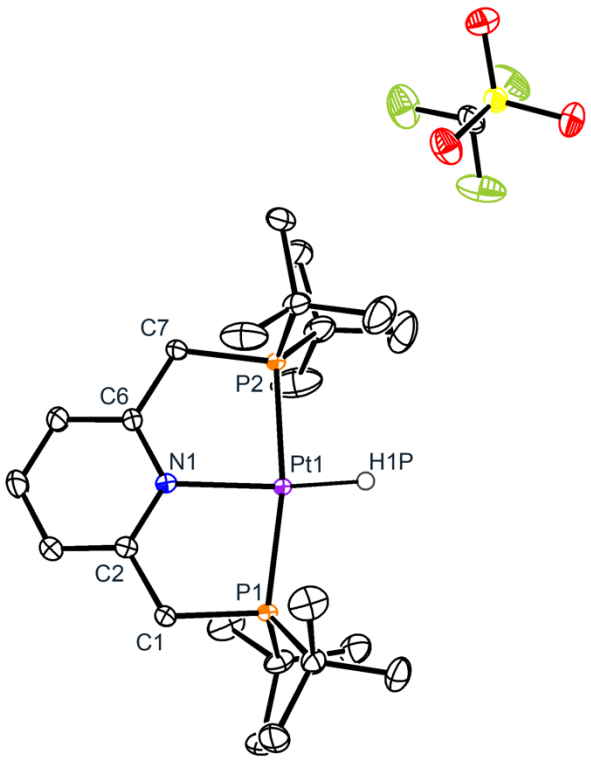

Figure 2.8. Single molecule ORTEP[32] of [($^{t\text{Bu}}$PNP)PtH]OTf **(15)** with ellipsoids shown at 50% probability. Hydrogen atoms bound to carbon atoms are omitted for clarity.

Synthesis of an Anionic ($^{t\text{Bu}}$PNP)Pt$^{\text{II}}$ Hydride Complex:** The anionic hydride K[($^{t\text{Bu}}$PNP**)PtH] **(15**)** can be prepared similarly to its Pd$^{\text{II}}$ analog complex **10****. Addition of excess KH to a THF solution of K[($^{t\text{Bu}}$PNP**)PtCl] generates the hydride **15****, confirmed by ^{1}H, ^{13}C{^{1}H} and ^{31}P{^{1}H} NMR spectroscopy (**Scheme 2.4**). The ^{31}P{^{1}H} NMR spectrum displays a singlet (68.7 ppm) with Pt satellites ($^{1}J_{\text{PtP}}$ = 2648 Hz), indicating equivalent phosphorus nuclei. The C_{2v} symmetry of the molecule was confirmed by the virtual triplet (1.25 ppm, $^{3}J_{\text{PH}}$ = 6.5 Hz) corresponding to the ^{t}Bu substituents and triplet (-11.6 ppm, $^{2}J_{\text{PH}}$ = 13.0 Hz, $^{1}J_{\text{PtH}}$ = 1038 Hz) for the hydride ligand in the ^{1}H NMR spectrum. Similar to the palladium analog **10**** described above, the anionic platinum species **15**** could not be isolated and all attempts to do so led to decomposition.

Dependence of M-H Bond Strength on Electronics of the Pincer Ligand: The relative *trans* influence exerted by the pincer ligand on the hydride ligand was examined through solution IR spectroscopy. All IR spectra of hydrides were recorded in THF (**Figure 2.9**, **Table 2.2**). As the ligand is deprotonated in both the Pt and the Pd series, the M-H stretching frequency was found to decrease. Thus the cationic complexes **10** (1977 cm^{-1}) and **15** (2163 cm^{-1}) have the highest M-H stretching frequencies and the anionic hydrides **10**** (1889 cm^{-1}) and **15**** (2082 cm^{-1}) have the lowest in each series. It is also notable that, consistent with expected M-H bond strengths, the stretching frequencies of the M-H bonds in all of the Pt^{II}-H complexes are higher in energy than those of the analogous Pd^{II}-H complexes. This trend shows that, as the ligand is deprotonated, there is greater electron donation to the metal center, which weakens the metal-hydride bond.

This trend is also supported by the coupling constants between Pt^{II} and the hydride ligand in the ^1H NMR spectra (**Table 2.2**). The $^1J_{PtH}$ coupling constant is 1179 Hz in the cationic **15**, 1068 Hz in neutral **15*** and 1038 Hz in anionic **15****. This trend is in agreement with the $^1J_{PtC}$ reported by Milstein *et al* for the series of cationic (623.5 Hz), neutral (615 Hz) and anionic (611.2 Hz) $^{t\text{Bu}}$PNP Pt^{II} methyl complexes.[27] The ability to tune the M-H bond strength through ligand protonation and deprotonation could prove valuable in reactions involving M-H bond cleavage. In particular, the information could be useful in oxygen insertion reactions where a homolytic M-H bond cleavage has been invoked.

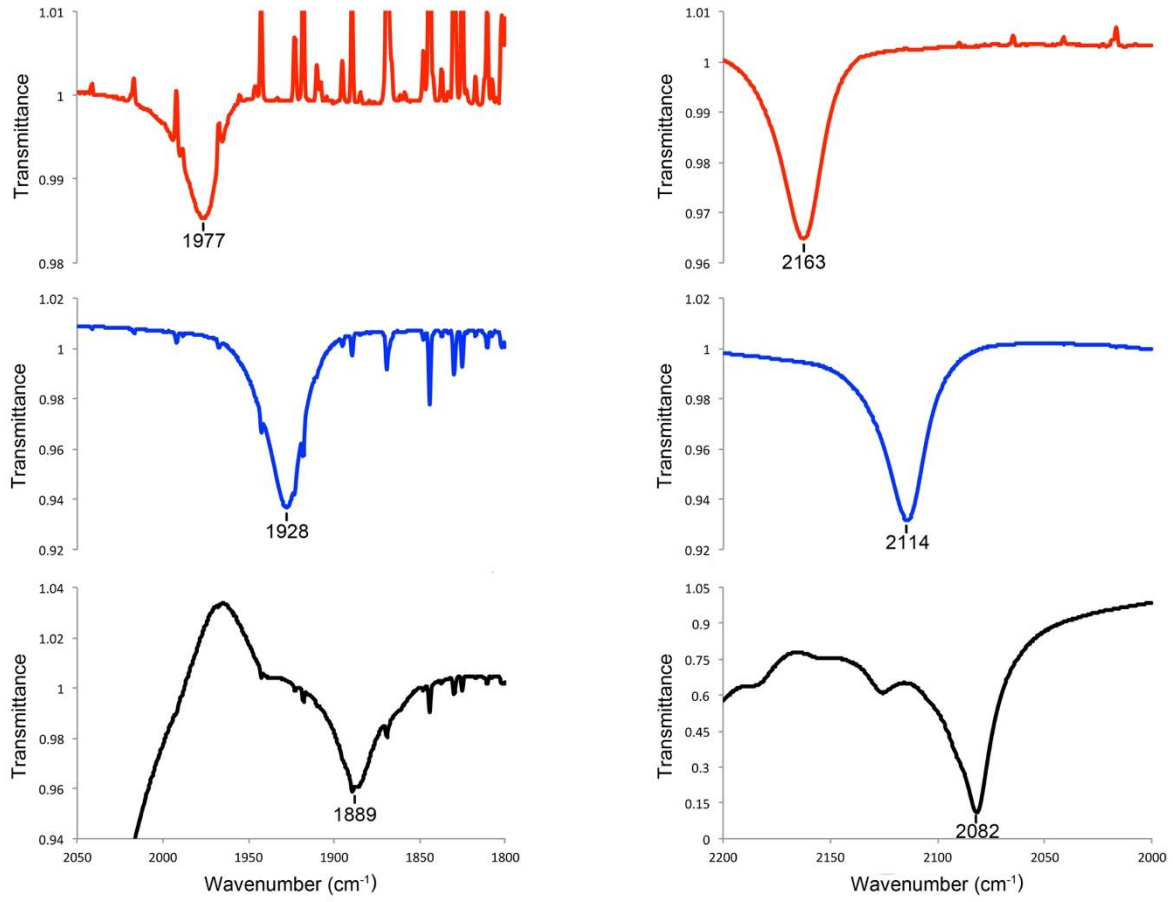

(a.) (b.)

Figure 2.9. Solution cell (THF) IR spectra displaying the M-H stretch for (a.) complexes **10** (top), **10*** (middle), and **10**** (bottom) and for (b.) complexes **15** (top), **15*** (middle), and **15**** (bottom).

Table 2.2. M-H stretching frequencies and coupling constants of the Pd/Pt hydrides.

Metal	Overall Charge	Complex	Stretching Frequency (cm^{-1})	$^{1}J_{PtH}$ (Hz)
Pd	+1	**10**	1977	-
Pd	0	**10***	1928	-
Pd	-1	**10****	1889	-
Pt	+1	**15**	2163	1179
Pt	0	**15***	2114	1068
Pt	-1	**15****	2082	1038

Metal hydride reactions with O_2: The reactivity of the metal hydrides towards O_2 was investigated. Exposure of degassed C_6D_6 solutions of the neutral Pd^{II}-H **10*** or Pt-H **15*** to 5 atm of O_2 resulted in an immediate color change from orange to yellow. Accompanying the

color change, a dark precipitate formed. Within 30 mins of O_2 addition, no starting material was observed in solution by NMR spectroscopy. The precipitate was found to be soluble in THF-d_8, and a ^{1}H NMR spectrum showed multiple intractable products suggesting decomposition of the hydride species. Similar decomposition was observed with the anionic species **10**** and **15****. These reactions were repeated with varying O_2 pressure from 1-5 atm with similar results. Low temperature NMR spectroscopy was attempted to observe possible intermediates, but none were seen. It is plausible that the decomposition of these complexes occurs from reactivity at the ligand backbone instead of the metal. Similar decomposition was observed when a C_6D_6 solution of neutral ($^{t\text{Bu}}$PNP*)PdCl was pressurized with O_2. Recently, one decomposition product was isolated by a member of the Goldberg group.[38] Indeed, reaction with O_2 at the deprotonated pincer arm was occurring, yielding ($^{t\text{Bu}}$PNO)PdCl and the corresponding oxidized phosphine (**Scheme 2.5**).

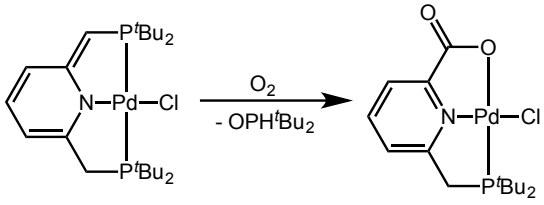

Scheme 2.5. Oxidative decomposition of ($^{t\text{Bu}}$PNP*)PdCl by O_2.

In contrast to the neutral and anionic hydrides, the cationic hydrides **10** and **15** were found to be relatively stable under a pressure of O_2. Exposure of a CD_2Cl_2 solution of **10** to 2 atm of O_2 resulted in no reaction with O_2 over three weeks at room temperature. Monitoring this reaction further saw overall conversion to the chloride [($^{t\text{Bu}}$PNP)PdCl]OTf **(10-Cl)**. Both **10** and **15** were found to be sparingly soluble in C_6D_6 at room temperature, and showed no reaction under 1 atm of O_2. At elevated temperatures, complex **10** showed no reaction with O_2

up to 60 °C, but over time decomposed at this temperature to intractable products. The platinum hydride **15** was stable and showed no reaction up to 80 °C for multiple days.

Previous studies of metal hydrides reacting with O_2 to form metal-hydroperoxide species propose two reaction mechanisms: a HX reductive elimination pathway (HXRE)[39] and a H-atom abstraction pathway (HAA).[40] Stahl and coworkers have shown through Hammett studies that more strongly electron withdrawing ligands *trans* to a metal hydride favor an HXRE pathway, whereas electron donating ligands favor a HAA.[39] This supports studies performed in this group that have shown favorable oxygen insertion into metal hydrides featuring strongly σ-donating pincer frameworks.[41-43] It is proposed that the relative stability of the cationic **10** and **15** results from the pincer ligand's resistance to a reductive elimination pathway. As such, the reactivity should be sensitive to the strength of the M-H bond. However, the relatively weak *trans* influence exhibited on the hydride ligand as shown by IR spectroscopy inhibits H-atom abstraction by O_2.

2.3 Summary

The synthesis and characterization of a series of $^{t\text{Bu}}$PNP and $^{t\text{Bu}}$PNN Pd^{II} and Pt^{II} hydrides have been discussed. The overall charge of the hydride complexes was varied systematically through deprotonation/protonation of the $^{t\text{Bu}}$PNP or $^{t\text{Bu}}$PNN backbone. The metal hydrides were synthesized using a variety of methods including reaction with common hydride reagents such as LAH and borohydride salts as well as through activation of H_2. The relative M-H bond strengths of the platinum and palladium hydrides were examined using IR spectroscopy. A direct relationship between the overall complex charge and M-H stretching frequency was observed for both the $^{t\text{Bu}}$PNP Pd and Pt analogs. The cationic complexes in each

series displayed the largest M-H stretching frequencies while the anionic complexes displayed the smallest M-H stretching frequencies. This trend could prove useful in the selective activation of a *trans* ligand (X) by reversible protonation/deprotonation of the $^{t\text{Bu}}$PNP ligand in ($^{t\text{Bu}}$PNP)MX compounds. The oxygen reactivity of the metal hydride complexes was examined, showing a stark difference in reactivity of the cationic metal hydrides and the neutral/anionic metal hydrides. The cationic species were found to be inert under pressures of O_2, as the M^{II}-H bond is not significantly activated by the weak *trans* donor. The neutral and anionic species, however, react with O_2 at the deprotonated sites in the ligand backbone. This type of reactivity is undesirable, and shows the importance of an inert supporting framework for the metal center.

2.4 Experimental

General Procedures: Unless otherwise noted, all experiments were carried out under an atmosphere of purified nitrogen in a drybox or by using standard Schlenk techniques. Non-deuterated solvents were dried by passage through columns of activated alumina and molecular sieves. Deuterated solvents were purchased from Cambridge Isotope Laboratories and dried over calcium hydride (CD_2Cl_2) or over sodium metal/benzophenone (THF-d_8, toluene-d_8 and C_6D_6). All other reagents were used as received from commercial suppliers. ^{1}H NMR and $^{13}C\{^1H\}$ NMR spectra are referenced to residual solvent signals and shifts are reported in parts per million (ppm) downfield of tetramethylsilane. ^{31}P NMR spectra are referenced to an external 85% H_3PO_4 sample set to 0 ppm. All spectra were taken at 25 °C unless otherwise noted. NMR spectra were carried out using Bruker AV300, AV500 and DRX499 spectrometers. Reactions of metal hydrides with O_2 were performed in medium walled J. Young NMR tubes in deuterated solvents. Samples were degassed (freeze, pump, thaw 3x)

before being exposed to O_2. The tubes were pressurized with 2-5 atm of O_2 on a high-pressure gas manifold equipped with a J. Young connection valve.[44] Precautions were taken for the handling of pressurized samples: samples were kept and transported in a protective sleeve. The complexes ($^{t\text{Bu}}$PNP*)PdCl, K[($^{t\text{Bu}}$PNP**)PdCl], ($^{t\text{Bu}}$PNP*)PtCl, and K[($^{t\text{Bu}}$PNP**)PtCl] were prepared according to literature procedures.[27]

X-ray Crystallography Methodology: Inclusion free single crystals were mounted on a loop with oil. Data was collected at -173°C on a Bruker APEX II single crystal X-ray diffractometer, Mo-radiation. Crystal-to-detector distance was 40 mm and exposure times were between 10 to 60 seconds per frame, depending on crystal size (see **Table 2.3**). The scan width was 0.5°. The data was integrated and scaled using SAINT, SADABS within the APEX2 software package by Bruker.[45] Solution by direct methods (SHELXS, SIR97[46]) produced complete heavy atom phasing models consistent with the proposed structures. The structures were completed by difference Fourier synthesis with SHELXL97.[47,48] Scattering factors are from Waasmair and Kirfel[49]. Hydrogen atoms were placed in geometrically idealized positions and constrained to ride on their parent atoms with C---H distances in the range 0.95-1.00 Angstrom. Isotropic thermal parameters U_{eq} were fixed such that they were $1.2U_{eq}$ of their parent atom Ueq for CH's and $1.5U_{eq}$ of their parent atom U_{eq} in case of methyl groups. All non-hydrogen atoms were refined anisotropically by full-matrix least-squares.

Table 2.3. Crystallographic data for complexes **10***, **10**, **13**, **10-Cl**, **15** and **15*-Pt**.

Complex	**(10*)**	**(10)**	**(13)**	**(10-Cl)**	**(15)**	**(15*-Pt)**
Empirical formula	$C_{23}H_{43}NP_2Pd$	$C_{24}H_{43.92}Cl_{0.09}F_3NO_3P_2PdS$	$C_{25}H_{41}Cl_2N_2PPd$	$C_{24}H_{43}ClF_3NO_3P_2PdS$	$C_{72}H_{131.71}Cl_{0.33}F_9N_3O_9P_6Pt_3S_3$	$C_{376}H_{684}N_{20}P_{32}Pt_{16}$
Formula weight	501.92	654.93	577.87	686.44	2233.48	9597.91
Temperature	100(2) K	100(2) K	100(2) K	100(2) K	100(2) K	100(2) K
Wavelength	0.71073 Å	0.71073 Å	0.71073 Å	0.71073 Å	0.71073 Å	0.71073 Å
Crystal system	Monoclinic	Triclinic	Monoclinic	Monoclinic	Triclinic	Tetragonal
Space group	P 2_1/c	P -1	P 2_1/c	P 2_1/c	P -1	I 41/a
Unit cell axes(Å)	a = 9.3997(13) b = 11.3514(15) c = 23.623(3)	a = 15.0598(15) b = 15.4771(14) c = 25.655(3)	a = 16.2577(15) b = 10.4928(10) c = 15.7558(14)	a = 12.0998(12) b = 9.8492(10) c = 24.725(3)	a = 15.062(2) b = 15.441(2) c = 19.890(3)	a = 23.320(3) b = 23.320(3) c = 19.575(4)
Unit cell angles (°)	α = 90 β = 90.021(9) γ = 90	α = 83.144(4) β = 81.714(5) γ = 83.180(4)	α = 90 β = 99.435(5) γ = 90	α = 90 β = 90.643(5) γ = 90	α = 106.715(7) β = 92.145(7) γ = 96.467(7)	α = 90 β = 90 γ = 90
Volume ($Å^3$)	2520.6(6)	5843.6(10)	2651.4(4)	2946.3(5)	4390.5(12)	10645(3)
Z	4	8	4	4	2	1
Density (Mg/m^3), calculated	1.323	1.489	1.448	1.548	1.689	1.497
Absorption coeff. (mm^{-1})	0.871	0.869	0.977	0.946	5.029	5.402
F(000)	1056	2715	1200	1416	2231	4808
Crystal size (mm^3)	0.20 x 0.10 x 0.08	0.17 x 0.14 x 0.13	0.18 x 0.13 x 0.10	0.20 x 0.07 x 0.04	0.20 x 0.15 x 0.08	0.10 x 0.05 x 0.04
Theta range for data collection	1.79 to 25.41°	1.61 to 28.57°	2.32 to 28.36°	1.65 to 28.44°	1.82 to 28.42°	2.21 to 25.44°
Reflections collected	26610	272155	105521	121179	202207	122941
Independent reflections, R(int)	4530, 0.1434	29404, 0.0414	6617, 0.0721	7391, 0.0536	21855, 0.0376	4860, 0.1750
Completeness to theta (%)	97.7 to 25.00°	99.9 to 25.00°	100.0 to 25.00°	100.0 to 25.00°	98.9 to 28.42°	98.9 to 25.00°
Max. and min. transmission	0.9336 and 0.8450	0.8955 and 0.8664	0.9086 and 0.8437	0.9632 and 0.8334	0.6891 and 0.4328	0.8129 and 0.6141
Data / restraints / parameters	4530 / 139 / 260	29404 / 487 / 1452	6617 / 0 / 276	7391 / 0 / 337	21855 / 176 / 1116	4860 / 45 / 294
Goodness-of-fit on F^2	0.990	1.069	1.048	1.057	0.956	1.061
Final R indices [I>2sigma(I)]	R1 = 0.0834, wR2 = 0.1639	R1 = 0.0339, wR2 = 0.0760	R1 = 0.0288, wR2 = 0.0598	R1 = 0.0265, wR2 = 0.0570	R1 = 0.0360, wR2 = 0.0801	R1 = 0.0428, wR2 = 0.0771
R indices (all data)	R1 = 0.1355, wR2 = 0.1824	R1 = 0.0439, wR2 = 0.0818	R1 = 0.0412, wR2 = 0.0645	R1 = 0.0368, wR2 = 0.0615	R1 = 0.0421, wR2 = 0.0825	R1 = 0.0971, wR2 = 0.0979
Largest diff. peak and hole ($e.Å^{-3}$)	2.712 and -1.421	3.226 and -1.160	0.843 and -0.455	0.617 and -0.722	4.462 and -2.199	1.368 and -0.637

($^{t\text{Bu}}$PNP*)PdH (10*): To a THF solution (3 mL) of ($^{t\text{Bu}}$PNP*)PdCl (53 mg, 0.099 mmol) in a heavy walled vessel equipped with a resealable Teflon pin was added a THF solution (1 mL) of $KN(SiMe_3)_2$ (20 mg, 0.10 mmol). The solution was stirred for 45 mins after which a small aliquot was taken to confirm completed deprotonation of the PNP ligand by the disappearance of the peak centered at 59.6 ppm and appearance of the singlet at 55.9 ppm in the $^{31}P\{^1H\}$ NMR spectra. The vessel was degassed (freeze, pump, thaw 3x), placed under 3 atm of H_2 on a high-pressure gas manifold and stirred for 3 days. The dark red solution became orange. The solvent was removed under vacuum to give an orange solid, which was extracted into pentane and filtered through Celite®. Solvent removal under vacuum yielded an orange solid, 49 mg (0.098 mmol, 99 % Yield). Crystals suitable for X-ray crystallography were grown by slow evaporation of a pentane solution of **10***. Compound **10*** can also be synthesized using LAH as the hydride agent from the neutral ($^{t\text{Bu}}$PNP*)PdCl.

$^{31}P\{^1H\}$ NMR (202 MHz, toluene-d_8): δ AB system 74.37 (d, J_{PP} = 320 Hz), 76.25 (d, J_{PP} = 320 Hz). ^1H NMR (500 MHz, toluene-d_8): δ -10.49 (bs, 1H, Pd-*H*), 1.04 (dd, 18H, J_{PH} = 12.4 Hz, J_{PH} = 1.2 Hz, $P(C(CH_3)_3)_2$), 1.36 (dd, 18H, J_{PH} = 12.4 Hz, J_{PH} = 1.2 Hz, $P(C(CH_3)_3)_2$), 2.82 (d, 2H, J_{PH} = 8.2 Hz, CH_2P), 3.49 (d, 1H, J_{PH} = 5.6, CHP), 5.49 (d, 1H, J_{HH} = 6.5, pyridine-H), 6.37 (d, 1H, J_{HH} = 8.8 Hz, pyridine-H), 6.53 (m, 1H, pyridine-H). $^{13}C\{^1H\}$ NMR (126 MHz, toluene-d_8): δ 29.01 (d, J_{PC} = 6.2 Hz, $P(C(CH_3)_3)_2$), 29.83 (d, J_{PC} = 5.9 Hz, $P(C(CH_3)_3)_2$), 33.30 (dd, J_{PC} = 11.6, J_{PC} = 3.5 Hz, CH_2P), 35.33 (dd, J_{PC} = 21.2 Hz, J_{PC} = 4.5 Hz, $P(C(CH_3)_3)_2$), 36.58 (d, J_{PC} = 15.0 Hz, $P(C(CH_3)_3)_2$), 61.49 (dd, J_{PC} = 48.6 Hz, J_{PC} = 4.3 Hz, CHP), 97.75 (d, J_{PC} = 9.6 Hz, pyridine-C), 113.06 (d, J_{PC} = 16.4 Hz, pyridine-C), 133.00 (s, pyridine-C), 158.47 (s, pyridine-C), 171.36 (dd, J_{PC} = 17.0 Hz, J_{PC} = 5.4 Hz, pyridine-C). IR (soln, THF): 1928

cm^{-1} (Pd^{II}-H stretch). Anal. for $C_{23}H_{43}NP_2Pd$: calcd: C, 55.03; H, 8.63; N, 2.79; found: C, 55.16; H, 8.64; N, 2.60.

(^{tBu}PNP*)PdH (10*) from K-Selectride: (^{tBu}PNP*)PdCl (10 mg, 0.019 mmol) was weighed into a medium walled NMR tube equipped with a resealable Teflon valve and dissolved in THF (0.4 mL). K-Selectride (1.0 M in THF, 25 μL, 0.025 mmol) was added to the solution which was then shaken and left for 1.5 hrs. The solvent was then removed in vacuo, and the residue was dissolved in C_6D_6. A new hydride species was observed by the broad singlet at -10.4 ppm in the ^{1}H NMR spectrum, as well as a contaminant that could not be removed (broad peaks at 0.90, 1.21 and 1.67 ppm in the ^{1}H NMR spectrum). The contaminant was proposed to be a tri-*sec*-butyl borane species originating from K-Selectride, and attempted removal by dynamic vacuum and washing with nonpolar solvents (pentane, toluene, and benzene) was unsuccessful.

(^{tBu}PNP*)PdH (10*) from LAH: To a solution of (^{tBu}PNP*)PdCl (30 mg, 0.056 mmol) in THF (4 mL) at -30 °C was added an excess of LAH (4.5 mg, 0.12 mmol). The solution was stirred overnight after which the solvent was removed in vacuo. The solid was extracted with pentane (5 x 2 mL), filtered and the solvent was removed in vacuo to give an orange solid, 21 mg (75% yield). This reaction showed limited reproducibility resulting in inconsistent yields and purity.

[(^{tBu}PNP)PdH]OTf (10): To a pentane solution (3 mL) of **10*** (25 mg, 0.050 mmol) at -30 °C was added triflic acid (4.4 μL, 0.050 mmol), which resulted in the formation of a tan precipitate. The solid was collected by filtration, washed with pentane (4 x 1 mL), and dried under vacuum to yield a tan powder, 29 mg (0.044 mmol, 89% yield). Crystals suitable for x-ray crystallography were grown by slow diffusion of pentane into a CH_2Cl_2 solution of **10**.

$^{31}P\{^{1}H\}$ NMR (202 MHz, THF-d_8): δ 76.32 (s). ^{1}H NMR (500 MHz, THF-d_8) δ -11.51 (t, 1H, J_{PH} = 2.5 Hz, Pd-*H*), 1.35 (vt, 36H, J_{PH} = 7.5 Hz, P(C(CH_3)$_3$)$_2$), 4.15 (vt, 4H, J_{PH} = 3.6 Hz, CH_2P), 7.82 (d, 2H, J_{HH} = 7.8 Hz, pyridine-H), 7.91 (t, 1H, J_{HH} = 7.8 Hz, pyridine-H). $^{13}C\{^{1}H\}$ NMR (126 MHz, THF-d_8): δ 29.27 (vt, J_{PC} = 3.5 Hz, P(C(*C*H$_3$)$_3$)$_2$), 35.06 (vt, J_{PC} = 9.0 Hz, *C*H$_2$P), 37.45 (vt, J_{PC} = 8.7 Hz, P(*C*(CH$_3$)$_3$)$_2$), 123.24 (vt, J_{PC} = 4.5 Hz, pyridine-C), 141.01 (s, pyridine-C), 163.63 (vt, J_{PC} = 4.5 Hz, pyridine-C). IR (soln, THF): 1977 cm^{-1} (Pd^{II}-H stretch). Anal. for $C_{24}H_{44}F_3NO_3P_2PdS$: calcd: C, 44.21; H, 6.80; N, 2.15; found: C, 44.50; H, 6.65; N, 2.03.

K[(^{t}BuPNP****)PdH] (10****)**: To a solution of (^{t}BuPNP*)PdCl (6.3 mg, 0.012 mmol) in THF-d_8 (0.5 mL) in a medium walled NMR tube equipped with a resealable Teflon valve was added KN(SiMe$_3$)$_2$ (2.6 mg, 0.013 mmol) at room temperature. The solution instantly became darker, and the absence of the peak centered at 59.6 ppm and appearance of the singlet at 55.9 ppm in the $^{31}P\{^{1}H\}$ NMR spectra showed full conversion to K[(^{t}BuPNP**)PdCl]. To this solution was added an excess of KH (2.5 mg, 0.062 mmol) and the solution was left for 24 hours. The dark red solution was filtered into a new medium walled NMR tube with a resealable Teflon valve for spectral analysis (60% yield by NMR, hexamethylbenzene IS). The anionic complex **10**** was not isolated as it readily reacts with trace oxygen and adventitious water to form multiple intractable products.

$^{31}P\{^{1}H\}$ NMR (121 MHz, THF-d_8): δ 72.87 (s). ^{1}H NMR (300 MHz, THF-d_8): δ -10.15 (t, 1H, J_{PH} = 4.8 Hz, Pd-*H*), 1.22 (vt, 36H, J_{PH} = 6.5 Hz, P(C(CH_3)$_3$)$_2$), 2.65 (vt, 2H, J_{PH} = 2.0 Hz, C*H*P), 4.82 (d, 2H, J_{HH} = 7.7 Hz, pyridine-H), 5.97 (tt, 1H, J_{PH} = 1.7 Hz, J_{HH} = 7.7 Hz, pyridine-H). $^{13}C\{^{1}H\}$ NMR (126 MHz, THF-d_8): δ 30.16 (vt, J_{PC} = 4.2 Hz, P(C(*C*H$_3$)$_3$)$_2$), 35.09 (vt, J_{PC} = 11.2 Hz, *C*HP), 52.90 (vt, J_{PC} = 25.1 Hz, P(*C*(CH$_3$)$_3$)$_2$), 89.68 (vt, J_{PC} = 8.7 Hz, pyridine-C),

133.80 (vt, J_{PC} = 2.7 Hz, pyridine-C), 172.53 (vt, J_{PC} = 11.8 Hz, pyridine-C). IR (soln, THF): 1889 cm^{-1} (Pd^{II}-H stretch).

[(^{tBu}PNP)PdCl]OTf (10-Cl): A CD_2Cl_2 solution of **10** was left for a month at room temperature. Full conversion to the product **10-Cl** was observed by NMR spectroscopy. X-ray suitable crystals were grown by layering pentane on a concentrated CD_2Cl_2 solution of **10-Cl**.

$^{31}P\{1H\}$ NMR (121 MHz, CD_2Cl_2): δ61.9 (s). ^{1}H NMR (300 MHz, CD_2Cl_2): δ1.46 (vt, J_{PH} = 7.7 Hz, 36H, P(C(CH_3)$_3$)$_2$), 3.78 (vt, J_{PH} = 3.6 Hz, 4H, CH_2P), 7.69 (d, J_{HH} = 7.9 Hz, 2H, pyridine- H), 8.00 (t, J_{HH} = 7.9 Hz, 1H, pyridine-H).

[(^{tBu}PNN)PdCl]Cl (13): To a CH_2Cl_2 solution (2 mL) of $Pd(PhCN)_2Cl_2$ (225 mg, 0.588 mmol) was added a methylene chloride solution (3 mL) of ^{t}BuPNN ligand (199 mg, 0.616 mmol) which resulted in an immediate color change from orange to deep red. The reaction mixture was stirred for 2 hours after which the solvent was removed under vacuum to yield a red-orange oil. The residue was washed with pentane, extracted into methylene chloride and the solvent was removed under vacuum to yield a glassy red-orange solid, 243 mg (0.486 mmol, 83% yield). Crystals of **16** were grown from a saturated benzene solution at room temperature.

$^{31}P\{^{1}H\}$ NMR (121 MHz, CD_2Cl_2): δ 87.27 (s). ^{1}H NMR (300 MHz, CD_2Cl_2): δ 1.51 (t, J_{HH} = 7.4 Hz, N(CH_2CH_3)$_2$), 1.52 (d, J_{PH} = 15.7 Hz, P(C(CH_3)$_3$)$_2$) the last two reported signals are overlapped, and their integral corresponds to 24H, 2.85 (m, 2H, N(CHHCH$_3$)), 3.26 (m, 2H, N(CHHCH$_3$)), 4.24 (d, 2H, J_{PH} = 10.5 Hz, CH_2P), 4.59 (s, 2H, CH_2N), 7.79 (d, 1H, J_{HH} = 7.8 Hz, pyridine-H), 8.10 (td, 1H, J_{PH} = 0.8 Hz, J_{HH} = 7.9 Hz, pyridine-H), 8.21 (d, 1H, J_{HH} = 7.8 Hz, pyridine-H). ^{13}C NMR (126 MHz, CD_2Cl_2): δ 13.02 (s, N(CH_2CH_3)$_2$), 28.82 (d, J_{PC} = 2.6 Hz, P(C(CH_3)$_3$)), 37.12 (d, J_{PC} = 25.9 Hz, CH_2P), 37.54 (d, J_{PC} = 18.4 Hz, P(C(CH$_3$)$_3$)), 55.26

(d, J_{PC} = 2.0 Hz, N(CH_2CH_3)$_2$), 64.56 (d, J_{PC} = 3.3 Hz, CH_2N), 121.60 (s, pyridine-C), 124.26 (d, J_{PC} = 11.6 Hz, pyridine-C), 141.69 (s, pyridine-C), 162.60 (d, J_{PC} = 1.6 Hz, pyridine-C), 162.68 (s, pyridine-C).

(^{tBu}PNN*)PdCl (13*): To an orange suspension of **13** (47 mg, 0.095 mmol) in THF (5 mL) was added ^{t}BuOK (11 mg, 0.10 mmol), at which point the solution turned deep red. The solution was stirred for 1 hour, after which the volatiles were removed leaving a red residue. The residue was extracted into benzene (5 x 1 mL) and filtered through a PTFE 0.2 μm syringe filter. The volatiles were removed under vacuum yielding **13*** as a dark red solid, 42 mg (0.090 mmol, 95% yield).

^{31}P{^{1}H} NMR (121 MHz, C_6D_6): δ 86.31 (s). ^{1}H NMR (300 MHz, C_6D_6): δ 1.23 (t, 6H, J_{HH} = 7.1 Hz, N(CH_2CH_3)$_2$), 1.49 (d, 18H, J_{PH} = 14.5 Hz, P(C(CH_3)$_3$)$_2$), 2.08 (m, 2H, N(CHCH$_3$)$_2$), 2.87 (m, 2H, N(CHCH$_3$)$_2$), 2.94 (s, 2H, CH_2N), 3.01 (d, 1H, J_{PH} = 4.5 Hz, CHP), 5.15 (d, 1H, J_{HH} = 6.6 Hz, pyridine-H), 6.20 (d, 1H, J_{HH} = 8.8 Hz, pyridine-H), 6.44 (ddd, 1H, J_{HH} = 8.8 Hz, J_{HH} = 6.2 Hz, J_{PH} = 1.8 Hz, pyridine-H). ^{13}C NMR (126 MHz, C_6D_6): δ 12.31 (s, N(CH_2CH_3)$_2$), 29.11 (d, J_{PC} = 3.7 Hz, P(C(CH_3)$_3$)$_2$), 37.68 (d, J_{PC} = 25.2 Hz, P(C(CH$_3$)$_3$)$_2$), 53.52 (s, N(CH_2CH_3)$_2$), 59.38 (d, J_{PC} = 60.8 Hz, CHP), 62.51 (d, J_{PC} = 2.4 Hz, CH_2N), 96.78 (s, pyridine-C), 112.79 (d, J_{PC} = 19.7 Hz, pyridine-C), 132.96 (s, pyridine-C), 158.22 (s, pyridine-C), 169.68 (d, J_{PC} = 13.8 Hz, pyridine-C).

(^{tBu}PNN*)PdH (14*): To a solution of (^{tBu}P*NN)PdCl (9.5 mg, 0.021 mmol) in C_6D_6 (0.4 mL) in a medium walled NMR tube equipped with a J. Young adapter was added Superhydride (21 μL, 1.0 M in THF). After 20 hours, the volatiles were removed and fresh C_6D_6 was added by vacuum transfer. Analysis by ^{1}H NMR indicated that the product **14*** had formed, but was

contaminated by a borane (broad multiplets at 0.68 and 1.35 ppm in the ^{1}H NMR spectrum. A similar contaminant was observed in the synthesis of **10*** from K-Selectride (*vide supra*).

^{31}P{^{1}H} NMR (121 MHz, C_6D_6): δ 91.7 (s). ^{1}H NMR (300 MHz, C_6D_6): δ -12.14 (d, 1H, J_{PH} = 6.3 Hz, Pd-*H*), 1.21 (t, J_{HH} = 7.1 Hz, N(CH_2CH_3)$_2$), 1.42 (d, J_{PH} = 14.1 Hz, P(C(CH_3)$_3$)$_2$) the last two reported signals are overlapping with the borane hydrogen signals, 2.26 (m, 2H, N($CHHCH_3$)$_2$), 2.38 (m, 2H, N($CHHCH_3$)$_2$), 3.06 (s, 2H, CH_2N), 3.26 (d, 1H, J_{PH} = 4.3 Hz, C*H*P), 5.37 (d, 1H, J_{HH} = 6.6 Hz, pyridine-H), 6.40 (d, 1H, J_{HH} = 8.7 Hz, pyridine-H), 6.64 (ddd, 1H, J_{HH} = 6.6 Hz, J_{HH} = 8.7 Hz, J_{PH} = 1.9 Hz, pyridine-H).

($^{t\text{Bu}}$PNP*)PtH (15*): To a heavy walled glass vessel with a resealable Teflon pin was added ($^{t\text{Bu}}$PNP*)PtCl (58 mg, 0.093 mmol). The solid was dissolved in THF (10 mL) and ^{n}BuLi (1.26 M in hexanes, 77 μL, 0.0970 mmol) was added by syringe, which turned the solution deep red. The solution was stirred for 15 mins and then pressurized with 3 atm of H_2 on a high pressure gas manifold. The vessel was sealed and stirred for 6 days. The now orange solution was then degassed, filtered through Celite® and the solvent was removed in vacuo to give an orange solid. The solid was extracted into pentane (5 mL), filtered through Celite, and the solvent was removed in vacuo to give an orange solid, 45 mg (0.076 mmol, 82% yield).

^{31}P{^{1}H} NMR (202 MHz, toluene-d_8): δ ABX system 70.65 (d, J_{PP} = 327 Hz, J_{PtP} = 2794 Hz), 74.48 (d, J_{PP} = 327 Hz, J_{PtP} = 2640 Hz). ^{1}H NMR (500 MHz, toluene-d_8): δ -12.29 (t, 1H, J_{PH} = 12.9 Hz, J_{PtH} = 1068 Hz, Pt-*H*), 1.06 (d, 18H, J_{PH} = 13.1 Hz, P(C(CH_3)$_3$)$_2$), 1.39 (d, 18H, J_{PH} = 13.1 Hz, P(C(CH_3)$_3$)$_2$), 2.84 (d, 2H, J_{PH} = 8.7, J_{PtH} = 10.6 Hz, CH_2P), 3.84 (dd, 1H, J_{PH} = 5.0 Hz, J_{PH} = 3.4 Hz, J_{PtH} = 28.0 Hz, C*H*P), 5.55 (d, 1H, J_{HH} = 6.4, pyridine-H), 6.45 (d, 1H, J_{HH} = 8.8 Hz, pyridine-H), 6.55 (m, 1H, pyridine-H). ^{13}C{^{1}H} NMR (126 MHz, toluene-d_8): δ 28.89 (d, J_{PC} = 3.4 Hz, J_{PtC} = 22.9 Hz, P(C(CH_3)$_3$)$_2$), 29.84 (d, J_{PC} = 2.8 Hz, J_{PtC} = 24.7 Hz,

P(C(CH_3)$_3$)$_2$), 34.09 (dd, J_{PC} = 19.3, J_{PC} = 2.5 Hz, CH_2P), 36.49 (dd, J_{PC} = 27.9 Hz, J_{PC} = 3.9 Hz, P(C(CH$_3$)$_3$)$_2$), 37.03 (d, J_{PC} = 22.5 Hz, P(C(CH$_3$)$_3$)$_2$), 62.03 (dd, J_{PC} = 59.6 Hz, J_{PC} = 1.9 Hz, CHP), 97.35 (d, J_{PC} = 9.9 Hz, pyridine-C), 112.84 (d, J_{PC} = 16.4 Hz, pyridine-C), 132.37 (s, pyridine-C), 159.51 (s, J_{PtC} = 8.5 Hz, pyridine-C), 172.42 (dd, J_{PC} = 15.1 Hz, J_{PC} = 4.9 Hz, pyridine-C). IR (soln, THF): 2114 cm^{-1} (Pt^{II}-H stretch). Anal. for $C_{23}H_{43}NP_2Pd$: calcd: C, 46.77; H, 7.34; N, 2.37; found: C, 46.81; H, 7.16; N, 2.21.

($^{t\text{Bu}}$PNP*)PtH (15*) from LAH: To a solution of ($^{t\text{Bu}}$PNP*)PtCl (12 mg, 0.019 mmol) in THF-d_8 (0.5 mL) in a J. Young NMR tube was added LAH (2.0 mg, 0.053 mmol). After 12 days at room temperature a new product was observed by ^{31}P{^{1}H} NMR spectroscopy. The solution was filtered and volatiles were removed in vacuo. The residue was extracted with pentane (3 x 0.5 mL) and filtered into a new J. Young NMR tube. Solvent was removed in vacuo and orange solid was disolved in toluene-d_8 for spectral analysis (59% yield by NMR, hexamethylbenzene IS).

[($^{t\text{Bu}}$PNP)PtH]OTf (15): To a pentane solution (3 mL) of **15*** (19 mg, 0.032 mmol) at -30 °C was added triflic acid (2.6 μL, 0.030 mmol), which resulted in the formation of a tan precipitate. The solid was collected by filtration, washed with pentane (3 x 5 mL), and dried in vacuo to yield a tan powder, 16 mg (0.022 mmol, 72% yield). Crystals suitable for x-ray crystallography were grown by slow diffusion of pentane into a concentrated THF solution of **15**.

^{31}P{^{1}H} NMR (202 MHz, THF-d_8): δ 75.82 (s, J_{PtP} = 2677 Hz). ^{1}H NMR (500 MHz, THF-d_8): δ -13.84 (t, J_{PH} = 12.0 Hz, J_{PtH} = 1179 Hz, Pt-H), 1.37 (vt, 36H, J_{PH} = 7.5 Hz, P(C(CH_3)$_3$)$_2$), 4.18 (vt, 4H, J_{PH} = 3.9 Hz, CH_2P) 7.88 (d, 2H, J_{HH} = 7.8 Hz, pyridine-H), 8.01 (t, 1H, J_{HH} = 7.8 Hz, pyridine-H). ^{13}C{^{1}H} NMR (126 MHz, THF-d_8): δ 28.97 (vt, J_{PC} = 2.9 Hz, J_{PtC} = 19.8

Hz, P(C(CH_3)$_3$)$_2$), 35.75 (vt, J_{PC} = 12.8 Hz, CH_2P), 37.61 (vt, J_{PC} = 12.5 Hz, P(C(CH$_3$)$_3$)$_2$), 123.04 (vt, J_{PC} = 4.9 Hz, pyridine-C), 140.24 (s, pyridine-C), 164.74 (vt, J_{PC} = 3.9 Hz, pyridine-C). IR (soln, THF): 2163 cm^{-1} (Pt^{II}-H stretch). Anal. for $C_{24}H_{44}F_3NO_3P_2PtS$: calcd: C, 38.92; H, 5.99; N, 1.89; found: C, 39.60; H, 5.69; N, 1.73.

K[($^{t\text{Bu}}$PNP)PtH] (15**)**: To a solution of ($^{t\text{Bu}}$PNP*)PtCl (7.6 mg, 0.012 mmol) in THF-d_8 (0.5 mL) in a medium walled NMR tube with a resealable Teflon valve was added KN(SiMe$_3$)$_2$ (2.6 mg, 0.013 mmol) at room temperature. The solution instantly became red. The absence of the peak centered at 51.5 ppm in the ^{31}P{^{1}H} NMR and appearance of the singlet at 47.7 ppm showed full conversion to K[($^{t\text{Bu}}$PNP**)PtCl]. To this solution was added an excess of KH (7.7 mg, 0.19 mmol) and was left for 6 days at room temperature. The formation of a hydride species was seen by the triplet at -11.79 ppm in the ^{1}H NMR spectrum with full conversion by a single peak at 70.6 ppm in the ^{31}P{^{1}H} NMR spectrum. The solution was filtered into a new medium walled NMR tube with a resealable Teflon valve for spectral analysis (75% yield by NMR, hexamethylbenzene IS). The anionic complex **15**** was not isolated as it readily reacts with trace oxygen and adventitious water to form multiple products.

^{31}P{^{1}H} NMR (121 MHz, THF-d_8): δ 68.69 (s, J_{PPt} = 2648 Hz). ^{1}H NMR (300 MHz, THF-d_8): δ -11.62 (t, 1H, J_{PH} = 13.0 Hz, J_{PtH} = 1038 Hz, Pt-H), 1.25 (vt, 36H, J_{PH} = 6.5 Hz, P(C(CH_3)$_3$)$_2$), 2.99 (vt, 2H, J_{PH} = 3.8 Hz, J_{PtH} = 27.8 Hz, CHP), 4.91 (dt, 2H, J_{PH} = 2.9 Hz, J_{HH} = 7.7 Hz, pyridine-H), 6.02 (tt, 1H, J_{PH} = 1.2 Hz, J_{HH} = 7.7 Hz, pyridine-H). ^{13}C{^{1}H} NMR (126 MHz, THF-d_8): δ 30.46 (vt, J_{PC} = 3.0 Hz, P(C(CH$_3$)$_3$)$_2$), 36.50 (vt, J_{PC} = 14.0 Hz, CHP), 51.78 (vt, J_{PC} = 29.9 Hz, P(C(CH$_3$)$_3$)$_2$), 89.45 (vt, J_{PC} = 7.4 Hz, pyridine-C), 133.05 (s, pyridine-C), 174.62 (vt, J_{PC} = 10.6 Hz, pyridine-C). IR (soln, THF): 2082 cm^{-1} (Pt^{II}-H stretch).

Li[(^{t}BuPNP****)PtCl] (16****)**: To a THF solution (0.4 mL) of (^{t}BuPNP*)PtCl (9.5 mg, 0.015 mmol) at - 30 °C was added ^{n}BuLi (1.66 M in hexanes, 9.2 μL, 0.015 mmol) by syringe. An immediate color change from orange to bright red was observed. The intermediate product **16**** was confirmed by comparing the NMR spectral data to the known complex K[(^{t}BuPNP**)PtCl].

^{31}P{1H} NMR (121 MHz, THF-d_8): δ 47.3 (s, J_{PPt} = 2574 Hz). ^{1}H NMR (499 MHz, THF-d_8): δ 1.33 (vt, J_{PH} = 6.4 Hz, 36H, P(C(CH_3)$_3$)$_2$), 2.62 (vt, J_{PH} = 4.0 Hz, J_{PtH} = 27.4 Hz, 2H, CHP), 4.72 (d, J_{HH} = 7.6 Hz, 2H, pyridine-H), 5.77 (tt, J_{HH} = 7.6 Hz, J_{PH} = 1.4 Hz, 1H, pyridine-H).

2.5 Notes to chapter 2

1. Albrecht, M.; van Koten, G. *Angew. Chem. Int. Ed*. **2001**, *40*, 3750.
2. van der Boom, M. E.; Milstein, D. *Chem. Rev.* **2003**, *103*, 1759.
3. Singleton, J. T. *Tetrahedron* **2003**, *59*, 1837.
4. Dupont, J.; Consorti, C. S.; Spencer, J. *Chem. Rev.* **2005**, *105*, 2527.
5. Benito-Garagorri, D.; Kirchner, K. *Acc. Chem. Res.* **2008**, *41*, 201.
6. Leis, W.; Mayer, H. A.; Kaska, W. C. *Coord. Chem. Rev.* **2008**, *252*, 1787.
7. Milstein, D. *Top. Catal.* **2010**, *53*, 915.
8. Gunanathan, C.; Milstein, D. *Acc. Chem. Res.* **2011**, *44*, 588.
9. Niu, J.-L.; Hao, X.-Q.; Gong, J.-F.; Song, M.-P. *Dalton Trans.* **2011**, *40*, 5135.
10. Albrecht, M.; Lindner, M. M. *Dalton Trans*. **2011**, *40*, 8733.
11. Haibach, M. C.; Kundu, S.; Brookhart, M.; Goldman, A. S. *Acc. Chem. Res.* **2012**, *45*, 947.
12. *Organometallic Pincer Chemistry;* Van Koten, G.; Milstein, D., Ed.; Top. Organomet. Chem.; Springer: Heidelberg, 2013; Vol. 40.
13. Suh, H.-W.; Schmeier, T. J.; Hazari, N.; Kemp, R. A.; Takase, M. K. *Organometallics* **2012**, *31*, 8225.
14. Roddick, D. M. *Top. Organomet. Chem.* **2013**, *40*, 49.
15. Gunanathan, C.; Ben-David, Y.; Milstein, D. *Science* **2007**, *317*, 790.
16. Gunanathan, C.; Milstein, D. *Top. Organomet. Chem.* **2011**, *37*, 55.
17. Schwartsburd, L.; Iron, M. A.; Konstantinovski, L.; Ben-Ari, E.; Milstein, D. *Organometallics* **2011**, *30*, 2721.
18. Gelman, D.; Musa, S. *ACS Catal.* **2012**, *2*, 2456.
19. Bichler, B.; Holzhacker, C.; Stöger, B.; Puchberger, M.; Veiros, L. F.; Kirchner, K. *Organometallics* **2013**, *32*, 4114.
20. Zeng, G.; Guo, Y.; Li, S. *Inorg. Chem.* **2009**, *48*, 10257.
21. Parkes, M. V. Ph.D. Dissertation, University of New Mexico, 2012.
22. Milstein, D. *Top. Catal.* **2010**, *53*, 915.
23. Gunanathan, C.; Milstein, D. *Acc. Chem. Res.* **2011**, *44*, 588.
24. Gunanathan, C.; Milstein, D. *Top. Organomet. Chem.* **2011**, *37*, 55.
25. Montag, M. Zhang, J.; Milstein, D. *J. Am. Chem. Soc.* **2012**, *134*, 10325.
26. Vogt, M.; Nerush, A.; Iron, M. A.; Leitus, G.; Diskin-Posner, Y.; Shimon, L. J.; Ben-David, Y.; Milstein, D. *J. Am. Chem. Soc.* **2013**, *135*, 17004.
27. Feller, M.; Ben-Ari, E.; Iron, M. A.; Diskin-Posner, Y.; Leitus, G.; Shimon, L. J. W.; Konstantinovski, L.; Milstein, D. *Inorg. Chem.* **2010**, *49*, 1615.
28. Ben-Ari, E. Activation of Strong Bonds by Electron-Rich Iridium and Rhodium. Ph. D. Dissertation, Weizmann Institute of Science, 2007.
29. Lachaize, S.; Essalah, K.; Montiel-Palma, V.; Vendier, L.; Chaudret, B.; Barthelat, J.-C. Sabo-Etienne, S. *Organometallics* **2005**, *24*, 2935.
30. Hebden, T. J.; Denney, M. C.; Pons, V.; Piccoli, P. M. B.; Koetzle, T. F.; Schultz, A. J., Kaminsky, W.; Goldberg, K. I.; Heinekey, D. M. *J. Am. Chem. Soc.* **2008**, *130*, 10812.
31. Rossin, A.; Peruzzini, M.; Zanobini, F. *Dalton Trans.* **2011**, *40*, 4447.
32. Farrugia, L. J. *J. Appl. Cryst.* **2012**, *45*, 849.

33. Poverenov, E.; Iron, M. A.; Gandelman, M.; Ben-David, Y.; Milstein, D. *Eur. J. Inorg. Chem.* **2010**, 1991.
34. Vuzman, D.; Poverenov, E.; Shimon, L. J. W.; Diskin-Posner, Y.; Milstein, D. *Organometallics,* **2008**, 27, 2627.
35. Milstein, D.; *Top. Catal.*, **2010**, 53, 915.
36. Zhang, J.; Gandelman, M.; Herrman, D.; Leitus, G.; Shimon, L. J. W.; Ben-David, Y.; Milstein, D.; *Inorg. Chim. Acta.* 359, **2006**, 1955.
37. Milstein, D.; *Top. Catal.*, **2010**, 53, 915.
38. Smoll, K. Manuscript in preparation, 2016.
39. Konnick, M. M.; Decharin, N.; Popp, B. V.; Stahl, S. S. *Chem. Sci.* **2011**, *2*, 326.
40. Keith, J. M.; Muller, R. P.; Kemp, R. A.; Goldberg, K. I.; Goddard III, W. A.; Oxgaard, J. *Inorg. Chem.* **2006**, *45*, 9631.
41. Denney, M. C.; Smythe, N. A.; Cetto, K. L.; Kemp, R. A.; Goldberg, K. I. *J. Am. Chem. Soc.* **2006**, *128*, 2508.
42. Boro, B. J. Ph.D. Dissertation, University of New Mexico, 2009.
43. Fulmer, G. R. Ph.D. Dissertation, University of Washington, 2010.
44. Fulmer, G. R.; Herndon, A. N.; Kaminsky, W.; Kemp, R. A.; Goldberg, K. I. *J. Am. Chem. Soc.* **2011**, *133*, 17713.
45. Bruker (**2007**) APEX2 (Version 2.1-4), SAINT (version 7.34A), SADABS (version 2007/4), BrukerAXS Inc, Madison, Wisconsin, USA.
46. (a) Altomare, A.; Burla, C.; Camalli, M.; Cascarano, G. L.; Giacovazzo, C.; Guagliardi, A.; Moliterni, A. G. G.; Polidori, G.; Spagna, R. *J. Appl. Cryst.* **1999**, *32***,** 115. (b) Altomare, A.; Cascarano, G. L.; Giacovazzo, C.; Guagliardi, A. *J. Appl. Cryst.* **1993**, *26*, 343.
47. Sheldrick, G. M. (**1997**) SHELXL-97, Program for the Refinement of Crystal Structures. University of Göttingen, Germany.
48. Mackay, S.; Edwards, C.; Henderson, A.; Gilmore, C.; Stewart, N.; Shankland, K.; Donald, A. (**1997**) *MaXus: a computer program for the solution and refinement of crystal structures from diffraction data*. University of Glasgow, Scotland.
49. Waasmaier, D.; Kirfel, A. *Acta Cryst. A* **1995**, *51*, 416.

Chapter 3*

Pyrazole-based PCN pincer complexes of Pd^{II}: Mono- and dinuclear hydroxide complexes and ligand rollover C-H activation

3.1 Introduction

The use of pincer ligated transition metal complexes as catalysts for organic transformations has grown dramatically in recent years.[1] The robust tridentate binding motif coupled with the tunability of the steric and electronic parameters of pincer ligands has proven highly effective in stabilizing and allowing isolation of a variety of uncommon types of metal complexes. For example, pincer ligands have been very useful in the preparation of mononuclear late metal complexes bearing M-OR and M-NR_2 bonds. Notably there are significantly fewer mononuclear late transition metal hydroxide, alkoxide and amide

* The majority of the data presented in this chapter has been previously published: Reprinted with permission from Bailey, W. D.; Luconi, L.; Rossin, A.; Yakhvarov, D.; Flowers, S. E.; Kaminsky, W.; Kemp, R. A.; Giambastiani, G.; Goldberg, K. I. *Organometallics* **2015**, *34*, 3998-4010. Copyright 2015 American Chemical Society. Luconi, Rossin, Giambastiani: Ligand and Pd-Cl complex synthesis. Luconi, Rossin, Yakhvarov, Giambastiani: DFT calculations. Flowers, Kaminsky: X-ray crystallography.

complexes relative to their metal alkyl (M-C) analogs.[2] However, such M-OR and M-NR_2 linkages are pertinent to catalysis,[3,4] and thus isolation and study of model metal-hydroxide and amide complexes are of great value. We are particularly intrigued by isolable terminal M-OH complexes as these species would result from O-atom transfer by M-OOH complexes. This transformation is crutial in a partial oxidative cycle that uses O_2 as the oxidant (**Scheme 3.1**). Understanding the chemistry of M-OH species is imperative for catalyst regeneration. A large part of that is choosing suitable ligands to promote selective reactivity at the hydroxide ligand.

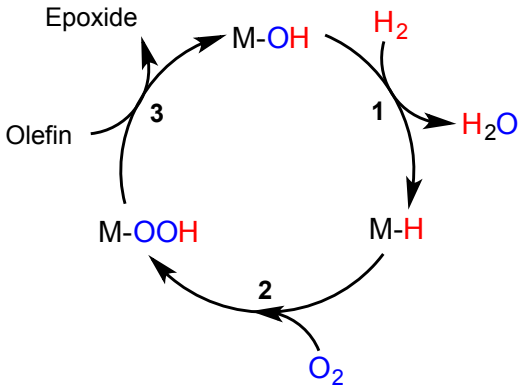

Scheme 3.1 Proposed catalytic cycle for the epoxidation of olefins using molecular oxygen.[4]

The variety of available pincer ligands has increased dramatically in recent years. While early pincer ligands were symmetric with respect to ligand "arms" (*e.g.* PCP, PNP, POCOP, etc.),[5] pincer-type complexes bearing unsymmetrical arms have begun to appear in greater numbers (NCC, PNN, PCO, PCS, etc.).[6] PCN-type systems in particular are intriguing, because in (PCN)$M(L)_n$ complexes (M = transition metal; L = ancillary ligand) the tridentate hybrid ligand contains both *hard* (N) and *soft* (P) donor atoms, thus leading to novel and unprecedented chemical properties.[7] In such species, there is a marked difference in the *trans* effect between the two different donors. This difference results in the group with the weaker

trans effect (N) being more likely to dissociate from the metal center due to its position *trans* to the group with a stronger *trans* effect (P). The stronger M-P bond remains intact. From a homogeneous catalysis perspective, the hemilability of the ligand provides access to a vacant coordination site at the metal center and so can allow for effective coordination, activation and transformation of substrate molecules. Such ligand hemilability has often been invoked as the critical factor when comparing the catalytic activity of $(PCP)M(L)_n$/$(NCN)M(L)_n$ and $(PCN)M(L)_n$ analogues; the unsymmetrical complex has consistently been shown to be *more active* than its symmetric counterparts.[6i,j,8,9]

In our laboratories, we have explored a variety of both symmetrical and unsymmetrical pincer systems (PCP,[10] PNP,[11] PCO,[6h] NNC[12]) to stabilize and study model complexes. While the symmetric ligand systems result in more stable complexes, the unsymmetrical analogs have yielded higher reactivity primarily through arm lability. For example, in a study on late transition metal PCO pincer systems, the ether O-arm was found to be labile, and allowed for reductive elimination of the pincer framework under reducing conditions.[6h]

The following is an account of a novel unsymmetrical PCN^R pincer ligand system designed to relieve steric bulk around the metal center relative to its PCP counterpart. The nitrogen donor (pyrazole group) was expected to be a stronger binding ligand than an ether linkage (as in a related PCO system),[6h] yet would potentially provide for hemilability at elevated temperatures. Notably, this is also a cautionary tale about unsymmetrical pincer ligands. Pincer ligands are often touted for their robustness, but here we find that N-heterocycles *trans* to phosphines can display undesired reactivity of their own. The metallation of two new pyrazole-containing PCN^R ligand frameworks on Pd^{II} and the exploration of the reactivity of the related chloro and hydroxo complexes is discussed. In a hydroxo derivative,

an unexpected pyrazole side-arm C-H bond activation was observed. C−H addition across the Pd−OH bond on the 5-position of the heterocycle occurred to transform the monoanionic {P,C-,N} ligand into a dianionic {P,C-,C-} donor. The thermodynamics are favorable with the driving force for the reaction to occur provided by the simultaneous formation of a stable neutral *aquo* ligand that exits the metal coordination sphere. The process was followed experimentally (multinuclear $^{31}P\{^{1}H\}$ and ^{1}H NMR spectroscopy) and then computationally modeled (DFT at the M06//6-31G* level of theory). By protecting the ligand in the 5-position through methylation (PCN^{Me}), this "rollover" reactivity was shut down and a stable terminal hydroxide complex was isolated.

3.2 Results and discussion

The PCN^{H} ligand was synthesized as described in **Scheme 3.2**.† Details for the preparation can be found in the published work on this system.[13]

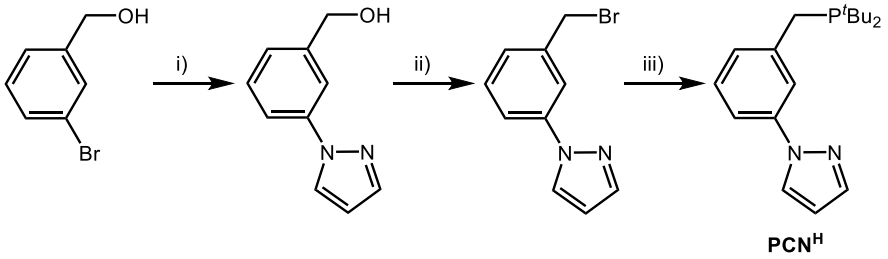

Scheme 3.2. Synthetic route for the **PCN^{H}** pincer ligand. Reagents and conditions: i) pyrazole, CuI, K_2CO_3, NMP, microwave irradiation, 210 °C, 5 h, 250 W; ii) Br_3CCO_2Et, PPh_3, CH_2Cl_2, rt, 0.5 h; iii) $^{t}Bu_2PH$, acetone, reflux, 12 h.

† The synthesis and characterization of the PCN^{H} ligand and complexes **17-19** were performed by our collaborators, the Giambastiani group, at the Institute of Chemistry of Organometallic Compounds ICCOM-CNR and Consorzio INSTM, Florence, Italy.

Metallation of PCN^{H}: Synthesis of Pd^{II} chloride complexes†: The reaction of PCN^{H} ligand with Pd(COD)Cl$_2$ in toluene (110 °C) was monitored through successive solution samplings and $^{31}P\{^{1}H\}$ NMR spectroscopy at room temperature. Full conversion to the Pd^{II} complex (PCN^{H})Pd-Cl (**17**) was observed after 4 hours with a new downfield $^{31}P\{^{1}H\}$ NMR signal at 95.1 ppm (**Scheme 3.3**).

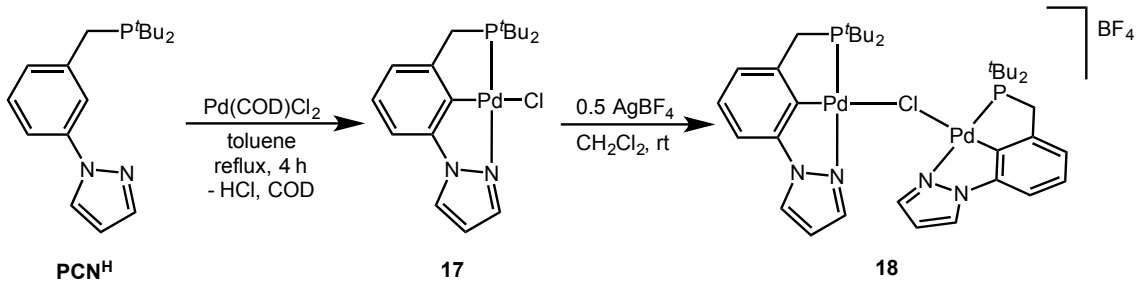

Scheme 3.3. Synthesis of (PCN^{H})Pd^{II} chloride complexes **17** and **18**.

The (PCN^{H})Pd-Cl complex **17** was isolated as a moderately air-sensitive white microcrystalline solid and was characterized by $^{31}P\{^{1}H\}$, ^{1}H and $^{13}C\{^{1}H\}$ NMR spectroscopy combined with single-crystal X-ray diffraction studies. The ^{1}H and $^{13}C\{^{1}H\}$ NMR patterns indicate that **17** possesses C_s symmetry in solution. The most representative ^{1}H and $^{13}C\{^{1}H\}$ NMR spectroscopic resonances related to the κ^3-coordinated ligand fall at lower fields when compared with those observed for the free ligand; the aryl carbon atom directly bound to the Pd^{II} center shows the largest resonance shift [from 120.1 (free PCN^{H}) to 150.3 (**17**) ppm]. Microcrystals suitable for X-ray analysis were grown from a concentrated acetone solution at −30 °C. An ORTEP[14] of the crystal structure of **17** is given in **Figure 3.1**. **Table 3.1** in the experimental section lists all the main crystal and structural-refinement data, and selected bond lengths and angles are summarized in **Table 3.2**.

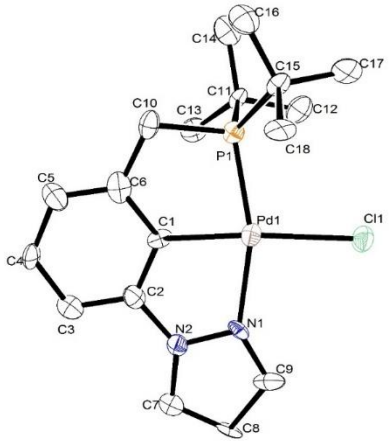

Figure 3.1. Single molecule ORTEP[14] of complex (PCN^{H})Pd-Cl **(17)**, with ellipsoids shown at 50% probability. Hydrogen atoms bound to carbon atoms omitted for clarity.

Complex **17** crystallizes in the orthorhombic *P2$_1$2$_1$2$_1$* space group with 4 molecules per unit cell. The Pd^{II} center adopts a distorted square-planar coordination geometry (τ_4 = 0.16).[15] Bond lengths and angles measured within the [(PCN^{H})Pd]$^{+}$ fragment of **17** fall in the typical range observed for related [(PCN)Pd]$^{+}$ fragments in square planar environments.[16,9b] It is notable that the Pd^{II}-P bond in **17** (2.227(4) Å)is shorter than those observed in symmetric ($^{t\text{Bu}}$PCP)Pd(L) analogues (mean Cambridge Structural Database (CSD) value = 2.31 Å)[10,17] and that the Pd^{II}-N bond length in **17** (2.094(10) Å) is longer than that found in symmetric pyrazole-based (NCN)Pd(L) species (mean CSD value = 2.03 Å).[18] This crystallographic evidence suggests that the pyrazole group is more likely to possess hemilabile properties in the unsymmetrical PCN^{H} environment.

It was found that the chloride ligand *trans* to the strongly donating aryl backbone in **17** could be abstracted by treatment with silver reagents. Treatment of a CH_2Cl_2 solution of **17** with only 0.5 equiv of $AgBF_4$ (**Scheme 3.3**) afforded a dinuclear Pd^{II} complex {[(PCN^{H})Pd]$_2$(μ-Cl)}[BF_4] (**18**), in the form of pale yellow microcrystals. Single crystals

suitable for X-ray diffraction were grown by layering a concentrated CH_2Cl_2 solution of the salt with cold pentane. The solid-state structure confirmed the identity of **18** (ORTEP[14] in **Figure 3.2** and relevant bond angles and distances in **Table 3.2**). The NMR spectra of the chloride bridged dimer show a similar, yet shifted pattern compared to its mononuclear analogue **17**. The ^{t}Bu and methylene "arm" signals in the ^{1}H NMR spectrum appear as doublets, coupling to phosphorus and indicate a high level of symmetry of the dimer in solution. The $^{13}C\{^1H\}$ NMR spectrum also supports this as separate signals for each [(PCN^H)Pd] fragment are not observed. It is possible that the dimer rotates about the Pd^{II}-Cl bond on the NMR timescale, yielding magnetically equivalent ^{t}Bu and methylene groups. It is also possible that dissociation of the dinuclear **18** and reformation of the [(PCN^H)Pd fragments could occur on the NMR timescale, resulting in the ^{t}Bu and methylene signals appearing as respectively averaged signals. If, instead, a rigid dimer existed in solution as it appears in the solid state, diastereotopic and thus magnetically unique ^{t}Bu and methylene signals would be expected. A sharp singlet is observed in the $^{31}P\{^1H\}$ NMR spectrum at 95.1 ppm.

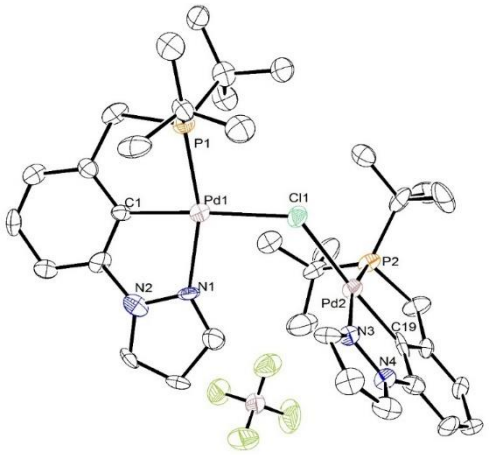

Figure 3.2. Single molecule ORTEP[14] of complex {[(PCN^H)Pd]$_2$(μ-Cl)}[BF_4] (**18**) , with ellipsoids shown at 50% probability. Hydrogen atoms bound to carbon atoms and crystallization solvent molecules omitted for clarity.

The dimer crystallizes in the orthorhombic *Pna2₁* space group, with 4 molecules per unit cell. In the chloride-bridged dinuclear cation, both palladium centers maintain a slightly distorted square-planar geometry (τ_4 = 0.15 and 0.19).[15] The main bond lengths and angles in **18** are very similar to those found in the monomeric complex **17**. Similar to related μ-Cl mono-bridged cationic dimers,[19] only slightly longer Pd^{II}–Cl distances are found in **18** [2.427(4) Å for Pd(1)-Cl(1) and 2.425(4) Å for Pd(2)-Cl(1)] compared to the bond length determined in **17** [2.388(4) Å].

The nitrile complex [(PCN^{H})Pd(MeCN)][BF_4] (**19**) was obtained as a finely divided white powder from the reaction of **17** with 1 equiv. of $AgBF_4$ in CH_2Cl_2 in the presence of a 5-fold excess (compared to Pd) of acetonitrile (**Scheme 3.4**). Complex **19** was characterized by multinuclear NMR spectroscopy and combustion analysis. Unfortunately, attempts to obtain crystals of **19** suitable for X-ray analysis were unsuccessful. The ^{1}H and $^{13}C\{^{1}H\}$ NMR resonances of **19** are very similar to those observed in the parent chloride precursor **17**, except for the appearance of a sharp singlet in the ^{1}H NMR spectrum at 2.51 ppm (ascribed to the methyl group of the coordinated CH_3CN molecule). The $^{31}P\{^{1}H\}$ NMR signal moves from 95.1 for **17** to 98.2 ppm for **19**.

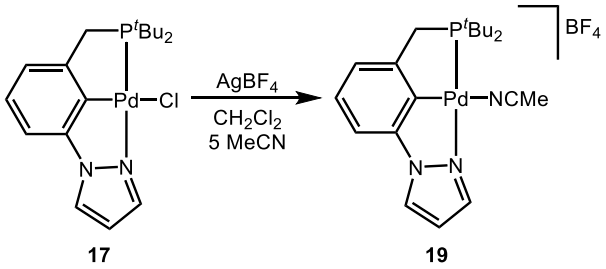

17 19

Scheme 3.4. Formation of [(PCN^{H})Pd(MeCN)][BF_4] (**19**) by halide abstraction from **17**.

The reaction of **17** with 1 equiv. of AgOTf in CH_2Cl_2 in the absence of acetonitrile yields the triflate species (PCN^H)Pd-OTf (**20**) (**Scheme 3.5**). Complex **20** was fully characterized by multinuclear NMR spectroscopy, X-ray crystallography and combustion analysis. The ^1H and $^{13}C\{^1H\}$ NMR spectra display very similar (albeit slightly shifted) patterns to those observed for the chloride analogue **17**. The $^{31}P\{^1H\}$ NMR spectrum displayed a singlet at 94.1 ppm. Complex **20** exhibits a typical square planar ligand arrangement about the Pd^{II} center with a κ^3-PCN^H and triflate ligands coordinated. An ORTEP[14] of **20** is shown in **Figure 3.3**. Relevant bond lengths and angles appear in **Table 3.2**. The nitrate species (PCN^H)Pd-ONO_2 was also synthesized and characterized by ^1H and $^{31}P\{^1H\}$ NMR spectroscopy and X-ray crystallography (see experimental section). Notably the triflate complex **20** was produced under milder conditions and in higher yield, and therefore was used for future reactivity studies.

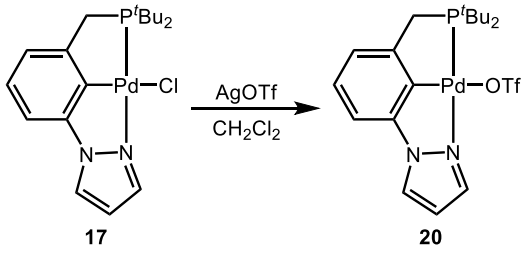

Scheme 3.5. Formation of (PCN^H)Pd-OTf (**20**) by halide abstraction from **17**.

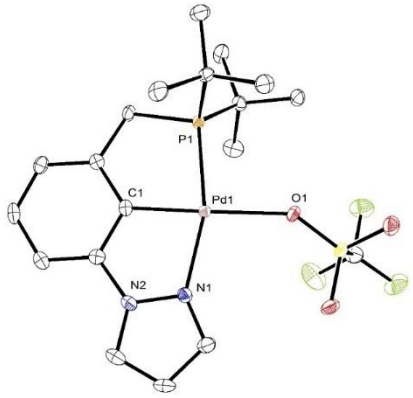

Figure 3.3. Single molecule ORTEP[14] of complex (PCN^H)Pd-OTf **(20)**, with ellipsoids shown at 50% probability. Hydrogen atoms bound to carbon atoms omitted for clarity.

Formation of hydroxide species containing the [(PCN^{H})Pd]$^{+}$ and [(PCC)Pd] fragments. "Rollover" C−H bond activation on the pyrazole side-arm: The synthesis of Pd^{II}-OH complexes was targeted in order to create catalytically relevant model species for olefin epoxidation reactions (**Scheme 3.1**). As previous transition metal hydroxide complexes have been synthesized primarily through metathesis reactions with alkali metal hydroxides,[20] preparation of the desired monomeric hydroxide complex was first attempted by addition of potassium hydroxide (KOH) to the chloride complex **17** in THF. No reaction was observed at room temperature, and only a slow reaction occurred at elevated temperatures (60 °C) to produce an array of intractable products, including palladium black, over long reaction times (4 days). As group 10 terminal hydroxides have also been made *via* metathesis of weakly bound anions rather than from the chloride precursor,[21] the reactivity of the triflate complex **20** with hydroxide salts was investigated.

Addition of an excess of KOH to a THF-d_8 solution of the triflate complex **20** yielded a new product **21** as observed by the disappearance of the signal at 94.1 ppm and the appearance of a new singlet at 93.3 ppm in the $^{31}P\{^{1}H\}$ NMR spectra (**Figure 3.4**). However, further monitoring of this reaction showed conversion of **21** to a second species **22** with a singlet at 91.8 ppm in the $^{31}P\{^{1}H\}$ NMR spectrum. A third product **23**, with two new signals at 91.1 and 71.0 ppm, then grows in concurrently with a relative decrease of the 91.8 ppm signal due to **22**. Some decomposition of the reaction mixture was also observed in the reaction vessel as palladium black became visible. When the reaction conditions were changed as described below, characterization of the various palladium species formed in this reaction (**21-23**) was possible.

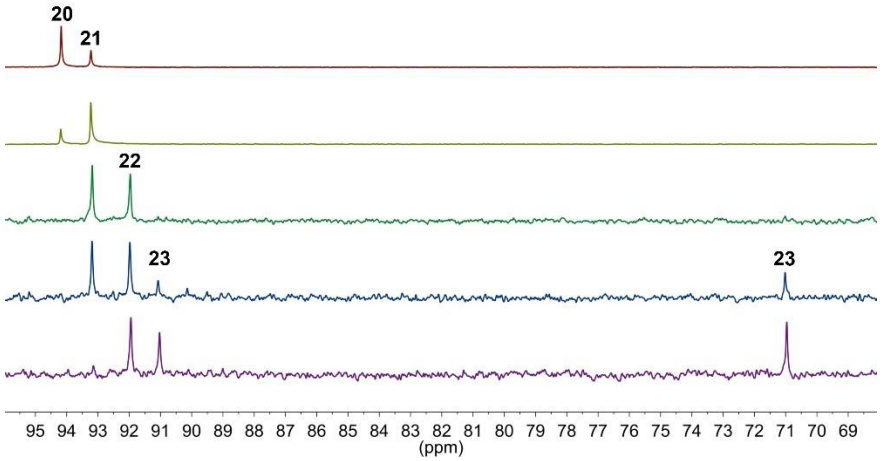

Figure 3.4. $^{31}P\{^{1}H\}$ NMR stack of the formation of species **21**-**23** over days.

When only 0.5 equivalents of KOH were added to the triflate **20**, the new species **21** was formed as the sole product (**Scheme 3.6**). The ^{1}H NMR spectrum of **21** displays a peak at −1.48 ppm, indicative of a Pd^{II} hydroxide species. The ^{t}Bu protons appear as two doublets at 1.44 and 1.51 ppm ($^{3}J_{PH}$ = 14.1 and 14.3 Hz, respectively). Integration of the doublets compared to the hydroxide signal yields a 18:18:1 ratio, suggesting a dinuclear species. The appearance of two signals for the ^{t}Bu protons demonstrates that these resonances are magnetically inequivalent (diastereotopic) as would be expected in a ridged dinuclear species. This observation contrasts what is observed for **18**, where only one resonance is observed for the ^{t}Bu signals at room temperature. As the steric profile between **18** and **21** are similar, the diastereotopic signals in **21** indicate a much more rigidly bound dinuclear compound. X-ray quality crystals were grown from a concentrated THF solution of **21** layered with pentane. The solid-state structure confirmed the spectroscopic assignment of **21** as the dinuclear species $\{[(PCN^{H})Pd]_2(\mu\text{-}OH)\}[OTf]$ (**Figure 3.5**).

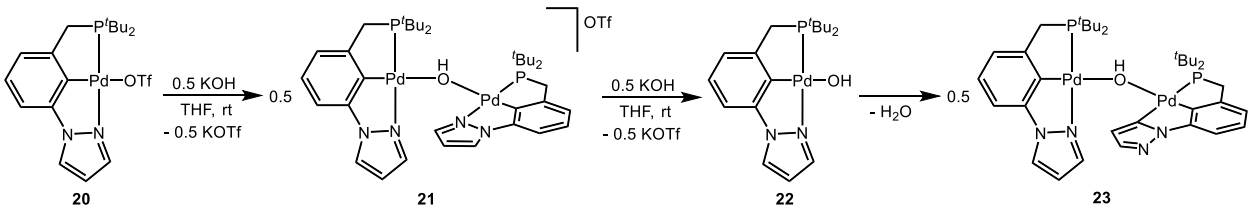

Scheme 3.6. Synthesis of the hydroxide pincer complexes (**21**-**23**) of the PCN^H ligand.

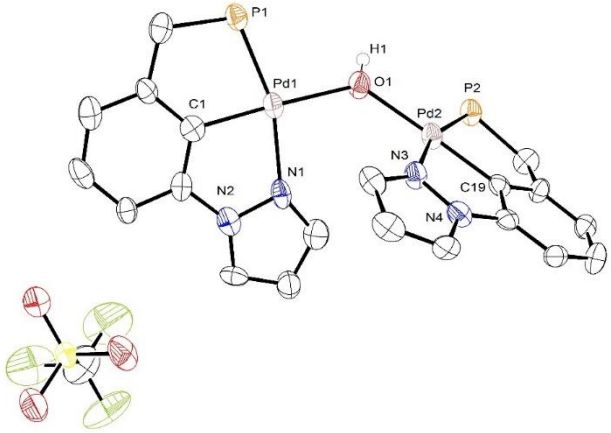

Figure 3.5. ORTEP[14] of the {[(PCN^H)Pd]$_2$(μ-OH)}[OTf] salt (**21**), with ellipsoids shown at 50% probability. Hydrogen atoms and ^{t}Bu groups on P omitted for clarity.

Dinuclear **21** is C_2 symmetric with the two distorted square planar (PCN^H)Pd^{II} units bridged by a single μ-OH (τ_4[Pd(1)] = 0.14; τ_4[Pd(2)] = 0.16).15 One non-coordinating triflate counterion is found in the asymmetric unit to balance the overall positive charge of the dinuclear complex. The structure of **21** is analogous to the chloride bridged dinuclear species **18**, with a bridging hydroxide instead of a bridging chloride. The hydroxyl hydrogen was refined by geometry optimization of the hydroxide ligand with respect to the Pd(1)-O(1) bond, while leaving the Pd(2)-O(1) bond free. The hydroxide is shielded by the bulky ^{t}Bu groups. No hydrogen bonding interactions were observed. The bond lengths within the (PCN^H)Pd units of **21** are similar to those observed in the mononuclear triflate complex **20**. While bis μ-OH

dimers are well known for Pd^{II}, this is a rare example of two palladium centers bridged only by a single μ-OH ligand.[22] **Table 3.2** contains a list of selected bond lengths and angles for **21**.

When a THF solution of the triflate **20** was treated with one full equivalent of KOH, **21** was observed as a transient intermediate and decayed into complex **22** as the major product. Complex **22** is characterized by a singlet at 91.8 ppm in the $P\{^1H\}$ NMR spectrum. Conversion into complex **22** was not clean, and peaks at 91.1 and 71.0 ppm (complex **23**) in the $^{31}P\{^1H\}$ NMR spectrum consistently appeared as a minor product, such that it was not possible to isolate pure **22**. However, it was found that the addition of water to **22** inhibited decomposition to **23**. Thus, addition of D_2O to a THF-d_8 (1:4 v/v) solution of **21** containing suspended KOH resulted in the formation of pure **22** which could be fully characterized in solution by NMR spectroscopy. On the basis of intermediacy of **21** in the formation of **22** and the ^1H and $^{31}P\{^1H\}$ NMR spectral signals assignable to **22**, complex **22** is proposed to be the mononuclear terminal hydroxide (PCN^H)Pd-OH (**Scheme 3.6**). The ^1H NMR spectrum of **22** displays a signal at –1.71 ppm (observed only in the absence of excess water), attributable to the Pd-OH group and the ^{t}Bu protons appear as a doublet at 1.43 ppm, integrating 18:1 compared to the hydroxide signal.

Efforts to recrystallize **22** from the reaction mixture in THF at low temperatures did yield crystals suitable for an X-ray diffraction study, as well as amorphous material. However, as shown in **Figure 3.6**, the crystallized product was not **22** but rather complex **23**, a mixed-ligand hydroxide-bridged dinuclear complex, [(PCN^H)Pd(μ-OH)](Pd(PCC)). This was confirmed as dissolution of the isolated crystalline sample in THF matched the spectral features displayed by **23** in the $^{31}P\{^1H\}$ NMR spectrum along with minor impurities attributed to the amorphous solid. The structure of **23** consists of two palladium centers bridged by a single μ-

OH ligand, similar to **21**. One of the Pd^{II} centers is bound by the {P, C^-,N} ligand as observed in **21**. However, unlike **21**, the other Pd^{II} center is bound to a *dianionic* tridentate {P, C^-,C^-} ligand; the pyrazolyl arm has undergone "rollover" C-H activation at the 5-position.

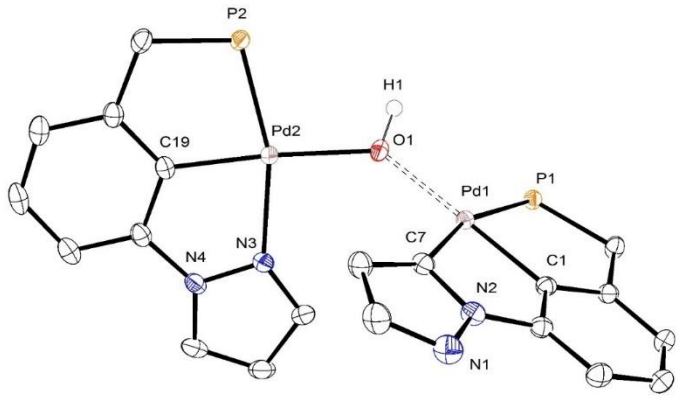

Figure 3.6. ORTEP[14] of [(PCN^H)Pd(μ-OH)](Pd(PCC)) (**23**), with ellipsoids shown at 50% probability. Hydrogen atoms and ^{t}Bu groups on P omitted for clarity. The dative bond between the [(PCC)Pd] fragment and O(1) is represented by a dotted line.

In the X-ray structure, the "rollover" and pyrazole rings were distinguished primarily by the observation of a H-bonding interaction between the assigned free N(1) of the rollover ring and a neighboring molecule's C(3')-H (**Figure 3.7**). This forms an octagonal ring interaction: N(1)---H-C(3'), C(3)-H---N(1'). A C(7)-H bond could not fill this space while the H-bonding interaction exists. Furthermore, assigning the atoms incorrectly (as two pyrazole rings) yields a displacement parameter mismatch: too large of a thermal ellipsoid for N(1), too small of a thermal ellipsoid for C(7). This results in a larger R_1-value. No visible electron density for a bound hydrogen atom to the N(1) position was observed. Notably all other hydrogens could be identified.

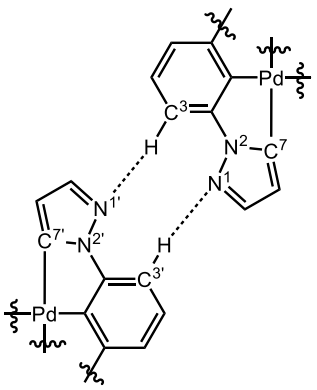

Figure 3.7. Intermolecular hydrogen bonding interaction in the solid state of **23**.

The $[(PCN^{H})Pd]^{+}$ fragment displays near identical bond angles and distances to those found in the hydroxide complex **21**. In contrast, the Pd(1)-P(1) bond in the [(PCC)Pd] fragment is somewhat longer than the corresponding bond in the $(PCN^{H})Pd$ fragment [2.3084(4) Å *vs.* 2.2260(4) Å]. This change is expected, as the phosphorus donor is *trans* to a stronger donor when moving from neutral N to an anionic C^{-}. Notably, no counterion was observed, which is consistent with the dianionic PCC character of the second pincer fragment. The Pd-O bond lengths in the cationic and neutral μ-hydroxo dimers (**21** and **23**, respectively) are very similar. However, when comparing the Pd(1)-O(1) and the Pd(2)-O(1) bond lengths within **23**, a clear difference is observed. In **23**, the hydroxide ligand is associated more with the cationic $[(PCN)Pd]^{+}$ fragment (2.0831(11) Å) than with the neutral [(PCC)Pd] fragment (2.1077(11) Å) and further supports a mixed ligand dinuclear species. It should be noted that for complex **21**, the hydroxide ligand is shared equally between palladium centers within error.

The activation of a pyrazole C-H bond at the 5-position has previously been observed in (poly)pyrazole-containing ligands in the presence of late transition metals (*e.g.* Ru,[23] Pd,[24] Pt,[25] and Ir[26]) and the activation of C-H bonds by palladium fragments in several N-heterocycles has been studied computationally.[27] Notably however, the "rollover" activation

to form **23** takes place under very mild conditions, in contrast to many previously reported literature examples that require elevated temperatures or the employment of photoirradiation. We propose that the room-temperature "rollover" C-H activation occurs at the monomeric hydroxide **22**, forming a neutral and coordinatively unsaturated [(PCC)Pd] unit after loss of an *aquo* ligand from the palladium coordination sphere. This is supported by the increased stability of **22** in the presence of water (*vide supra*). Subsequent combination of the [(PCC)Pd] fragment with another molecule of (yet unreacted) **22** yields the bridged species **23** (**Scheme 3.6**). When a THF solution of a mix of **22** as the major product and **23** as a minor impurity was left at room temperature for 6 days, decomposition of **22** occurred yielding **23** as the major product, along with unidentified side products as observed by multinuclear NMR spectroscopy. Attempts to achieve a pure sample of **23** in solution were unsuccessful. However, by analyzing a mixture of **22** converting to **23** by NMR spectroscopy before further decomposition, signals attributed to the mixed ligand complex **23** could be, in part, assigned. Notably, the ^{1}H NMR spectrum of the mixture shows 4 new ^{t}Bu signals (1.36, 1.39, 1.44 and 1.51 ppm), each as doublets, indicating that the substituents are not only diastereotopic as in complex **21**, but are bound to two chemically inequivalent phosphorous atoms. This is expected, as one phosphine arm is *trans* to N and the other *trans* to C. This mixed ligand framework is also consistent with the 4 sets of doublet of doublets observed for the diastereotopic methylene protons (3.08, 3.12, 3.42 and 3.49 ppm), as well as 4 ^{t}Bu primary carbon signals in the ^{13}C{^{1}H} NMR spectrum (29.46, 29.51, 29.91 and 30.10 ppm; $^{2}J_{PC}$ = 3.9, 3.5, 6.0 and 6.0 Hz, respectively). Unfortunately, due to the complexity of the mixture and the inability to isolate **23**, the other resonances in the ^{13}C{^{1}H} NMR spectrum could not be assigned confidently. To explore this "rollover" activation in more detail, DFT simulations of the reaction were undertaken.

DFT simulation of the "rollover" cyclometallation in the conversion of the mononuclear hydroxide 22 to the dinuclear μ-OH complex 23[‡]: The pyrazole "rollover" and related activation of the C(5)-H pyrazole bond to form H_2O was examined computationally, on the real system at the M06//6-31G* level of theory. THF solvent was included in the calculation through a *continuum* model (SMD), and all the figures reported here should be considered as ΔG or $\Delta G^{\ddagger}$ values evaluated in THF (see Computational Details). A water molecule generated by an intermolecular rearrangement of the hydroxide complex **22** implies a $(PCN^{H})^{-} \leftrightarrow (PCC)^{2-}$ conversion. The rotation of the pyrazole ring around the C(2)-N(2) bond (**Figure 3.1** for atom numbering) within the pincer can lead to an activation of the C-H bond in the 5-position by the palladium center, with concomitant formation of the *aquo* species (PCC)Pd(H_2O) (**24**) as the result of a proton transfer to the -OH group on palladium. Beginning with the mononuclear hydroxide complex **22**, rotation of the pyrazole substituent by 180° with respect to the starting geometry yields an isomeric form of the hydroxide (PCCH)Pd(OH) (**22′**) wherein the C-H bond in the 5-position interacts with the metal center through an agostic interaction {optimized d[C-Pd] = 2.58 Å; d[H-Pd] = 2.29 Å; d[C-H] = 1.09 Å}. This optimized structure is drawn in **Figure 3.8**. Unsurprisingly, N-coordination is more stabilizing than a C-H agostic interaction and the Gibbs energy of **22′** is higher than that of **22** by 17.0 kcal mol^{-1}.

[‡] DFT calculations and analysis performed by our collaborators, the Giambastiani group, at the Institute of Chemistry of Organometallic Compounds ICCOM-CNR and Consorzio INSTM, Florence, Italy.

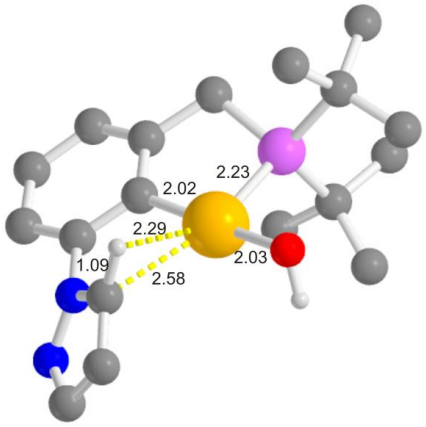

Figure 3.8. Optimized structure of (PCCH)Pd(OH) (**22′**). Selected bond lengths (Å) reported. H atoms on the pincer omitted for clarity. Atom color code: gray, C; white, H; red, O; blue, N; purple, P; orange, Pd.

An estimation of the rotation barrier of the pyrazole ring was made through a scan of the θ[C(1)-C(2)-N(2)-N(1)] dihedral angle reaction coordinate (**Figure 3.9**). The maximum of the energy profile along this coordinate is located at 24.5 kcal mol^{-1} from the starting geometry [at θ(C-C-N-N) ≈ 75°], and it can be reasonably considered the "Transition State", $\mathbf{TS_{rot}}$, for this ligand rearrangement (**Figure 3.9**).

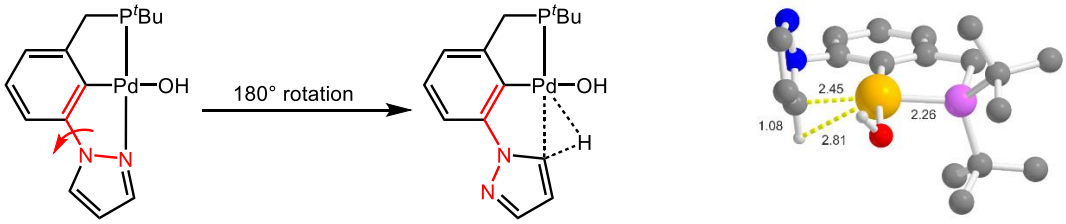

Figure 3.9. Pincer rearrangement around the Pd center through 180° rotation of the pyrazole ring (left) with calculated transition state, $\mathbf{TS_{rot}}$ (right). Dihedral angle varied shown in red.

From **22′**, a direct proton transfer through a four-centered transition state ($\mathbf{TS_1}$, **Figure 3.10**, left; $\Delta G^{\ddagger}$ = 20.8 kcal mol^{-1}) leads to the *aquo* complex **24** [**Figure 3.10**, right; ΔG(**9a′/11a**) = -11.4 kcal mol^{-1}]. The dimer formation reaction **22** + **24** → **23**···$\mathbf{H_2O}$ is

thermodynamically favored with a ΔG = -12.0 kcal mol^{-1}. In the final structure, the water molecule engages in a hydrogen bond with the bridging hydroxide group {optimized d[μ-HO···H_2O] = 1.83 Å} and it is responsible for an extra-stabilization of the dinuclear product. The optimized structure of **23**···**H_2O** is reported in **Figure 3.11**. Evolution to the dimeric product provides the strong driving force for the reaction to take place. Interestingly, the pyrazole rotation and the C-H activation barriers are almost identical at the computational level used; thus, the heterocycle rotation (albeit slow at ambient temperature, owing to the relatively high $\Delta G^{\ddagger}$ found) is accompanied by a *simultaneous* C-H activation on the 5-position and dimer formation, as found experimentally. Notably, this analysis is consistent with experimental results as the *aquo* species **24** was never detected in the course of the transformation of **22** to **23** by $^{31}P\{^{1}H\}$ NMR spectroscopy. The overall Gibbs energy *vs.* reaction coordinate profile for this transformation is reported in **Figure 3.12**.

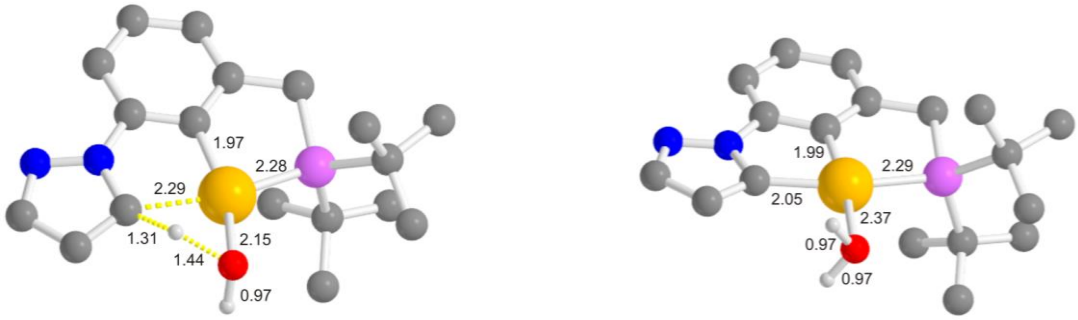

Figure 3.10. Optimized structure of **TS_1** (left) and (PCC)Pd(H_2O) (**24**) (right). Selected bond lengths (Å) reported. H atoms on the pincer omitted for clarity. Atom color code: gray, C; white, H; red, O; blue, N; purple, P; orange, Pd.

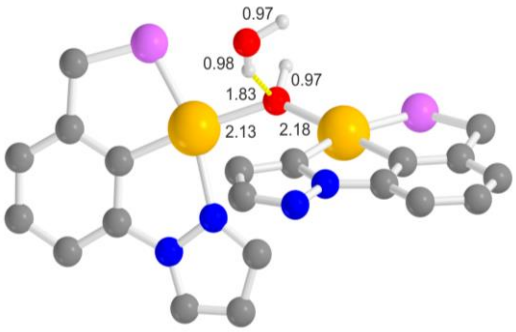

Figure 3.11. Optimized structure of [(PCN^{H})Pd(μ-OH)Pd(PCC)]···H_2O (**23···H_2O**). Selected bond lengths (Å) reported. H atoms on the pincer and ^{t}Bu groups on phosphorus omitted for clarity. Atom color code: gray, C; white, H; red, O; blue, N; purple, P; orange, Pd.

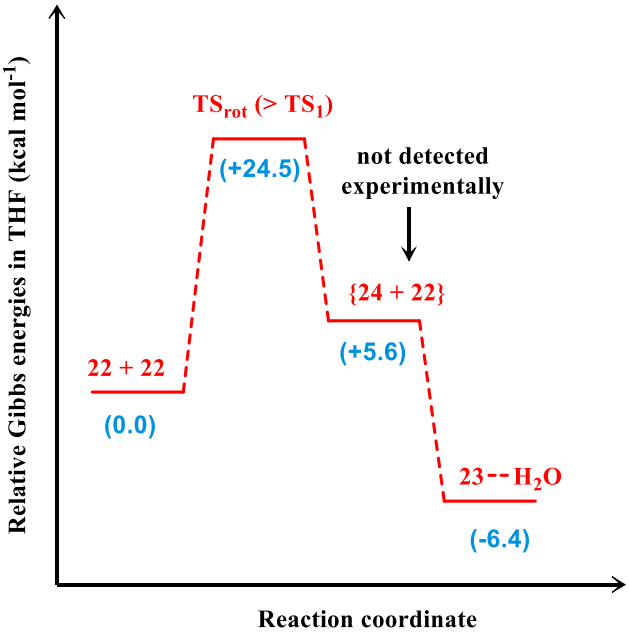

Figure 3.12. Gibbs energy (THF) vs. reaction coordinate profile for the formation of the dinuclear species **23···H_2O** starting from the hydroxide complex **22**.

Synthesis of the protected PCN^{Me} ligand and the corresponding species of the [(PCN^{Me})Pd]$^{+}$ fragment: Conversion of the mononuclear hydroxide complex **22** to the rollover cyclometallated dinuclear **23** should be inhibited if the 5-position of the pyrazolyl ring is blocked. With this in mind, the ligand PCN^{Me}, which bears a methyl group at the 5-position of the pyrazolyl was prepared (**Scheme 3.7**). The PCN^{Me} ligand was synthesized following a

similar preparation from the PCN^H ligand, but starting from the previously reported 3-(5-methyl-1H-pyrazol-1-yl)benzaldehyde.[6b] The phosphine arm was installed from the benzyl-bromide derivative, which after workup gave the analytically pure white viscous and air-sensitive oil in 52% isolated yields from the aldehyde starting complex shown in **Scheme 3.7**.

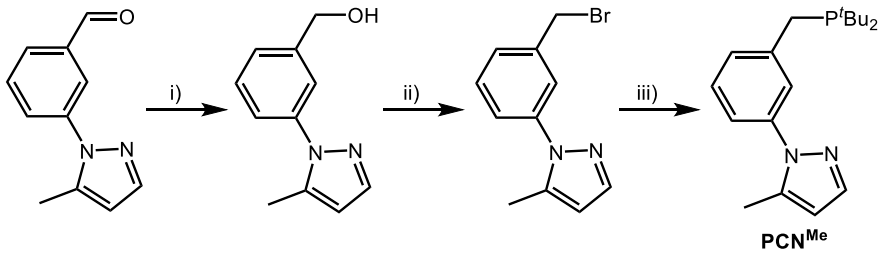

Scheme 3.7. Synthesis of the **PCN^{Me}** pincer ligand. Reagents and conditions: i) $NaBH_4$, EtOH, rt, 1 h; ii) Br_3CCO_2Et, PPh_3, CH_2Cl_2, rt, 0.5 h; iii) $^tBu_2PH$, acetone, reflux, 12 h.

Metallation of PCN^{Me} onto Pd^{II} to form the chloride complex (PCN^{Me})Pd-Cl (**25**) was carried out in an analogous manner to the metallation of PCN^H (*vide supra* and **Scheme 3.8**). Complex **25** was characterized by multinuclear $^{31}P\{^1H\}$, ^1H and $^{13}C\{^1H\}$ NMR spectroscopy as well as by single-crystal X-ray diffraction. Similar to its PCN^H analogue **17**, complex **25** displays C_s symmetry in solution. The spectroscopic signals for **25** are nearly identical to **17**, with the exception of the appearance of a methyl signal in the ^1H and $^{13}C\{^1H\}$ NMR spectra at 2.71 and 13.9 ppm, respectively, and a corresponding loss of the pyz-H signal at the 5-position. A singlet at 93.3 ppm is observed in the $^{31}P\{^1H\}$ NMR spectrum. An ORTEP[14] of the solid-state structure of **25** is reported in **Figure 3.13**. The bond distances and angles of **25** are very similar to **17**.

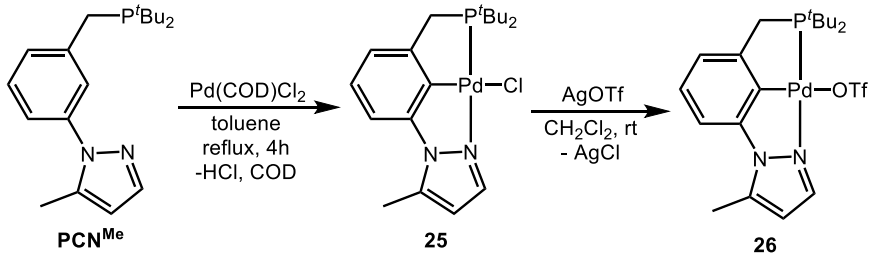

Scheme 3.8. Synthesis of the chloride (**25**) and triflate (**26**) pincer complexes of PCN^{Me}.

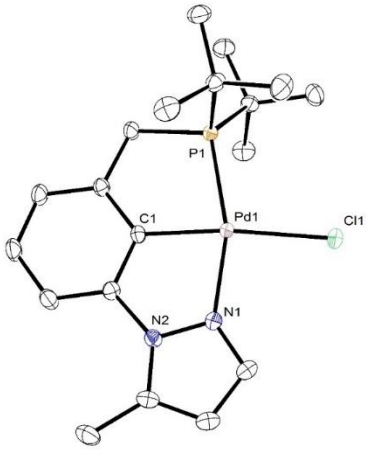

Figure 3.13. Single molecule ORTEP[14] of complex (PCN^{Me})Pd-Cl (**25**) with ellipsoids shown at 50% probability. Hydrogen atoms bound to carbon atoms are omitted for clarity.

When **25** was treated with 1 equivalent of AgOTf in CH_2Cl_2 at room temperature, AgCl precipitation occurred over 5 h and the Pd^{II} triflate complex, (PCN^{Me})Pd-OTf (**26**, **Scheme 3.8**) was formed. Complex **26** was characterized by NMR spectroscopy, X-ray diffraction and elemental analysis. The ^{1}H and ^{13}C{^{1}H} NMR spectra of **26** are very similar to those of the non-methylated analogue **18**, differing by the appearance a methyl resonance at 2.68 ppm and 14.56 ppm, respectively. The ^{31}P{^{1}H} NMR spectrum of **26** displays a singlet at 92.1 ppm. Similar to **18**, the solid-state structure of **26** shows a square planar complex with the triflate ligand directly bound to the Pd^{II} center (**Figure 3.14**). The physical metrics of **26** are closely related to the PCN^{H} analogue **18**, diverging with respect to the Pd-N interaction; a shorter Pd-

N distance of 2.0779(16) Å is found in **26** as compared to 2.112(2) Å in **18**. **Table 3.2** lists a selection of bond lengths and angles of X-ray structure of **26**.

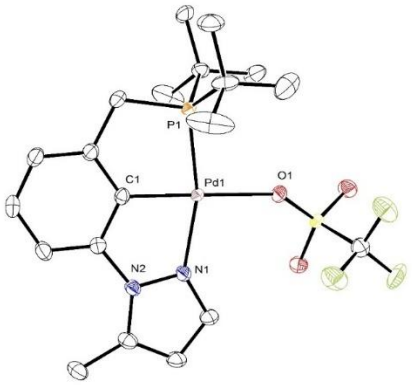

Figure 3.14. Single molecule ORTEP[14] of complex (PCN^{Me})Pd-OTf **(26)** with ellipsoids shown at 50% probability. Hydrogen atoms bound to carbon atoms are omitted for clarity.

When 0.5 equivalents of KOH were added to a solution of **26** in THF (**Scheme 3.9**), formation of a new species **27** was observed by $^{31}P\{^{1}H\}$ NMR spectroscopy through the appearance of a new singlet at 91.6 ppm. This chemical shift variation (from the triflate species **26** at 92.1 ppm) was very similar to the shift observed going from **18** to **19** in the PCN^{H} system, suggesting that a similar μ-OH species had formed. Indeed, **27** was identified as the symmetric dinuclear species, {[(PCN^{Me})Pd]$_2$(μ-OH)}[OTf], by NMR spectroscopy and single-crystal X-ray diffraction. The ^{1}H NMR spectrum shows a diagnostic Pd-OH signal at -1.46 ppm and integration of the ^{1}H NMR signals was consistent with the presence of two equivalents of PCN^{Me} ligand per hydroxide group. Similar to **19**, the ^{t}Bu protons in **27** are diastereotopic and appear as two doublets at 1.43 and 1.49 ppm ($^{3}J_{PH}$ = 14.0 Hz and 14.2 Hz, respectively). The solid state structure (**Figure 3.15**) displays two nearly identical [(PCN^{Me})Pd]$^{+}$ fragments equally sharing the bridging hydroxide ligand. An outersphere triflate counterion is associated with the dinuclear species. While the Pd-N distance of **27** is comparable to **19**, the Pd-P bond

of **27** (2.2381(11) Å) is lengthened compared to **19** (2.218(2) Å). Otherwise, the physical metrics in the solid state between **27** and **19** are nearly indistinguishable. Select bond lengths and angles for **27** are listed in **Table 3.2**.

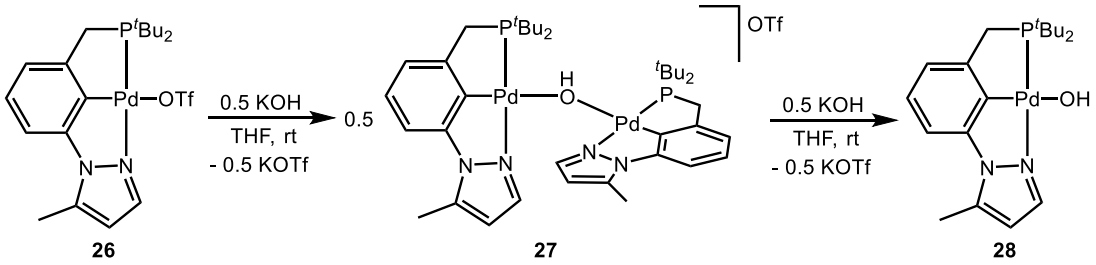

Scheme 3.9. Synthesis of the hydroxide (**27**, **28**) pincer complexes of (PCN^{Me})Pd^{II}.

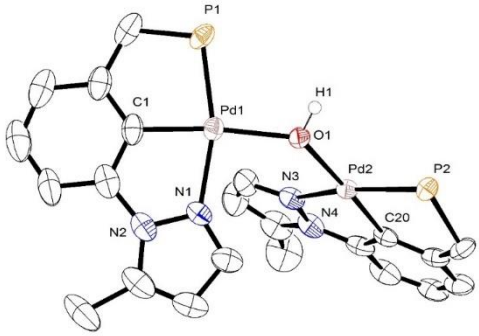

Figure 3.15. ORTEP[14] of the {[(PCN^{Me})Pd]$_2$(μ-OH)}[OTf] salt (**27**), with ellipsoids shown at 50% probability. Hydrogen atoms and ^{t}Bu groups on P omitted for clarity. Because of the explicit disorder, the model seemed incomplete, indicated by an elevated second parameter in the weighting scheme. SQUEEZE[28] was used to resolve the situation and remove the solvent and triflate molecules.

Addition of a full equivalent of KOH to the bridging dinuclear hydroxide complex **27**, or addition of an excess of KOH to the mononuclear triflate complex **26** cleanly yielded a new product **28** as observed by NMR spectroscopy (**Scheme 3.9**). A singlet at 90.2 ppm appeared with no additional signals in the $^{31}P\{^1H\}$ NMR spectrum. The similarity of the reaction and the chemical shift change to that found for the PCN^H analogue is suggestive that **28** is a monomeric Pd^{II} hydroxide complex. Indeed, a new signal was observed at −1.97 ppm in the ^1H NMR spectrum, corresponding to a palladium hydroxide group. The upfield signal

integrated to one equivalent relative to the PCN^{Me} signals. The $^{13}C\{^{1}H\}$ NMR signals for this complex were also consistent with the assignment of **28** as (PCN^{Me})Pd-OH. While the reaction of the palladium triflate complex **26** or the dinuclear bridging hydroxide complex **27** with KOH produced **28**, it was also determined that the same complex could be prepared directly from the chloride **25**. Thus, a metathesis reaction between **25** and an excess of KOH in THF performed with sonication, yielded **28** directly with no observation of any bridging species like **27**. As hypothesized, the mononuclear hydroxide complex **28** was not found to undergo further reaction (*i.e.* "rollover" cyclometallation) as was observed for the PCN^{H} analogue **22**. Thus, it was possible to purify complex **28** through crystallization and X-ray diffraction was used to confirm the solid-state structure (**Figure 3.16**). A list of select bond lengths and angles for **28** is compiled in **Table 3.2**.

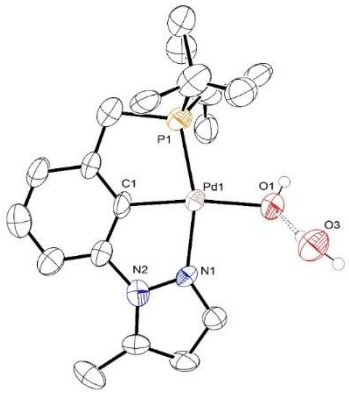

Figure 3.16. ORTEP[14] of (PCN^{Me})Pd-OH **28**, with ellipsoids shown at 50% probability. Hydrogen atoms and THF solvent molecules omitted for clarity. The Pd-OH···H_2O hydrogen bond between the hydroxyl group and the crystallization water molecule is depicted with a yellow dotted line.

Complex **28** crystallizes in the orthorhombic $P2_12_12$ space group, with 2 monomers, 2 water molecules and 3 disordered THF solvent molecules per asymmetric unit. The square planar Pd^{II} center is bound by the tridentate PCN^{Me} ligand with a hydroxide ligand occupying the fourth coordination site. Each complex is hydrogen bound to a symmetry related copy of

itself *via* two water molecules and the hydroxyl ligand. This water-bridged mode has been observed previously in terminal hydroxides.[21,29] The $[(PCN^{Me})Pd]^{+}$ fragment has similar metrics (bond angles and distances) to the other monomeric $(PCN^{H,Me})$Pd-X (X = Cl, OTf) structures described above. The Pd−O bond length [2.078(7) and 2.080(7) Å from two molecules in the asymmetric unit] is comparable to that found in the handful of other monomeric Pd^{II}−OH complexes that have been characterized in the solid state (mean CSD value = 2.05 Å).[30] For example, the Pd^{II}-OH bond length reported for the pincer complex ($^{t\text{Bu}}$PCP)PdOH···H_2O was 2.095 Å.[31]

3.3 Summary

The synthesis and characterization of a new unsymmetrical pincer ligand scaffold and complexation of these novel PCN ligands to Pd^{II} has been reported. With a bulky phosphine and a less sterically hindered pyrazoyl as the arms on the PCN pincer ligand, both mononuclear and dinuclear Pd^{II} hydroxide complexes were formed and characterized. Furthermore, a pyrazoyl ring "rollover" activation at the metal center was observed on a pyrazolyl pincer complex bearing an available C-H bond at the 5-position of the pyrazolyl side-arm. Observation of this reactivity provides opportunities for the synthesis of new derivatives of the dianionic tridentate $(PCC)^{2-}$ fragment and it also serves as a warning to those interested in exploiting the "stability" of PCN ligated structures. Notably, the use of the methylated analogue (PCN^{Me}) inhibits the "rollover" reactivity, allowing for a clean isolation of the mononuclear hydroxide species. The reactivity of these mono- and dinuclear hydroxide species was investigated and will be discussed in Chapter 4.

3.4 Experimental

General considerations and materials characterization. All air- and/or moisture-sensitive reactions were performed under inert atmosphere in flame-dried flasks using standard Schlenk-type techniques or in a glove-box filled with nitrogen. Tetrahydrofuran (THF) was purified by distillation from sodium/benzophenone ketyl, after drying over KOH. Benzene, *n*-hexane, pentane, CH_3CN and toluene were purified by distillation from sodium/triglyme benzophenone ketyl or were obtained by means of a MBraun solvent purification system. THF-d_8, benzene-d_6 and toluene-d_8 were dried over sodium/benzophenone ketyl, condensed *in vacuo* over activated 4Å molecular sieves and degassed by several freeze-pump-thaw cycles prior to use. CD_2Cl_2 was dried over activated 4 Å molecular sieves. All other reagents and solvents were used as purchased from commercial suppliers. ^1H, $^{13}C\{^1H\}$ and $^{31}P\{^1H\}$ NMR spectra were obtained on either a Bruker Avance 700, Bruker Avance 500, Bruker Avance DRX-400 or a Bruker Avance 300 MHz instrument. Chemical shifts are reported in ppm (δ) relative to TMS, referenced to the chemical shifts of residual solvent resonances (^1H and ^{13}C), and coupling constants are given in Hz. $^{31}P\{^1H\}$ NMR spectra are referenced to an external 85% H_3PO_4 sample (0 ppm). The N, C, H elemental analyses were carried out at ICCOM by means of a Carlo Erba Model 1106 elemental analyzer or at the CENTC Elemental Analysis Facility at the University of Rochester. The GC/MS analyses were performed on a Shimadzu QP2010S apparatus equipped with a column identical with that used for GC analysis.

X-ray Diffraction Data. X-ray diffraction intensity data were collected on an *Oxford Diffraction XcaliburPX* (**17**, **18** and **25**) equipped with a CCD area detector or on a *Bruker APEX II* (**20**, **21**, **23**, **26**, **27**, **28** and (PCN^H)Pd-ONO_2) diffractometer using a *Mo-K*α radiation

(λ = 0.71073 Å) at low temperature (either T = 100 or 120 K, see **Table 3.1**). The dataset was integrated and scaled using SAINT, SADABS within the APEX2 software package by Bruker.[32] The program used for the data collection was *CrysAlis CCD* 1.171.[33] Data reduction was carried out with the program *CrysAlis RED* 1.171[34] and the absorption correction was applied with the program *ABSPACK* 1.17. Direct methods implemented in *Sir97*[35] were used to solve the structures and the refinements were performed by full-matrix least-squares against F^2 implemented in *SHELX97*.[36] All the non-hydrogen atoms were found from Fourier syntheses of electron density and were refined anisotropically, while the hydrogen atoms were fixed in calculated positions and refined isotropically with the thermal factor depending on the one of the atom to which they are bound (riding model) with C---H distances in the range 0.95-1.00 Angstrom. The geometrical calculations were performed by *PARST97*.[37] The details of crystallographic, collection and refinement data are shown in **Table 3.1**. Molecular plots were produced by the program *ORTEP3*.[14]

Computational Details. Density Functional Theory (DFT) calculations were performed using the *Gaussian09* program (revision C.01).[38] Model structures were optimized with a M06 functional[39] using the SDD/MWB10 pseudopotential and related basis set[40] on the palladium and phosphorus atoms plus a 6-31G* basis set on all the other atoms. Introduction of diffuse functions is essential to well-reproduce conformational equilibria and experimental electron affinities.[41] An extra *d*-type polarization function for P and an extra *f*-type function for Pd were added to the standard set.[42] Gibbs energy calculations to infer relative thermodynamic stabilities were carried out on the real system. The initial guess geometry for the optimization was obtained starting from the XRD structure of the dimeric species **23**. IRC analysis[43] was performed, to find the two minima linked by the related transition structure. When IRC

calculations failed to reach the minima, geometry optimizations from the initial phase of the IRC path were performed. Frequency calculations were made on all the optimized structures, to characterize the stationary points as minima or TSs, as well for the calculation of zero-point energies, enthalpies, entropies and gas phase Gibbs energies at 298 K. Evaluation of the solvent effects was performed through a continuum modeling of the reaction medium. Bulk solvent effects (THF, $\varepsilon = 7.42$) were expressed through the SMD Continuum Model,[44] with the same basis set used for the gas phase optimizations. Gibbs energy in solution was calculated according to the following simplified equation: $G_{THF} = G_{gas} + (E_{THF} - E_{gas})$.

Table 3.1. Collection of the main crystal data and structure refinement details of the compounds presented in this study.

	17	**25**	**18**	**20**	**21**
CCDC number	1048866	1048867	1048868	1061228	1061230
Empirical formula	$C_{18}H_{26}Cl N_2 P Pd$	$C_{19}H_{28}Cl N_2 P Pd$	$C_{38}H_{56}B Cl_5 F_4 N_4 P_2 Pd_2$	$C_{19}H_{26}F_3 N_2 O_3 P Pd S$	$C_{37}H_{53}F_3 N_4 O_4 P_2 Pd_2 S$
FW	443.23	457.25	1107.67	556.85	981.63
T, K	120(2)	120(2)	120(2)	100(2)	100(2)
Crystal system	Orthorhombic	Monoclinic	Orthorhombic	Monoclinic	Monoclinic
Space group	*P 2₁ 2₁ 2₁*	*P 2₁/n*	*P n a 2₁*	*P 2₁/n*	*P 2₁/n*
Unit cell dimensions	*a* [Å] = 11.054(7) *b* [Å] = 12.843(8) *c* [Å] = 13.303(8) α [°] = 90 β [°] = 90 γ [°] = 90	*a* [Å] = 12.302(2) *b* [Å] = 12.201(2) *c* [Å] = 13.250(2) α [°] = 90 β [°] = 100.019(2) γ [°] = 90	*a* [Å] = 30.989(2) *b* [Å] = 12.597(10) *c* [Å] = 11.852(9) α [°] = 90 β [°] = 90 γ [°] = 90	*a* [Å] = 10.0547(4) *b* [Å] = 8.3459(4) *c* [Å] = 25.8456(12) α [°] = 90 β [°] = 92.588(2) γ [°] = 90	a [Å] = 23.6110(11) b [Å] = 15.5658(7) c [Å] = 24.9876(11) α [°] = 90 β [°] = 103.310(3) γ [°] = 90
V, Å^3	1888.6(2)	1958.5(11)	4627(8)	2166.63(17)	8936.9(7)
Z	4	4	4	4	8
D_{calc}, mg/m^3	1.559	1.551	1.590	1.707	1.459
Abs coeff, mm^{-1}	1.209	1.169	1.184	1.076	0.975
F(000)	904	936	2240	1128	4000
Crystal size, mm	0.01 x 0.01 x 0.04	0.1 x 0.1 x 0.3	0.01 x 0.01 x 0.03	0.06 x 0.06 x 0.12	0.07 x 0.10 x 0.15
θ range for collection, [°]	4.30 - 25.85	4.29 - 30.95	4.16 - 26.87	2.14 - 26.50	2.14 - 26.49
Index ranges	$-11 \le h \le 13$ $-13 \le k \le 15$ $-13 \le l \le 16$	$-17 \le h \le 17$ $-17 \le k \le 17$ $-18 \le l \le 18$	$-34 \le h \le 38$ $-14 \le k \le 14$ $-14 \le l \le 14$	$-12 \le h \le 12$ $-10 \le k \le 10$ $-32 \le l \le 32$	$-29 \le h \le 29$ $-19 \le k \le 19$ $-31 \le l \le 31$
Reflns collected	8113	50449	21117	58493	71608
Independent reflns	2862	5771	7191	4483	18320
R_{int}	0.1106	0.0281	0.1177	0.0539	0.1235
Completeness to θ	89.3 (θ = 25.0°)	99.5 (θ = 25.0°)	97.1 (θ = 25.0°)	99.9	99.8
Data / restraints / parameters	2862 / 0 / 214	5771 / 0 / 224	7191 / 1 / 517	4483 / 0 / 277	18320 / 0 / 981
GOF on F^2	0.981	1.110	1.030	1.044	0.867
Final *R* indices *[I>2σ(I)]*	R_1 = 0.0640 wR_2 = 0.0895	R_1 = 0.0219 wR_2 = 0.0501	R_1 = 0.0703 wR_2 = 0.1102	R_1 = 0.0265 wR_2 = 0.0530	R_1 = 0.0615 wR_2 = 0.1159
R indices (all data)	R_1 = 0.1091 wR_2 = 0.1084	R_1 = 0.0262 wR_2 = 0.0522	R_1 = 0.1417 wR_2 = 0.1441	R_1 = 0.0335 wR_2 = 0.0552	R_1 = 0.1597 wR_2 = 0.1372
Largest diff peak and hole, [e Å^3]	1.089 and −0.739	0.582 and −0.587	0.943 and −0.703	0.541 and −0.514	0.730 and −0.730

Table 3.1 *cont.*

	23	**26**	**27**	**28**	**(PCN^{H})Pd-ONO$_2$**
CCDC number	1061233	1061229	1061231	1061232	
Empirical formula	C_{36} H_{52} N_4 O P_2 Pd_2	C_{20} H_{28} F_3 N_2 O_3 P Pd S	C_{38} H_{57} N_4 O P_2 Pd_2	C_{88} H_{148} N_8 O_{11} P_4 Pd_4	C_{18} H_{26} N_3 O_3 P Pd
FW	831.56	570.87	860.62	2043.62	469.79
T, K	100(2)	100(2)	100(2)	100(2)	100(2)
Crystal system	Monoclinic	Monoclinic	Monoclinic	Orthorhombic	Monoclinic
Space group	*P* $2_1/n$	*C* 2/*c*	*P* $2_1/n$	*P* 2_1 2_1 2	P 2_1/n
Unit cell dimensions	*a* [Å] = 12.2394(9) *b* [Å] = 14.7557(10) *c* [Å] = 20.5708(13) α [°] = 90 β [°] = 101.235(3) γ [°] = 90	*a* [Å] = 19.5576(6) *b* [Å] = 19.4772(6) *c* [Å] = 14.2865(5) α [°] = 90 β [°] = 123.118(2) γ [°] = 90	*a* [Å] = 16.2762(6) *b* [Å] = 24.7065(8) *c* [Å] = 24.1256(9) α [°] = 90 β [°] = 105.583(2) γ [°] = 90	*a* [Å] = 15.791(5) *b* [Å] = 16.128(5) *c* [Å] = 18.562(5) α [°] = 90 β [°] = 90 γ [°] = 90	*a* [Å] = 7.9124(5) *b* [Å] = 22.3001(14) *c* [Å] = 11.2644(7) α [°] = 90 β [°] = 96.407(3) γ [°] = 90
V, Å^3	3643.9(4)	4558.0(3)	9345.0(6)	4727(2)	1975.2(2)
Z	4	8	8	2	4
Dcalc, mg/m^3	1.516	1.664	1.223	1.436	1.580
Abs coeff, mm^{-1}	1.108	1.025	0.867	0.876	1.043
F(000)	1704	2320	3544	2128	960
Crystal size, mm	0.22 x 0.22 x 0.30	0.30 x 0.30 x 0.45	0.05 x 0.05 x 0.18	0.05 x 0.05 x 0.12	0.15 x 0.14 x 0.11
θ range for collection, [°]	2.19 - 33.37	2.70 - 26.56	1.87 - 26.45	2.11 - 25.43°	2.04 to 28.39°
Index ranges	$-18 \le h \le 18$ $-22 \le k \le 22$ $-31 \le l \le 31$	$-24 \le h \le 24$ $-24 \le k \le 24$ $-17 \le l \le 17$	$-20 \le h \le 20$ $-30 \le k \le 30$ $-30 \le l \le 30$	$-18 \le h \le 19$ $-19 \le k \le 19$ $-22 \le l \le 22$	-10<=h<=10 0<=k<=29 0<=l<=15
Reflns collected	213749	74676	144883	58367	138227
Independent reflns	14074	4749	19197	8670	4949
Rint	0.0525	0.0233	0.0706	0.1568	0.0301
Completeness to θ	99.6	99.8	99.8	99.7	99.9
Data / restraints / parameters	14074 / 0 / 406	4749 / 0 / 287	19197 / 0 / 877	8670 / 195 / 605	4949 / 0 / 241
GOF on F^2	1.068	1.028	1.005	1.011	1.108
Final *R* indices	R_1 = 0.0255	R_1 = 0.0221	R_1 = 0.0449	R_1 = 0.0637	R_1 = 0.0191
[I>2σ(I)]	wR_2 = 0.0574	wR_2 = 0.0532	wR_2 = 0.1018	wR_2 = 0.1081	wR_2 = 0.0447
R indices (all data)	R_1 = 0.0361 wR_2 = 0.0630	R_1 = 0.0251 wR_2 = 0.0553	R_1 = 0.0708 wR_2 = 0.1092	R_1 = 0.1448 wR_2 = 0.1328	R_1 = 0.0204 wR_2 = 0.0451
Largest diff peak and hole, [e Å^3]	1.856 and −0.988	0.899 and −0.456	1.128 and −1.080	1.032 and −1.016	0.418 and -0.437

Table 3.2. Select bond lengths (Å) and angles (°) for complexes **17**, **25**, **18**, **20**, **26**, **21**, **27**, **28**, and **23**.

	17	**25**	**18**	**20**	**26**	**21**	**27**	**28**	**23**
C(1)-Pd(1)	1.962(14)	1.9689(14)	1.975(15)	1.959(2)	1.9584(18)	1.971(7)	1.959(4)	1.966(9)	1.9816(15)
C(7)-Pd(1)	-	-	-	-	-	-	-	-	2.0477(15)
C(10)-P(1)	1.839(14)	1.8509(15)	1.817(17)	1.844(2)	1.841(2)	1.855(7)	1.847(5)	1.896(14)	1.8547(15)
C(19)-Pd(2)a	-	-	1.972(18)	-	-	1.955(7)	1.966(4)	-	1.9619(15)
N(1)-N(2)	1.372(14)	1.3685(17)	1.368(17)	1.366(3)	1.375(2)	1.389(7)	1.376(5)	1.376(9)	1.3622(18)
N(1)-Pd(1)	2.094(10)	2.0653(14)	2.089(12)	2.112(2)	2.0779(16)	2.098(7)	2.084(3)	2.043(7)	-
N(3)-N(4)	-	-	1.363(17)	-	-	1.350(7)	1.368(5)	-	1.3651(18)
P(1)-Pd(1)	2.227(4)	2.2376(7)	2.249(4)	2.2573(6)	2.2599(5)	2.218(2)	2.2381(11)	2.230(3)	2.3084(4)
Pd(1)-Cl(1)	2.388(4)	2.3949(7)	2.427(4)	-	-	-	-	-	-
Pd(1)-O(1)	-	-	-	2.1752(17)	2.1701(14)	2.103(4)	2.091(3)	2.078(7)	2.1077(11)
Pd(2)-Cl(1)	-	-	2.425(4)	-	-	-	-	-	-
Pd(2)-O(1)	-	-	-	-	-	2.087(5)	2.095(3)	-	2.0831(11)
O(1)-H	-	-	-	-	-	0.84	0.84	0.84	0.95
C(1)-Pd(1)-Cl(1)	175.6(4)	173.09(4)	176.5(5)	-	-	-	-	-	-
C(1)-Pd(1)-O(1)	-	-	-	178.73(9)	179.38(7)	177.42(6)	173.32(2)	171.9(3)	175.00(5)
C(7)-Pd(1)-P(1)	-	-	-	-	-	-	-	-	162.91(5)
C(19)-Pd(2)-Cl(1)	-	-	170.5(5)	-	-	-	-	-	-
C(19)-Pd(2)-O(1)a	-	-	-	-	-	174.7(2)	176.9(1)	-	175.01(6)
P(1)-Pd(1)-N(1)	162.3(3)	161.76(4)	162.1(4)	162.97(6)	163.70(5)	162.48(16)	162.79(11)	162.3(2)	-
P(2)-Pd(2)-N(3)	-	-	163.0(4)	-	-	162.96(17)	162.07(10)	-	162.49(4)
Pd(1)-Cl(1)-Pd(2)	-	-	126.30(17)	-	-	-	-	-	-
Pd(1)-O(1)-Pd(2)	-	-	-	-	-	130.48(6)	130.7(1)	-	134.28(6)

[a] For complex **27**, this is the C(20)-Pd(2) bond length.

The syntheses of PCN^{H} and PCN^{Me} were performed by our collaborators in the Giambastiani group, and details can be found in our published report.[13]

PCN^{H}: $^{31}P\{^{1}H\}$ NMR (121 MHz, CD_2Cl_2, 293K): δ 35.2 (s). ^{1}H NMR (300 MHz, CD_2Cl_2, 293K): δ 1.18 (d, $^{3}J_{PH}$ = 10.8 Hz, 18H, P-C(C*H*$_3$)$_3$), 2.94 (d, $^{2}J_{PH}$ = 2.8 Hz, 2H, Ar-C*H*$_2$-P), 6.48 (m, 1H, C*H*), 7.38-7.30 (m, 2H, C*H* Ar), 7.48 (m, 1H, C*H* Ar), 7.69 (m, 1H, C*H*), 7.75 (m, 1H, C*H* Ar), 7.98, (m, 1H, C*H*). $^{13}C\{^{1}H\}$ NMR (75 MHz, CD_2Cl_2, 293 K): δ 28.5 (d, $^{1}J_{PC}$ = 24.7 Hz, Ar-*C*H$_2$-P), 29.5 (d, $^{2}J_{PC}$ = 13.2 Hz, P-C(*C*H$_3$)$_3$), 31.6 (d, $^{1}J_{PC}$ = 22.7 Hz, P-*C*(CH$_3$)$_3$), 107.2 (s), 115.8 (s), 120.1 (d, J_{PC} = 9.3 Hz), 126.6 (s), 127.6 (d, J_{PC} = 8.5 Hz), 129.0 (s), 140.0 (s), 140.7 (s), 143.8 (d, J_{PC} = 13.0 Hz). Anal. Calcd (%) for $C_{18}H_{27}N_2P$ (302.39): C 71.49, H 9.00, N, 9.26; found: C 71.60, H 9.21, N, 9.30.

PCN^{Me}: $^{31}P\{^{1}H\}$ NMR (121 MHz, CD_2Cl_2, 293K): δ 35.7 (s). ^{1}H NMR (300 MHz, CD_2Cl_2, 293K): δ 1.16 (d, $^{3}J_{PH}$ = 10.8 Hz, 18H, P-C(C*H*$_3$)$_3$), 2.34 (s, 3H, C*H*$_3$), 2.92 (d, $^{2}J_{PH}$ = 2.8 Hz, 2H, Ar-C*H*$_2$-P), 6.20 (m, 1H, C*H*), 7.24-7.20 (m, 1H, C*H* Ar), 7.38-7.34 (m, 2H, C*H* Ar), 7.45 (br s, 1H, C*H* Ar), 7.53 (m, 1H, C*H*). $^{13}C\{^{1}H\}$ NMR (75 MHz, CD_2Cl_2, 293 K): δ 12.2 (s), 28.3 (d, $^{1}J_{PC}$ = 24.7 Hz, Ar-*C*H$_2$-P), 29.4 (d, $^{2}J_{PC}$ = 13.2 Hz, P-C(*C*H$_3$)$_3$), 31.7 (d, $^{1}J_{PC}$ = 22.7 Hz, P-*C*(CH$_3$)$_3$), 106.5 (s), 121.6 (s), 125.8 (d, J_{PC} = 9.2 Hz), 128.6 (s), 128.7 (d, J_{PC} = 8.4 Hz), 138.7 (s), 139.4 (s), 143.4 (d, J_{PC} = 12.7 Hz). Anal. Calcd (%) for $C_{19}H_{29}N_2P$ (316.42): C 72.12, H 9.24, N 8.85; found: C 72.33, H 9.40, N 8.92.

General procedure for the synthesis of the chloride complexes 17 and 25: To a stirred solution of the selected PCN^{R} ligand (R= H, **PCN^{H}**; R = Me, **PCN^{Me}**) (0.5 mmol) in dry and degassed toluene (3 mL), a suspension of $Pd(COD)Cl_2$ (0.50 mmol) in dry and degassed toluene (4 mL) was added in one portion. The reaction mixture was stirred at reflux for 4 h and

was allowed to cool to rt. Afterwards, the solvent was removed in *vacuo* to give a crude mixture as a yellow pale viscous material. The crude sample was washed with pentane and filtered to afford analytically pure white crystals of **17** and **25** in 90 % and 93 % isolated yield, respectively. For both palladium compounds, crystals suitable for X-ray diffraction analysis were growth from concentrated acetone solutions.

(PCN^{H})Pd-Cl (17): $^{31}P\{^{1}H\}$ NMR (161 MHz, CD_2Cl_2, 293K): δ 95.0 (s). ^{1}H NMR (400 MHz, CD_2Cl_2, 293K): δ 1.48 (d, $^{3}J_{PH}$ = 14.3 Hz, 18H, P-C(C*H*$_3$)$_3$), 3.41 (d, $^{2}J_{PH}$ = 9.3 Hz, 2H, Ar-C*H*$_2$-P), 6.55 (m, 1H, C*H*), 7.06-7.15 (m, 3H, C*H* Ar), 7.98-8.02 (m, 2H, C*H* Ar). $^{13}C\{^{1}H\}$ NMR (100 MHz, CD_2Cl_2, 293 K): δ 29.2 (d, $^{2}J_{PC}$ = 4.3 Hz, P-C(*C*H$_3$)$_3$), 35.3 (d, $^{1}J_{PC}$ = 31.6 Hz, Ar-*C*H$_2$-P), 35.6 (d, $^{1}J_{PC}$ = 19.7 Hz, P-*C*(CH$_3$)$_3$), 107.1 (s), 110.1 (s), 122.5 (d, $^{3}J_{PC}$ = 20.4 Hz), 125.7 (s), 126.0 (s), 139.3 (s), 143.7 (s), 148.6 (s), 150.3 (d, $^{3}J_{PC}$ = 14.0 Hz). Anal. Calcd (%) for $C_{18}H_{26}ClN_2PPd$ (443.26): C 48.77, H 5.91, N 6.32; found C 48.82, H 5.97, N 6.39.

(PCN^{Me})Pd-Cl (25): $^{31}P\{^{1}H\}$ NMR (161 MHz, CD_2Cl_2, 293K): δ 93.3 (s). ^{1}H NMR (400 MHz, CD_2Cl_2, 293K): δ 1.48 (d, $^{3}J_{PH}$ = 14.2 Hz, 18H, P-C(C*H*$_3$)$_3$), 2.71 (s, 3H, C*H*$_3$), 3.39 (d, $^{2}J_{PH}$ = 9.4 Hz, 2H, Ar-C*H*$_2$-P), 6.29 (m, 1H, C*H*), 7.06 (m,1H, C*H*), 7.13 (m,1H, C*H*), 7.23 (m, 1H, C*H* Ar), 7.91 (m, 1H, C*H* Ar). $^{13}C\{^{1}H\}$ NMR (100 MHz, CD_2Cl_2, 293 K): δ 13.9 (s, *C*H$_3$), 28.8 (d, $^{2}J_{PC}$ = 4.3 Hz, P-C(*C*H$_3$)$_3$), 34.9 (d, $^{1}J_{PC}$ = 28.7 Hz, Ar-*C*H$_2$-P), 35.0 (d, $^{1}J_{PC}$ = 17.4 Hz, P-*C*(CH$_3$)$_3$), 108.0 (s), 111.3 (s), 121.6 (d, $^{3}J_{PC}$ = 20.4 Hz), 125.0 (s), 138.4 (s), 140.1 (s), 144.9 (s), 149.0 (s), 150.1 (d, $^{3}J_{PC}$ = 14.4 Hz). Anal. Calcd (%) for $C_{19}H_{28}ClN_2PPd$ (457.29): C 49.90, H 6.17, N 6.13; found C 49.93, H 6.21, N 6.15.

{[(PCN^{H})Pd]$_2$(μ-Cl)}[BF$_4$] (18): To a stirred solution of **17** (0.100 g, 0.23 mmol) in dry and degassed CH_2Cl_2 (10 mL), 0.5 equivalents of $AgBF_4$ (0.022 g, 0.11 mmol) was added under a

nitrogen atmosphere. The resulting mixture was stirred at rt for 5 h, then the solution was filtered *via* cannula and concentrated to approximately one-third of its initial volume. To this concentrated solution was added dropwise dry and degassed pentane until the formation of a precipitate. The final pale yellow solid was washed with several portions of pentane and dried under vacuum for 1 h (0.062 g, 60 % isolated yield). Crystals suitable for X-ray diffraction were obtained from a concentrated solution of the complex in a mixture of CH_2Cl_2/pentane cooled at -30 °C.

$^{31}P\{^1H\}$ NMR (121 MHz, CD_2Cl_2, 293K): δ 95.1 (s). ^1H NMR (300 MHz, CD_2Cl_2, 293K): δ 2.17 (d, $^3J_{PH}$ = 14.4 Hz, 36H, P-C(C*H*$_3$)$_3$), 3.44 (d, $^2J_{PH}$ = 8.7 Hz, 2H, Ar-C*H*$_2$-P, H), 6.39 (m, 2H, C*H*), 7.11-7.16 (6H, C*H* Ar), 8.03-8.09 (4H, C*H* Ar). $^{13}C\{^1H\}$ NMR (75 MHz, CD_2Cl_2, 293 K): δ 28.8 (d, J_{PC} = 3.5 Hz, P-C(*C*H$_3$)$_3$), 34.0 (d, J_{PC} = 30.3 Hz, Ar-*C*H$_2$-P), 35.6 (d, J_{PC} = 17.5 Hz, P-*C*(CH$_3$)$_3$), 107.2 (s), 110.6 (s), 122.8 (d, J_{PC} = 20.5 Hz), 126.6 (s), 139.8 (s), 142.9 (s), 144.6 (s), 149.8 (d, J_{PC} = 13.3 Hz). $^{11}B\{^1H\}$ NMR (96 MHz, CD_2Cl_2, 293K): δ -1.1. Anal. Calcd (%) for $C_{36}H_{52}BClF_4N_4P_2Pd_2$ (937.87): C 46.10, H 5.59, N 5.97; found C 46.20, H 5.63, N 5.93.

[(PCN^H)Pd(MeCN)][BF$_4$] (19): To a stirred solution of **17** (0.100 g, 0.23 mmol) in dry and degassed CH_2Cl_2 (5 mL), dry and degassed CH_3CN (23 µL, 0.44 mmol) and $AgBF_4$ (0.065 g, 0.33 mmol) were added in sequence, under nitrogen atmosphere. The resulting mixture was stirred at rt for 5 h, then the solution was filtered *via* cannula and concentrated to approximately three-fourth of its initial volume. To this concentrated solution was added dropwise dry and degassed pentane until the formation of a precipitate. The final white solid was washed with several portions of pentane and dried under vacuum for 1 h (0.090 g, 75 % isolated yield).

$^{31}P\{^{1}H\}$ NMR (161 MHz, CD_2Cl_2, 293K): δ 98.2 (s). ^{1}H NMR (400 MHz, CD_2Cl_2, 293K): δ 1.41 (d, $^{3}J_{PH}$ = 14.7 Hz, 18H, P-C(C*H*$_3$)$_3$), 2.51 (s, 1H, C*H*$_3$CN), 3.43 (d, $^{2}J_{PH}$ = 9.6 Hz, 2H, Ar-C*H*$_2$-P), 6.64 (m, 1H, C*H*), 7.07 (m, 1H, C*H* Ar), 7.13 (m, 1H, C*H* Ar), 7.20 (m, 1H, C*H* Ar), 7.90 (m, 1H, C*H* Ar), 8.07 (m, 1H, C*H* Ar). $^{13}C\{^{1}H\}$ NMR (100 MHz, CD_2Cl_2, 293 K): δ 2.9 (s, *C*H$_3$CN), 28.6 (d, $^{2}J_{PC}$ = 4.2 Hz, P-C(*C*H$_3$)$_3$), 33.7 (d, $^{1}J_{PC}$ = 31.2 Hz, Ar-*C*H$_2$-P), 35.5 (d, $^{1}J_{PC}$ = 17.7 Hz, P-*C*(CH$_3$)$_3$), 107.8 (s), 110.6 (s), 122.7 (d, J_{PC} = 21.0 Hz), 126.8 (s), 126.9 (s), 140.5 (s), 143.3 (s), 143.4 (s), 150.4 (d, J_{PC} = 13.5 Hz). $^{11}B\{^{1}H\}$ NMR (128 MHz, CD_2Cl_2, 293K): δ -1.0. Anal. Calcd (%) for $C_{20}H_{29}BF_4N_3PPd$ (535.66): C 44.84, H 5.46, N 7.84; found C 44.88, H 5.50, N 7.80.

(PCN^{H})Pd-ONO$_2$. $AgNO_3$ (26.3 mg, 0.155 mmols) and (PCN)PdCl (59.0 mg, 0.133 mmols) were dissolved in THF (5 mL) and stirred at 80 °C for 16 h in the absence of light. The light brown suspension was then filtered through Celite®. Solvent removal yielded (PCN^{H})PdONO$_2$ as a light yellow solid (58.0 mg, 93% yield). Crystals suitable for X-ray diffraction were grown from slow diffusion of pentane into a concentrated THF solution of (PCN^{H})PdONO$_2$. The solid state structure is shown in **Figure 3.17**.

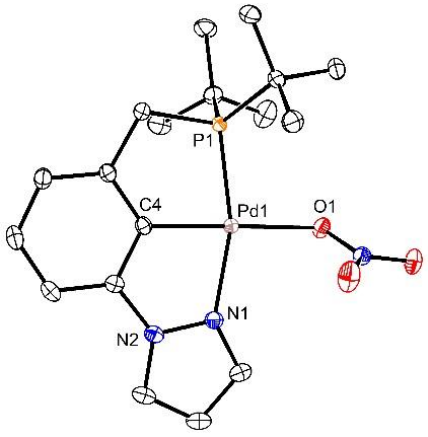

Figure 3.17. ORTEP[14] of the (PCN^{H})PdONO$_2$ with ellipsoids shown at 50% probability. Hydrogen atoms omitted for clarity.

$^{31}P\{^{1}H\}$ NMR (THF-d_8) δ 93.2 (s). ^{1}H NMR (500 MHz, THF-d_8) δ 1.41 (d, $^{3}J_{PH}$ = 14.3 Hz, 18H, P-C(CH_3)$_3$), 3.43 (d, $^{2}J_{PH}$ = 9.5 Hz, 2H, Ar-CH_2-P), 6.54 (m, 1H), 6.98 (d, $^{3}J_{HH}$ = 7.6 Hz, 1H), 7.06 (td, $^{3}J_{HH}$ = 7.7, 1.5 Hz, 1H), 7.21 (d, $^{3}J_{HH}$ = 7.9 Hz, 1H), 7.68 (s, 1H), 8.32 (d, $^{3}J_{HH}$ = 2.7 Hz, 1H).

(PCN^{H})Pd-OTf (20). AgOTf (33.0 mg, 0.128 mmols) was added to a solution of **17** (51.2 mg, 0.116 mmols) in CH_2Cl_2 (2 mL) in the absence of light. The suspension was allowed to stir for 4 h, and filtered through Celite®. Solvent removal yielded **20** as an off white solid (62.7 mg, 97% yield). Recrystallization from layering pentane on a concentrated solution of **20** in CH_2Cl_2 yielded clear crystals that were suitable for X-ray crystallography.

$^{31}P\{^{1}H\}$ NMR (202 MHz, CD_2Cl_2) δ 94.1 (s). ^{1}H NMR (500 MHz, CD_2Cl_2) δ 1.43 (d, $^{3}J_{PH}$ = 14.5 Hz, 18H, P-C(CH_3)$_3$), 3.31 (d, $^{2}J_{PH}$ = 9.6 Hz, 2H, Ar-CH_2-P), 6.55 (m, 1H, C*H*), 7.01 (dd, $^{3}J_{HH}$ = 7.6 Hz, 0.9 Hz, 1H, C*H*), 7.05 (d, $^{3}J_{HH}$ = 7.9 Hz, 1H, C*H*), 7.14 (td, $^{3}J_{HH}$ = 7.8, 1.3 Hz, 1H, C*H*), 7.98-7.99 (m, 1H, C*H*), 8.32-8.33 (m, 1H, C*H*). $^{13}C\{^{1}H\}$ NMR (176 MHz, CD_2Cl_2) δ 28.9 (d, $^{2}J_{PC}$ = 4.3 Hz, P-C(*C*H$_3$)$_3$), 33.0 (d, $^{1}J_{PC}$ = 30.6 Hz, Ar-*C*H$_2$-P), 35.7 (d, $^{1}J_{PC}$ = 17.6 Hz, P-*C*(CH$_3$)$_3$), 107.8 (d, J_{PC} = 3.7 Hz), 110.7 (s), 122.9 (d, J_{PC} = 20.8 Hz), 126.4 (s), 126.6 (s), 139.8 (s), 142.6 (d, J_{PC} = 2.8 Hz), 143.5 (s), 150.7 (d, J_{PC} = 13.7 Hz). Anal. Calc. for $C_{19}H_{26}F_3N_2O_3PPdS$: C, 40.98; H, 4.71; N, 5.03. Found: C, 40.97; H, 4.56; N, 4.96.

{[(PCN^{H})Pd]$_2$(μ-OH)}[OTf] (21). Ground KOH (1.4 mg, 0.0250 mmols, 1 eq.) was added to a solution of **20** (26.7 mg, 0.0479, 2 eq.) in THF (3 mL) and stirred for 24 h. The golden mixture was filtered through Celite® and concentrated (*ca*. 1 mL). The product was crystallized in a pentane-vapor diffusion chamber at -30 °C. The isolated golden crystals of **21** were suitable for X-ray crystallography (16.0 mg, 68% yield).

$^{31}P(^{1}H\}$ NMR (202 MHz, THF-d_8) δ 93.3 (s). ^{1}H NMR (500 MHz, THF-d_8) δ -1.48 (s, 1H, Pd-O*H*), 1.44 (d, $^{3}J_{PH}$ = 14.1 Hz, 18H, P-C(CH_3)$_3$), 1.51 (d, $^{3}J_{PH}$ = 14.3 Hz, 18H, P-C(CH_3)$_3$), 3.54 (dd, $^{2}J_{PH}$ = 9.3 Hz, $^{2}J_{HH}$ = 18.1 Hz, 2H, Ar-CH_2-P), 3.58 (dd, $^{2}J_{PH}$ = 10.2 Hz, $^{2}J_{HH}$ = 18.1 Hz, 2H, Ar-CH_2-P), 6.40-6.42 (m, 2H, C*H*), 7.07 (dd, $^{3}J_{HH}$ = 7.7, 1.1 Hz, 2H, C*H*), 7.11 (td, $^{3}J_{HH}$ = 7.7, 1.3 Hz, 2H, C*H*), 7.34 (dd, $^{3}J_{HH}$ = 7.8, 1.1 Hz, 2H, C*H*), 8.32-8.33 (m, 2H, C*H*), 8.45-8.46 (m, 2H, C*H*). $^{13}C\{^{1}H\}$ NMR (176 MHz, THF-d_8) δ 29.31 (d, $^{2}J_{PC}$ = 4.4 Hz, P-C(*C*H$_3$)$_3$), 29.52 (d, $^{2}J_{PC}$ = 4.4 Hz, P-C(*C*H$_3$)$_3$), 34.88 (d, $^{1}J_{PC}$ = 31.3 Hz, Ar-*C*H$_2$-P), 35.86 (d, $^{1}J_{PC}$ = 17.6 Hz, P-*C*(CH$_3$)$_3$), 36.13 (d, $^{1}J_{PC}$ = 17.6 Hz, P-*C*(CH$_3$)$_3$), 107.56 (d, J_{PC} = 3.3 Hz), 111.48 (s), 123.34 (d, J_{PC} = 21.1 Hz), 126.62 (s), 128.11 (s), 140.41 (d, J_{PC} = 1.9 Hz), 144.59 (s), 144.65 (s), 151.13 (d, J_{PC} = 14.1 Hz). Anal. Calc. for $C_{37}H_{53}F_3N_4O_4P_2Pd_2S$: C, 45.27; H, 5.44; N, 5.71. Found: C, 46.17; H, 5.51; N, 5.49.

(PCN^{H})Pd-OH (22) and [(PCN^{H})Pd(μ-OH)](Pd(PCC)) (23). In a medium-walled NMR tube with a resealable Teflon pin, ground KOH (0.8 mg, 0.0143 mmols) was added to a solution of **20** (7.0 mg, 0.0126 mmols) in THF-d_8 (0.4 mL). The mixture was shaken intermittently until full conversion to **21** was observed by NMR spectroscopy. An excess of ground KOH (1.2 mg, 0.214 mmols) was then added and the NMR tube was rotated slowly using a NMR tube rotary device over 16 h. Full conversion of **21** to a mixture of **22** (70% yield based on internal standard, hexamethylbenzene) and **23** was observed by NMR spectroscopy. Compound **22** can also be prepared by the addition of D_2O (0.1 mL) to a THF-d_8 (0.4 mL) solution of **21** (5.0 mg, 8.98 μmol) containing suspended KOH (0.6 mg, 10.7 μmol). Using this procedure, the resulting solution contained only **22** as determined by solution NMR spectroscopy.

22: $^{31}P(^{1}H\}$ NMR (202 MHz, THF-d_8) δ 91.9 (s). ^{1}H NMR (500 MHz, THF-d_8) δ -1.71 (s, 1H, Pd-O*H*), 1.43 (d, $^{3}J_{PH}$ = 13.9 Hz, 18H, P-C(CH_3)$_3$), 3.38 (d, $^{2}J_{PH}$ = 9.2 Hz, 2H, Ar-CH_2-P), 6.49

(m, 1H, C*H*), 6.92-6.95 (m, 2H, C*H*), 7.15 (m, 1H, C*H*), 8.05 (m, 1H, C*H*), 8.30 (m, 1H, C*H*). ^{1}H NMR (700 MHz, THF-d_8/D_2O) δ 1.38 (d, $^{3}J_{PH}$ = 14.1 Hz, 18H, P-C(CH_3)$_3$), 3.36 (d, $^{2}J_{PH}$ = 9.3 Hz, 2H, Ar-CH_2-P), 6.59 – 6.56 (m, 1H, C*H*), 6.93 (d, $^{3}J_{HH}$ = 7.5 Hz, 1H, C*H*), 6.98 (t, $^{3}J_{HH}$ = 7.6 Hz, 1H, C*H*), 7.18 (d, $^{3}J_{HH}$ = 7.8 Hz, 1H, C*H*), 8.08 (m, 1H, C*H*), 8.32 (m, 1H, C*H*). ^{13}C{^{1}H} NMR (176 MHz, THF-d_8/D_2O) δ 29.47 (d, $^{2}J_{PC}$ = 4.8 Hz, P-C(*C*H$_3$)$_3$), 35.61 (d, $^{1}J_{PC}$ = 31.0 Hz, Ar-*C*H$_2$-P), 35.75 (d, $^{1}J_{PC}$ = 17.3 Hz, P-*C*(CH$_3$)$_3$), 107.98 (d, J_{PC} = 3.5 Hz), 110.61 (s), 122.57 (d, J_{PC} = 20.4 Hz), 125.72 (s), 127.21 (s), 140.72 (d, J_{PC} = 2.8 Hz), 144.8 (s), 147.85 (s), 150.96 (d, J_{PC} = 14.5 Hz). LRMS (ESI-MS) m/z: [M – OH]$^{+}$ Calcd for $C_{18}H_{26}N_2PPd$ 407; Found 407.3.

23: ^{31}P(^{1}H} NMR (120 MHz, THF-d_8) δ 71.0 (s, *P trans* to C), 91.1 (s, *P trans* to N). ^{1}H NMR (700 MHz, THF-d_8) δ -1.75 (bs, 1H, Pd-O*H*), 1.36 (d, $^{3}J_{PH}$ = 12.4 Hz, 9H, P-C(CH_3)$_3$), 1.39 (d, $^{3}J_{PH}$ = 12.5 Hz, 9H, P-C(CH_3)$_3$), 1.44 (d, $^{3}J_{PH}$ = 13.8 Hz, 9H, P-C(CH_3)$_3$), 1.51 (d, $^{3}J_{PH}$ = 14.2 Hz, 9H, P-C(CH_3)$_3$), 3.08 (dd, $^{2}J_{PH}$ = 8.9 Hz, $^{2}J_{HH}$ = 17.4 Hz, 1H, Ar-CH_2-P), 3.12 (dd, $^{2}J_{PH}$ = 8.3 Hz, $^{2}J_{HH}$ = 17.4 Hz, 1H, Ar-CH_2-P), 3.42 (dd, $^{2}J_{PH}$ = 9.3 Hz, $^{2}J_{HH}$ = 17.9 Hz, 1H, Ar-CH_2-P), 3.49 (dd, $^{2}J_{PH}$ = 9.3 Hz, $^{2}J_{HH}$ = 17.9 Hz, 1H, Ar-CH_2-P), 6.11-6.12 (m, 1H, C*H*), 6.31-6.32 (m, 1H, C*H*), 6.60 (d, *J* = 7.6 Hz, 1H, C*H*), 6.74 (td, *J* = 7.6, 1.1 Hz, 1H, C*H*), 6.90-6.91 (m, 1H, C*H*), 6.91-6.93 (m, 1H, C*H*), 6.96-6.98 (m, 1H, C*H*), 7.02 (td, *J* = 7.7, 1.0 Hz, 1H, C*H*), 7.16-7.18 (m, 1H, C*H*), 8.17-8.19 (m, 1H, C*H*), 8.74-8.75 (m, 1H, C*H*).

(PCN^{Me})Pd-OTf (26). AgOTf (42.1 mg, 0.164 mmols) was added to a solution of (PCN^{Me})PdCl (75.0 mg, 0.164 mmols) in CH_2Cl_2 (3 mL) in the absence of light. The suspension was allowed to stir for 5 h, and filtered through Celite®. Layering pentane on the CH_2Cl_2 solution at room temperature yielded clear light yellow crystals of **26** suitable for X-ray crystallography (81.8 mg, 87% yield).

$^{31}P\{^{1}H\}$ NMR (202 MHz, CD_2Cl_2) δ 92.1 (s). ^{1}H NMR (500 MHz, CD_2Cl_2) δ 1.42 (d, $^{3}J_{PH}$ = 14.5 Hz, 18H, P-C(C*H*$_3$)$_3$), 2.68 (s, 3H, pyz-C*H*$_3$), 3.29 (d, $^{2}J_{PH}$ = 9.59 Hz, 2H, Ar-C*H*$_2$-P), 6.28 (s, 1H, C*H*), 7.01 (d, $^{3}J_{HH}$ = 7.11 Hz, 1H, C*H*), 7.13 (t, $^{3}J_{HH}$ = 7.11 Hz, 1H, C*H*), 7.19 (d, $^{3}J_{HH}$ = 7.51 Hz, 1H, C*H*), 8.22 (s, 1H, C*H*). $^{13}C\{^{1}H\}$ NMR (126 MHz, CD_2Cl_2) δ 14.56 (s, pyz-*C*H$_3$), 28.96 (d, $^{2}J_{PC}$ = 3.9 Hz, P(C(*C*H$_3$)$_3$)$_2$), 32.96 (d, $^{1}J_{PC}$ = 29.8 Hz, P(*C*(CH$_3$)$_3$)$_2$), 35.49 (d, $^{1}J_{PC}$ = 17.3 Hz, *C*H$_2$P), 109.3 (d, J_{PC} = 2.75 Hz), 112.3 (s), 122.5 (d, J_{PC} = 20.8 Hz), 126.4 (s), 140.6 (d, J_{PC} = 2.1 Hz), 140.9 (s), 141.9 (s), 145.2 (s), 150.9 (d, J_{PC} = 13.8 Hz). Anal. Calc. for $C_{20}H_{28}F_3N_2O_3PPdS$: C, 42.08; H, 4.94; N, 4.91. Found: C, 42.06; H, 4.81; N, 4.75.

{[(PCN^{Me})Pd]$_2$(μ-OH)}[OTf] (27). To a solution of (PCN^{Me})Pd-OTf (14.5 mg, 0.0254 mmols) in THF (3 mL) was added ground KOH (1.0 mg, 0.0178 mmols). The solution was stirred for 16 h after which it was filtered through a teflon filter. The solution was concentrated (*ca*. 1 mL) and recrystallization was accomplished by slow diffusion of pentane into the solution at -30 °C. The dark yellow crystals were washed with water (3 x 1 mL) and dried in vacuum yielding **27** (11.8 mg, 92% yield).

$^{31}P\{^{1}H\}$ NMR (202 MHz, THF-d_8) δ 91.6 (s). ^{1}H NMR (700 MHz, THF-d_8) δ -1.46 (s, 1H, Pd-O*H*), 1.43 (d, $^{3}J_{PH}$ = 14.0 Hz, 18H, P-C(C*H*$_3$)$_3$), 1.49 (d, $^{3}J_{PH}$ = 14.2 Hz, 18H, P-C(C*H*$_3$)$_3$), 2.67 (s, 3H, C*H*$_3$), 3.54 (dd, $^{2}J_{HH}$ = 18.1, $^{2}J_{PH}$ = 10.1 Hz, 2H, Ar-C*H*$_2$-P), 3.58 (dd, $^{2}J_{HH}$ = 18.1, $^{2}J_{PH}$ = 10.0 Hz, 2H, Ar-C*H*$_2$-P), 6.20 (m, 2H, C*H*), 7.10 (dd, $^{3}J_{HH}$ = 7.7 Hz, 1.4 Hz, 2H, C*H*), 7.12 (td, $^{3}J_{HH}$ = 7.6, 1.1 Hz, 2H, C*H*), 7.30 (dd, $^{3}J_{HH}$ = 7.7, 1.4 Hz, 2H, C*H*), 8.34 (m, 2H, C*H*). $^{13}C\{^{1}H\}$ NMR (176 MHz, THF-d_8) δ 14.1 (s, pyz-*C*H$_3$), 29.30 (d, $^{2}J_{PC}$ = 4.0 Hz, P(C(*C*H$_3$)$_3$)$_2$), 29.58 (d, $^{2}J_{PC}$ = 4.0 Hz, P(C(*C*H$_3$)$_3$)$_2$), 34.82 (d, $^{1}J_{PC}$ = 30.6 Hz, *C*H$_2$P), 35.65 (d, $^{1}J_{PC}$ = 17.6 Hz, P(*C*(CH$_3$)$_3$)$_2$), 36.00 (d, $^{1}J_{PC}$ = 17.7 Hz, P(*C*(CH$_3$)$_3$)$_2$), 108.9 (d, J = 1.6 Hz, pyz-*C*), 112.8 (s, Ar-*C*), 123.14 (d, J = 20.9 Hz, Ar-*C*), 126.4 (s, pyz-*C*), 139.7 (s, pyz-*C*), 141.8 (s, Ar-*C*),

145.7 (s, Ar-*C*), 145.8 (s, Ar-*C*), 151.48 (d, *J* = 14.2 Hz, Ar-*C*). Anal. Calc. for $C_{39}H_{57}F_3N_4O_4P_2Pd_2S$: C, 46.39; H, 5.69; N, 5.55. Found: C, 47.02; H, 5.70; N, 5.26.

(PCN^{Me})Pd-OH (28). To a solution of **25** (30.0 mg, 0.0656 mmols) in THF (5 mL) was added an excess of ground KOH (15.2 mg, 0.271 mmols). The mixture was sonicated for 2.5 h, then left for 20 h at room temperature. The mixture was filtered through Celite® and concentrated to ca. 1 mL. The golden solution was layered with pentane and cooled to -30 °C to yield tan crystals of **28** suitable for X-ray diffraction (20.3 mg, 71% yield).

$^{31}P\{^1H\}$ NMR (121 MHz, THF-d_8) δ 90.2 (s). ^1H NMR (500 MHz, THF-d_8) δ -1.97 (s, 1H, Pd-O*H*), 1.43 (d, $^3J_{PH}$ = 13.7 Hz, 18H, P-C(C*H*$_3$)$_3$), 2.66 (s, 3H, C*H*$_3$), 3.36 (d, $^2J_{PH}$ = 9.2 Hz, 2H, Ar-C*H*$_2$-P), 6.25 (m, 1H, C*H*), 6.91-6.93 (m, 2H, C*H*), 7.17 (dd, $^3J_{HH}$ = 6.1, 2.8 Hz, 1H, C*H*), 7.79 (m, 1H, C*H*). $^{13}C\{^1H\}$ NMR (126 MHz, THF-d_8) δ 14.07 (s, pyz-*C*H$_3$), 29.40 (d, $^2J_{PC}$ = 5.0 Hz, P(C(*C*H$_3$)$_3$)$_2$), 35.38 (d, $^1J_{PC}$ = 16.9 Hz, P(*C*(CH$_3$)$_3$)$_2$), 36.16 (d, $^1J_{PC}$ = 28.9 Hz, *C*H$_2$P), 108.1 (s), 111.6 (s), 121.89 (d, J_{PC} = 20.2 Hz), 124.1 (s), 138.1 (s), 140.2 (s), 146.3 (s), 150.90 (d, J_{PC} = 14.8 Hz). Anal. Calc. for $C_{19}H_{29}N_2OPPd$: C, 52.00; H, 6.66; N, 6.38. Found: C, 51.89; H, 6.76; N, 6.18.

3.5 Notes to chapter 3

1. For general reviews and books, see: (a) *Pincer and Pincer-Type Complexes: Application in Organic Synthesis and Catalysis;* Szabo, K. J., Ed.; Wendt, O. F., Ed; Wiley-VCH: Weinheim, Germany, 2014. (b) *Organometallic Pincer Chemistry;* Van Koten, G.; Milstein, D., Ed.; Top. Organomet. Chem.; Springer: Heidelberg, 2013; Vol. 40. (c) Niu, J.-L.; Hao, X.-Q.; Gong, J.-F.; Song, M.-P. *Dalton Trans.* **2011**, *40*, 5135. (d) Benito-Garagorri, D.; Kirchner, K. *Acc. Chem. Res.* **2008**, *41*, 201. (e) van der Boom, M. E.; Milstein, D. *Chem. Rev.* **2003**, *103*, 1759. (f) Singleton, J. T. *Tetrahedron* **2003**, *59*, 1837.
2. Roesky, H. W.; Singh, S.; Yusuff, K. K. M.; Maguire, J. A.; Hosmane, N. S. *Chem. Rev.* **2006**, *106*, 3813.
3. Wenzel, T. T. *Stud. Surf. Sci. Catal.* **1991**, *66*, 545.
4. Bailey, W. D.; Parkes, M. V.; Kemp, R. A.; Goldberg, K. I. *Reactions of Square Planar d^8 Pincer Complexes with Oxygen and Hydrogen.* Pincer and Pincer-Type Complexes: Application in Organic Synthesis and Catalysis*;* Szabo, K. J., Ed.; Wendt, O. F., Ed; Wiley-VCH: Weinheim, Germany, 2014; pp 281-298.
5. The pioneering work on PCP-pincer complexes is: (a) Moulton, C. J.; Shaw, B. L. *J. Chem. Soc., Dalton Trans.* **1976**, 1020. More recent (selected) examples are: PCP-type: (b) Roddick, D. M. *Top. Organomet. Chem.* **2013**, *40*, 49. (c) Kundu, S.; Choliy, Y.; Zhuo, G.; Ahuja, R.; Emge, T. J.; Warmuth, R.; Brookhart, M.; Krogh-Jespersen, K.; Goldman, A. S. *Organometallics* **2009**, *28*, 5432. (d) Leis, W.; Mayer, H. A.; Kaska, W. C. *Coord. Chem. Rev.* **2008**, *252*, 1787. (e) Jensen, C. M. *Chem. Commun.* **1999**, 2443. PNP-type: (f) Schneider, S.; Meiners, J.; Askevold, B; *Eur. J. Inorg. Chem.* **2012**, 412. (g) Milstein, D. *Top. Catal.* **2010**, *53*, 915. POCOP-type: (h) Timpa, S. D.; Pell, C; Zhou, J.; Ozerov, O. V. *Organometallics* **2014**, *33*, 5254. (i) Jonasson, K. J.; Wendt, O. F. *Chem.−Eur. J.* **2014**, *20*, 11894. (j) Lao, D. B.; Owens, A. C. E.; Heinekey, D. M.; Goldberg, K. I. *ACS Catal.* **2013**, *3*, 2391. (k) Pandarus, V.; Zargarian, D. *Chem. Commun.* **2007**, 978. (l) Hebden, T. J.; St. John, A. J.; Gusev, D. G.; Kaminsky, W.; Goldberg, K. I.; Heinekey, D. M. *Angew. Chem. Int. Ed.* **2011**, *50*, 1873.
6. Some (selected) examples are: CCN/CNN/NCN′-type: (a) Luconi, L.; Klosin, J.; Smith, A. J.; Germain, S.; Schulz, E.; Hannedouche, J.; Giambastiani, G. *Dalton Trans.* **2013**, *42*, 16056. (b) Luconi, L.; Rossin, A.; Motta, A.; Tuci, G.; Giambastiani, G. *Chem. Eur. J.* **2013**, *19*, 4906. (c) Bröring, M.; Kleeberg, C.; Köhler, S. *Inorg. Chem.* **2008**, *47*, 6404. PNN-type: (d) Balaraman, E.; Gunanathan, C.; Zhang, J.; Shimon, L. J. W.; Milstein, D. *Nature Chem.* **2011**, *3*, 609. (e) Gnanaprakasam, B.; Milstein, D. *J. Am. Chem. Soc.* **2011**, *133*, 1682. (f) Zhang, J.; Balaraman, E.; Leitus, G.; Milstein, D. *Organometallics* **2011**, *30*, 5716. (g) Balaraman, E.; Gnanaprakasam, B.; Shimon, L. J. W.; Milstein, D. *J. Am. Chem. Soc.* **2010**, *132*, 16756. PCO-type: (h) Fulmer, G. R.; Kaminsky, W.; Kemp, R. A.; Goldberg, K. I. *Organometallics* **2011**, *30*, 1627. PCS-type: (i) Li, J.; Siegler, M.; Lutz, M.; Spek, A. L.; Gebbink, R. J. M. K.; van Koten, G. *Adv. Synth. Catal.* **2010**, *352*, 2474. (j) Gagliardo, M.; Selander, N.; Mehendale, N. C.; van Koten, G.; Klein G., R. J. M.; Szabó, K. J. *Chem. Eur. J.* **2008**, *14*, 4800.
7. Examples of PCN-type complexes can be found in: (a) Hao, X.-Q.; Huang, J.-J.; Wang, T.; Lv, J.; Gong, J.-F.; Song, M.-P. *J. Org. Chem.* **2014**, 79, 9512. (b) Khake, S. M.; Soni, V.; Gonnade, R. G.; Punji, B. *Dalton Trans.* **2014**, *43*, 16084. (c) Herbert, D. E.; Ozerov, O. V. *Organometallics* **2011**, *30*, 6641. (d) Moreno, I.; SanMartin, R.; Inés, B.; Herrero, M. T.; Domínguez, E. *Curr. Org. Chem.* **2009**, *13*, 878. (e) Poverenov, E.; Leitus, G.; Shimon, L. J. W.; Milstein, D. *Organometallics* **2005**, *24*, 5937.

8. Mehendale, N. C.; Sietsma, J. R. A.; de Jong, K. P.; van Walree, C. A.; Klein Gebbink R. J. M. and van Koten, G. *Adv. Synth. Catal.* **2007**, *349*, 2619.
9. As a comparison of the catalytic activity of NCP and NCN pyrazole-based pincers, see: (a) Zhang, X.; Suzuki, S.; Kozaki, M.; Okada, K., *J. Am. Chem. Soc.* **2012**, *134*, 17866. (b) Inés, B.; SanMartin, R.; Churruca, F.; Domínguez, E.; Urtiaga M. K.; Arriortua, M. I. *Organometallics*, **2008**, *27*, 2833. (c) Gong, J.-F.; Zhang, Y.-H.; Song, M.-P.; Xu, C. *Organometallics* **2007**, *26*, 6487.
10. (a) Chierotti, M. R.; Rossin, A.; Gobetto, R.; Peruzzini, M. *Inorg. Chem.* **2013**, *52*, 12616. (b) Rossin, A.; Bottari, G.; Lozano-Vila, A. M.; Paneque, M.; Peruzzini, M.; Rossi, A. and Zanobini, F. *Dalton Trans.* **2013**, *42*, 3533. (b) Levina, V. A.; Rossin, A.; Belkova, N. V.; Chierotti, M. R.; Epstein, L. M.; Filippov, O. A.; Gobetto, R.; Gonsalvi, L.; Lledòs, A.; Shubina, E. S.; Zanobini, F. and Peruzzini, M. *Angew. Chem. Int. Ed.* **2011**, *50*, 1367. (c) Rossin, A.; Peruzzini, M.; Zanobini, F. *Dalton Trans.* **2011**, *40*, 4447. (d) Fulmer, G. R.; Herndon, A. N.; Kaminsky, W.; Kemp, R. A.; Goldberg, K. I. *J. Am. Chem. Soc.* **2011**, *133*, 17713. (e) Denney, M. C.; Smythe, N. A.; Cetto, K. L.; Kemp, R. A.; Goldberg, K. I. *J. Am. Chem. Soc.* **2006**, *128*, 2508.
11. Bailey, W. D.; Kaminsky, W.; Kemp, R. A.; Goldberg, K. I. *Organometallics* **2014**, *33*, 2503.
12. (a) Luconi, L.; Rossin, A.; Tuci, G.; Germain, S.; Schulz, E.; Hannedouche, J.; Giambastiani, G. *ChemCatChem* **2013**, *5*, 1142 (b) Luconi, L.; Rossin, A.; Tuci, G.; Tritto, I.; Boggioni, L.; Klosin, J. J.; Theriault, C. N.; Giambastiani, G. *Chem. Eur. J.* **2012**, *18*, 671. (c) Luconi, L.; Giambastiani, G.; Rossin, A.; Bianchini, C.; Lledós, A. *Inorg. Chem*. **2010**, *49*, 6811. (d) Luconi, L.; Lyubov, D. M.; Bianchini, C.; Rossin, A.; Faggi, C.; Fukin, G. K.; Cherkasov, A. V.; Shavyrin, A. S.; Trifonov, A. A.; Giambastiani, G. *Eur. J. Inorg. Chem.* **2010**, 608. (e) Lyubov, D. M.; Fukin, G. K.; Cherkasov, A. V.; Shavyrin, A. S.; Trifonov, A. A.; Luconi, L.; Bianchini, C.; Meli, A.; Giambastiani, G. *Organometallics* **2009**, *28*, 1227.
13. Bailey, W. D.; Luconi, L.; Rossin, A.; Yakhvarov, D.; Flowers, S. E.; Kaminsky, W.; Kemp, R. A.; Giambastiani, G.; Goldberg, K. I. *Organometallics* **2015**, *34*, 3998.
14. Farrugia, L. J. *J. Appl. Cryst.* **2012**, *45*, 849.
15. Yang, L.; Powell, D. R.; Houser, R. P. *Dalton Trans.* **2007**, 955.
16. The (few) structurally determined (PCN)PdCl complexes can be found in: (a) Cook, E.; Iwasaki, K.; Masuda, J. D.; Xia, A. *Polyhedron* **2015**, *87*, 38. (b) Hou, A.-T.; Liu, Y.-L.; Hao, X.-Q.; Gong, J.-F.; Song, M.-P. *J. Organomet. Chem.* **2011**, *696*, 2857. (c) Gong, J.-F.; Zhang, Y.-H.; Song, M.-P.; Xu, C. *Organometallics* **2007**, *26*, 6487. (d) Motoyama, Y.; Shimozono, K.; Nishiyama, H. *Inorg. Chim. Acta*, **2006**, *359*, 1725.
17. Some examples are: (a) (^{tBu}PCP)PdCl: Johnson M. T.; Dzolic, Z.; Cetina, M.; Lahtinen, M.; Ahlquist, M. S. G.; Rissanen, K.; Ohrstrom, L.; Wendt, O. F. *Dalton Trans.* **2013**, *42*, 8484. (b) (^{tBu}PCP)Pd(COOH): Johansson, R.; Wendt, O. F. *Organometallics* **2007**, *26*, 2426. (c) (^{tBu}PCP)Pd(I_3): Johnson M. T.; Dzolic, Z.; Cetina, M.; Wendt, O. F.; Ohrstrom, L.; Rissanen, K. *Cryst. Growth Des.* **2012**, *12*, 362.
18. (a) Hartshorn, C. M.; Steel, P. J. *Organometallics* **1998**, *17*, 3487. (b) Canty, A. J.; Patel, J.; Skelton, B. W.; White, A. H. *J. Organomet. Chem.* **2000**, *607*, 194.
19. (a) Grove, D. M.; van Koten, G.; Ubbels, H. J. C.; Spek, A. L. *J. Am. Chem. Soc.,***1982**, *104*, 4285. (b) Fornies, J.; Navarro, R.; Sicilia, V.; Martinez, F.; Welch, A. J. *J. Organomet. Chem.* **1991**, *408*, 425. (c) Ara, I.; Fornies, J.; Martin, A.; Martin, L. F.; Menjon, B.; Miedes, H. *Dalton Trans.* **2010**, *39*, 7301.
20. Bryndza, H. E.; Tam, W. *Chem. Rev.* **1988**, *88*, 1163.
21. Cámpora, J.; Palma, P.; del Río, D.; Álvarez, E. *Organometallics* **2004**, *23*, 1652.
22. Some examples are: (a) Khusnutdinova, J. R.; Rath, N. P.; Mirica, L. M. *J. Am. Chem. Soc.* **2012**, *134*, 2414. (b) Cao, L.; Jennings, M. C.; Puddephatt, R. J. *Dalton Trans.* **2009**, 5171. (c) Klein, A.; Dogan, A.; Feth, M.; Bertagnolli, H. *Inorg. Chim. Acta* **2003**, *343*, 189.

23. Joslin, E. E.; Quillian, B.; Gunnoe, T. B.; Cundari, T. R.; Sabat, M.; Myers, W. H. *Inorg. Chem.* **2014**, *53*, 6270.
24. (a) Salanouve, E.; Retailleau, P.; Janin, Y. L. *Tetrahedron* **2012**, *68*, 2135. (b) Alonso, M. T.; Juanes, O.;de Mendoza, J.; Rodríguez-Ubis, J. C. *J. Organomet. Chem.* **1994**, *484*, 19.
25. (a) Canty, A. J.; Honeyman, R. T.; Skelton, B. W.; White, A. H. *Inorg. Chim. Acta* **1986**, *114*, L39. (b) Canty, A. J.; Minchin, N. J. *J. Organomet. Chem.* **1982**, *226*, C14. (c) Canty, A. J.; Honeyman, R. T. *J. Organomet. Chem.* **1992**, *430*, 245. (d) Canty, A. J.; Honeyman, R. T. *J. Organomet. Chem.* **1990**, *387*, 247.
26. (a) Maenaka, Y. Suenobu, T.; Fukuzumi, S. *J. Am. Chem. Soc.* **2012**, *134*, 9417. (b) Wiley, J. S.; Oldham, Jr., W. J.; Heinekey, D. M. *Organometallics* **2000**, *19*, 1670.
27. Petit, A.; Flygare, J.; Miller, A. T.; Winkel, G.; Ess, D. H. *Org. Lett.* **2012**, *14*, 3680.
28. (a) Spek, A. L. *J. Appl. Cryst.* **2003**, *36,* 7. (b) van der Sluis P.; Spek, A. L. *Acta Crystallogr. A* **1990**, *46*, 194.
29. Johansson, R.; Öhrström, L.; Wendt, O. F. *Cryst. Growth Des.* **2007**, *7*, 1974.
30. (a) Hayashi, Y.; Wada, S.; Yamashita, M.; Nozaki, K. *Organometallics* **2012**, *31*, 1073. (b) Canty, A. J.; Jin, H.; Roberts, A. S.; Skelton, B. W.; White, A. H. *Organometallics* **1996**, *15*, 5713. (c) Canty, A. J.; Jin, H.; Skelton, B. W.; White, A. H. *J. Organomet. Chem.* **1995**, *503*, C16. (d) Castan, P.; Dahan, F.; Wimmer, S.; Wimmer, F. L. *J. Chem Soc., Dalton Trans.* **1990**, 2679.
31. Fulmer, G. R.; Muller, R. P.; Kemp, R. A.; Goldberg, K. I. *J. Am. Chem. Soc.* **2009**, *131*, 1346.
32. Bruker (**2007**) APEX2 (Version 2.1-4), SAINT (version 7.34A), SADABS (version 2007/4), BrukerAXS Inc, Madison, Wisconsin, USA.
33. CrysAlis CCD 1.171.31.2 (release 07-07-2006), CrysAlis171 .NET, Oxford Diffraction Ltd.
34. CrysAlis RED 1.171.31.2 (release 07-07-2006), CrysAlis171 .NET, Oxford Diffraction Ltd.
35. Altomare, A.; Burla, M. C.; Camalli, M.; Cascarano, G. L.; Giacovazzo, C.; Guagliardi, A.; Moliterni, A. G. G.; Polidori, G.; Spagna, R. *J. Appl. Crystallogr.* **1999**, *32*, 115.
36. Sheldrick, G. M. SHELXL (**1997**).
37. Nardelli, M. *Comput. Chem.* **1993**, *7*, 95.
38. Frisch, M. J. *et al.*, *Gaussian09*, Revision C.01, Gaussian Inc., Wallingford CT, **2009**.
39. Zhao, Y. and Truhlar, D. G. *Theor. Chem. Account* **2008**, *120*, 215.
40. (a) Andrae, D.; Haeuessermann, U.; Dolg, M.; Stoll, H.; Preuss, H. *Theor. Chem. Acc.* **1990**, *77*, 123. (b) Dunning Jr., T. H.; Hay P. J. in *Modern Theoretical Chemistry*, Ed. H. F. Schaefer III, Vol. 3 (Plenum, New York, **1976**) 1-28.
41. Lynch, B. J.; Zhao Y.; Truhlar, D. G. *J. Phys. Chem. A* **2003**, *107*, 1384.
42. (a) Höllwarth, A.; Böhme, M.; Dapprich, S.; Ehlers, A. W.; Gobbi, A.; Jonas, V.; Köhler, K. F.; Stegmann, R.; Veldkamp A.; Frenking, G. *Chem. Phys. Lett.* **1993**, *208*, 237. (b) Ehlers, A. W.; Böhme, M.; Dapprich, S.; Gobbi, A.; Höllwarth, A.; Jonas, V.; Köhler, K. F.; Stegmann, R.; Veldkamp, A.; Frenking, G. *Chem. Phys. Lett.* **1993**, *208*, 111.
43. Fukui, K. *Acc. Chem. Res.* **1981**, *14*, 363.
44. Marenich, A. V.; Cramer C. J.; Truhlar, D. G. *J. Phys. Chem. B* **2009**, *113*, 6378.

Chapter 4

Hydrogenolysis of mono- and dinuclear (PCN^{R})Pd^{II} hydroxides

4.1 Introduction

The combination of dihydrogen and transition metal complexes has been heavily used in the reduction of organic substrates, catalyst regeneration, and stoichiometric synthesis.[1-3] The activation of dihydrogen has become a fundamental tool in organometallic chemistry. However, transformations regarding hydrogenation by H_2 have been investigated far more than other potentially powerful uses of H_2.[4,5] For example, hydrogenolysis reactions, or the cleaving of M-X bonds by H_2, have been underutilized, yet could represent a method for catalyst regeneration, organic substrate release, as well as metal hydride formation.[6] Metal hydride species play a significant role as intermediates in a wide range of catalytic and stoichiometric transformations.

Hydrogenolysis of M-OR bonds would result in the formation of a metal hydride as well as the release of an alcohol or water molecule. This reaction has been utilized in both stoichiometric and catalytic transformations, for example the reduction of CO_2 to formic acid,[7]

in the activation of Adam's[8] and Pearlman's[9] catalysts, and the generation of Stryker's reagent.[10] However, in order for hydrogenolysis reactions to find use in new chemical transformations, the mechanism by which it occurs must be well understood. Only recently have mechanistic investigations been performed for the hydrogenolysis of M-OR complexes.[11]

Previously, our group has shown that the hydroxide complex ($^{t\text{Bu}}$PCP)Pd-OH reacts cleanly under an H_2 atmosphere to produce the hydride ($^{t\text{Bu}}$PCP)Pd-H and an equivalent of water.[11] Through experimental kinetics, as well as DFT calculations, a mechanism was proposed where H_2 is heterolytically cleaved across the Pd-O(H) bond through a four-centered transition state.[11,12] The available lone pair on oxygen was required, as formally a proton is delivered to the hydroxide ligand while a hydride is added to the Pd^{II} center.

We recently reported the synthesis and characterization of the asymmetric pincer ligands PCN^R (PCN^H = 1-[3-[(di-*tert*-butylphosphino)methyl]phenyl]-1H-pyrazole) and PCN^{Me} = 1-[3-[(di-*tert*-butylphosphino)methyl]phenyl]-5-methyl-1H-pyrazole) and the corresponding Pd^{II} hydroxide complexes (**Figure 4.1**).[13] Both dinuclear μ-OH and mononuclear terminal hydroxides were reported. The PCN^{Me} ligand, with the 5-position of the pyrazole arm methylated, was used to inhibit pyrazole "rollover" C-H activation, which was observed in the unprotected PCN^H systems. Reported below is the examination of the PCN^R hydroxide complexes susceptibility towards hydrogenolysis. Both dinuclear μ-OH complexes were found to react cleanly with H_2, yielding the analogous dinuclear μ-H complexes. Experimental kinetic studies were performed on the hydrogenolysis of {[(PCN^{Me})Pd]$_2$(μ-OH)}(OTf) (**27**) to provide mechanistic insight. Reactions of the terminal hydroxide (PCN^H)Pd-OH (**22**) with H_2 yielded a mixed-ligand μ-H through pyrazole rollover C-H

activation, while the protected hydroxide (PCN^{Me})Pd-OH (**28**) did not produce a stable hydride species under H_2.

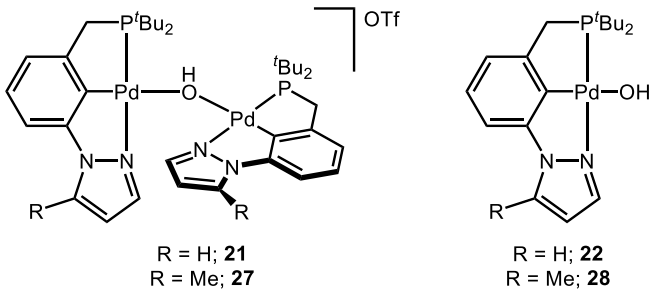

Figure 4.1. Pd^{II}-OH complexes investigated in this study.

4.2 Results and discussion

Hydrogenolysis of {[(PCN^H)Pd]$_2$(μ-OH)}(OTf) (21): When THF-d_8 solutions of {[(PCN^H)Pd]$_2$(μ-OH)}(OTf)[13] (**21**) were pressurized with H_2 (1-7 atm), reaction at the bridging hydroxide occurred over days at room temperature yielding the μ-hydride {[(PCN^H)Pd]$_2$(μ-H)}(OTf) (**29**). The reaction, shown in **Scheme 4.1**, was monitored by both ^{1}H and ^{31}P NMR spectroscopy. In the ^{1}H NMR spectrum of **29**, the hydride signal is observed as a triplet ($^2J_{PH}$ = 12.6 Hz) at -8.68 ppm, coupling to two equivalent phosphorus nuclei of the PCN^H ligands. Similar to the starting μ-OH **21**, the ^{t}Bu and methylene signals of the pincer ligand in **29** are diastereotopic, and appear as doublets at 1.44 and 1.49, and doublet-of-doublets at 3.70 and 3.82, respectively. This exemplifies the rigid character of the dinuclear species, as no rotation about the Pd-H-Pd bonds is observed at room temperature on the NMR timescale. Furthermore, this indicates that **29** indeed exists as a dinuclear species in solution. A singlet at 105.2 ppm is observed in the ^{31}P NMR spectrum.

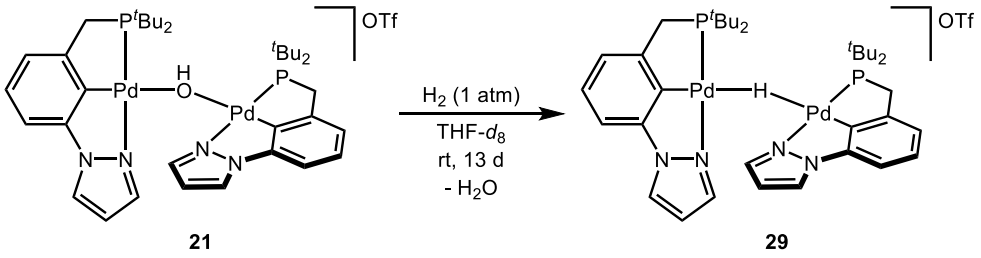

Scheme 4.1. Hydrogenolysis of **21**.

Complex **29** was recrystallized from a concentrated THF solution layered with pentane at -30 °C. A solid-state structure was determined by X-ray diffraction, which confirms the dinuclear structure of **29** (**Figure 4.2**). The two cationic [(PCN^{H})Pd^{II}] fragments of **29** share indistinguishable metrics. A triflate counter-ion balances the overall cationic complex. Both Pd^{II} centers are distorted square planar (τ_4 = 0.17 and 0.18).[14] Complex **29** represents, to our knowledge, the first structurally characterized dinuclear Pd^{II} species bridged only by a single hydride ligand. Other examples of structurally characterized dinuclear Pd^{II} μ-H complexes contain additional bridging groups between the two metal centers (bis-phosphines, bis-imides, heterometals, hydrides, carbonyls).[15-28] The two Pd^{II} atoms in **29** exist further apart (3.0563(17) Å) compared to the average distance between other dinuclear Pd^{II} μ-H complexes (CSD average = 2.89 Å).

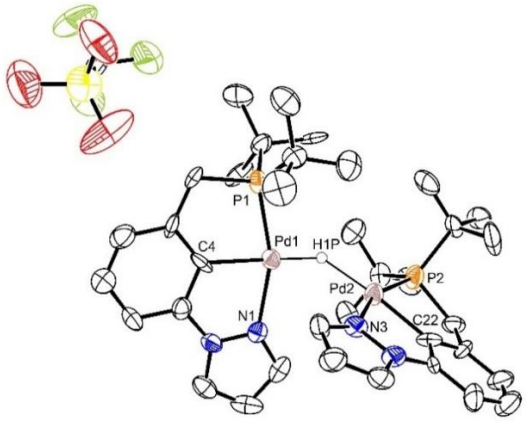

Figure 4.2. ORTEP[29] of the {[(PCN^{H})Pd]$_2$(μ-H)}(OTf) salt (**29**), with ellipsoids shown at 50% probability. Hydrogen atoms on the ligands omitted for clarity.

Complex **29** was found to be stable in the solid state and in solution under an inert atmosphere (N_2), but slowly decomposed under an H_2 atmosphere. The decomposition route under H_2 appeared to go through reduction at the metal center, as Pd^0 particles could be observed over time. Notably, no reaction was observed when an authentic sample of (PCN^H)Pd-OTf (**20**) was pressurized with H_2 (3 atm), even at elevated temperatures (60 °C), indicating that decomposition of **29** occurs from the intact dinuclear complex. If the dinuclear species **29** underwent dissociation into a terminal Pd-H species and **20**, then complex **20** would be observed under the reaction conditions. DFT studies suggest pyrazolyl dissociation as a critical step in the decomposition to a Pd^0 product (discussed below).[12]

Hydrogenolysis of {[(PCN^H)Ni]$_2$(μ-OH)}(OTf) (31): The Ni^{II} analogue of **21** was also investigated for its propensity to undergo hydrogenolysis. Beginning from (PCN^H)Ni-Br,[30] the halide was abstracted with AgOTf, forming the triflate complex (PCN^H)Ni-OTf (**30**) (**Scheme 4.2**). Complex **30** was characterized by NMR spectroscopy and X-ray diffraction. In the $^{31}P\{^1H\}$ NMR spectrum, a singlet is observed at 86.4 ppm, shifting upfield from 89.4 ppm corresponding to the bromide complex. Large yellow crystals were grown from a concentrated CH_2Cl_2 solution layered with pentane at -30 °C. The solid-state structure of **30** is shown in **Figure 4.3**, confirming an innersphere triflate ligand. Complex **30** appears as a slightly distorted square planar structure (τ_4 = 0.12).[14] The Ni-ligand bonds of **30** all appear shorter than its Pd^{II} analogue (PCN^H)Pd-OTf (**20**), as expected for the smaller Ni^{II} ion.[31]

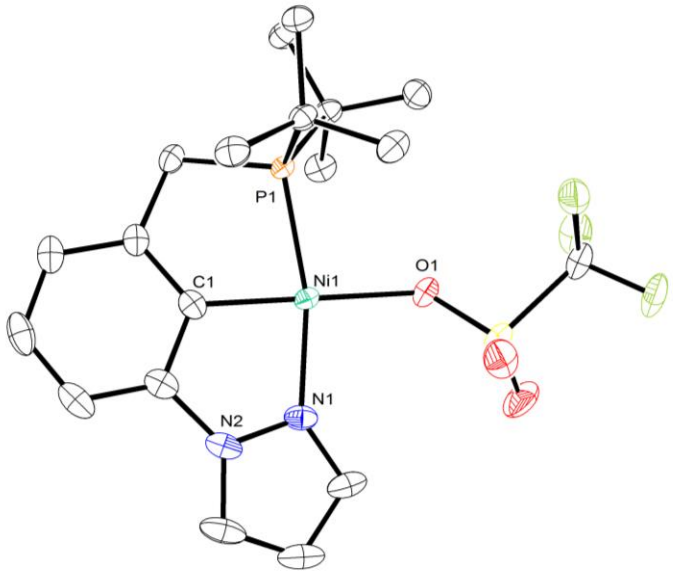

Figure 4.3. ORTEP[29] of the (PCN^{H})Ni-OTf (**30**), with ellipsoids shown at 50% probability. Hydrogen atoms on the ligands omitted for clarity.

Addition of 0.5 equiv. of KOH to a THF-d_8 solution of **30** resulted in the formation of the dinuclear {[(PCN^{H})Ni]$_2$(μ-OH)}(OTf) (**31**) over 3 days at room temperature (**Scheme 4.2**). The ^{1}H NMR spectrum displays an upfield singlet at -3.38 ppm, indicating a metal-hydroxide had formed. The ^{t}Bu and methylene signals are diastereotopic, appearing as two doublets at 1.48 and 1.53 ppm ($^3J_{PH}$ = 13.3 and 13.4 Hz) and two doublet of doublets at 3.31 ($^2J_{HH}$ = 17.9 Hz, $^2J_{PH}$ = 10.2 Hz) and 3.43 ($^2J_{HH}$ = 17.9 Hz, $^2J_{PH}$ = 8.2 Hz), respectively. In the ^{31}P{^{1}H} NMR spectrum, a singlet at 84.2 ppm indicates equivalent phosphorus nuclei. The spectroscopic signals indicate a symmetric dinuclear hydroxide species. Yellow crystals spontaneously formed during the reaction period. X-ray diffraction of the crystal sample confirmed the identity of **31** (**Figure 4.4**).

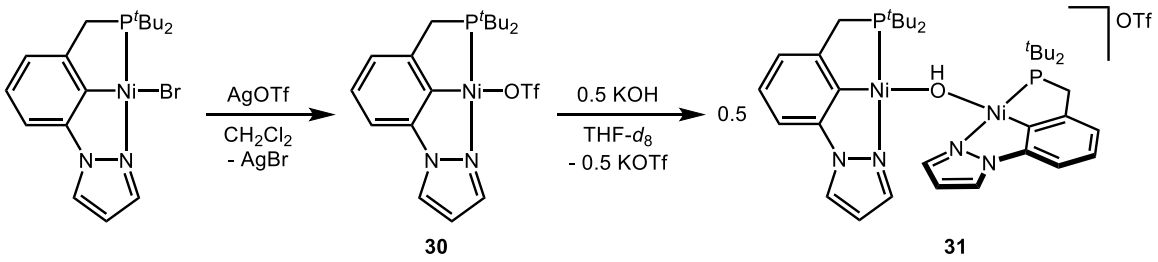

Scheme 4.2. Synthesis of the dinuclear hydroxide {[(PCN^H)Ni]$_2$(μ-OH)}(OTf) (**31**).

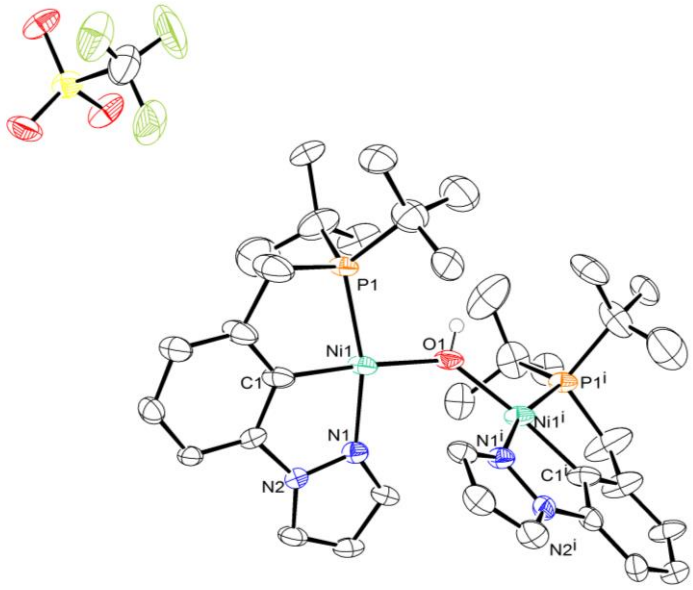

Figure 4.4. ORTEP[29] of the {[(PCN^H)Ni]$_2$(μ-OH)}(OTf) (**31**), with ellipsoids shown at 50% probability. Hydrogen atoms on the ligands omitted for clarity.

Complex **31** exists as two [(PCN^H)Ni] fragments bridged by a single hydroxide ligand with a distorted outersphere triflate ion. The hydroxide ligand is shared equally, as a two-fold rotation through the bridging hydroxyl relates half of the structure to the other. This rotation also folds a half triflate into itself, which leads to slightly extended displacement parameters of atoms in the vicinity of the disordered anion. The Ni^{II} centers are distorted square planar (τ_4 = 0.15). The dinuclear **31** shares indistinguishable metrics with **30** except for a smaller Ni-O bond length to the hydroxide ligand compared to a weakly bound triflate (1.933(3) and 1.9979(14) Å, respectively).

The susceptibility of **31** to undergo hydrogenolysis was investigated. A degassed sample of **31** in THF-d_8 was pressurized with 5 atm of H_2 at room temperature and monitored by NMR spectroscopy. No reaction was observed over 3 days. The sample was then heated to 60 °C for 24 h. A very small amount of a new monomeric species could be observed by a new ^{t}Bu signal overlapping with the signals for **31**. However, no hydride signal was observed. The sample was further heated at 100 °C for 6 h, at which point complex degradation was detected. Ni^0 particles could be seen precipitating out of solution, while no signals for a hydride complex were observed by NMR spectroscopy. The lack of reactivity at **31** may be due to the lower propensity of first row metals to undergo 2-electron processes. Given the similar steric profile of **31** compared to **21**, the lack of reactivity in **31** would seem to be electronic in nature. However, an argument could be made that the Ni-OH is more shielded by the PCN^H ligand compared to **21** due to the shorter metal-ligand bond lengths. Furthermore, bond dissociation energy of M-O bonds follow the trend of Ni>Pt>Pd, while M-H bond dissociation energy follows the trend of Pt>Pd>Ni, and therefore a thermodynamic argument could also be made for the lack of reactivity at **31**.[32]

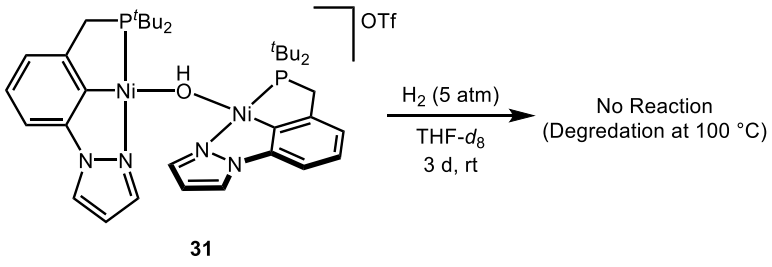

31

Scheme 4.3. Attempted hydrogenolysis of {[(PCN^H)Ni]$_2$(μ-OH)}(OTf) (**31**).

Hydrogenolysis of {[(PCN^{Me})Pd]$_2$(μ-OH)}(OTf) (27): Similar to complex **21**, when a solution of the bridged hydroxide **27** in THF-d_8 was exposed to H_2 (7 atm) at room temperature, a reaction occurred over 8 days yielding a new hydridic species **32** (**Scheme 4.4**). The ^{1}H NMR

spectrum of **32** displays an upfield triplet at -8.77 ppm ($^2J_{PH}$ = 13.2 Hz), indicating once again that a μ-H species has formed. The ^{t}Bu signals on phosphorus appear as two doublets at 1.42 and 1.47 ppm ($^3J_{PH}$ = 8.4 and 8.6 Hz, respectively). The methylene protons on the pincer "arm" are also diastereotopic, appearing as two doublet-of-doublets at 3.69 and 3.82 ppm. The protons in the square plane of each metal center are equivalent by the C_2 rotation through the bridged hydride. Similarly, the phosphorus nuclei are equivalent, appearing as a singlet at 105.2 ppm. The spectroscopic similarities to **29** led to the assignment of **32** as the dinuclear {[(PCN^{Me})Pd]$_2$(μ-H)}(OTf).

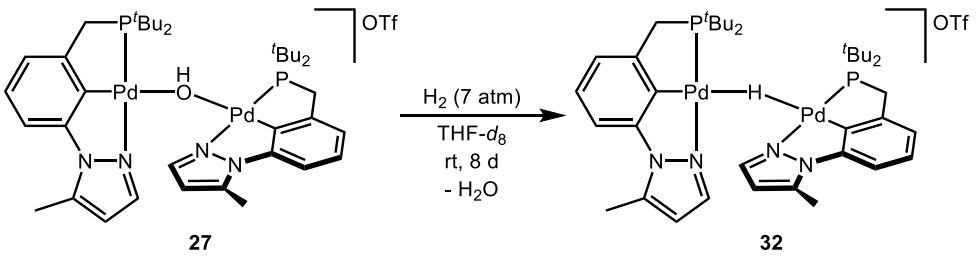

Scheme 4.4. Hydrogenolysis of **27**.

Single crystals suitable for X-ray analysis were grown from a concentrated THF solution of **32** layered with pentane. The solid-state structure, shown in **Figure 4.5**, confirms the identity of **32**. Complex **32** crystalizes in the P 2_1/c point group, with 2 molecules in the asymmetric unit. The structure of **32** is composed of two [(PCN^{Me})Pd] cationic units oriented closely in space. No electron density was observed for the hydride ligand; however, its existence is evident by the diagnostic ^{1}H NMR signal at -8.77 ppm. A triflate counterion is found in the outersphere to balance the two formally Pd^{II} centers. The physical metrics are nearly indistinguishable to those found in **29**. The notable difference is that the Pd(1)-Pd(2) separation distance (2.977(3) Å) in **32** is slightly shorter than the **29** analogue (3.0563(17) Å).

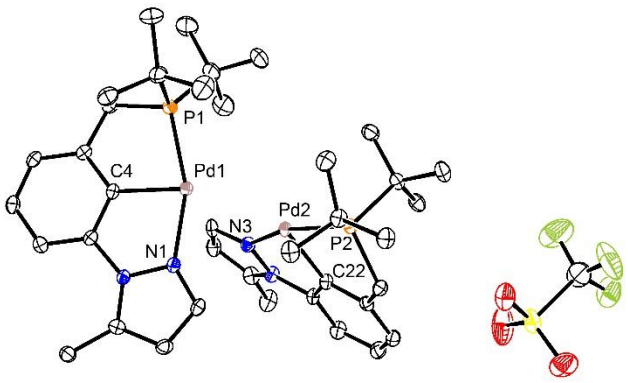

Figure 4.5. ORTEP[29] of {[(PCN^{Me})Pd]$_2$(μ-H)}(OTf) salt (**32**), with ellipsoids shown at 50% probability. Hydrogen atoms on the ligands omitted for clarity. No electron density for the μ-H atom was found.

Kinetic studies of the hydrogenolysis of 27: In order to understand the mechanism by which the dinuclear hydroxide **27** undergoes hydrogenolysis to form the μ-hydride **32**, kinetic studies were performed. Complex **27** was chosen to study for its increased stability compared to **21**. The reaction was monitored by ^{1}H NMR spectrometry, following the disappearance of the multiplet at 6.19-6.22 ppm compared to the hexamethylbenzene internal standard (2.17 ppm).

The hydrogenolysis of **27** was performed under 1, 2, and 5 atm of H_2 at 50 °C. In each case, the reaction followed first order kinetics in [**27**]. Plots of ln[**27**] versus time over 3 half-lives yielded linear relationships (**Figure 4.6**). A direct dependence of k_{obs} on [H_2] was observed (**Figure 4.7**). This first order dependence of the rate on [H_2] indicates that the reaction follows a second order rate law overall. The rate law is thus -d[**27**]/dt = k_{obs}[**27**][H_2]. The hydrogenolysis of **27** shows a similar kinetic profile to the hydrogenolysis of the mononuclear ($^{t\text{Bu}}$PCP)Pd-OH.[11]

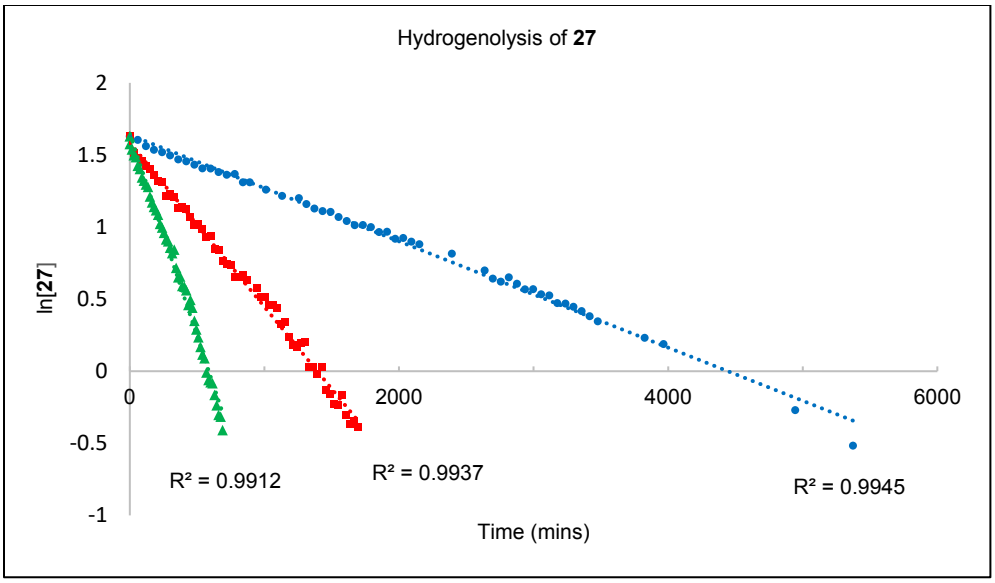

Figure 4.6. Combined first-order rate plots for the hydrogenolysis of **27** under 1 (●), 2 (■), and 5 (▲) atm of H_2. Reaction conditions: $[\mathbf{27}]_0$ = 5.1 mM, THF-d_8, 50 °C.

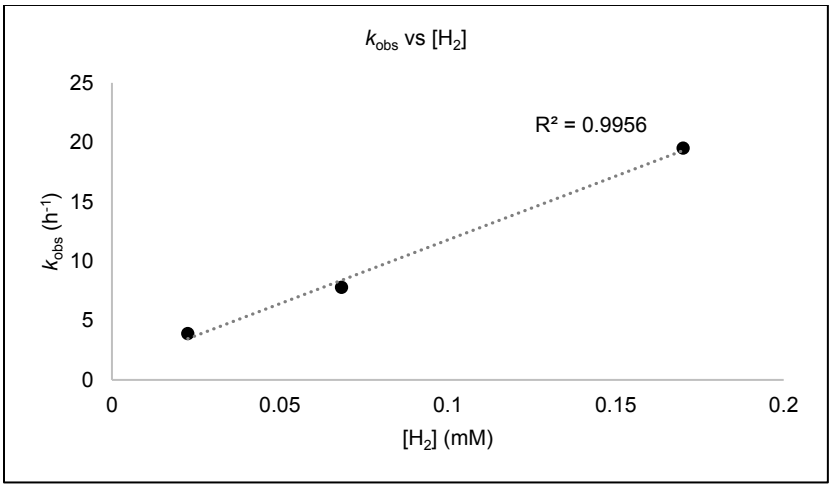

Figure 4.7. Plot of k_{obs} versus [H_2] for the hydrogenolysis of **27** at 1, 2, and 5 atm of H_2. Dihydrogen concentration in solution calculated through extrapolation of mol fraction (χ_{H2}) data gathered at 323 K in THF.[33]

The kinetic data suggests a reaction pathway where a dihydrogen molecule interacts with the intact dinuclear **27**. No evidence for separation of the dinuclear complex into the terminal hydroxide **28** and the triflate **26** prior to rate determining interaction with H_2 was observed. Furthermore, reaction of **28** and H_2, as described below, does not yield hydride formation. Based on previous literature involving hydrogenolysis of Pd^{II}-OH complexes, a

mechanism involving concerted internal electrophilic substitution (IES) was considered. IES has been shown to be a favorable pathway in similar pincer Pd^{II}-OH systems by DFT.[11,12] DFT calculations of the hydrogenolysis of **27** were attempted, however a transition state at the intact dinuclear structure was never located.[34]

Hydrogenolysis of (PCN^{H})PdOH (22): The reaction of **22** formed *in situ*, with H_2 was followed by NMR spectroscopy in THF-d_8, C_6D_6, and toluene-d_8. All reactions formed a mixture of species, however the cleanest reaction was observed in toluene-d_8. Exposing a solution of the mononuclear hydroxide **22** in toluene-d_8 at room temperature to H_2 (7 atm) resulted in the formation of a new hydride species **33**. Within minutes of pressurization, the majority of the hydroxide **22** was consumed. However, a minor amount of **22** still persisted over 24 hours. The ^{1}H NMR spectrum of **33** displays a doublet of doublets at -8.65 ppm ($^2J_{PH}$ = 15.3, 10.2 Hz), indicating that the hydride is not only bridging two Pd^{II} centers, but also is coupling to two inequivalent phosphorus nuclei. This was confirmed by performing a $^1H\{^{31}P\}$ NMR experiment: only a singlet at -8.65 ppm remains. This assessment is echoed by the observation of two singlets at 85.9 and 103.8 ppm in the ^{31}P NMR spectrum. Furthermore, a break in symmetry is observed in the ligand ^{t}Bu, methylene and aromatic signals in the ^{1}H NMR spectrum. This evidence and similarities to our previous observation of rollover activation of the pyrazole arm of the PCN^{H} ligand suggests that this same activation is occurring, forming a dinuclear (PCN^{H})Pd(μ-H)Pd(PCC) complex (**33**) (**Scheme 4.5**). These experimental findings were followed up by DFT studies.

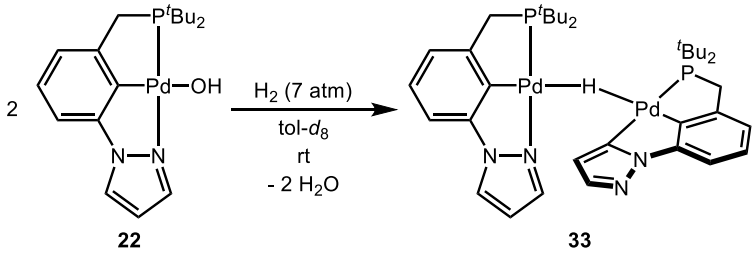

Scheme 4.5. Hydrogenolysis and rollover C-H activation of **22**.

The hydrogenolysis of **22** was evaluated by DFT at the M06/6-31G* level of theory. THF solvent was included in the calculation through a *continuum* model (SMD), and all the figures reported here should be considered as ΔG or $\Delta G^{\ddagger}$ values evaluated in THF (see Computational Details). An H_2 molecule was found to interact with the terminal hydroxide **22** initially above the Pd^{II} center and hydroxide ligand, forming a (PCN^{H})Pd-OH···H_2 adduct **22·H₂** (**Figure 4.8**, left). This interaction is endergonic (+7.6 kcal/mol) compared to the starting materials due to the entropic cost of coordinating free H_2. From the adduct, a 4-centered transition state (**TS₂**) is located at +25.8 kcal/mol (**Figure 4.8**, center). Notably, this TS energy is nearly identical to that calculated for the hydrogenolysis of (^{tBu}PCP)Pd-OH previously (+25.7 kcal/mol) and other pincer Pd^{II}-OH species.[11,12] From **TS₂**, formation of the mononuclear hydride (PCN^{H})Pd-H (**34**) occurs, releasing water. The water molecule engages with the hydride ligand of **34** through a H-bond by one of its own hydrogen (**Figure 4.8**, right). Formation of the terminal hydride is exergonic by 7.8 kcal/mol (**Figure 4.9**).

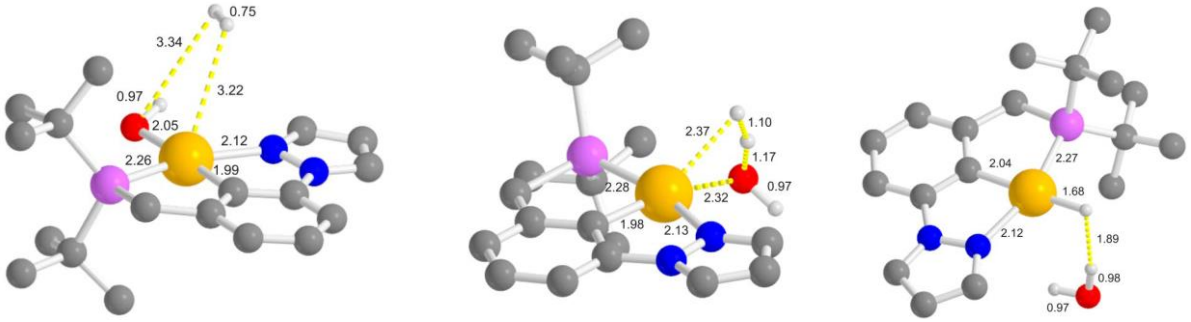

Figure 4.8. Optimized structure of the adduct **22·H₂** (left), **TS₂** (center), and (PCN^{H})Pd-H···H_2O (**34·H₂O**) (right). Selected bond distances (Å) reported. H atoms on the pincer omitted for clarity. Atom color code: gray, C; white, H; red, O; blue, N; purple, P; orange, Pd.

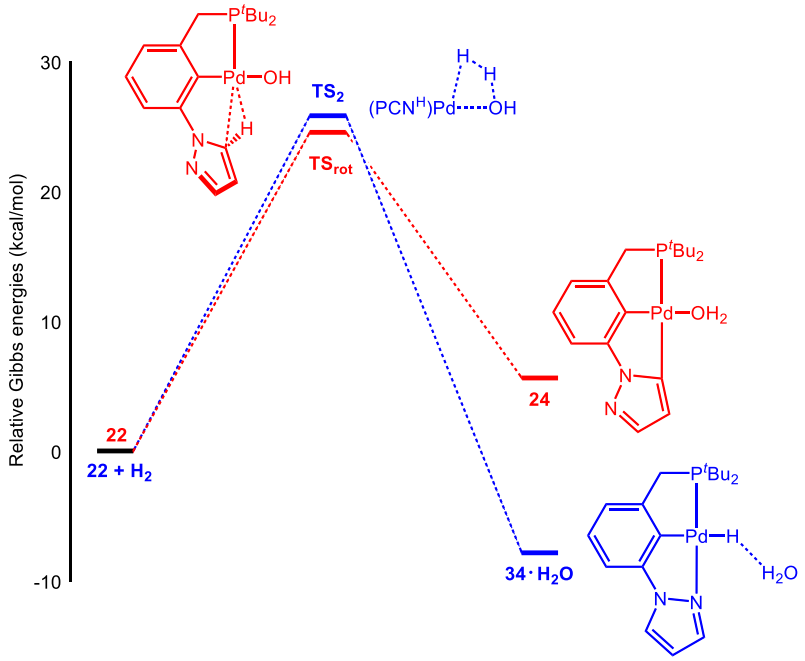

Figure 4.9. Combined reaction coordinate diagram for the hydrogenolysis (blue) and "rollover" C-H activation of the pyrazolyl arm (red) of **22**, respectively.

The formation of the terminal hydride **34** represents half of the required fragments to form **33**. An unsaturated (PCC)Pd^{II} fragment, formed by "rollover" activation of the pyrazolyl arm, is still required. Notably, no experimental evidence for a terminal hydride has been observed. It is possible that the hydroxide starting material **22** undergoes "rollover" C-H activation, as the barrier calculated for this process was found to be +24.5 kcal/mol (**Figure**

4.9). The formation of the *aquo* species (PCC)Pd-OH_2 (**24**) could then react with **34** to ultimately form the dinuclear **33** with the release of water.

It is also possible that the hydride **34** undergoes "rollover" C-H activation, forming (PCC)Pd-(η^2-H_2) (**35**). This complex could then lose H_2 and react with unreacted terminal hydride **34** to form **33**. This route was also calculated. The overall reaction is shown in **Scheme 4.6**. Similar to the "rollover" activation at **22**, the first step calculated for **34** was detachment of the pyrazolyl arm. An intermediate was found (**34'**), containing an agostic interaction of the pyrazolyl C-H bond at the 5-position with the Pd^{II} center (**Figure 4.10**, left). The barrier for rotation was calculated to reach a maximum at +25.2 kcal/mol, very similar to the barrier of rotation calculated for **22** (+24.5 kcal/mol). From **34'**, a "rollover" 4-centered transition state (**TS_3**) with a relative Gibbs energy of +34.7 kcal/mol was found (**Figure 4.10**, center). **TS_3** currently has only been calculated in the gas phase, explaining the large barrier. It is expected that in a solvent continuum, a similar barrier to that calculated for **22** rollover would be determined. This led to the dihydrogen complex **35** (**Figure 4.10**, right). Loss of H_2 from **35** with combination of **34** was found to be the driving force of this reaction (exergonic by 23.1 kcal/mol), yielding the final product **33**.

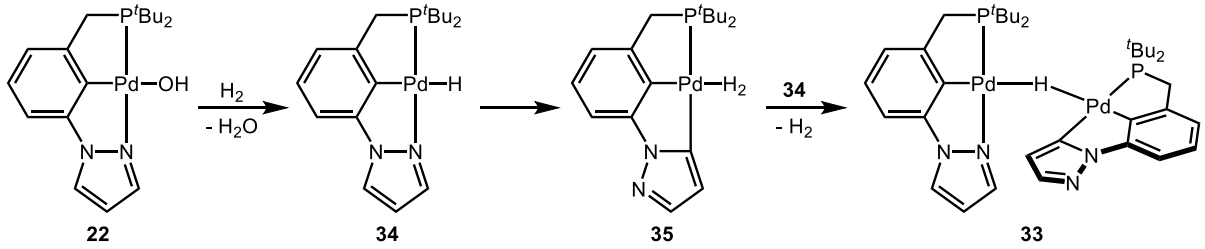

Scheme 4.6. Overall DFT calculated hydrogenolysis of **22.**

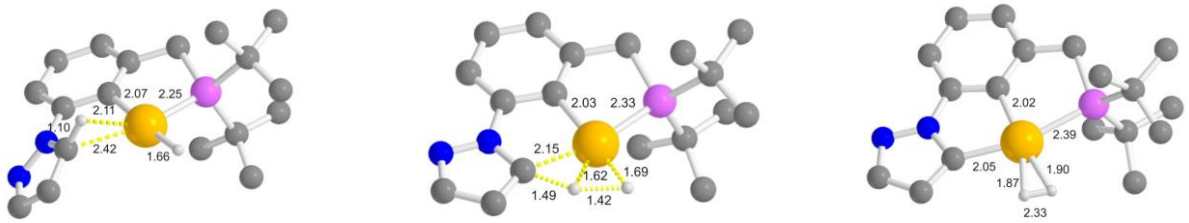

Figure 4.10. Optimized structure of (PCCH)Pd-H (**34'**) (left), **TS$_3$** (center), and (PCC)Pd-(η^2-H$_2$) (**35**) (right). Selected bond distances (Å) reported. H atoms on the pincer omitted for clarity.

After 24 hours, a second product **36** is observed in the reaction mixture of **33** and H_2 with the growth of a singlet at 61.1 ppm in the ^{31}P NMR spectrum. The sample appears as a dark yellow suspension, with black particles precipitating out of solution. From these observations, it was proposed that reduction of the complex occurred, forming the bisphosphine Pd^0 species (PCN^H)$_2$Pd^0 (**36**) and Pd^0 black (**Scheme 4.7**). The assignment of **36** was confirmed by independent synthesis and comparison of the ^{1}H and ^{31}P{^{1}H} NMR spectral data. Notably, reduction of a similar (PCO)Pd-OH complex under H_2 to form the bisphosphine species (PCO)$_2$Pd^0 and Pd^0 black has been previously observed by our group.[35] In order to understand the route by which the reduction took place, DFT calculations of the hydrogenolysis of **33** were performed.

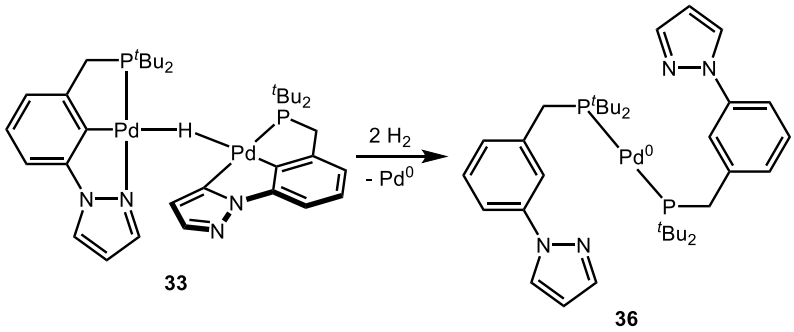

Scheme 4.7. Reduction of **33** under H_2.

Complex **33** is considered as two Pd fragments, [(PCN^H)Pd-H] and [(PCC)Pd]. To computationally simplify **33** degradation, DFT calculations were performed on how complex

(PCN^{H})Pd-H (**34**) reacts with H_2. The overall calculated reduction of **34** to Pd^0 is shown in **Scheme 4.8**. Notably, no transition state for the hydrogenation of the Pd^{II}-Ar backbone was found if starting from the tridentate pincer complex. Instead, pyrazolyl dissociation was required, allowing H_2 coordination to form the mixed hydride, dihydrogen complex **37** (**Figure 4.11,** left). From **37**, a transition state for the hydrogenation of the Pd^{II}-Ar bond of the pincer ligand was located (**TS$_4$**) (**Figure 4.11,** middle). The transition state was calculated to be +25.8 kcal/mol relative to the starting compounds. The 5-centered **TS$_4$** represents the concerted formation of the Ar-H and H-H bonds with reduction at the Pd-center, yielding a monodentate P-coordinated (PC(H)N^{H})Pd-(η^2-H_2) complex **38** (**Figure 4.11,** right). Reduction of the metal center was found to be exergonic (-7.2 kcal/mol overall). The overall reaction coordinate diagram is depicted in **Figure 4.12**.

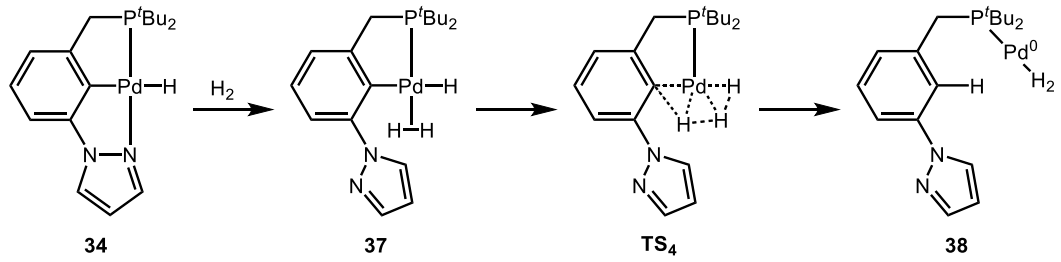

Scheme 4.8. Overall calculated degradation of **34** under H_2.

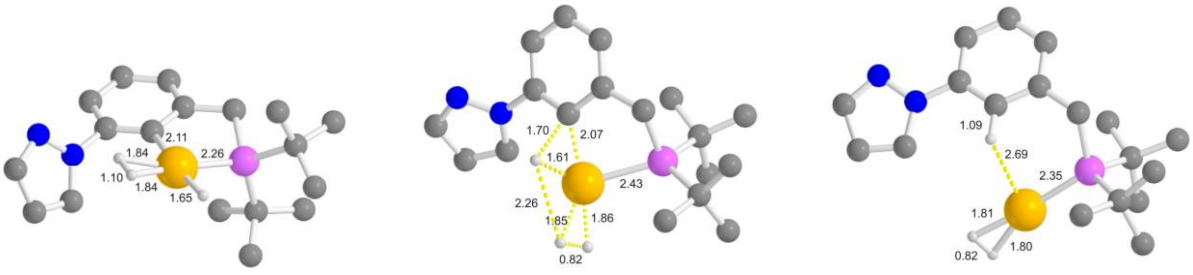

Figure 4.11. Optimized structure of (κ^2-P,C-PCN)Pd(H)(η^2-H_2) (**37**) (left), **TS$_4$** (middle), and (κ-P-PC(H)N)Pd-(η^2-H_2) (**38**) (right). Selected bond distances (Å) reported. H atoms on the pincer omitted for clarity.

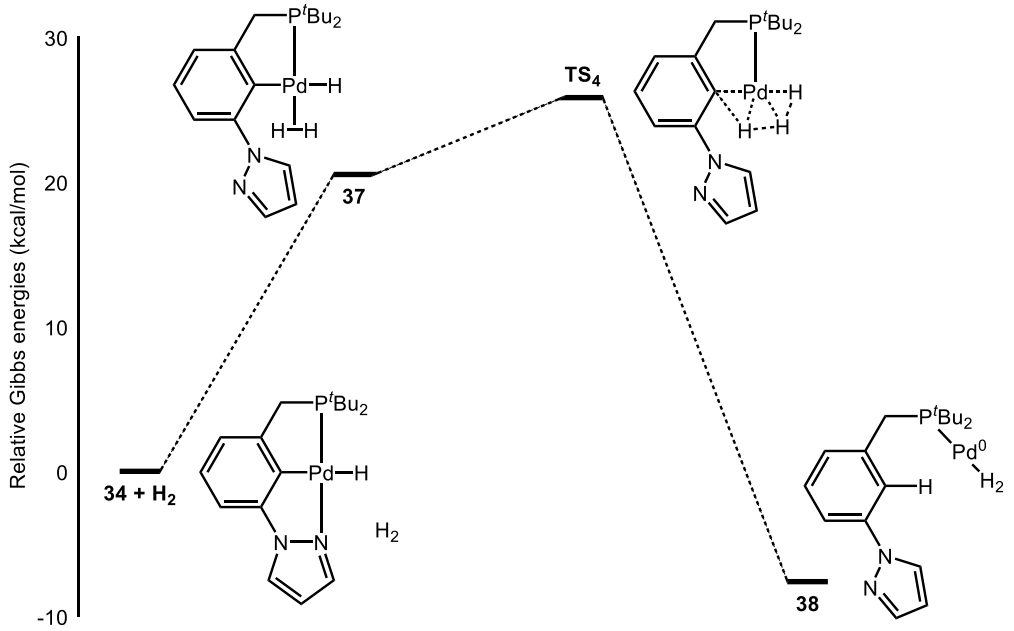

Figure 4.12. Reaction coordinate diagram for the reduction of the [(PCN^{H})Pd-H] fragment (**34**).

Displacement of the H_2 ligand of **38** by free PCN^{H} would yield the final reduced species **36**. Reduction of the [(PCC)Pd] fragment of **33** has yet to be investigated computationally. However, by the principle of microscopic reversibility, it is possible that the dihydrogen complex **35** could form from [(PCC)Pd] and free H_2 and undergo σ-bond metathesis, forming the terminal hydride **34** (**Scheme 4.9**). This second equivalent of **34** could then undergo reduction as described above. This is one possible mechanism but, without sufficient experimental evidence, remains purely a hypothesis.

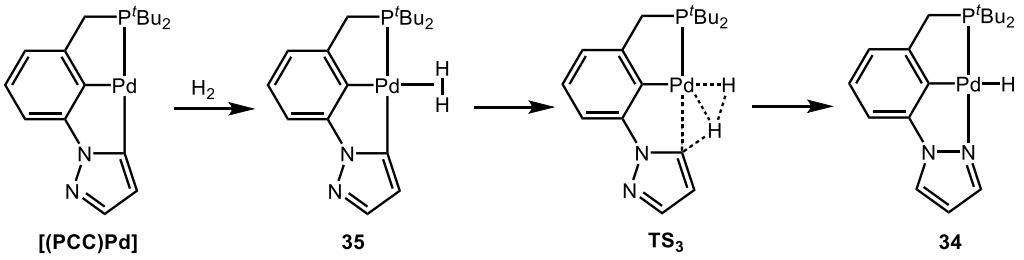

Scheme 4.9. Proposed hydrogenation of the [(PCC)Pd] fragment of **33** to form **34** based on rollover calculations.

Hydrogenolysis of (PCN^{H})PdOPh (39): The basic nature of the hydroxide ligand, and its ability to bridge metal centers caused a variety of different pathways to be followed upon hydrogenolysis. Therefore, a less basic, bulky aryloxide complex was investigated in order to probe the possibility of terminal hydride formation. The phenoxide complex (PCN^{H})Pd-OPh (**39**) was synthesized by addition of sodium phenoxide (NaOPh) to a THF-d_8 solution of the triflate **21** (**Scheme 4.10**). Salt metathesis resulted in clean formation of **39**. The ^{1}H NMR spectrum of **39** shows a doublet for both the ^{t}Bu (1.45 ppm, $^{3}J_{PH}$ = 14.1 Hz) and methylene protons (3.42 ppm, $^{2}J_{PH}$ = 9.3 Hz), consistent with its characterization as a mononuclear species. Aromatic signals (6.1-8.2 ppm) integrating to a total of 11 protons indicate the PCN^{H} backbone and phenoxide are bound to Pd^{II}. The ^{31}P{^{1}H} NMR spectrum displays a singlet at 91.3 ppm, shifted upfield from the triflate **21** (94.1 ppm). Single crystals were grown from a saturated THF solution of **39** layered with pentane. The solid state structure confirms the identity of **39** (**Figure 4.13**). Complex **39** crystallizes as a slightly distorted square planar Pd^{II} center (τ_4 = 0.15). The physical metrics are comparable to other [(PCN^{R})Pd]$^{+}$ frameworks (R = H or Me). The Pd-O bond (2.1021(14) Å) falls in a similar range to the Pd-O bonds in the dinuclear and mononuclear Pd-OH complexes **21**, **27** and **28**.

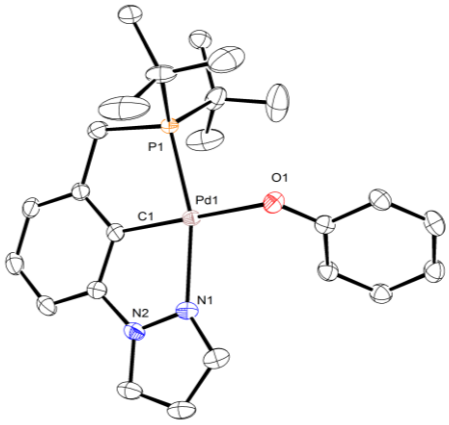

Figure 4.13. ORTEP[29] of (PCN^{H})Pd-OPh (**39**), with ellipsoids shown at 50% probability. Hydrogen atoms on the ligands omitted for clarity.

Addition of 7 atm of H_2 to a degassed solution of the Pd-OPh complex **39** in THF-d_8 at room temperature yielded a slow reduction of **39** to the Pd^0 complex **36** (**Scheme 4.10**). The reaction reaches 20% conversion over 14 days. No hydride intermediate was observed. The acidity of phenol, the conjugate acid produced by hydrogenolysis of the phenoxide, shifts the equilibrium of hydrogenolysis towards the reactants **39** and free H_2 (**Scheme 4.11**). This has been observed previously in the hydrogenolysis of (^{tBu}PCP)Pd-OPh.[11] As such, an appreciable amount of the hydride would never form, and instead hydrolysis of the Ar-Pd backbone through pyrazolyl displacement is most probable. If the terminal hydride **34** did form, similar products (complex **33**) to the hydrogenolysis of the terminal hydroxide **22** would be expected, as **34** would be a common intermediate between the reactions (**Scheme 4.6**). As only reduction to the Pd^0 complex **36** was observed experimentally, it further exemplifies that the PCN^H ligand is not capable of stabilizing a terminal, mononuclear Pd^{II}-H complex.

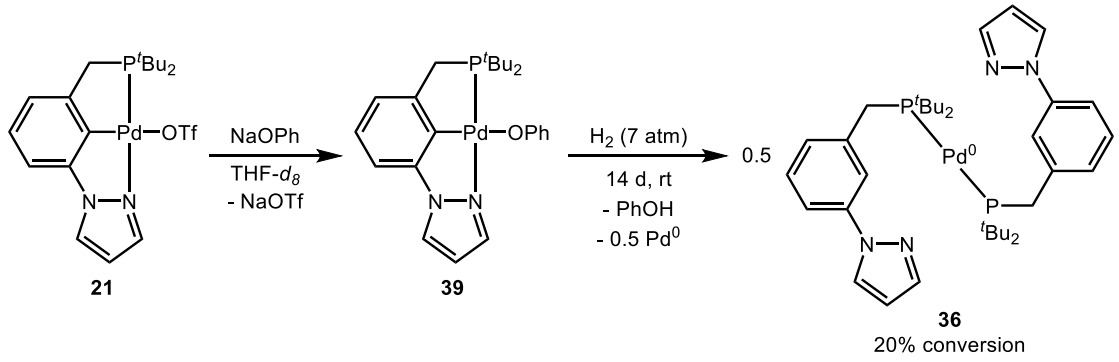

Scheme 4.10. Synthesis and hydrogenolysis of (PCN^H)Pd-OPh (**39**).

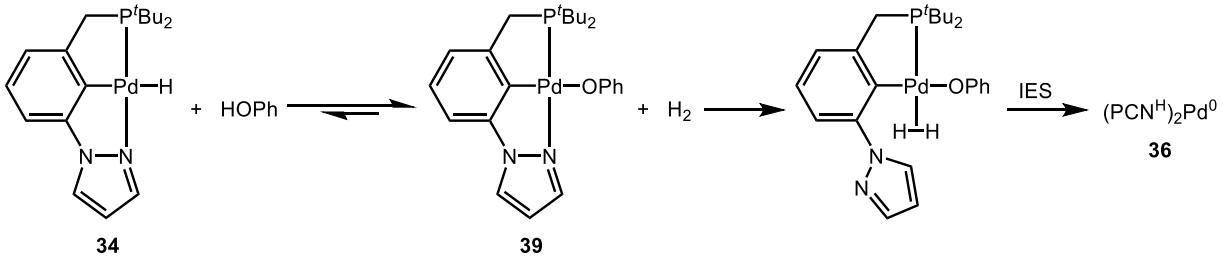

Scheme 4.11. Proposed equilibrium of the hydrogenolysis of **39**, favoring the Pd-OPh as only **36** is observed experimentally.

Hydrogenolysis of (PCN^{Me})PdOH (28): The reaction of the terminal hydroxide **28** with H_2 (1 atm) was followed to completion by ^{1}H and ^{31}P NMR spectroscopy over 40 hours at room temperature. However, no hydride species was observed throughout the reaction period. A singlet at 60.8 ppm in the ^{31}P NMR spectrum and a virtual triplet at 1.28 ppm ($^3J_{PH}$ = 6.1 Hz) in the ^{1}H NMR spectrum instead suggest that full reduction to a Pd^0 bisphosphine complex (**40**) occurred (**Scheme 4.12**). Indeed, complex **40** was confirmed as (κ-P-PCN^{Me})$_2$Pd^0 by independent synthesis.

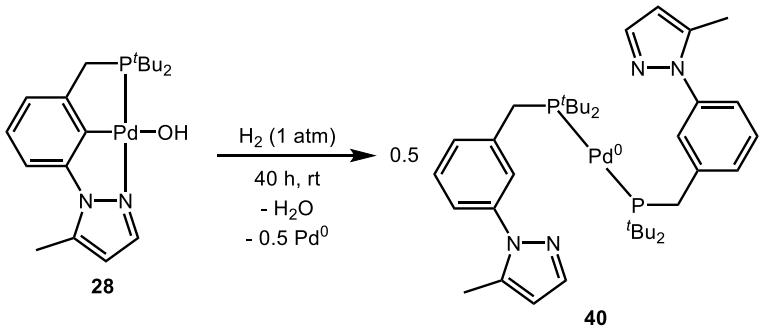

Scheme 4.12. Reduction of (PCN^{Me})Pd-OH (**28**) under H_2 to form the Pd^0 complex **40**.

Presumably, this reduction is occurring through an unstable terminal hydride intermediate. Hydrogenation of an aryl backbone has been previously investigated by us, and was found to proceed through displacement of the *cis* pincer arm by H_2.[12] As the pyrazole arm in these complexes has been established as hemilabile, reductive elimination could occur through dissociation of the pyrazolyl ring either before or after hydrogenolysis of the hydroxide ligand (**Scheme 4.13** top and bottom, respectively). The DFT results on the hydrogenolysis of the (PCN^H)Pd-OH (**22**) were used to assist in proposing a mechanism for **28** reduction, as the experimental physical metrics of the PCN^{Me} and the PCN^H Pd complexes are nearly identical based on single crystal X-ray diffractometry. Comparing the calculated energies for the hydrogenolysis of **22** to **34** (+25.8 kcal/mol), to the displacement of a pyrazole arm by H_2

(+20.6 kcal/mol) as well as our previous DFT findings,[12] reductive elimination through a *cis* hydride (formed from IES of H_2 with the hydroxide ligand) is more probable (**Scheme 4.13**, top).

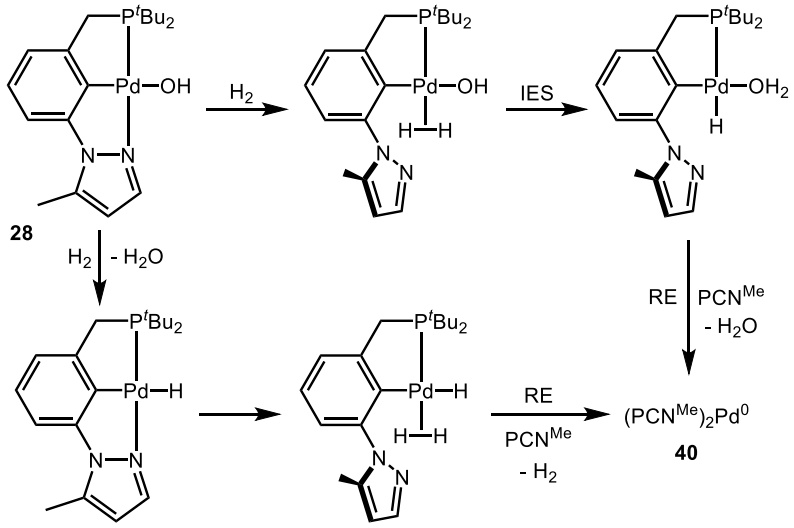

Scheme 4.13. Mechanisms considered for the reduction of **28**.

4.3 Summary

Mono- and dinuclear Pd-OH complexes supported by a PCN^R pincer were evaluated for their reactivity with H_2. The dinuclear $\{[(PCN^R)Pd]_2(\mu\text{-}OH)\}[OTf]$ (R = H, Me) complexes **21** and **27** were found to react cleanly to the analogous μ-hydride complexes **29** and **32**. The nickel analogue $\{[(PCN^H)Ni]_2(\mu\text{-}OH)\}[OTf]$ did not react with H_2 under similar conditions. The mononuclear (PCN^H)Pd-OH (**22**) reacts quickly with H_2, forming the proposed "rollover" product (PCN^H)Pd(μ-H)Pd(PCC) (**33**). This species further reacted under H_2 to yield the Pd^0 complex $(PCN^H)_2Pd^0$ (**36**). A similar reduction of (PCN^{Me})Pd-OH (**28**) to $(PCN^{Me})_2Pd^0$ (**40**) under H_2 was observed, however no hydride intermediate was detected. Assisted by DFT studies, it was proposed that the hemilabile pyrazole arm of PCN^R dissociated from the metal, allowing H_2 to coordinate and further hydrogenate the aryl backbone.

4.4 Experimental

General considerations and materials characterization. All air- and/or moisture-sensitive reactions were performed under inert atmosphere in flame-dried flasks using standard Schlenk-type techniques or in a glove-box filled with nitrogen. Tetrahydrofuran (THF), benzene, pentane and toluene were purified by means of a MBraun solvent purification system. THF-d_8, C_6D_6 and toluene-d_8 were dried over sodium/benzophenone ketyl. CD_2Cl_2 was dried over activated 4 Å molecular sieves. Hydrogen gas was introduced to reactions in J. Young NMR tubes on a high pressure gas manifold.[11] Complexes **21**, **22**, **27** and **28** were synthesized previously.[13] All other reagents and solvents were used as purchased from commercial suppliers. ^1H, $^{13}C\{^1H\}$ and $^{31}P\{^1H\}$ NMR spectra were obtained on either a Bruker Avance 700, Bruker Avance 500, Bruker Avance DRX-400 or a Bruker Avance 300 MHz instrument. Chemical shifts are reported in ppm (δ) relative to TMS, referenced to the chemical shifts of residual solvent resonances (^1H and ^{13}C), and coupling constants are given in Hz. $^{31}P\{^1H\}$ NMR spectra are referenced to an external 85% H_3PO_4 sample (0 ppm).

X-ray Diffraction Data. X-ray diffraction intensity data were collected on a *Bruker APEX II* diffractometer using a *Mo-K*α radiation (λ = 0.71073 Å) at low temperature (either T = 100 or 120 K, see **Table 4.1**). The dataset was integrated and scaled using SAINT, SADABS within the APEX2 software package by Bruker.[36] The program used for the data collection was *CrysAlis CCD* 1.171.[37] Data reduction was carried out with the program *CrysAlis RED* 1.171[38] and the absorption correction was applied with the program *ABSPACK* 1.17. Direct methods implemented in *Sir97*[39] were used to solve the structures and the refinements were performed by full-matrix least-squares against F^2 implemented in *SHELX97*.[40] All the non-hydrogen atoms were found from Fourier syntheses of electron density and were refined anisotropically,

while the hydrogen atoms were fixed in calculated positions and refined isotropically with the thermal factor depending on the one of the atom to which they are bound (riding model) with C---H distances in the range 0.95-1.00 Angstrom. The geometrical calculations were performed by *PARST97*.[41] The details of crystallographic, collection and refinement data are shown in **Table 4.2**. Molecular plots were produced by the program *ORTEP3*.[42]

Computational Details. Density Functional Theory (DFT) calculations were performed using the *Gaussian09* program (revision C.01).[43] Model structures were optimized with a M06 functional[44] using the SDD/MWB10 pseudopotential and related basis set[45] on the palladium and phosphorus atoms plus a 6-31G* basis set on all the other atoms. Introduction of diffuse functions is essential to well-reproduce conformational equilibria and experimental electron affinities.[46] An extra *d*-type polarization function for P and an extra *f*-type function for Pd were added to the standard set.[47] Gibbs energy calculations to infer relative thermodynamic stabilities were carried out on the real system. The initial guess geometry for the optimization was obtained starting from the XRD structure of the dimeric species **23**. IRC analysis[48] was performed, to find the two minima linked by the related transition structure. When IRC calculations failed to reach the minima, geometry optimizations from the initial phase of the IRC path were performed. Frequency calculations were made on all the optimized structures, to characterize the stationary points as minima or TSs, as well for the calculation of zero-point energies, enthalpies, entropies and gas phase Gibbs energies at 298 K. Evaluation of the solvent effects was performed through a continuum modeling of the reaction medium. Bulk solvent effects (THF, $\varepsilon = 7.42$) were expressed through the SMD Continuum Model,[49] with the same basis set used for the gas phase optimizations. Gibbs energy in solution was calculated according to the following simplified equation: $G_{THF} = G_{gas} + (E_{THF} - E_{gas})$.

Table 4.1. Collection of the main crystal data and structure refinement details of the compounds presented in this study.

	29	**30**	**31**	**32**	**39**
Empirical formula	$C_{49}H_{77}F_3N_4O_6P_2Pd_2S$	$C_{19}H_{26}F_3N_2NiOPS$	$C_{37}H_{53}F_3N_4Ni_2O_4P_2S$	$C_{47}H_{72}F_3N_4O_5P_2Pd_2S$	$C_{76}H_{101}N_6O_4P_3Pd_3$
FW	1181.95	509.16	886.25	1136.89	1574.74
T, K	100(2)	100(2)	100(2)	100(2)	100(2)
Crystal system	Monoclinic	Triclinic	Monoclinic	Monoclinic	Triclinic
Space group	P 2_1/n	P -1	C 2/c	P 2_1/c	P -1
Unit cell dimensions	*a* [Å] = 28.393(5) *b* [Å] = 12.542(5) *c* [Å] = 29.920(5) α [°] = 90.000(5) β [°] = 91.193(5) γ [°] = 90.000(5)	*a* [Å] = 8.0982(4) *b* [Å] = 8.8317(4) *c* [Å] = 16.3416(8) α [°] = 102.901(2) β [°] = 94.745(2) γ [°] = 104.105(2)	*a* [Å] = 13.833(4) *b* [Å] = 19.325(6) *c* [Å] = 16.879(6) α [°] = 90 β [°] = 113.38(2) γ [°] = 90	*a* [Å] = 18.661(17) *b* [Å] = 12.935(12) *c* [Å] = 22.69(2) α [°] = 90 β [°] = 113.101(16) γ [°] = 90	*a* [Å] = 15.7572(10) *b* [Å] = 15.8387(11) *c* [Å] = 16.3363(12) α [°] = 81.614(4) β [°] = 87.205(4) γ [°] = 63.022(3)
V, Å^3	10652(5)	1093.23(9)	4142(2)	5038(8)	3593.9(4)
Z	8	2	4	4	2
Dcalc, mg/m^3	1.474	1.547	1.421	1.499	1.455
Abs coeff, mm^{-1}	0.834	1.105	1.093	0.878	0.862
F(000)	4896	528	1856	2348	1628
Crystal size, mm	0.07 x 0.03 x 0.02	0.28 x 0.15 x 0.12	0.15 x 0.03 x 0.03	0.17 x 0.17 x 0.08	0.15 x 0.11 x 0.06
θ range for collection, [°]	1.91 to 25.49	1.29 to 28.25	1.92 to 25.15	1.97 to 28.44	2.05 to 28.42
Index ranges	$-34 \le h \le 34$ $-15 \le k \le 15$ $-35 \le l \le 35$	-10<=h<=10 -11<=k<=11 -21<=l<=21	-16 ≤ h ≤ 16 -23 ≤ k ≤ 23 -20 ≤ l ≤ 20	$-25 \le h \le 24$ $-16 \le k \le 16$ $-30 \le l \le 30$	-20<=h<=21 -21<=k<=21 -21<=l<=21
Reflns collected	36611	35843	31514	160601	227896
Independent reflns	19366	5374	3719	12483	17903
Rint	0.3815	0.0466	0.2303	0.0549	0.0403
Completeness to θ	99.1 (θ = 25.0°)	99.9 (θ = 25.0°)	99.9 (θ = 25.0°)	99.9 (θ = 25.0°)	99.9 (θ = 25.0°)
Data / restraints / parameters	19366 / 301 / 1237	5374 / 0 / 277	3719 / 9 / 278	12483 / 30 / 613	17903 / 0 / 847
GOF on F^2	0.910	1.049	1.037	1.082	1.029
Final *R* indices	*R1* = 0.0958	R1 = 0.0378	R1 = 0.0852	*R1* = 0.0376	R1 = 0.0264
[I>2σ(I)]	*wR2* = 0.1172	wR2 = 0.0823	wR2 = 0.1990	*wR2* = 0.0826	wR2 = 0.0581
R indices (all data)	*R1* = 0.3498 *wR2* = 0.1811	R1 = 0.0517 wR2 = 0.0874	R1 = 0.1803 wR2 = 0.2535	*R1* = 0.0550 *wR2* = 0.0937	R1 = 0.0354 wR2 = 0.0630
Largest diff peak and hole, [e Å^3]	0.966 and −0.792	0.802 and -0.378	1.384 and -0.714	1.856 and -0.927	1.430 and -0.742

Table 4.2. Select bond lengths (Å) and angles (°) for complexes **29**-**32** and **39**.

	29	**30**	**31**[a,b]	**32**	**39**[c]
C(1)-Pd(1)	1.976(15)	1.877(2)	1.888(9)	2.005(3)	1.9667(19)
C(7)-Pd(1)	-	-	-	-	-
C(19)-Pd(2)	2.008(15)	-	-	2.011(3)	-
N(1)-N(2)	1.323(14)	1.369(3)	1.380(9)	1.381(3)	1.368(2)
N(1)-Pd(1)	2.135(14)	1.9485(18)	1.932(7)	2.100(3)	2.1034(16)
O(1)-Ni(1)		1.9979(14)	1.933(3)		2.1021(14)
N(3)-N(4)	1.361(14)	-	-	1.378(4)	-
N(3)-Pd(2)	2.115(11)	-	-	2.105(3)	-
P(1)-Pd(1)	2.242(5)	2.1782(6)	2.172(2)	2.2502(15)	2.2356(5)
P(2)-Pd(2)	2.248(4)	-	-	2.2451(15)	-
Pd(1)-Pd(2)	3.0563(17)	-	-	2.977(3)	-
Ni(1)-O(1)-Ni(2)		-	135.4(4)		-
C(1)-Ni(1)-O(1)		178.10(7)	174.9(3)		176.14(7)
C(7)-Pd(1)-P(1)	-	-	-	-	-
P(1)-Pd(1)-N(1)	160.2(4)	165.44(6)	164.5(2)	159.12(7)	162.83(5)
P(2)-Pd(2)-N(3)	159.7(4)	-	-	157.85(8)	-

[a] A two-fold rotation through the bridging hydroxyl relates half of the dimer to the other, and the metrics of each were kept the same.
[b] Bonds listed as Pd(1) are Ni(1).
[c] Bonds listed as Ni(1) are Pd(1).

{[(PCN^{H})Pd]$_2$(μ-H)}(OTf) (29): Complex **21** (4.2 mg, 0.00428 mmol) and hexamethylbenzene (IS, 0.9 mg, 0.00555 mmol) were added to a J. Young NMR tube and dissolved in THF-d_8 (0.4 mL). The clear solution was degassed (freeze, pump, thaw 3x), and placed under H_2 (5 atm). The reaction was monitored over 18 days at room temperature until full conversion of **21** was achieved, yielding **29** (83% yield based on IS). Single crystals were grown from slow diffusion of pentane into a concentrated THF solution of **29** at -30 °C.

^{31}P{^{1}H} NMR (202 MHz, THF-d_8) δ 105.2 (s). ^{1}H NMR (500 MHz, THF-d_8) δ -8.68 (t, J = 12.6 Hz, 1H, Pd-*H*), 1.44 (d, J = 5.1 Hz, 18H, P(C(C*H*$_3$)$_3$)$_2$), 1.49 (d, J = 5.3 Hz, 18H, P(C(C*H*$_3$)$_3$)$_2$), 3.70 (dd, J = 17.9, 10.0 Hz, 2H, C*H*$_2$P), 3.82 (dd, J = 18.0, 9.0 Hz, 2H, C*H*$_2$P),

6.30-6.33 (m, 2H), 7.21–7.17 (m, 4H), 7.43–7.38 (m, 2H), 8.33-8.35 (m, 2H), 8.43-8.46 (m, 2H).

(PCN^{H})Ni-OTf (30): In the dark, (PCN^{H})Ni-Br (100 mg, 0.227 mmols) and AgOTf (63.8 mg, 0.248 mmols) were dissolved in CH_2Cl_2 and stirred for 5 hours. The mixture was then filtered through Celite® and the resulting clear yellow solution was layered with pentane and left to recrystallize at -30 °C. The resulting large yellow crystals were isolated and dried, yielding **30** (104 mg, 90 % yield).

$^{31}P\{^{1}H\}$ NMR (121 MHz, THF-d_8) δ 86.5 (s). ^{1}H NMR (300 MHz, THF-d_8) δ 1.48 (d, $^{3}J_{PH}$ = 13.6 Hz, 18H, P(C(CH_3)$_3$)$_2$), 3.24 (d, $^{2}J_{PH}$ = 9.1 Hz, 2H, CH_2P), 6.45-6.48 (m, 1H), 6.75-6.81 (m, 1H), 6.95-7.02 (m, 2H), 8.21-8.26 (m, 2H).

{[(PCN^{H})Ni]$_2$(μ-OH)}(OTf) (31): Complex **30** (5.4 mg, 0.0106 mmols) and KOH (0.4 mg, 0.00713 mmols) were added to a J. Young NMR tube and dissolved in THF-d_8 (0.4 mL). The sample was rotated for 3 days, at which point full conversion to **31** was observed by NMR spectroscopy. Single crystals suitable for X-ray diffraction spontaneously grew over the reaction period.

$^{31}P\{^{1}H\}$ NMR (202 MHz, THF-d_8) δ 84.2 (s). ^{1}H NMR (500 MHz, THF-d_8) δ -3.38 (s, 1H, Ni-OH), 1.48 (d, $^{3}J_{PH}$ = 13.3 Hz, 18H, P(C(CH_3)$_3$)$_2$), 1.53 (d, $^{3}J_{PH}$ = 13.4 Hz, 18H, P(C(CH_3)$_3$)$_2$), 3.31 (dd, $^{2}J_{HH}$ = 17.9, $^{2}J_{PH}$ = 10.2 Hz, 2H, CH_2P), 3.43 (dd, $^{2}J_{HH}$ = 17.9, $^{2}J_{PH}$ = 8.2 Hz, 2H, CH_2P), 6.39-6.41 (m, 2H), 6.86 (d, $^{3}J_{HH}$ = 7.4 Hz, 2H), 7.03 (t, $^{3}J_{HH}$ = 7.6 Hz, 2H), 7.08 (d, $^{3}J_{HH}$ = 7.8 Hz, 2H), 8.29-8.33 (m, 2H), 9.79-9.83 (m, 2H).

{[(PCN^{Me})Pd]$_2$(μ-H)}(OTf) (32): To a degassed (freeze, pump, thaw 3x) solution of **27** (7.2 mg, 0.00713 mmols) and hexamethylbenzene (IS, <1 mg) in a medium walled J. Young NMR

tube was added gaseous H_2 (7 atm) at room temperature. The solution was mixed, and allowed to react for 6 days at which full conversion to complex **32** was observed (96% yield based on IS). Suitable crystals for X-ray diffraction were grown from a concentrated THF-d_8 solution of **32** layered with pentane.

$^{31}P\{^1H\}$ NMR (121 MHz, THF-d_8) δ 105.2 (s). ^1H NMR (300 MHz, THF-d_8) δ -8.77 (t, J = 13.2 Hz, 1H, Pd-*H*), 1.42 (d, J = 8.4 Hz, 18H, P(C(C*H*$_3$)$_3$)$_2$), 1.47 (d, J = 8.6 Hz, 18H, P(C(C*H*$_3$)$_3$)$_2$), 2.65 (s, 6H, pyz-C*H*$_3$), 3.69 (dd, J = 17.9, 10.3 Hz, 2H, C*H*$_2$P), 3.83 (dd, J = 18.0, 8.9 Hz, 2H, C*H*$_2$P), 6.10-6.13 (m, 2H), 7.16-7.23 (m, 2H), 7.21-7.24 (m, 2H), 7.39 (dd, J = 6.9, 2.2 Hz, 2H), 8.42-8.45 (m, 2H). $^{13}C\{^1H\}$ NMR (176 MHz, THF-d_8) δ 14.2 (s, Pyz-*C*H$_3$), 29.49 (d, J = 4.3 Hz, PC(*C*H$_3$)$_3$), 30.39 (d, J = 4.5 Hz, PC(*C*H$_3$)$_3$), 35.29 (d, J = 17.8 Hz, P*C*(CH$_3$)$_3$), 36.85 (d, J = 18.6 Hz, P*C*(CH$_3$)$_3$), 37.19 (d, J = 30.1 Hz, P*C*H$_2$), 109.4 (d, J = 2.4 Hz, Ar-C), 112.6 (s, Ar-C), 123.09 (d, J = 20.8 Hz, Pyz-C), 127.4 (s, Ar-C), 141.8 (s, Ar-C), 145.0 (s, Ar-C), 145.5 (s, Ar-C), 151.42 (d, J = 13.4 Hz, Pyz-C), 154.0 (s, Pyz-C).

(PCN^H)Pd(μ-H)Pd(PCC) (33): To a degassed solution of (PCN^H)Pd-OH (**22**), formed *in situ* by addition of KOH (2.0 mg, 0.036 mmols) to (PCN^H)Pd-OTf (**20**) (6.2 mg, 0.011 mmols), in toluene-d_8 (0.4 mL) was added H_2 (7 atm) at room temperature. The reaction was monitored by ^1H and $^{31}P\{^1H\}$ NMR spectroscopy, and after 5 mins from H_2 addition, the hydride **33** could be observed. The reaction appeared complete after 5 hours, with a small amount of (PCN^H)$_2$Pd^0 (**36**) observed as well. Attempts to recrystallize **33** in toluene-d_8 layered with pentane at -30 °C yielded dark microcrystals that decomposed at room temperature.

$^{31}P\{^1H\}$ NMR (121 MHz, toluene-d_8) δ 85.9 (s, P *trans* to C), 103.8 (s, P *trans* to N). ^1H NMR (500 MHz, toluene-d_8) δ -8.65 (dd, $^2J_{PH}$ = 15.3, 10.2 Hz, 1H, Pd-*H*), 1.16 (d, $^3J_{PH}$ = 14.0 Hz, 9H, P(C(C*H*$_3$)$_3$)), 1.19 (d, $^3J_{PH}$ = 14.5 Hz, 9H, P(C(C*H*$_3$)$_3$)), 1.21 (d, $^3J_{PH}$ = 13.0 Hz, 9H,

P(C(CH_3)$_3$)), 1.23 (d, $^3J_{PH}$ = 12.5 Hz, 9H, P(C(CH_3)$_3$)), 3.00 (dd, $^2J_{HH}$ = 9.8 Hz, $^2J_{PH}$ = 17.6 Hz, 2H, CH_2P), 5.33-5.27 (m, 1H), 5.78-5.82 (m, 1H), 6.55-6.60 (m, 1H), 7.47-7.51 (m, 1H), 7.78-7.83 (m, 1H), 8.33-8.38 (m, 1H), 8.46-8.49 (m, 1H). Some assignments could not be made due to side product or solvent overlap.

(PCN^H)$_2$Pd^0 (36): The reduced species **36** was observed as a decomposition product from the further reaction of **33** with H_2. Complex **36** was synthesized independently. To a solution of the PCN^H ligand (0.050 g, 0.165 mmol) in dry and degassed C_6H_6 (1 mL) a solution of Pd(dba)2 (0.047 g, 0.082 mmol) in dry and degassed C_6H_6 (1.5 mL) was added in one portion. The reaction was stirred at 50 °C for 24 h and its course was periodically monitored by sampling the mixture and analyzing it via ^{31}P NMR spectroscopy until complete conversion. The solvent was removed at room temperature under reduced pressure to give a yellow pale solid as crude material. Attempts to completely eliminate free dba from the mixture by successive washing with cold pentane were not successful.

^{31}P{^{1}H} NMR (283 MHz, THF-d_8) δ 61.1 (s). ^{1}H NMR (700 MHz, THF-d_8) δ 1.28 (vt, 36H, P(C(CH_3)$_3$)$_2$), 3.08 (vt, 4H, CH_2P), 6.29-6.31 (m, 2H), 7.11-7.15 (m, 4H), 7.47-7.49 (m, 2H), 7.52 (d, $^4J_{PH}$ = 1.7 Hz, 2H), 8.08 (d, $^4J_{PH}$ = 2.4 Hz, 2H), 8.13-8.16 (m, 2H), 8.25-8.26 (m, 2H).

(PCN^H)Pd-OPh (39): To a solution of (PCN^H)Pd-OTf (**20**) (8.2 mg, 0.0147 mmols) in THF-d_8 (0.4 mL) was added NaOPh (1.7 mg, 0.0146 mmols). Complete conversion to the phenoxide **39** was observed after 1 hour by ^{1}H and ^{31}P{^{1}H} NMR spectroscopy.

^{31}P{^{1}H} NMR (202 MHz, THF-d_8) δ 91.3 (s). ^{1}H NMR (500 MHz, THF-d_8) δ 1.45 (d, $^3J_{PH}$ = 14.1 Hz, 18H, P(C(CH_3)$_3$)$_2$), 3.42 (d, $^2J_{PH}$ = 9.3 Hz, 2H, CH_2P), 6.19 (td, $^3J_{HH}$ = 7.1, $^4J_{HH}$ 1.2

Hz, 1H), 6.32-6.34 (m, 1H), 6.64-6.70 (m, 2H), 6.80-6.84 (m, 2H), 6.96-7.03 (m, 3H), 7.14-7.18 (m, 1H), 8.21-8.23 (m, 1H).

(PCN^{Me})$_2$Pd^0 (40): A degassed (freeze, pump, thaw 3x) solution of **28** (6.8 mg, 0.0155 mmols) in THF-d_8 (0.4 mL) and hexamethylbenzene (IS, 0.5 mg) in a J. Young medium walled NMR tube was pressurized with H_2 (1 atm) and left at room temperature. The clear solution turned to a dark suspension over 3 days at room temperature, yielding complex **40** (80% yield assessed via integration versus IS). No hydride intermediate was observed.

$^{31}P\{^1H\}$ NMR (202 MHz, THF-d_8) δ 60.8 (s). ^1H NMR (500 MHz, THF-d_8) δ 1.28 (vt, J = 6.1 Hz, 36H, P(C(CH_3)$_3$)$_2$), 2.27 (s, 6H, pyz-CH_3), 3.08 (vt, J = 2.8 Hz, 4H, CH_2P), 6.08–6.06 (m, 2H), 7.18–7.14 (m, 2H), 7.36 (d, J = 1.7 Hz, 2H), 7.82-7.85 (m, 2H), 8.30-8.35 (m, 2H).

Kinetic studies of the hydrogenolysis of 27: Complex **27** (10.3 mg, 0.0102 mmol) and hexamethylbenzene (1.7 mg, 0.0105 mmol, IS) were dissolved in THF-d_8 (2.0 mL), forming a 5.1 mM stock solution. Each kinetic experiment was run with 0.4 mL of stock solution (0.00204 mmol **27**) in a J. Young NMR tube. The sample was degassed (freeze, pump, thaw 3x), put under a pressure of H_2 (1.0, 2.0, or 5.0 atm) and heated to 50 °C. The reactions were monitored by ^1H NMR spectroscopy. For the experiments with 2.0 and 5.0 atm of H_2, heating was carried out completely inside the NMR probe (323.5 and 323.2 K respectively, ethylene glycol calibrated). For the experiment with 1.0 atm of H_2, heating at 50 °C was carried out in a thermocouple controlled oil bath as well as inside the NMR probe during data collection. For samples heated in the oil bath, the tube was cooled to rt in an acetone bath prior to data collection. Rates were determined by monitoring the disappearance of the pyrazole C-H signal (6.19-6.22 ppm) through three half-lives compared to the hexamethylbenzene internal standard.

4.5 Notes to Chapter 4

1. Esteruelas, M. A.; Oro, L. A. *Chem. Rev.* **1998**, *98*, 577.
2. Ito, M.; Ikariya, T. *Chem. Commun.* **2007**, 5134.
3. Jessop, P. G.; Morris, R. H. *Coord. Chem. Rev.* **1992**, *121*, 155.
4. Wang, W.; Wang, S.; Ma, X.; Gong, J. *Chem. Soc. Rev.* **2011**, *40*, 3703.
5. Clapham, S. E.; Hadzovic, A.; Morris, R. H. *Coord. Chem. Rev.* **2004**, *248*, 2201.
6. Bailey, W. D.; Parkes, M. V.; Kemp, R. A.; Goldberg, K. I. *Reactions of Square* Planar d^8 Pincer Complexes with Oxygen and Hydrogen. Pincer and Pincer-Type Complexes: Application in Organic Synthesis and Catalysis*;* Szabo, K. J., Ed.; Wendt, O. F., Ed; Wiley-VCH: Weinheim, Germany, 2014; pp 281-298.
7. Jessop, P. G.; Ikariya, T.; Noyori, R. *Chem. Rev.* **1995**, *95*, 259.
8. Voorhees, V.; Adams, R. *J. Am. Chem. Soc.* **1922**, *44*, 1397.
9. Pearlman, W. M. *Tetrahedron Lett.* **1967**, *8*, 1663.
10. Mahoney, W. S.; Brestensky, D. M.; Stryker, J. M. *J. Am. Chem. Soc.* **1988**, *110*, 291.
11. Fulmer, G. R.; Herndon, A. N.; Kaminsky, W.; Kemp, R. A.; Goldberg, K. I. *J. Am. Chem. Soc.* **2011**, *133*, 17713.
12. Parkes, M. V.; Bailey, W. D.; Goldberg, K. I.; Kemp, R. A. *Manuscript in preparation*, 2016.
13. Bailey, W. D.; Luconi, L.; Rossin, A.; Yakhvarov, D.; Flowers, S. E.; Kaminsky, W.; Kemp, R. A.; Giambastiani, G.; Goldberg, K. I. *Organometallics* **2015**, *34*, 3998.
14. Yang, L.; Powell, D. R.; Houser, R. P. *Dalton Trans.* **2007**, 955.
15. Portnoy, M.; Frolow, F.; Milstein D. *Organometallics* **1991**, *10*, 3960.
16. Fryzuk, M. D.; Lloyd, B. R.; Clentsmith, G. K. B.; Rettig, S. J. *J. Am. Chem. Soc.* ***1991***, *113*, 4332.
17. Fryzuk, M. D.; Lloyd, B. R.; Clentsmith, G. K. B.; Rettig, S. J. *J. Am. Chem. Soc.* **1994**, *116*, 3804.
18. Chan, S.; Lee, S.-M.; Lin, Z.; Wong W.-T. *J. Organomet. Chem.* **1996**, *510*, 219.
19. Stockland Junior, R. A.; Anderson, G. K.; Rath, N. P. *Inorg. Chim. Acta* **1997**, *259*, 173.
20. Stockland Junior, R. A.; Anderson, G. K.; Rath, N. P. *J. Am. Chem. Soc.* **1999**, *121*, 7945.
21. Stockland Junior, R. A.; Anderson, G. K.; Rath, N. P. *Inorg. Chim. Acta* **2000**, *300*, 395.
22. Zhuravel, M. A.; Moncarz, J. R.; Glueck, D. S.; Lam, K.-C.; Rheingold A. L. *Organometallics* **2000**, *19*, 3447.
23. Evrard, D.; Meilleur, D.; Drouin, M.; Mugnier, Y.; Harvey P. D. *Z. Anorg. Allg. Chem.* **2002**, *628*, 2286.
24. Goto, E.; Begum, R. A.; Zhan, S.; Tanase, T.; Tanigaki, K.; Sakai, K. *Angew. Chem. Int. Ed.* **2004**, *43*, 5029.
25. Baya, M.; Houghton, J.; Konya, D.; Champouret, Y.; Daran, J.-C.; Lenero, K. Q. A.; Schoon, L.; Mul, W. P.; van Oort, A. B.; Meijboom, N.; Drent, E.; Orpen, A. G.; Poli R. *J. Am. Chem. Soc.* **2008**, *130*, 10612.
26. Tanabe, M.; Ishikawa, N.; Chiba, M.; Ide, T.; Osakada, K.; Tanase T. *J. Am. Chem. Soc.* **2011**, *133*, 18598.
27. Adams, R. D.; Pearl Junior, W. C.; Wong, Y. O.; Zhang, Q.; Hall, M. B.; Walensky, J. R. *J.Am.Chem.Soc.* **2011**, *133*, 12994.
28. Herbert, D. E.; Ozerov, O. V. *Organometallics* **2011**, *30*, 6641.
29. Farrugia, L. J. *J. Appl. Cryst.* **2012**, *45*, 849.
30. (PCN^H)Ni-Br was synthesized in the laboratory of Dr. Giuliano Giambastiani and sent to us for further study.
31. Bondi, A. *J. Phys. Chem.* **1964**, *68*, 441.

32. Data compiled from (a) Cottrell, T. L. *The Strengths of Chemical Bonds*, 2d ed., Butterworth, London, 1958. (b) Darwent, B. B. *National Standard Reference Data Series, National Bureau of Standards, no. 31*, Washington, 1970. J. A. Kerr, Chem. Rev. 66:465 (1966).
33. Brunner, E. *J. Chem. Eng. Data* **1985**, *30*, 269.
34. Bailey, W. D.; Luconi, L.; Rossin, A.; Yakhvarov, D.; Flowers, S. E.; Kaminsky, W.; Kemp, R. A.; Giambastiani, G.; Goldberg, K. I. *Unpublished communication*, **2016**.
35. Fulmer, G. R.; Kaminsky, W.; Kemp, R. A.; Goldberg, K. I. *Organometallics* **2011**, *30*, 1627.
36. Bruker (**2007**) APEX2 (Version 2.1-4), SAINT (version 7.34A), SADABS (version 2007/4), BrukerAXS Inc, Madison, Wisconsin, USA.
37. CrysAlis CCD 1.171.31.2 (release 07-07-2006), CrysAlis171 .NET, Oxford Diffraction Ltd.
38. CrysAlis RED 1.171.31.2 (release 07-07-2006), CrysAlis171 .NET, Oxford Diffraction Ltd.
39. Altomare, A.; Burla, M. C.; Camalli, M.; Cascarano, G. L.; Giacovazzo, C.; Guagliardi, A.; Moliterni, A. G. G.; Polidori, G.; Spagna, R. *J. Appl. Crystallogr.* **1999**, *32*, 115.
40. Sheldrick, G. M. SHELXL (**1997**).
41. Nardelli, M. *Comput. Chem.* **1993**, *7*, 95.
42. Farrugia, L. J. *J. Appl. Crystallogr.* **1997**, *30*, 565.
43. Frisch, M. J. *et al.*, *Gaussian09*, Revision C.01, Gaussian Inc., Wallingford CT, **2009**.
44. Zhao, Y. and Truhlar, D. G. *Theor. Chem. Account* **2008**, *120*, 215.
45. (a) Andrae, D.; Haeuessermann, U.; Dolg, M.; Stoll, H.; Preuss, H. *Theor. Chem. Acc.* **1990**, *77*, 123. (b) Dunning Jr., T. H.; Hay P. J. in *Modern Theoretical Chemistry*, Ed. H. F. Schaefer III, Vol. 3 (Plenum, New York, **1976**) 1-28.
46. Lynch, B. J.; Zhao Y.; Truhlar, D. G. *J. Phys. Chem. A* **2003**, *107*, 1384.
47. (a) Höllwarth, A.; Böhme, M.; Dapprich, S.; Ehlers, A. W.; Gobbi, A.; Jonas, V.; Köhler, K. F.; Stegmann, R.; Veldkamp A.; Frenking, G. *Chem. Phys. Lett.* **1993**, *208*, 237. (b) Ehlers, A. W.; Böhme, M.; Dapprich, S.; Gobbi, A.; Höllwarth, A.; Jonas, V.; Köhler, K. F.; Stegmann, R.; Veldkamp, A.; Frenking, G. *Chem. Phys. Lett.* **1993**, *208*, 111.
48. Fukui, K. *Acc. Chem. Res.* **1981**, *14*, 363.
49. Marenich, A. V.; Cramer C. J.; Truhlar, D. G. *J. Phys. Chem. B* **2009**, *113*, 6378.

Chapter 5

Metal-ligand cooperation designed to assist oxygen atom transfer

5.1 Introduction

Historically, the catalysts for epoxidation have primarily been homo/heterogeneous early transition metals or heterogeneous Ag/Au surfaces.[1,2-6] The partial oxidation of olefins to epoxides is performed by early transition metal hydroperoxide complexes at the industrial scale.[7] The primary catalyst of choice is a titanium center supported on silicate (catalyst TS-1). A variety of mechanisms by which the epoxidation takes place have been proposed.[8] The most prevalent mechanisms are outlined in **Scheme 5.1**. Ancillary ligand cooperation has been proposed in assisting O-atom transfer (OAT) of both β and α oxygen to a nucleophilic olefin (**Scheme 5.1**, a and e, respectively). A similar mechanism is proposed for epoxidation by organic peracids (**Scheme 5.1**, b).[9] The oxophilic nature of the early metal can also allow for η^2 coordination of the hydroperoxide moiety, and transfer of the α oxygen to a nucleophilic olefin (**Scheme 5.1**, d). In all cases, it should be noted that the olefin acts as a nucleophile, and

the oxophilic early metal imparts a high degree of electrophilicity to the hydroperoxide ligand, allowing OAT. However, the same oxophilicty of the early metals renders them practically incapable of utilizing O_2 as the oxidant; the M-O bond is far too inert for catalyst turnover. As such, hydrogen peroxide or alkyl hydroperoxides are utilized to regenerate the active species. As our goal is to use the less expensive, more available, and less hazardous O_2 as an oxidant, less oxophilic metals (late transition metals) are more attractive. However, late-transition metals are less likely to endow the hydroperoxide ligand a high enough degree of electrophilicity, rendering it inert towards nucleophilic attack by olefins. And so, the question that we face is how can we manipulate the metal complex to increase the electrophilicity of the hydroperoxide to promote OAT? As it is the early/middle transition metal centers that show the most proclivity for this OAT step, we can gain inspiration from the mechanisms by which these metals carry out this reaction and use that in the design of our late metal systems. For example, as shown in **Scheme 5.1**, additional basic sites and proton movement can be intimately involved in these transfers.

Proton transfer and/or hydrogen bonding have been proposed to be important in OAT reactions involving both early and late metal systems and organic peracids. **Scheme 5.1** reactions a and e illustrate examples of the proposed OAT mechanism for early metals where an oxo/hydroxo ligand participates by accepting a proton in the concerted transformation, forming a bound hydroxide or free water molecule, respectively. Notably epoxidation mechanisms by organic peracids (**Scheme 5.2**, a),[10] for example *m*-chloroperbenzoic acid (mCPBA), mimics the proton movement shown in **Scheme 5.1**, a. These interactions continue to be found in OAT reactions. Musaev and coworkers proposed that an adventitious water

molecule assisted OAT from a tungsten-hydroperoxide complex by an H-bonding network (**Scheme 5.2**, b).[11] In their second

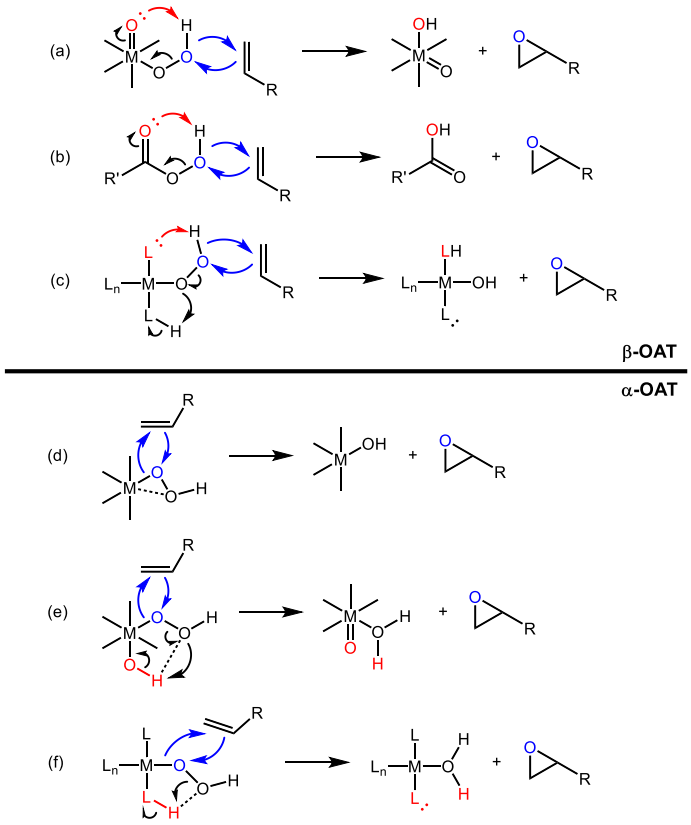

Scheme 5.1. Proposed mechanism for β-OAT by early transition metals (a), organic peracids (b), and our targeted late transition metal complexes (c), and α-OAT by early transition metals (d, e) and our targeted late transition metal complexes (f).

generation catalyst, Strukul and coworkers propose H-bonding of H_2O_2 with a perfluorophenyl ligand assists in activating the oxidant (**Scheme 5.2**, c).[12] Therefore, we have devised a new strategy to prepare late-metal complexes that would operate in an analogous manner by incorporating ligands with available H-bonding and/or protic functionality in the second coordination sphere to address the difficulties in OAT from late metal hydroperoxides (**Scheme 5.1**, c and f).

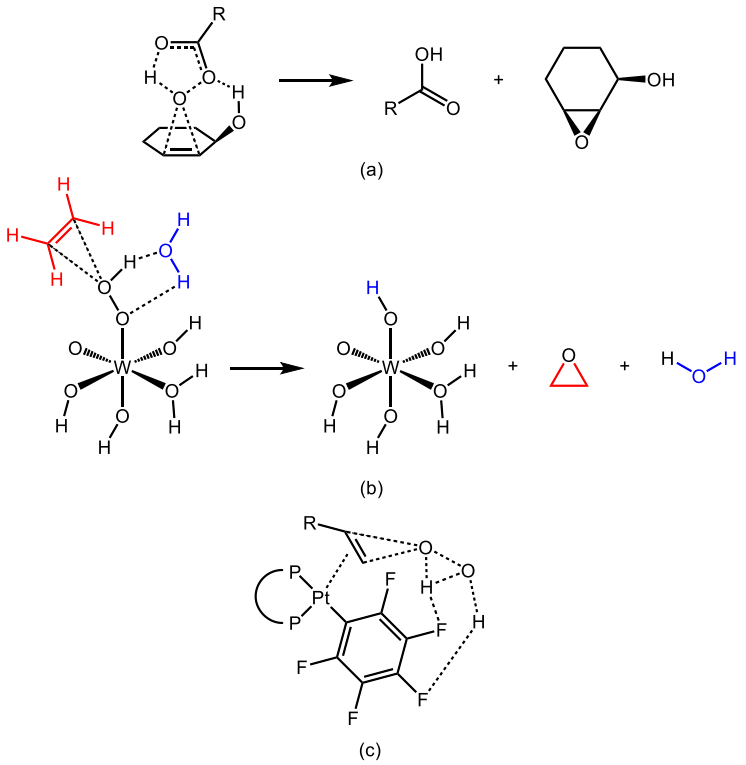

Scheme 5.2. Examples of proposed H-bonding/proton transfer in OAT mechanisms.

Prioritizing the OAT step and including the H-bonding/proton transfer interactions described above, a new catalytic cycle has been targeted, which operates with a M^n/M^{n+2} couple (**Scheme 5.3**). The advantages of this new strategy are: 1) the oxygen transfer step models the very well precedented epoxidation by organic peracids and early metal centers; 2) since the oxygen activation and incorporation does not operate via a H-atom abstraction (HAA) pathway, the strength of the M-H bond should not be a critical factor (see Chapter 1). Notably, the only late-transition metal system that has been shown to epoxide olefins (using hydrogen peroxide as the oxidant and oxygen atom source) is platinum. Our efforts in the past to use platinum with O_2 as the oxidant were hampered by the challenge in promoting the HAA pathway for O_2 insertion at a Pt^{II}-H. And 3) with the HX reductive elimination (HXRE) pathway, a wider range of ligands (with low *trans* influence groups) and different metals are available for use in this system.

Beginning with a hydroperoxide species, OAT to an olefin substrate will take place, assisted by ligand cooperation. The basic ligand (L) can kinetically assist in OAT by accepting the hydroperoxo proton during attack of the substrate (**Scheme 5.1**, c). The protonated ligand, or a second ligand (LH) could then protonate the proximal O-atom, yielding a hydroxide complex and the oxygenated substrate (**Scheme 5.3**, step 1). Another possibility is transfer of the proximal O-atom from the M-OOH species to substrate with cooperative protonation of the distal O-atom by an acidic ligand (LH) (**Scheme 5.1**, f)

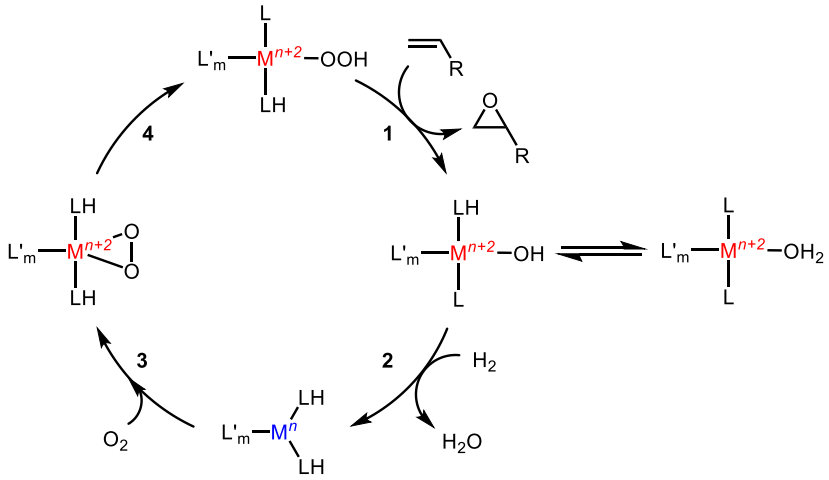

Scheme 5.3. Targeted metal-ligand cooperative catalytic cycle for the epoxidation of olefins.

The hydroxide complex can then undergo hydrogenolysis, forming a metal hydride. The basic ligand (L) can then deprotonate the M^{n+2}-H complex, formally reducing the metal center without dissociation of the ligand (**Scheme 5.3**, step 2). We have observed reduction of the metal center by hydrogenolysis before as unwanted degradation with the use of PCO and PCN hemilabile ligands,[13,14] however our new systems are designed to specifically carry out this transformation in a productive manner. This deprotonation of the metal hydride is reminiscent of the first step in the HXRE mechanism for O_2 insertion into a Pd^{II}-H bond described by Stahl and coworkers.[15,16]

The low valent metal complex could then be oxidized by O_2. Considerable literature precedent is available and indicates that binding as a η^2 peroxo ligand is expected (**Scheme 5.3**, step 3). This reaction is commonly observed in low coordinate Pd^0 and Pt^0 complexes[17] as well as other low valent late transition metal complexes (Rh^I,[18] Ir^I,[19]). It is also known that the side on peroxo ligand is basic in nature, reacting with acids to form monoanionic hydroperoxide ligands.[20] This method of O_2 activation to form late metal hydroxperoxide complexes is inspired by the HXRE mechanism for O_2 insertion proposed by Stahl and coworkers.[15] Their system utilizes an amphoteric benzoate moiety to deprotonate a Pd^{II}-H and then later perform an outersphere protonation of a Pd^{II}-peroxo complex. We intend to incorporate a protic functionality into the ligand such that the protonation of the bound peroxo is an intramolecular reaction (**Scheme 5.3**, step 4).

Described below are preliminary investigations of new tridentate and bidentate ligands capable of cooperative activation and utilization of O_2 at late transition metal centers (**Figure 5**). The chosen ligands contain functional groups that have been shown to exhibit cooperative hydrogen bonding or proton transfer properties. Many of the ligands have been used specifically to cooperate with a metal center in both catalytic and stoichiometric transformations involving the protonation/deprotonation of the ligand ancillary groups. The discussion below is not a complete narrative, but shows the potential of this new approach to drive this project in a promising new direction.

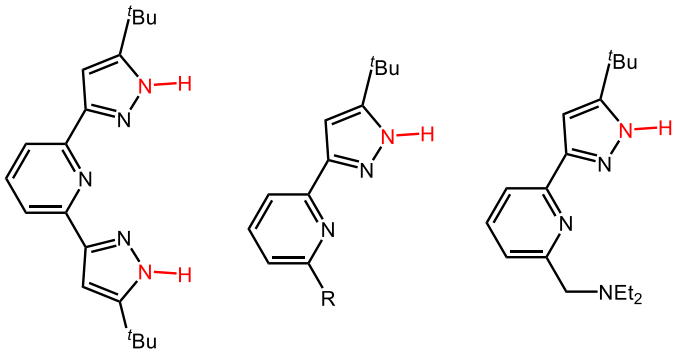

Figure 5.1. Bifunctional ligands investigated to assist in OAT to olefins.

5.2 Results and discussion

Symmetric NNN^{pyz} pincer ligand with pyrazolyl arms: Initial investigations into cooperative systems for OAT began with a pyrazole-based pincer ligand NNN^{pyz}. The symmetric NNN^{pyz} ligand shown in **Figure 5.1** contains a central pyridine backbone with ancillary pyrazolyl arms. This ligand was attractive to us due to its documented properties. The NNN^{pyz} ligand has been previously synthesized in high yield and metallated on a variety of transition metal centers.[21-23] Bulky substituents (^{t}Bu) on the α-carbon to the secondary amine were found to hinder coordination of a second metal ion.[23] Metal complexes of the NNN^{pyz} ligand have been shown previously to be reversibly deprotonated/protonated by mild bases/acids.[23] Furthermore, the ligand itself has been shown to be unreactive under an O_2 atmosphere, even in its deprotonated state. The protic N-H sites have been demonstrated to engage in H-bonding interactions with a fourth ligand in the pincer plane, and to protonate basic ligands and assist in N-N cleavage of hydrazines (**Scheme 5.4**).[21] The deprotonated form of the ligand shown in **Scheme 5.4** has been invoked in proton transfer activity as well, indicating that the pyrazole N-H functionality has a pK_a desirable for the desired cooperative transformations.[21]

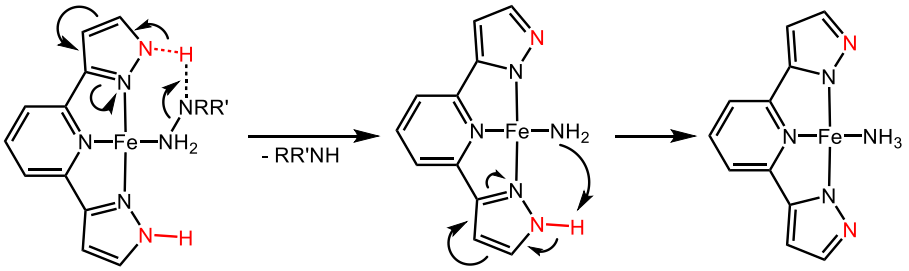

Scheme 5.4. Previously proposed ML cooperation for the degradation of hydrazines.

The NNN^{pyz} ligand was synthesized following the published procedure.[23] The first attempts at metalation were at zero valent Pd and Pt starting materials. Addition of the NNN^{pyz} ligand to $Pd_2(dba)_3$ in CD_2Cl_2 under N_2 resulted in a multitude of species as observed by NMR spectroscopy. Gentle heating of the reaction mixture at 40 °C did not result in the convergence to one product. Addition of NNN^{pyz} to CD_2Cl_2 solution of $Pd(P^nBu^tBu_2)_2$ under N_2 yielded similar results. A slow conversion to a variety of species without phosphine dissociation was observed by NMR spectroscopy. Addition of NNN^{pyz} to a CD_2Cl_2 solution of $Pt(PPh_3)_2(C_2H_4)$ resulted in the loss of ethylene and slight shifts in the NNN^{pyz} ligand signals by ^1H NMR spectroscopy. No free PPh_3 was observed. However, pressurizing a degassed sample of this reaction mixture with O_2 (3 atm) resulted in the clean conversion to a new Pt species **41** over 16 h (**Scheme 5.5**). Notably, addition of O_2 to the reaction mixture of NNN^{pyz} and $Pd_2(dba)_3$ did not result in any observed reaction. In the $^{31}P\{^1H\}$ NMR spectrum of the reaction mixture containing **41**, two signals are observed: a singlet at 26.6 ppm, and a singlet at 15.4 ppm with Pt satellites ($^1J_{Pt\text{-}P}$ = 3857 Hz). The singlet at 26.6 ppm was identified as triphenylphosphine oxide ($OPPh_3$), and confirmed by addition of an authentic sample to the reaction mixture. The Pt species appeared to be the doubly deprotonated (NNN^{pyz})Pt-PPh_3, as no N-H signal was observed in the ^1H NMR spectrum. Instead, a singlet for H_2O was observed, integrating to 1 molar equiv. compared to the NNN ligand. Large, yellow, luminescent single crystals of **41**

were grown from a concentrated methanol solution at -15 °C and analyzed by X-ray diffraction, confirming the assignment of (NNN^{pyz})Pt-PPh$_3$ (**Figure 5.2**).

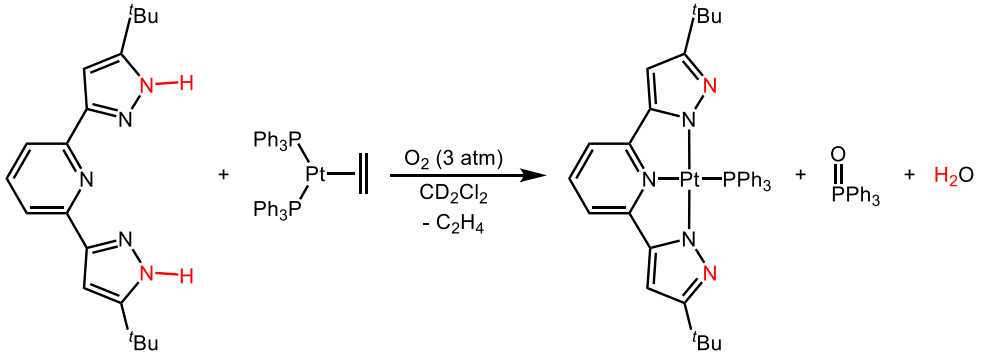

NNN^{pyz} **41**

Scheme 5.5. Metalation of NNN^{pyz} onto Pt under O_2 to form **41** with subsequent oxidation of PPh_3.

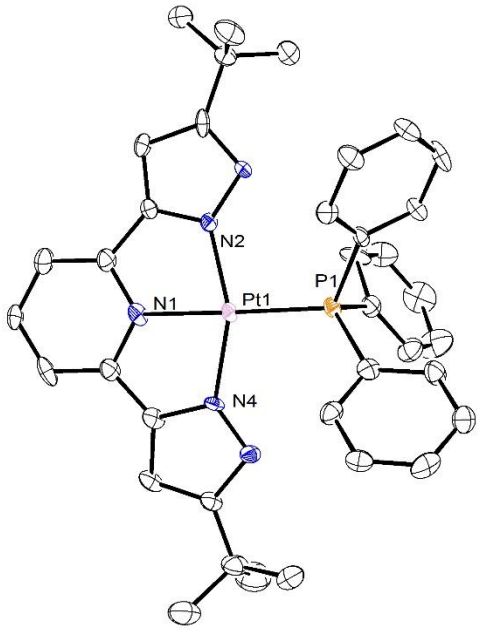

Figure 5.2. ORTEP[24] of (NNN^{pyz})Pt-PPh$_3$ (**41**) with ellipsoids shown at 50% probability. Hydrogen atoms on the ligands omitted for clarity.

The formation of **41** represents the reduction of O_2 to water with concomitant oxidation of a substrate molecule, yet it was unclear what species had activated O_2. As mentioned above, there exist numerous examples of Pt^0 species, commonly chelated by phosphine ligands,

reacting with O_2 to yield a Pt^{II}-peroxo complex.[17] As little reaction was observed on the addition of NNN^{pyz} to the Pt^0 species prior to addition of O_2, it is feasible that a free NNN^{pyz} ligand could protonate a Pt^{II}-peroxo formed *in situ* to yield the observed products. To test this theory, the peroxo $(PPh_3)_2PtO_2$ was synthesized independently,[25] and combined with free NNN^{pyz} ligand (**Scheme 5.6**). Indeed, a clean reaction occurred yielding (NNN)Pt-PPh_3 (**41**), $OPPh_3$, and an equivalent of H_2O.

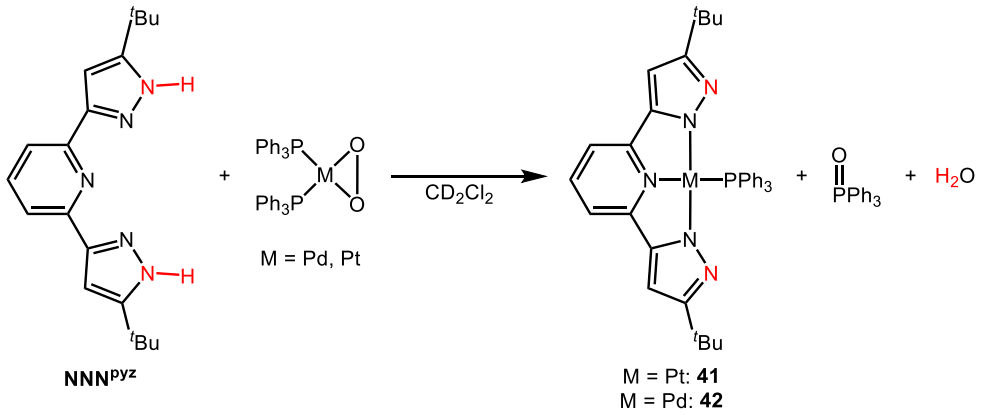

Scheme 5.6. Protonation of a M^{II}-peroxo by NNN^{pyz} yielding $(NNN^{pyz})M\text{-}PPh_3$, $OPPh_3$ and an equivalent of H_2O.

This synthetic method described in **Scheme 5.6** was then applied to Pd systems. The peroxo $(PPh_3)_2PdO_2$ was synthesized and combined with the NNN^{pyz} ligand in CD_2Cl_2. Within minutes, the formation of $(NNN^{pyz})Pd\text{-}PPh_3$ (**42**), $OPPh_3$ and an equivalent of H_2O was observed by NMR spectroscopy. A singlet at 29.7 ppm appears in the $^{31}P\{^1H\}$ NMR spectrum. Single crystals grown by slow evaporation of a pentane solution of **42** were analyzed by X-ray diffraction. The solid-state structure obtained confirms the identity of **42** (**Figure 5.3**). Notably, performing the same reaction shown in **Scheme 5.6** but using a bulkier phosphine complex $(P^nBu^tBu_2)_2PdO_2$ resulted in $(NNN^{pyz})Pd\text{-}P^nBu^tBu_2$, $OPPh_3$ and H_2O, yet the reaction required a significantly longer time to reach completion. As $P^nBu^tBu_2$ is a stronger electron donor than

PPh_3, the peroxo ligand is expected to be more basic and we hypothesized that the reaction would conclude faster. Since the opposite was observed, it may be that NNN^{pyz} association to the metal center is occurring first, allowing protonation of the peroxo and subsequent chelation of the pincer. Since the steric profile of $P^nBu^tBu_2$ is larger than PPh_3, association could be more hindered, increasing the reaction time.

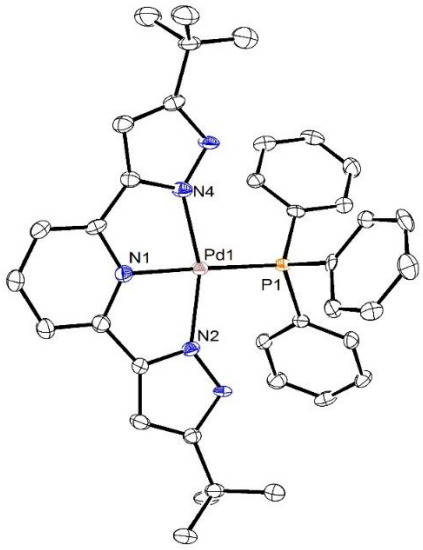

Figure 5.3. ORTEP[24] of (NNN^{pyz})Pd-PPh_3 (**42**) with ellipsoids shown at 50% probability. Hydrogen atoms on the ligands omitted for clarity.

Revisiting our targeted catalytic cycle in **Scheme 5.3**, species **41** and **42** resemble the expected product after OAT from a M-OOH (step 1). While a single oxidation event has occurred ($OPPh_3$), a hydroxide ligand is not present, but instead water has formed through subsequent protonation by the NNN^{pyz} ligand. As the second phosphine is a much better ligand than water, **41** or **42** result. The next step would be the reduction of these species to yield a low valent Pd^0 or Pt^0 complex that could react with O_2 (**Scheme 5.3**, step 2). Therefore, **41** and **42** were exposed to H_2.

When a degassed solution of **41** in CD_2Cl_2 was pressurized with H_2 (3 atm), no reaction was observed at room temperature over 24 hrs. Heating the reaction mixture to 60 °C for 16 hrs and then 80 °C for 16 hrs still yielded no spectroscopic change. However, running the same reaction but with the Pd analogue **42** resulted in complete conversion (96% based on hexamethylbenzene internal standard) of the Pd-PPh_3 complex in 16 hrs at room temperature. The yellow solution of **42** in CD_2Cl_2 grew steadily darker over the reaction period. The $^{31}P\{^1H\}$ NMR spectrum becomes featureless. In the ^1H NMR spectrum, a symmetric single NNN-containing product is observed. A singlet at 1.37 ppm for the ^{t}Bu substituents, as well as a singlet (6.69 ppm), doublet (7.63 ppm, $^3J_{HH}$ = 8.1 Hz) and triplet (7.72 ppm, $^3J_{HH}$ = 8.1 Hz) for the pyrazole and pyridine aromatic signals indicate C_2 symmetry of the NNN^{pyz} ligand. The signals are similar but not exactly the same as those associated with the free ligand. A broad peak at 8.01 ppm indicates N-H formation. A similar broad peak is observed in the free protonated ligand, albeit further downfield (11-12 ppm). The spectroscopic and physical evidence of the reaction mixture would indicate that a reduction of the metal center has occurred, however further investigation is required. Notably, a singlet for benzene also appears as the reaction with **42** and H_2 proceeds (confirmed by comparison with an authentic sample). The aromatic source is presumably the PPh_3 ligand, as the lack of a ^{31}P signal indicates decomposition of this moiety. Pd^0 has been shown computationally and experimentally to cleave P-Ph bonds in an $OPPh_3$ derivative to form a $Ph_2(O)P$-Pd-Ph complex.[26] A similar decomposition pathway could be occurring here, at which point the Pd-Ph complex could be hydrogenated by H_2 to give free benzene. Exposing this "reduced species" to O_2 resulted in the appearance of new products. However, this reaction was not clean, and the products were never isolated or further characterized.

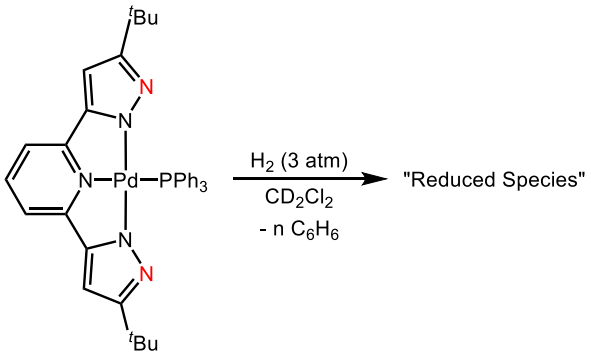

42

Scheme 5.7. Reduction of **42** under and H_2 atmosphere.

The reduction of **42** appears to be specific to the solvent CD_2Cl_2 and only to the Pd-PPh_3 analogue. Running the reaction shown in **Scheme 5.7** but in C_6D_6 results in no observable reaction by NMR spectroscopy. Further heating at 60 °C yields no change. Furthermore, exposing (NNN^{pyz})Pd-$P^nBu^tBu_2$ to H_2 (3 atm) in CD_2Cl_2 results in no observable reaction. The lack in generality to this hydrogenation reaction lead to the search for (NNN^{pyz})M complexes lacking a phosphine ligand.

As the reaction shown in **Scheme 5.6** is essentially a deprotonation/coordination reaction, other Pd/Pt starting materials with basic groups were investigated for NNN^{pyz} coordination. Addition of NNN^{pyz} to a solution of $Ph_2Pt(SMe_2)_2$ in CD_2Cl_2 resulted in the clean formation of a new product by ^1H NMR spectroscopy (**Scheme 5.8**). One set of NNN^{pyz} ligand signals is observed, as well as 2 equivalents of free benzene, 1 equivalent of free SMe_2 and 1 equivalent of a SMe_2 group with Pt satellites ($^3J_{PtH}$ = Hz). The spectroscopic signals indicate double deprotonation of NNN^{pyz} with protonation of the phenyl ligands and coordination of NNN^{pyz} by displacement of a SMe_2 ligand to yield (NNN^{pyz})Pt-SMe_2 (**43**). Complex **43** was found to be quite inert, as exposure to vacuum, heat (100 °C, H_2 (5 atm), 35% *aq.* H_2O_2 or other ligands (MeCN) resulted in no reaction, similar to **41**.

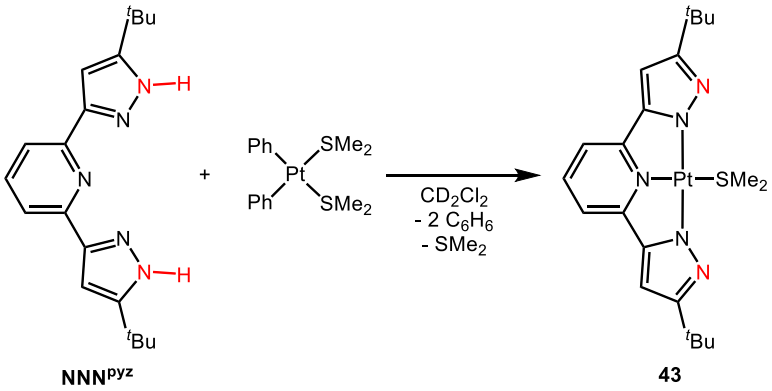

Scheme 5.8. Synthesis of (NNN^{pyz})$PtSMe_2$ (**43**).

Attempts to reach the doubly deprotonated species through a metal-halide were also performed. Addition of NNN^{pyz} to CH_2Cl_2 solutions of $M(SMe_2)Cl_2$ resulted in the formation of [(NNN^{pyz})MCl]Cl through displacement of the SMe_2 ligands (M = Pd (**44**), Pt (**45**)) (**Scheme 5.9**). The cation complexes showed limited solubility in most organic solvents, with methanol being an exception. Addition of base to methanolic solutions of **44** or **45** resulted in the formation of a plethora of species by NMR spectroscopy. Bases that were examined included KHMDS, LiOH, KOH, K_2CO_3, NEt_3, Ag_2O and ^{t}BuOK. No combination yielded the formation of a single species. Notably, single crystals were grown from a sample of **45** and ^{t}BuOK in a THF-pentane mixture at -30 °C. X-ray diffraction analysis yielded a solid-state structure of a deprotonated dimer bridged by two K^+ ions (**Figure 5.4**, a). This structure is not representative of the batch sample, as dissolving the crystals in CD_3OD gave two clean species by NMR spectroscopy, presumably the dimer and the dissociated monomer. As the chloride ligand is still bound to the metal center, it appears that the pyridine backbone is not a strong enough *trans* donor to yield species of the type (NNN^{pyz})M-L from the halides **44** or **45**. This is further exemplified as the addition of an excess of AgOTf to **45** results in abstraction of only the outersphere chloride ion, while the Pt-Cl is untouched (**Figure 5.4**, b).

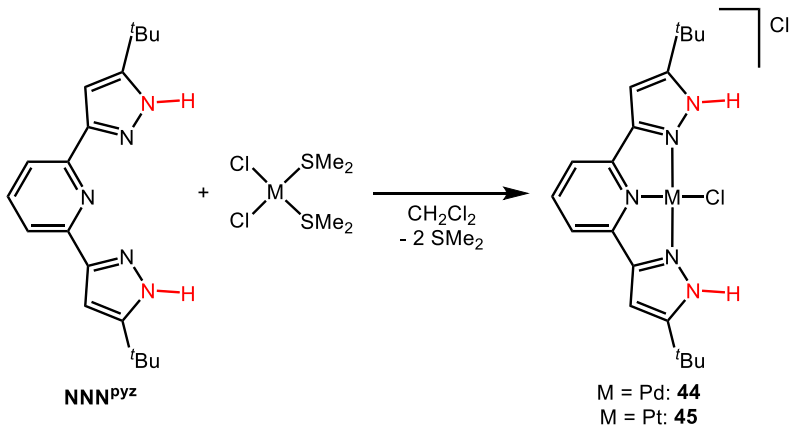

Scheme 5.9. Synthesis of the chloride cations [(NNN^{pyz})MCl]Cl, M = Pd (**44**); Pt (**45**).

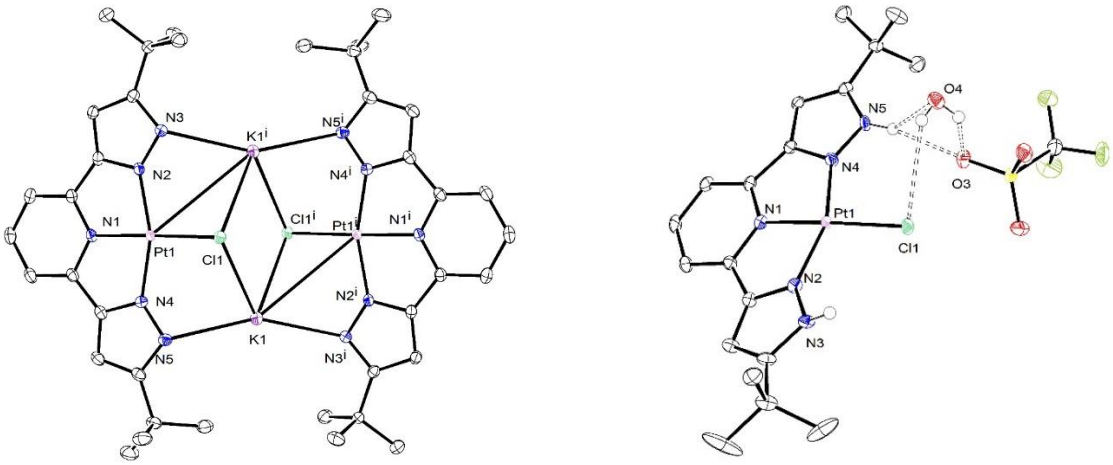

(a) (b)

Figure 5.4. ORTEP[24] of (a) {K[(NNN^{pyz})PtCl]}$_2$(THF)$_4$ and (b) [(NNN^{pyz})PtCl]OTf (H_2O) with ellipsoids shown at 50% probability. Hydrogen atoms attached to carbon and THF solvent molecules omitted for clarity. H-bonding interactions are shown by the dashed bonds. In (a), Pt1-Cl1: 2.3087(5); Pt1-N1: 1.9558(15); Pt1-N2: 2.0058(16); Pt1-N4: 1.9984(15); N3-K1^i: 2.8497(16); Cl1-K1: 3.1309(6) Å. In (b), Pt1-Cl1: 2.2943(6); Pt1-N1: 1.960(2); Pt1-N2: 1.982(2); Pt1-N4: 1.995(2) Å.

The NNN^{pyz} system's most promising development thus far are the reactions of the ligand with peroxo complexes of the form $(R_3P)_2M(O_2)$ (M = Pd, Pt). This represents a full reduction of O_2 under mild conditions, a relevant and desirable transformation consistent with the goals set out for this project. However, the rigid, tridentate nature of NNN^{pyz} appears not

to be the best choice to promote an M^0/M^{II} cycle for group 10 metals due to geometric constraints of the low valent system.

Bidentate pyridine-pyrazole NN ligand: Revisiting the targeted catalytic cycle which uses metal ligand cooperation (**Scheme 5.3**), a successful supporting ligand would need to stabilize both low valent M^n and high valent M^{n+2} species. In group 10 chemistry, the ligand must support the geometric constraints that are imposed when moving from square planar M^{II} to low valent M^0 (typically tetrahedral or linear). With the lack of success in the synthesis of Pd^0/Pt^0 complexes of NNN^{pyz}, a bidentate analogue of this ligand was targeted. The pyridine/pyrazole NN ligand could support M^0 complexes, the oxidation by O_2 to the peroxo complex, and further to the M-OOH species (**Scheme 5.10**). Stahl and coworkers have shown the oxidation of a similar bidentate (NN)Pd-olefin complex to the peroxo by O_2.[27]

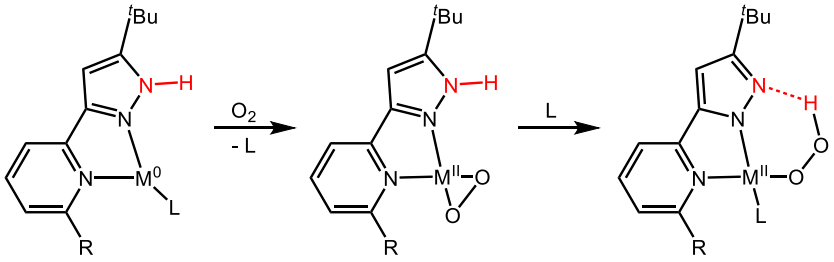

Scheme 5.10. Catalytic species that could be stabilized by bidentate NN ligand. L = olefin under catalytic conditions.

The 2-pyridyl pyrazole NN ligand was synthesized in high yield according to a published procedure.[28] Addition of NN ligand to $Pd(dba)_2$ in a 1:1 molar ratio in CD_2Cl_2 resulted in no reaction over 24 hours. On addition of more ligand (0.5 molar equiv.), the reaction progressed to what appeared to be 3 species by NMR spectroscopy followed by the convergence to one major product (**46**) over 24 hrs. One large singlet for the ^{t}Bu protons of the final product is observed in the ^{1}H NMR spectrum at 1.63 ppm. One of the pyridine signals is

observed far downfield (10.37 ppm), indicating proximity to the metal center. Complex **46** showed no reactivity to oxygen. Furthermore, complex **46** formed both in the presence and absence of O_2 but required an excess of NN ligand to be added to $Pd(dba)_2$ under both conditions. Single crystals were grown from the slow evaporation of a CD_2Cl_2 solution of **46** and a solid-state structure was obtained (**Figure 5.5**). Complex **46** is a homoleptic Pd^{II} species with two NN ligands coordinated in the square plane. A C_2 rotation axis relates the two NN ligands.

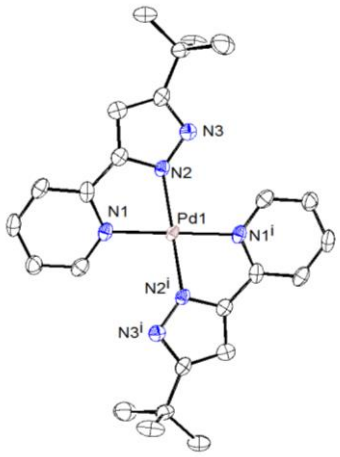

Figure 5.5. ORTEP[24] of $(NN)_2Pd$ (**46**) with ellipsoids shown at 50% probability. Hydrogen atoms on the ligands omitted for clarity.

Methods to form species with only one NN ligand coordinated were unsuccessful. Deprotonation of NN in the presence of Pd always resulted in complex **46** as the major product. Due to the undesirable bis-coordination of the NN ligand, steric derivation was performed. Examining the crystal structure, placing a bulky group at the 6-position of pyridine would hinder a second ligand coordinating in the plane. Therefore, 2-[3-*tert*-butyl-1*H*-pyrazol-5-yl]-6-methyl-pyridine (NN^{Me}) was synthesized.[28] Addition of the NN^{Me} ligand to $Pd(dba)_2$ or $Pt(PPh_3)_2(C_2H_4)$ resulted in a multitude of products or no reaction, respectively. However, reactions using M^{II} sources were more successful.

The reaction of NN^{Me} and $Pd(SMe_2)Cl_2$ with an equivalent of NEt_3 proceeded to form one major product (**47**). Free SMe_2 was observed, as well as one set of NN^{Me} ligand signals. However, two singlets for what appeared to be a bound Pd-SMe_2 moiety were observed at 1.76 and 2.72 ppm, integrating to 3 protons each. This result was unexpected, as no break in symmetry is observed for the rest of the complex. Single crystals were grown of **47** in a CH_2Cl_2/Et_2O mixed system at -30 °C. The result of X-ray diffraction analysis is shown in **Figure 5.6**. Complex **47** is a dinuclear species, where a pyrazole bridges two Pd^{II} centers, which are coordinated by a Cl and SMe_2 ligand. This species, while highly symmetric, would not have equivalent Me groups on SMe_2, indicating that this dinuclear structure persists in solution. Notably, N(1) and N(4) are oriented directly in line with S(2) and S(1), respectively. The two Pd centers are separated by a distance of 2.9857(4) Å, indicating a weak metal-metal sigma bond.

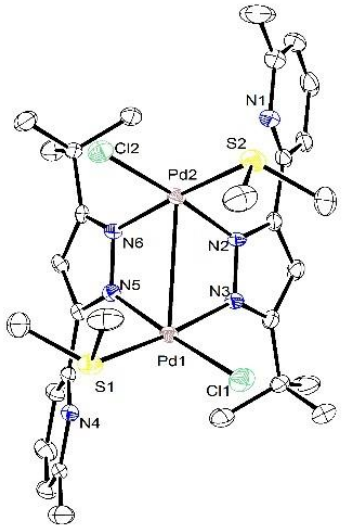

Figure 5.6. ORTEP[24] of $[(NN)PdCl(SMe_2)]_2$ (**47**) with ellipsoids shown at 50% probability. Hydrogen atoms on the ligands omitted for clarity.

While complex **47** was not a targeted structure, it was still intriguing as the dangling pyridine moiety could potentially participate in second coordination sphere reactivity. It may

also be interesting to investigate its reactivity in small molecule activation,[29] although beyond the scope of this project. Attempts to transform **47** into a catalytically relevant hydroxide complex were performed. Addition of AgOTf, both equimolar or excess, yielded a multitude of intractable products. Direct salt metathesis by KOH in THF-d_8 was also unsuccessful, either yielding no reaction or decomposition under sonication. The undesirable binding modes displayed by the bidentate NN^R ligand as well as the lack of isolable M^0 species dissuaded any further study of complexes containing this ligand.

Unsymmetrical NNN^{Et} pincer ligand with a hemilabile arm: While the NNN^{pyz} pincer appeared unfavorable for stabilizing M^0 species, and the bidentate NN^R ligand was not compliant in stabilizing catalytically relevant species, a "goldilocks" pincer ligand with a hemilabile arm was targeted in order to facilitate a M^0/M^{II} cycle. It was anticipated that a hemilabile pincer ligand would stabilize the M^{II} geometry as a tridentate ligand, as well as the reduced M^0 geometry as a bidentate ligand. The NNN^{Et} ligand (NNN^{Et} = 6-[5-*tert*-butyl-1*H*-pyrazol-3-yl] -*N*,*N*-diethyl-2-pyridinemethanamine) was synthesized according to published procedure.[30] Amine arms in unsymmetrical ligands have been shown to be hemilabile.[30,31] Our previous work with unsymmetrical PCO and PCN systems with hemilabile arms were plagued by reduction to low valent complexes under H_2.[13,14] With the new proposed M^0/M^{II} system and NNN^{Et}, we sought to use this result to our advantage.

As with the other pyridine-pyrazole ligands, NNN^{Et} was first added to M^0 starting materials in order to enter the catalytic cycle (**Scheme 5.3**) at the low valent state. Addition of NNN^{Et} to $Pd_2(dba)_3$ in C_6D_6 gave multiple species. Addition of a neutral ligand 1-hexene did not produce a single product. Addition of O_2 to the reaction mixture resulted in the precipitation of Pd^0 particles with no change to 1-hexene by NMR spectroscopy. Addition of NNN^{Et} to

$(PPh_3)_2Pt(C_2H_4)$ resulted in the displacement of ethylene, but no change to free ligand resonances and no loss of phosphine by NMR spectroscopy. However, addition of O_2 to the reaction mixture resulted in the formation of a new minor species (**Scheme 5.11**). As Pt^0 phosphine complexes are known to react with O_2 to form metal peroxide species,[17] it is possible that $(PPh_3)_2Pt(C_2H_4)$ reacted with O_2, yielding the peroxo $(PPh_3)_2PtO_2$ which then reacts with the NNN^{Et} ligand. Therefore, isolated peroxo complexes $(PPh_3)_2MO_2$ (M = Pd, Pt) were investigated as starting materials.[25]

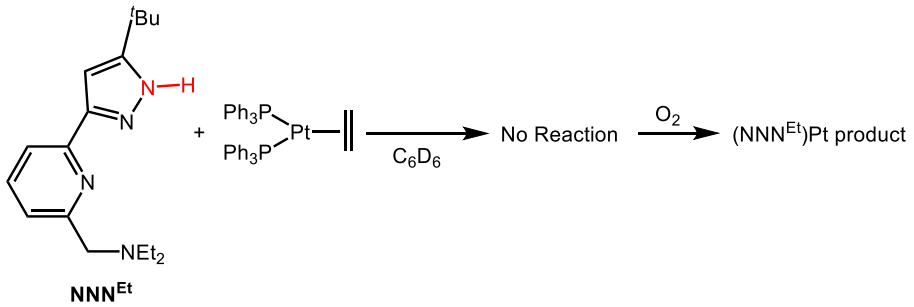

Scheme 5.11. Reaction of Pt^0 and NNN^{Et} under O_2.

When $(PPh_3)_2PdO_2$ was added to a C_6D_6 solution of free NNN^{Et} ligand, a reaction occurred yielding $OPPh_3$, H_2O and one phosphorus containing Pd product **48** as observed by $^{31}P\{^1H\}$ (30.6 ppm) and ^1H NMR spectroscopy. Notably, this ^{31}P shift is very similar to $(NNN^{pyz})Pd\text{-}PPh_3$ (29.7 ppm), suggesting a comparable species had formed. The ^1H NMR spectrum displays one set of ligand peaks, however the methylene signals of the amine pincer arm appear as two doublets, displaying germinal coupling of 16.9 Hz. This indicates a break of symmetry in the plane of the pincer ligand. Furthermore, integration of the PPh_3 ligand does not give a 1:1 ratio to NNN^{Et}, but instead a 1:2 ratio. This further indicates that two NNN^{Et} ligands are bound to a $Pd\text{-}PPh_3$ moiety. The solid state structure confirms this hypothesis (**Figure 5.7**).

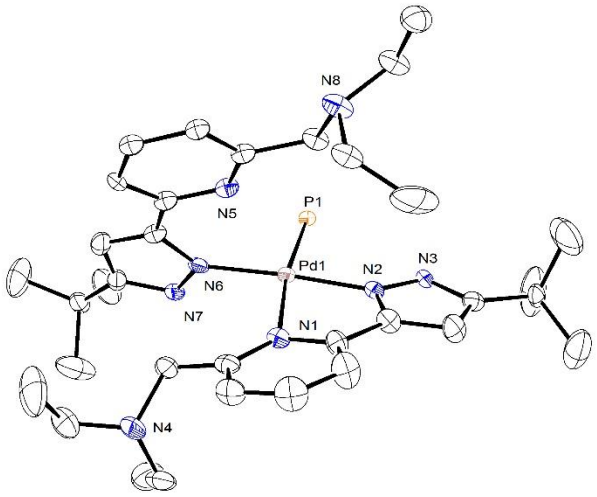

Figure 5.7. ORTEP[24] of $(NNN^{Et})_2$Pd-PPh_3 (**48**) with ellipsoids shown at 50% probability. Hydrogen atoms on the ligands and phenyl groups on P1 omitted for clarity.

Complex **48** is a slightly distorted square planar complex bound through the pyrazolyl-pyridine N's of one NNN^{Et} ligand and a pyrazolyl N from a second NNN^{Et} ligand. One PPh_3 ligand completes the four coordinate system. N(5) is weakly associated with the Pd^{II} center (2.807 Å) and is positioned to associate and displace N(1). This process must be occurring at a fast rate, as the NMR spectrum only shows inequivalent ligand signals for the methylene protons. If **48** was static, two complete sets of ligand signals would be observed in the ^{1}H NMR spectrum. Cooling the sample to 180 K in toluene-d_8 broadens the ligand signals, but they still do not separate completely. Notably, in each NNN^{Et} ligand, the amine arm is not associated with the metal. **Scheme 5.12** displays the full balanced reaction.

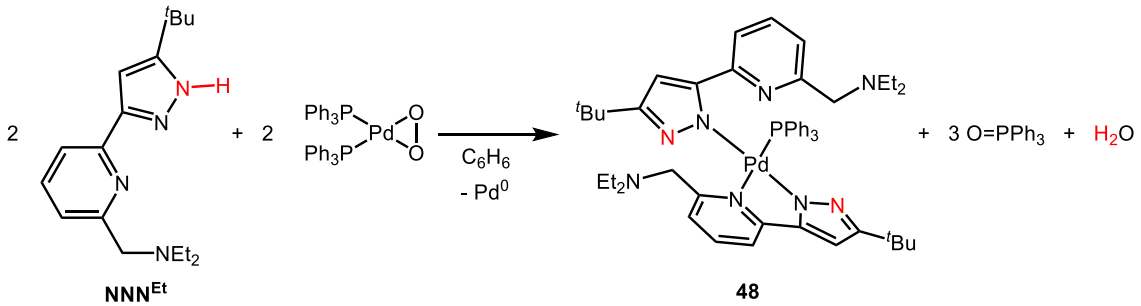

Scheme 5.12. Bis coordination of NNN^{Et} to Pd^{II}.

While the reaction shown in **Scheme 5.12** highlights the hemilability of the NNN^{Et} amine arm, the coordination mode was undesirable for future studies. Instead, halogenated starting materials were investigated to achieve 1:1 NNN^{Et}:metal coordination. The chloride species could then be transformed into the hydroxide complex and enter the catalytic cycle (**Scheme 5.3**). The addition of NNN^{Et} to $(SMe_2)_2MCl_2$ in the presence of excess NEt_3 yielded the complex $(NNN^{Et})MCl$ cleanly (M = Pd (**49**), Pt (**50**)). The neutral complexes **49** and **50** were characterized by ^1H NMR spectroscopy and X-ray crystallography (**Figure 5.8**). Complex **50** exists as a distorted square planar Pt^{II} center with the NNN^{Et} ligand bound κ^3. The Pt-Cl bond (2.2884(13) Å) is comparable to other Pt-Cl species *trans* to pyridine.

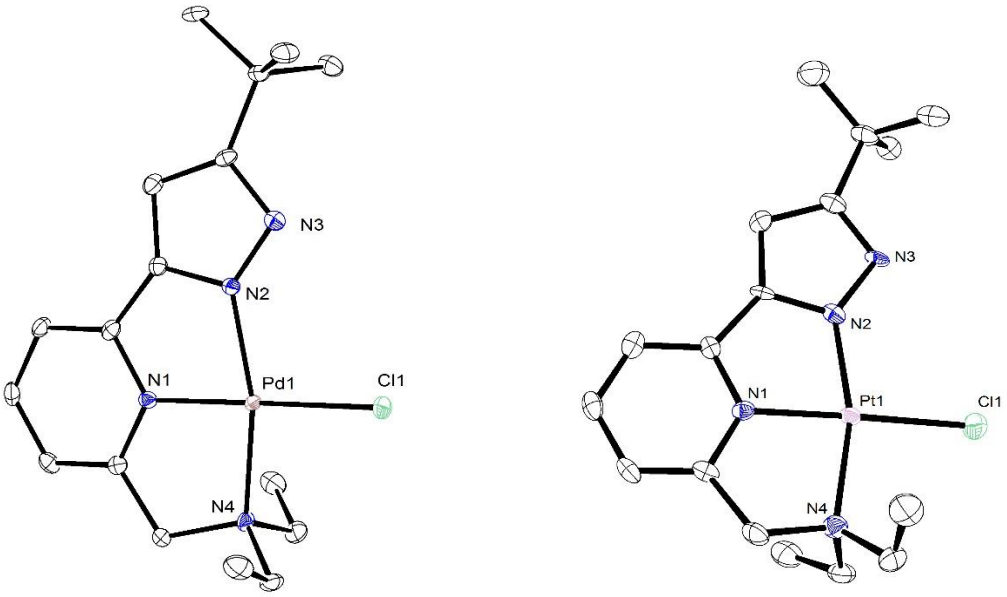

Figure 5.8. ORTEP[24] of (NNN^{Et})Pd-Cl (**49**) (left) and (NNN^{Et})Pt-Cl (**50**) (right) with ellipsoids shown at 50% probability. Hydrogen atoms on the ligands omitted for clarity.

In an attempt to form the hydroxide complex, excess KOH was combined with **50** in THF-d_8. A new complex **50*** evolves, with a drastic color change of the solution from yellow to dark red. In the ^1H NMR spectrum of **50***, the pyridine aromatic signals have shifted dramatically upfield (5.09, 5.44, and 6.23 ppm). Furthermore, the methylene arm signal at 3.30

ppm integrates to 1 proton only. No Pt-OH signal is observed. Instead, these resonances suggest that the ligand backbone has been deprotonated, formulating the dearomatized product K[(NNN^{Et}*)PtCl] (**50***) (* indicates ligand arm deprotonation). This assignment is in agreement with previous spectral observations in the dearomatization of pyridine based PNP complexes of Pd^{II} and Pt^{II}.[3233] It is unclear if the chloride ligand remains in the coordination sphere. However, the isolation of the anionic {K[(NNN^{pyz})PtCl]}$_2$(THF)$_4$ discussed above indicates that the pyridine backbone does not significantly activate the chloride ligand, hence the assignment of **50***. A large excess of KOH is required to push the deprotonation of **50**. Addition of water to **50*** instantly converts the anion back to the neutral **50**. Notably, the diethylamine arm of previously reported unsymmetrical (PNN*)Pt complexes was not observed to be deprotonated even in the presence of strong alkyllithium reagents.

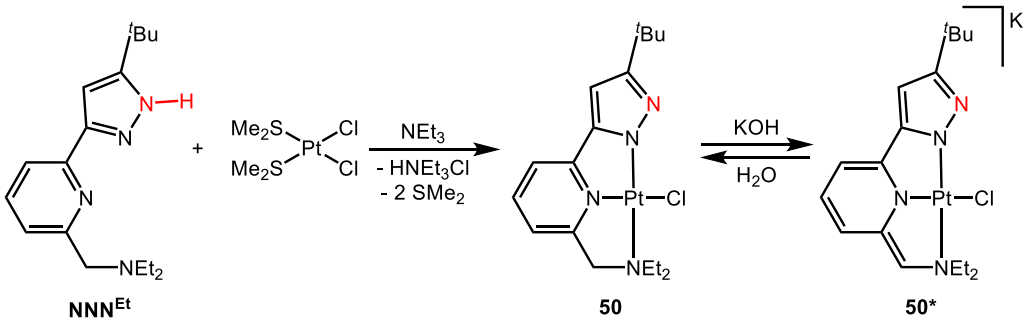

Scheme 5.13. Formation and pincer arm deprotonation of (NNN^{Et})PtCl (**50**).

In contrast to the Pt-Cl **50**, the Pt-I analogue (NNN^{Et})Pt-I (**51**) was found to lose KI on reaction of KOH in THF-d_8. The *in situ* deprotonation of a mixture of NNN^{Et} and (SMe$_2$)PtI$_2$ by an excess of KOH produced the neutral (NNN^{Et}*)Pt-SMe$_2$ (**52**) (**Scheme 5.14**). The ^{1}H NMR spectrum of **52** displays an upfield shift of the pyridyl signals (5.17, 5.59, and 6.27 ppm) and a 1 proton singlet for the methylene arm at 3.41 ppm. A Pt-bound SMe$_2$ ligand is observed by the 6 proton singlet at 2.84 ppm with Pt satellites ($^3J_{PtH}$ = 35 Hz). It is plausible that isolating

complex **51** prior to addition of KOH could assist in isolating a terminal hydroxide species. Complexes **50*** and **52** were studied for their reactivity with H_2.

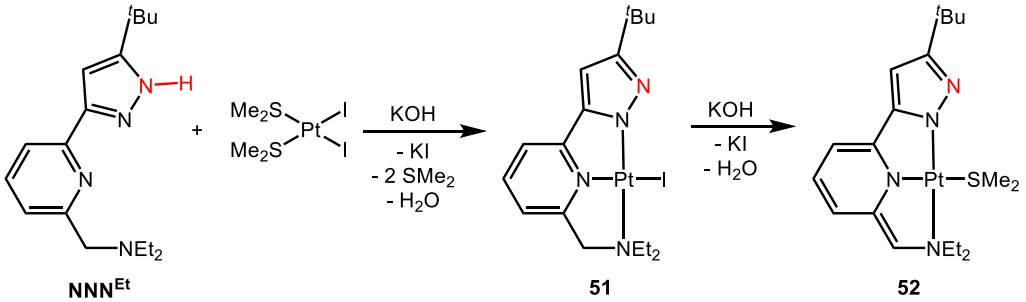

Scheme 5.14. Formation and pincer arm deprotonation of (NNN^{Et})PtI (**51**).

A solution of **50*** in THF-d_8 was pressurized with 3 atm of H_2. No noticeable reaction occurred over 20 h. A small amount of rearomatized species was observed, as well as a very small (~5 % compared to **50***) hydride signal (s, -16.05 ppm). The reaction was heated to 60 °C, resulting in complete reduction of the complex. Free ligand was observed by NMR spectroscopy, as well as Pt^0 particles. A similar overall result was observed when **52** was pressurized with H_2 (3 atm) at room temperature. Over 16h, the complete reduction of **52** to free NNN^{Et} and Pt^0 was observed.

In an alternative route, (NNN^{Et})M-alkyl/aryl complexes were targeted to undergo hydrolysis to form mononuclear hydroxide complexes. Coordination of NNN^{Et} with concomitant protonolysis of methyl or phenyl complexes of the form $[PtR_2(SMe_2)]_2$ was achieved at 60 °C, forming (NNN^{Et})Pt-R (R = Me (**53**), Ph (**54**)) (**Scheme 5.15**). The Pd analogue (NNN^{Et})Pd^{II}-Me (**55**) was synthesized in the similar manner, using (TMEDA)$PdMe_2$ as a starting metal source. A solid-state structure was collected from single crystals of **55**, which formed spontaneously upon cooling of the reaction mixture to room temperature (**Figure 5.9**). Complex **55** is a slightly distorted Pd^{II} square planar complex with a κ^3

deprotonated NNN^{Et} and methyl ligand coordinated. The metrics of **55** are nearly identical to **50**, except for the longer M-N(1) bond (2.012(3) Å) due to the stronger methyl σ-donor compared to Cl (1.948(4)Å). The Pd-C(18) bond is 2.033(4) Å.

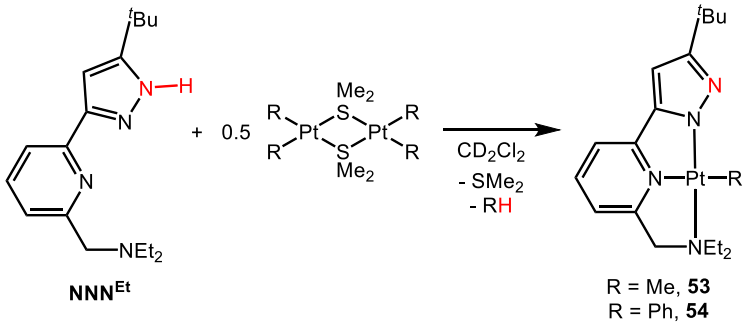

Scheme 5.15. Formation of Pt^{II} methyl and phenyl complexes of NNN^{Et}.

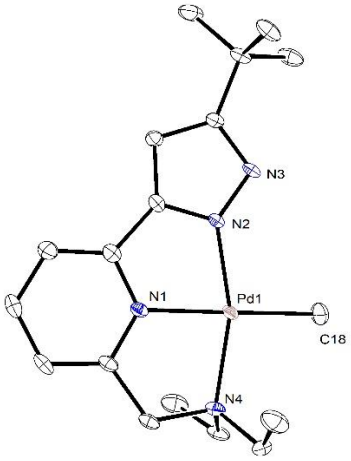

Figure 5.9. ORTEP[24] of (NNN^{Et})Pd-Me (**55**) with ellipsoids shown at 50% probability. Hydrogen atoms on the ligands omitted for clarity.

No reaction of complexes **53-55** in the presence of excess H_2O was observed. Heating a solution of **53** or **54** in CD_3CN with 0.5 μL of H_2O to 60 °C for up to 16 h yielded no change by NMR spectroscopy. Addition of 1 equiv. of triflic acid (HOTf) to the reaction mixtures cleanly converted the neutral **53** or **54** to the cationic [(NNN^{Et})Pt-R]OTf (R = Me (**56**), Ph (**57**), respectively) where the ligand pyrazole N had been protonated (**Scheme 5.16**). Complex **56**

and **57**, with alkyl/aryl groups in close proximity to a β-hydrogen, were remarkably stable. Only upon heating **56** to 100 °C overnight was loss of methane observed. The metal containing product was not identified. Complex **57** did not lose benzene as easily, with only a minor amount of decomposition occurring upon excess heating (5 days) at 80 °C and in the presence of excess HOTf. This is to be expected, as Pt-Ph are generally stronger than Pt-Me bonds.[34]

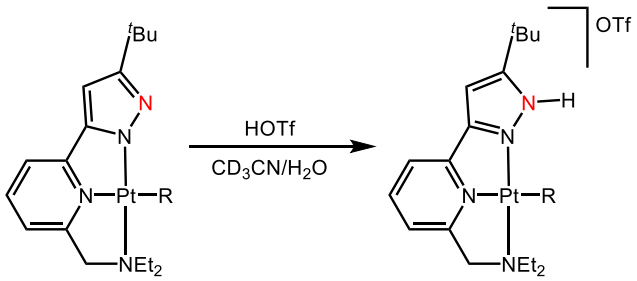

R = Me, **53**
R = Ph, **54**

R = Me, **56**
R = Ph, **57**

Scheme 5.16. Protonation of (NNN^{Et})Pt-R species by HOTf.

5.3 Summary and future outlook

Initial results of the reactivity of pyrazole-based pincer and bidentate complexes of Pd^{II} and Pt^{II} were presented. Although species relevant to the targeted M-L cooperative catalytic cycle (**Scheme 5.3**) for partial oxidation of olefins were not readily prepared and studied, a basis for using cooperative systems for O_2 activation and utilization was presented. Bidentate ligands containing acid/conjugate base sites in the second coordination sphere should be avoided due to the potential of undesirable bridging and bis-chelation. The symmetric NNN^{pyz} and NNN^{Et} systems show potential for cooperative reactivity, however the lack of stable M^0 complexes containing these ligands is disconcerting. While the pyrazole functionality appears to provide the necessary acid/base characteristics desirable for peroxo protonation and hydride deprotonation, other functional groups should be investigated. For example, the hydroxy

pyridine functionality used by Szymczak,[35] the imidazolyl phosphine used by Grotjahn,[36] and the frequently used amides in enzyme mimics.[37-40] It is the hope that the initial results here inspire future metal-ligand cooperation for the activation and application of O_2 as an oxidant.

5.4 Experimental

General considerations and materials characterization. All air- and/or moisture-sensitive reactions were performed under inert atmosphere in flame-dried flasks using standard Schlenk-type techniques or in a glove-box filled with nitrogen. Tetrahydrofuran (THF), benzene, pentane and toluene were purified by means of a MBraun solvent purification system. THF-d_8, C_6D_6 and toluene-d_8 were dried over sodium/benzophenone ketyl. CD_2Cl_2 was dried over activated 4 Å molecular sieves. Hydrogen or oxygen gas was introduced to reactions in J. Young NMR tubes on a high pressure gas manifold.[41] All other reagents and solvents were used as purchased from commercial suppliers. ^1H, $^{13}C\{^1H\}$ and $^{31}P\{^1H\}$ NMR spectra were obtained on either a Bruker Avance 700, Bruker Avance 500, Bruker Avance DRX-400 or a Bruker Avance 300 MHz instrument. Chemical shifts are reported in ppm (δ) relative to TMS, referenced to the chemical shifts of residual solvent resonances (^1H and ^{13}C), and coupling constants are given in Hz. $^{31}P\{^1H\}$ NMR spectra are referenced to an external 85% H_3PO_4 sample (0 ppm).

X-ray Diffraction Data. X-ray diffraction intensity data were collected on a *Bruker APEX II* diffractometer using a *Mo-K*α radiation (λ = 0.71073 Å) at low temperature (either T = 100 or 120 K). The dataset was integrated and scaled using SAINT, SADABS within the APEX2 software package by Bruker.[42] The program used for the data collection was *CrysAlis CCD* 1.171.[43] Data reduction was carried out with the program *CrysAlis RED* 1.171[44] and the

absorption correction was applied with the program *ABSPACK* 1.17. Direct methods implemented in *Sir97*[45] were used to solve the structures and the refinements were performed by full-matrix least-squares against F^2 implemented in *SHELX97*.[46] All the non-hydrogen atoms were found from Fourier syntheses of electron density and were refined anisotropically, while the hydrogen atoms were fixed in calculated positions and refined isotropically with the thermal factor depending on the one of the atom to which they are bound (riding model) with C---H distances in the range 0.95-1.00 Angstrom. The geometrical calculations were performed by *PARST97*.[47] Molecular plots were produced by the program *ORTEP3*.[48]

Table 5.1. Select bond lengths (Å) and angles (°) for complexes **41**, **42**, **46-50**, and **55**.

	41	**42**	**46**	**47**	**48**	**49**	**50**	**55**
M-N1	2.010(5)	2.009(3)	2.035(3)	-	2.215(4)	1.947(2)	1.948(4)	2.012(3)
M-N2	2.007(4)	2.016(3)	1.994(4)	2.045(3)[a]	1.989(4)	1.998(2)	1.990(4)	2.018(3)
M-N4	2.027(4)	2.027(3)	-	2.007(3)[b]	1.992(4)[b]	2.094(2)	2.081(4)	2.116(3)
M-P1	2.2546(16)	2.2874(12)	-	-	2.2438(14)	-	-	-
M-Cl1	-	-	-	2.3099(9)	-	2.3062(7)	2.2884(13)	-
M-C18	-	-	-	-	-	-	-	2.033(4)
M-S1	-	-	-	2.2863(10)	-	-	-	-
N1-M-X[c]	177.25(13)	177.65(10)	-	174.59(8)[d]	171.95(12)	179.32(7)	178.34(13)	178.22(15)
N2-M-N4	157.08(19)	157.71(14)	-	176.95(8)[e]	176.11(16)	162.64(9)	163.73(17)	161.88(12)

[a] M-N3 bond. [b] M-N5 bond. [c] X = atom *trans* to N1. [d] N3-M-S1 angle. [e] N5-M-Cl1 angle.

(NNN^{pyz})Pt-PPh$_3$ (41): The NNN^{pyz} ligand (22.2 mg, 0.0686 mmols) and Pt(PPh$_3$)$_2$(O$_2$) (50.9 mg, 0.0677 mmols) were dissolved in CH_2Cl_2 (2 mL) and stirred for 24 h. Solvent removal left a bright yellow solid, which was washed with cold methanol (0 °C) and then recrystallized from a saturated hot methanol solution left at -15 °C yielding large glowing yellow crystals of **41** (44.5 mg, 84% yield).

$^{31}P\{^1H\}$ NMR (121 MHz, CD_2Cl_2) δ 15.4 (s, $^1J_{PtP}$ = 3857 Hz). ^1H NMR (500 MHz, CD_2Cl_2) δ 1.03 (s, 18H), 6.30 (s, 2H), 7.11 (dd, J = 7.9, 1.5 Hz, 2H), 7.36-7.41 (m, 6H), 7.42-7.47 (m, 3H), 7.69 (t, J = 7.9 Hz, 1H), 7.79-7.85 (m, 6H).

(NNN^{pyz})Pd-PPh$_3$ (42): The NNN^{pyz} ligand (51.0 mg, 0.158 mmols) and Pd(PPh$_3$)$_2$(O$_2$) (102 mg, 0.154 mmols) were dissolved in CH_2Cl_2 (6 mL) and stirred for 1 h. The yellow solution was filtered through neutral alumina multiple times until no $OPPh_3$ was observed by NMR spectroscopy. Solvent removal of the clean solution left **42** as a yellow powder (79.8 mg, 75% yield).

$^{31}P\{^1H\}$ NMR (121 MHz, CD_2Cl_2) δ 29.7 (s). ^1H NMR (301 MHz, CD_2Cl_2) δ 1.04 (s, 18H), 6.34 (s, 2H), 7.07 (dd, J = 7.9, 1.5 Hz, 2H), 7.35-7.43 (m, 6H), 7.44-7.52 (m, 3H), 7.70 (t, J = 7.9 Hz, 1H), 7.77-7.87 (m, 6H).

(NNN^{pyz})Pt-SEt$_2$ (43): The NNN^{pyz} ligand (52.5 mg, 0.162 mmols) and Pt(Ph)$_2$(SEt$_2$)$_2$ (82.4 mg, 0.156 mmols) were dissolved in CH_2Cl_2 (5 mL) in a 10 mL bomb flask. The solution was heated to 60 °C for 22 h. Solvent removal left **43** as an orange solid (90.7 mg, 96.1% yield).

^1H NMR (300 MHz, C_6D_6) δ 1.13 (t, $^3J_{HH}$ = 7.3 Hz, 6H), 1.57 (s, 18H), 3.33 (bs, 4H), 6.36 (s, 2H), 6.37 (d, $^3J_{HH}$ = 7.6 Hz, 2H), 6.69 (t, $^3J_{HH}$ = 7.9 Hz, 1H).

[**(NNN^{pyz})Pd-Cl]Cl (44)**: The NNN^{pyz} ligand (90.8 mg, 0.281 mmols) and Pd(SMe$_2$)$_2$Cl$_2$ (83.9 mg, 0.278 mmols) were dissolved in CH_2Cl_2 (4 mL) and stirred vigorously for 72 h. Diethyl ether (4 mL) was added to the yellow suspension. The yellow solid was collected by filtration, washed with ether (3 x 2 mL) and dried yielding **44** as a yellow powder (119.6 mg, 86% yield).

^1H NMR (700 MHz, CD_3OD) δ 1.45 (s, 18H), 7.08 (s, 2H), 7.97 (d, J = 7.9 Hz, 2H), 8.29 (t, J = 7.9 Hz, 1H). ^{13}C NMR (176 MHz, CD_3OD) δ 30.0 (s), 33.2 (s), 104.1 (s), 121.5 (s), 144.4 (s), 151.6 (s), 155.0 (s), 160.4 (s).

[**(NNN^{pyz})Pt-Cl]Cl (45)**: The NNN^{pyz} ligand (52.2 mg, 0.161 mmols) and Pt(SMe$_2$)$_2$Cl$_2$ (62.0 mg, 0.159 mmols) were dissolved in CH_2Cl_2 (3 mL) and stirred vigorously for 6 h. Diethyl

ether (3 mL) was added to the yellow suspension. The yellow solid was collected by filtration, washed with ether (3 x 3 mL) and dried yielding **45** as a yellow powder (71.6 mg, 76% yield).

^{1}H NMR (301 MHz, CD_3OD) δ 1.47 (s, 18H), 7.09 (s, 2H), 7.94 (d, J = 8.0 Hz, 2H), 8.24 (t, J = 8.0 Hz, 1H).

$(NN)_2Pd$ (46): In a J. Young NMR tube, $Pd(dba)_2$ (15.5 mg, 0.0270 mmols) and NN ligand (5.6 mg, 0.0278 mmols) were dissolved in CD_2Cl_2 (0.4 mL). After 1 h, more NN ligand (3.0 mg, 0.0149 mmols) was added to the tube. After 24 h, more NN ligand (2.5 mg, 0.0124 mmols) was added to the reaction mixture, totaling 2 equiv. of NN compared to Pd. After 48 h, complex **46** was observed as the major species in solution by NMR spectroscopy.

^{1}H NMR (500 MHz, CD_2Cl_2) δ 1.43 (s, 18H), 6.56 (s, 2H), 7.86 (td, J = 7.7, 1.5 Hz, 2H), 10.36-10.39 (m, 2H). Some assignments could not be made due to overlap with free dba.

$[(NN^{Me})Pd(SMe_2)Cl]_2$ (47): The NN^{Me} ligand (55.3 mg, 0.257 mmols) and $Pd(SMe_2)_2Cl_2$ (76.7 mg, 0.254 mmols) were dissolved in C_6H_6 (4 mL). To the orange solution, NEt_3 (50 μL, 0.358 mmols) was added, and the mixture was stirred for 2 h. The solution was filtered and the solvent was removed to yield **47** as an orange powder (105.9 mg, 99.5% yield).

^{1}H NMR (500 MHz, C_6D_6) δ 1.58 (s, 6H), 1.60 (s, 18H), 2.62 (s, 6H), 2.85 (s, 6H), 6.17 (s, 2H), 6.68 (d, $^3J_{HH}$ = 7.5 Hz, 2H), 6.92 (d, $^3J_{HH}$ = 7.7 Hz, 2H), 7.07 (t, $^3J_{HH}$ = 7.7 Hz, 2H).

$(NNN^{Et})_2$Pd-PPh_3 (48): To a solution of NNN^{Et} (24.9 mg, 0.0869 mmols) in C_6H_6 (3 mL) was added $Pd(PPh_3)_2(O_2)$ (56.7 mg, 0.0855 mmols) and the dark solution was stirred for 72 h. Solvent removal left a dark solid that was extracted with pentane (3 x 1 mL), filtered and combined. The golden yellow solution was concentrated (1.5 mL) and left at -30 °C to yield single crystals of **48** suitable for X-ray diffraction.

$^{31}P\{^{1}H\}$ NMR (121 MHz, C_6D_6) δ 30.6 (s). ^{1}H NMR (500 MHz, C_6D_6) δ 0.82 (t, J = 7.1 Hz, 12H), 1.33 (s, 18H), 2.15-2.42 (m, 8H), 3.40 (d, J = 16.9 Hz, 2H), 3.49 (d, J = 16.9 Hz, 2H), 6.31 (s, 2H), 6.91-7.01 (m, 9H), 7.06 (d, J = 7.7 Hz, 2H), 7.13 (t, J = 7.7 Hz, 2H), 7.41 (d, J = 7.6 Hz, 2H), 7.83-7.91 (m, 6H).

(NNN^{Et})Pd-Cl (49): In a J. Young NMR tube, $Pd(SMe_2)_2Cl_2$ (5.9 mg, 0.0196 mmols) and an excess of NEt_3 was added to a solution of NNN^{Et} (5.6 mg, 0.0196 mmols) in C_6D_6 (0.4 mL). The solution was decanted off of the formed solid. The isolated solid was dried and dissolved in CD_2Cl_2 (0.4 mL). Slow evaporation of this solution yielded single crystals of **49** suitable for X-ray diffraction. The solid was washed with water in air, and dried under vacuum.

^{1}H NMR (500 MHz, CD_2Cl_2) δ 1.32 (s, 9H), 1.65 (t, J = 7.1 Hz, 6H), 2.64-2.73 (m, 2H), 3.29-3.45 (m, 2H), 4.20 (s, 2H), 6.45 (s, 1H), 6.99 (d, J = 7.8 Hz, 1H), 7.36 (d, J = 8.0 Hz, 1H), 7.80 (t, J = 7.9 Hz, 1H).

(NNN^{Et})Pt-Cl (50) and **K[(NNN^{Et}*)Pt-Cl] (50*)**: The NNN^{Et} ligand (15.8 mg, 0.0552 mmols) and $Pt(SMe_2)_2Cl_2$ (21.6 mg, 0.0554 mmols) were dissolved in CH_2Cl_2 (1 mL). To the solution was added an excess of NEt_3 (1 drop), and the mixture was stirred for 15 h. The formed **50** was confirmed by NMR spectroscopy, but was not isolated. Solvent removal left a yellow solid that was dissolved in THF (2 mL), and KOH was added (15.5 mg, 0.276 mmols). The mixture was stirred for 16 h upon which a color change from yellow to red occurred. The solution was filtered through Celite. Solvent removal yielded **50*** as a dark red solid (24.6 mg, 80% yield).

50: ^{1}H NMR (500 MHz, CD_2Cl_2) δ 1.33 (s, 9H), 1.55 (t, J = 7.1 Hz, 6H), 2.84-2.98 (m, 2H), 3.36-3.49 (m, 2H), 4.25 (s, J_{PtH} = 18.2 Hz, 2H), 6.48 (s, 1H), 7.02 (d, J = 7.8 Hz, 1H), 7.34 (d, J = 7.9 Hz, 1H), 7.86 (t, J = 7.9 Hz, 1H).

50*: ^{1}H NMR (700 MHz, C_6D_6) δ 1.37 (s, 9H), 1.63 (bs, 6H), 2.20-2.36 (m, 2H), 3.38-3.51 (m, 2H), 3.51 (s, 1H), 5.56 (d, J = 6.4 Hz, 1H), 5.86 (d, J = 9.3 Hz, 1H), 6.27 (s, 1H), 6.55 (dd, J = 9.2, 6.1 Hz, 1H).

(NNN^{Et})Pt-I (51) and **(NNN^{Et}*)Pt-SMe$_2$ (52)**: In a J. Young NMR tube was combined NNN^{Et} (3.2 mg, 0.0112 mmols), Pt(SMe$_2$)$_2$I$_2$ (6.4 mg, 0.0112 mmols) and KOH (3.0 mg, 0.0535 mmols). The solids were dissolved in THF-d_8 (0.4 mL) and stirred for 24 h. Complex **51** was observed as an intermediate by NMR spectroscopy, but was not isolated. Complex **52** was produced as the final product.

52: ^{1}H NMR (500 MHz, THF-d_8) δ 1.25 (s, 9H), 1.59 (t, J = 7.1 Hz, 6H), 2.60-2.69 (m, 2H), 2.84 (s, J_{PtH} = 32.1 Hz, 6H), 3.29-3.37 (m, 2H), 3.41 (s, 1H), 5.17 (d, J = 6.5 Hz, 1H), 5.58 (d, J = 9.1 Hz, 1H), 5.95 (s, 1H), 6.27 (dd, J = 9.2, 6.6 Hz, 1H).

(NNN^{Et})Pt-Me (53): To a solution of NNN^{Et} (3.3 mg, 0.0115 mmols) in CD_2Cl_2 (0.4 mL) at -30 °C was added [PtMe$_2$(SMe$_2$)]$_2$ (3.4 mg, 0.00592 mmols). Within 5 mins, complete conversion to **53** was observed by NMR spectroscopy.

^{1}H NMR (300 MHz, CD_2Cl_2) δ 0.81 (s, J_{PtH} = 77.2 Hz, 3H), 1.32 (s, 9H), 1.46 (t, J = 7.1 Hz, 6H), 2.84-2.99 (m, 2H), 3.10-3.25 (m, 2H), 4.21 (s, J_{PtH} = 24.6 Hz, 2H), 6.46 (s, 1H), 7.06 (d, J = 7.8 Hz, 1H), 7.31 (d, J = 7.9 Hz, 1H), 7.82 (t, J = 7.9 Hz, 1H).

(NNN^{Et})Pt-Ph (54): To a solution of NNN^{Et} (3.5 mg, 0.0122 mmols) in CD_2Cl_2 (0.4 mL) at -30 °C was added [PtPh$_2$(SMe$_2$)]$_2$ (5.0 mg, 0.00608 mmols). After 5 mins, a (NN)PtPh$_2$ intermediate was observed by NMR spectroscopy. Solvent removal yielded a yellow solid that was dissolved in CD_3CN (0.4 mL) and heated to 60 °C for 2 h, yielding complex **54**.

^{1}H NMR (700 MHz, CD_3CN) δ 1.21 (s, 14H), 1.48 (t, J = 7.1 Hz, 6H), 2.76-2.90 (m, 2H), 2.95-3.07 (m, 2H), 4.42 (s, 2H), 6.52 (s, 1H), 6.80-6.84 (m, 1H), 6.86 (t, J = 7.2 Hz, 1H), 6.97-7.02 (m, 2H), 7.18 (d, J = 7.8 Hz, 1H), 7.44 (d, J = 8.0 Hz, 1H), 7.46-7.51 (m, 1H), 7.91 (t, J = 7.9 Hz, 1H).

(NNN^{Et})Pd-Me (55): To a solution of NNN^{Et} (5.0 mg, 0.0175 mmols) in C_6D_6 (0.4 mL) was added (TMEDA)$PdMe_2$ (4.5 mg, 0.0178 mmols) and heated to 60 °C for 3 d. Upon cooling, yellow crystals of **55** suitable for X-ray diffraction formed spontaneously.

^{1}H NMR (700 MHz, THF-d_8) δ 0.41 (s, 3H), 1.28 (s, 9H), 1.51 (t, J = 7.1 Hz, 6H), 2.68-2.75 (m, 2H), 2.95-3.02 (m, 2H), 4.15 (s, 2H), 6.32 (s, 1H), 6.98 (d, J = 7.6 Hz, 1H), 7.26 (d, J = 8.0 Hz, 1H), 7.67 (t, J = 7.8 Hz, 1H).

[(NNN^{Et})Pt-Me]OTf (56): Complex **53** (0.0115 mmols) was suspended in CD_3CN (0.4 mL) in a J. Young NMR tube. H_2O (0.6 μL, 0.0333 mmols) was added to the suspension, followed by HOTf (1.0 μL, 0.0192 mmols), yielding complex **56**.

^{1}H NMR (700 MHz, CD_3CN) δ 0.85 (s, J_{PtH} = 74.1 Hz, 3H), 1.40 (t, J = 7.1 Hz, 6H), 1.40 (s, 9H), 2.95-3.01 (m, J_{PtH} = 61.7 Hz, 2H), 3.15-3.23 (m, 2H), 4.52 (s, J_{PtH} = 23.2 Hz, 2H), 6.92 (d, J = 2.0 Hz, 1H), 7.59 (d, J = 8.0 Hz, 1H), 7.81 (d, J = 7.9 Hz, 1H), 8.18 (t, J = 7.9 Hz, 1H), 11.82 (bs, 1H).

[(NNN^{Et})Pt-Ph]OTf (57): Complex **54** (0.0122 mmols) was dissolved in CD_3CN (0.4 mL) in a J. Young NMR tube. H_2O (0.5 μL, 0.0278 mmols) was added to the solution, followed by HOTf (0.9 μL, 0.0102 mmols), yielding complex **57**.

^{1}H NMR (300 MHz, CD_3CN) δ 1.30 (s, 9H), 1.53 (t, J = 7.1 Hz, 6H), 2.84-3.10 (m, 4H), 4.64 (s, J_{PtH} = 29.4 Hz, 2H), 6.92 (d, J = 2.0 Hz, 1H), 6.98-7.06 (m, 2H), 7.09-7.16 (m, 2H), 7.45-

7.50 (m, 1H), 7.60 (dd, J = 8.1, 0.9 Hz, 1H), 7.87 (d, J = 7.8 Hz, 1H), 8.21 (t, J = 8.0 Hz, 1H), 11.96 (bs, 1H).

5.5 Notes to chapter 5

1. Monnier, J. R. *Appl. Catal. A-Gen.* **2001**, *221*, 73.
2. Sheldon, R. A. *J. Mol. Catal.* **1980**, *7*, 107.
3. Katsuki, T.; Sharpless, K. B. *J. Am. Chem. Soc.*, **1980**, *102*, 5974.
4. Zhang, W.; Loebach, J. L.; Wilson, S. R.; Jacobsen, E. N. *J. Am. Chem. Soc.*, **1990**, *112*, 2801.
5. De Vos, D. E.; Sels, B. F.; Jacobs, P. A. *Adv. Synth. Catal.* **2003**, *345*, 457.
6. Mizuno, N.; Yamaguchi, K.; Kamata, K. *Coord. Chem. Rev.* **2005**, *249*, 1944.
7. Cavani, F.; Teles, J. H.; *ChemSusChem,* **2009**, *2*, 508.
8. (a)Wells, D. H.; Joshi, A. M.; Delgass, W. N.; Thomson, K. T. *J. Phys. Chem. B.* **2006**, *110*, 14627. (b)Khouw, C. B.; Dartt, C. B.; Labinger, J. A.; Davis, M. E. *J. Catal.* **1994**, *149*, 195.
9. Hornback, J. M.; *Organic Chemistry*, 2nd ed.; 2006; pp 376-378.
10. Adam, W.; Wirth, T. *Acc. Chem. Res.* **1999**, *32*, 703.
11. Prabhakar, R.; Morokuma, K.; Hill, C. L.; Musaev, D. G. *Inorg. Chem.* **2006**, *45*, 5703.
12. Colladon, M.; Scarso, A.; Sgarbossa, P.; Michelin, R. A.; Strukul, G. *J. Am. Chem. Soc.* **2007**, *129*, 7680.
13. Fulmer, G. R.; Kaminsky, W.; Kemp, R. A.; Goldberg, K. I. *Organometallics* **2011**, *30*, 1627.
14. Bailey, W. D.; Luconi, L.; Rossin, A.; Yakhvarov, D.; Flowers, S. E.; Kaminsky, W.; Kemp, R. A.; Giambastiani, G.; Goldberg, K. I. *Organometallics* **2015**, *34*, 3998.
15. Konnick, M. M.; Stahl, S. S. *J. Am. Chem. Soc.* **2008**, *130*, 5753.
16. Konnick, M. M.; Decharin, N.; Popp, B. V.; Stahl, S. S. *Chem. Sci.* **2011**, *2*, 326.
17. Scheuermann, M. L.; Goldberg, K. I. *Chem. Eur. J.* **2014**, *20*, 14556.
18. (a) Read, G.; Urgelles, M. *J. Chem. Soc. Dalton Trans.* **1985**, 1591. (b) Dorta, R.; Shimon, L. J. W.; Rozenberg, H.; Milstein, D. *Eur. J. Inorg. Chem.* **2002**, 1827.
19. (a) Lawson, H. J.; Atwood, J. D. *J. Am. Chem. Soc.* **1989**, *111*, 6223. (b) Dutta, D. K.; Deb, B.; Sarmah, B. J.; Woolins, J. D.; Slawin, A. M.; Fuller, A. L.; Randall, R. A. M. *Eur. J. Inorg. Chem.* **2011**, 835. (c) Lanci, M. P.; Brinkley, D. W.; Stone, K. L.; Smirnov, V. V.; Roth, J. P. *Angew. Chem. Int. Ed.* **2005**, *44*, 7273. (d). Polukeev, A. V.; Wendt, O. F. *Organometallics* **2015**, *34*, 4262. (e) Kelley, M. R.; Rohde, J.-U. *Chem. Commun.* **2012**, *48*, 2876.
20. Ahijado, M.; Braun, T.; Noveski, D.; Kocher, N.; Neumann, B.; Stalke, D.; Stammler, H.-G. *Angew. Chem. Int. Ed.* **2005**, *44*, 6947.
21. Umehara, K.; Kuwata, S.; Ikariya, T. *J. Am. Chem. Soc.* **2013**, *135*, 6754.
22. Umehara, K.; Kuwata, S.; Ikariya, T. *Inorg. Chima. Acta* **2014**, *413*, 136.
23. Yoshinari, A.; Tazawa, A.; Kuwata, S.; Ikariya, T. *Chem. Asian J.* **2012**, *7*, 1417.
24. Farrugia, L. J. *J. Appl. Cryst.* **2012**, *45*, 849.
25. Wilke, G.; Schott, H.; Heimbach, P. *Angew. Chem.* **1967**, *79*, 62.
26. Derrah, E. J.; Ladeira, S.; Bouhadir, G.; Miqueu, K.; Bourissou, D. *Chem. Commun.* **2011**, *47*, 8611.
27. Stahl, S. S.; Thorman, J. L.; Nelson, R. C.; Kozee, M. A. *J. Am. Chem. Soc.* **2001**, *123*, 7188.
28. Yu, W.-S.; Cheng, C.-C.; Cheng, Y.-M.; Wu, P.-C.; Song, Y.-H.; Chi, Y.; Chou, P.-T. *J. Am. Chem. Soc.* **2003**, *125*, 10800.
29. Powers, D. C.; Ritter, T. *Nat. Chem.* **2009**, *1*, 302.
30. Toda, T.; Kuwata, S.; Ikariya, T. *Z. Anorg. Allg. Chem.* **2015**, *641*, 2135.
31. (a) Poverenov, E.; Gandelman, M.; Shimon, L. J. W.; Rozenberg, H.; Ben-David, Y.; Milstein, D. *Organometallics* **2005**, *24*, 1082. (b) Linder, R.; van den Bosch, B.; Lutz, M.; Reek, J. N. H.; van der Vlugt, J. I. *Organometallics*, **2011**, *30*, 499.

32. Feller, M.; Ben-Ari, E.; Iron, M. A.; Diskin-Posner, Y.; Leitus, G.; Shimon, L. J. W.; Konstantinovski, L.; Milstein, D. *Inorg. Chem.* **2010**, *49*, 1615.
33. Bailey, W. D.; Kaminsky, W.; Kemp, R. A.; Goldberg, K. I. *Organometallics* **2014**, *33*, 2503.
34. Crabtree, R. H. The Organometallic Chemistry of the Transition Metals; Wiley: New York, 2005.
35. Dahl, E. W.; Szymczak, N. K. *Angew. Chem. Int. Ed.* **2016**, *55*, 3101.
36. (a) Grotjahn, D. B.; Larsen, C. R.; Gustafson, J. L.; Nair, R.; Sharma, A. *J. Am. Chem. Soc.* **2007**, *129*, 9592. (b) Grotjahn, D. B. *Dalton Trans.* **2008**, 6497. (c) Grotjahn, D. B. *Chem. Eur. J.* **2005**, *11*, 7146.
37. Peterson, R. I.; Himes, R. A.; Kotani, H.; Suenobu, T.; Tian, L.; Siegler, M. A.; Solomon, E. I.; Fukuzumi, S.; Karlin, K. D. *J. Am. Chem. Soc.* **2011**, *133*, 1702.
38. Ng, G. K.-Y.; Ziller, J. W.; Borovik, A. S. *Inorg. Chem.* **2011**, *50*, 7922.
39. Shook, R. L.; Peterson, S. M.; Greaves, J.; Moore, C.; Rheingold, A. L.; Borovik, A. S. *J. Am. Chem. Soc.* **2011**, *133*, 5810.
40. Borovik, A. S. *Acc. Chem. Res.* **2005**, *38*, 54.
41. Fulmer, G. R.; Herndon, A. N.; Kaminsky, W.; Kemp, R. A.; Goldberg, K. I. *J. Am. Chem. Soc.* **2011**, *133*, 17713.
42. Bruker (**2007**) APEX2 (Version 2.1-4), SAINT (version 7.34A), SADABS (version 2007/4), BrukerAXS Inc, Madison, Wisconsin, USA.
43. CrysAlis CCD 1.171.31.2 (release 07-07-2006), CrysAlis171 .NET, Oxford Diffraction Ltd.
44. CrysAlis RED 1.171.31.2 (release 07-07-2006), CrysAlis171 .NET, Oxford Diffraction Ltd.
45. Altomare, A.; Burla, M. C.; Camalli, M.; Cascarano, G. L.; Giacovazzo, C.; Guagliardi, A.; Moliterni, A. G. G.; Polidori, G.; Spagna, R. *J. Appl. Crystallogr.* **1999**, *32*, 115.
46. Sheldrick, G. M. SHELXL (**1997**).
47. Nardelli, M. *Comput. Chem.* **1993**, *7*, 95.
48. Farrugia, L. J. *J. Appl. Crystallogr.* **1997**, *30*, 565.

Bibliography

Adam, W.; Wirth, T. *Acc. Chem. Res.* **1999**, *32*, 703-710.

Adams, R. D.; Pearl Junior, W. C.; Wong, Y. O.; Zhang, Q.; Hall, M. B.; Walensky, J. R. *J.Am.Chem.Soc.* **2011**, *133*, 12994.

Ahijado, M.; Braun, T.; Noveski, D.; Kocher, N.; Neumann, B.; Stalke, D.; Stammler, H.-G. *Angew. Chem. Int. Ed.* **2005**, *44*, 6947-6951.

Albrecht, M.; Lindner, M. M. *Dalton Trans*. **2011**, *40*, 8733.

Albrecht, M.; van Koten, G. *Angew. Chem. Int. Ed*. **2001**, *40*, 3750.

Alonso, M. T.; Juanes, O.;de Mendoza, J.; Rodríguez-Ubis, J. C. *J. Organomet. Chem.* **1994**, *484*, 19.

Altomare, A.; Burla, M. C.; Camalli, M.; Cascarano, G. L.; Giacovazzo, C.; Guagliardi, A.; Moliterni, A. G. G.; Polidori, G.; Spagna, R. *J. Appl. Crystallogr.* **1999**, *32*, 115-119.

Altomare, A.; Cascarano, G. L.; Giacovazzo, C.; Guagliardi, A. *J. Appl. Crystallogr.* **1993**, *26*, 343.

Anastas, P. T.; Warner, J. C. Green Chemistry: Theory and Practice, Oxford University Press: New York, 1998; pp 30.

Andrae, D.; Haeuessermann, U.; Dolg, M.; Stoll, H.; Preuss, H. *Theor. Chem. Acc.* **1990**, *77*, 123-141.

Ara, I.; Fornies, J.; Martin, A.; Martin, L. F.; Menjon, B.; Miedes, H. *Dalton Trans.* **2010**, *39*, 7301-7309.

Bailey, W. D.; Kaminsky, W.; Kemp, R. A.; Goldberg, K. I. *Organometallics* **2014**, *33*, 2503-2509.

Bailey, W. D.; Luconi, L.; Rossin, A.; Yakhvarov, D.; Flowers, S. E.; Kaminsky, W.; Kemp, R. A.; Giambastiani, G.; Goldberg, K. I. *Organometallics* **2015**, *34*, 3998-4010.

Bailey, W. D.; Luconi, L.; Rossin, A.; Yakhvarov, D.; Flowers, S. E.; Kaminsky, W.; Kemp, R. A.; Giambastiani, G.; Goldberg, K. I. Manuscript in preparation, 2016.

Bailey, W. D.; Parkes, M. V.; Kemp, R. A.; Goldberg, K. I. *Reactions of Square Planar d^8 Pincer Complexes with Oxygen and Hydrogen.* Pincer and Pincer-Type Complexes: Application in Organic Synthesis and Catalysis*;* Szabo, K. J., Ed.; Wendt, O. F., Ed; Wiley-VCH: Weinheim, Germany, 2014; pp 281-298.

Balaraman, E.; Gnanaprakasam, B.; Shimon, L. J. W.; Milstein, D. *J. Am. Chem. Soc.* **2010**, *132*, 16756-16758.

Balaraman, E.; Gunanathan, C.; Zhang, J.; Shimon, L. J. W.; Milstein, D. *Nature Chem.* **2011**, *3*, 609-614.

Barteau, M. A.; Madix, R. J. *J. Am. Chem. Soc.* **1983**, *105*, 344.

Baya, M.; Houghton, J.; Konya, D.; Champouret, Y.; Daran, J.-C.; Lenero, K. Q. A.; Schoon, L.; Mul, W. P.; van Oort, A. B.; Meijboom, N.; Drent, E.; Orpen, A. G.; Poli R. *J. Am. Chem. Soc.* **2008**, *130*, 10612.

Bayson, J. H.; Winfield, M. E. *J. Catal.* **1964**, *3*, 123.

Ben-Ari, E. Activation of Strong Bonds by Electron-Rich Iridium and Rhodium. Ph. D. Dissertation, Weizmann Institute of Science, 2007.

Benito-Garagorri, D.; Kirchner, K. *Acc. Chem. Res.* **2008**, *41*, 201-213.

Beran, S.; Jiru, P.; Wichterlova, B.; Zahrandik, R. *React. Kinet. Catal. Lett.* **1976**, *5*, 131-134.

Bichler, B.; Holzhacker, C.; Stöger, B.; Puchberger, M.; Veiros, L. F.; Kirchner, K. *Organometallics* **2013**, *32*, 4114.

Bondi, A. *J. Phys. Chem.* **1964**, *68*, 441.

Boro, B. J. Ph.D. Dissertation, University of New Mexico, 2009.

Borovik, A. S. *Acc. Chem. Res.* **2005**, *38*, 54.

Bröring, M.; Kleeberg, C.; Köhler, S. *Inorg. Chem.* **2008**, *47*, 6404-6412.

Bruker (**2007**) APEX2 (Version 2.1-4), SAINT (version 7.34A), SADABS (version 2007/4), BrukerAXS Inc, Madison, Wisconsin, USA.

Brunner, E. *J. Chem. Eng. Data* **1985**, *30*, 269-273.

Bryndza, H. E.; Tam, W. *Chem. Rev.* **1988**, *88*, 1163-1188.

Campbell, C. *J. Catal.* **1985**, *94*, 436.

Cámpora, J.; Palma, P.; del Río, D.; Álvarez, E. *Organometallics* **2004**, *23*, 1652-1655.

Canty, A. J.; Honeyman, R. T. *J. Organomet. Chem.* **1990**, *387*, 247.

Canty, A. J.; Honeyman, R. T. *J. Organomet. Chem.* **1992**, *430*, 245.

Canty, A. J.; Honeyman, R. T.; Skelton, B. W.; White, A. H. *Inorg. Chim. Acta* **1986**, *114*, L39.

Canty, A. J.; Jin, H.; Roberts, A. S.; Skelton, B. W.; White, A. H. *Organometallics* **1996**, *15*, 5713-5722.

Canty, A. J.; Jin, H.; Skelton, B. W.; White, A. H. *J. Organomet. Chem.* **1995**, *503*, C16.

Canty, A. J.; Minchin, N. J. *J. Organomet. Chem.* **1982**, *226*, C14.

Canty, A. J.; Patel, J.; Skelton, B. W.; White, A. H. *J. Organomet. Chem.* **2000**, *607*, 194.

Cao, L.; Jennings, M. C.; Puddephatt, R. J. *Dalton Trans.* **2009**, 5171-5176.

Castan, P.; Dahan, F.; Wimmer, S.; Wimmer, F. L. *J. Chem Soc., Dalton Trans.* **1990**, 2679-2683.

Cavani, F.; Gaffney, A. M. *Synthesis of Propene Oxide: A Successful Example of Sustainable Industrial Chemistry, in Sustainable Industrial Chemistry*; Cavani, F., Ed.; Centi, G., Ed.;

Perathoner, S., Ed.; Trifiró, F., Ed.; Wiley-VCH Verlag GmbH & Co. KGaA, Weinheim, Germany, 2009; pp 319-365.

Cavani, F.; Teles, J. H. *ChemSusChem*, **2009**, *2*, 508.

Chan, S.; Lee, S.-M.; Lin, Z.; Wong W.-T. *J. Organomet. Chem.* **1996**, *510*, 219.

Chierotti, M. R.; Rossin, A.; Gobetto, R.; Peruzzini, M. *Inorg. Chem.* **2013**, *52*, 12616-12623.

Clapham, S. E.; Hadzovic, A.; Morris, R. H. *Coord. Chem. Rev.* **2004**, *248*, 2201-2237.

Clerici, M. G.; Ingallina, P. *J. Catal.* **1993**, *140*, 71.

Clerici, M. G.; Bellussi, G.; Romano, U. *J. Catal.* **1991**, *129*, 159.

Colladon, M.; Scarso, A.; Sgarbossa, P.; Michelin, R. A.; Strukul, G. *J. Am. Chem. Soc.* **2007**, *129*, 7680-7689.

Cook, E.; Iwasaki, K.; Masuda, J. D.; Xia, A. *Polyhedron* **2015**, *87*, 38.

Cottrell, T. L. *The Strengths of Chemical Bonds*, 2d ed., Butterworth, London, 1958.

Crabtree, R. H. The Organometallic Chemistry of the Transition Metals; Wiley: New York, 2005.

CrysAlis CCD 1.171.31.2 (release 07-07-2006), CrysAlis171 .NET, Oxford Diffraction Ltd.

CrysAlis RED 1.171.31.2 (release 07-07-2006), CrysAlis171 .NET, Oxford Diffraction Ltd.

Cundari, T. R.; Grimes, T. V.; Gunnoe, T. B. *J. Am. Chem. Soc.* **2007**, *129*, 13172.

Dahl, E. W.; Szymczak, N. K. *Angew. Chem. Int. Ed.* **2016**, *55*, 3101-3105.

Darwent, B. B. *National Standard Reference Data Series, National Bureau of Standards, no. 31*, Washington, 1970.

De Vos, D. E.; Sels, B. F.; Jacobs, P. A. *Adv. Synth. Catal.* **2003**, *345*, 457.

Denney, M. C.; Smythe, N. A.; Cetto, K. L.; Kemp, R. A.; Goldberg, K. I. *J. Am. Chem. Soc.* **2006**, *128*, 2508-2509.

Derrah, E. J.; Ladeira, S.; Bouhadir, G.; Miqueu, K.; Bourissou, D. *Chem. Commun.* **2011**, *47*, 8611-8613.

Dorta, R.; Shimon, L. J. W.; Rozenberg, H.; Milstein, D. *Eur. J. Inorg. Chem.* **2002**, 1827-1834.

Dunning Jr., T. H.; Hay P. J. in *Modern Theoretical Chemistry*, Ed. H. F. Schaefer III, Vol. 3 (Plenum, New York, **1976**) 1-28.

Dupont, J.; Consorti, C. S.; Spencer, J. *Chem. Rev.* **2005**, *105*, 2527.

Dutta, D. K.; Deb, B.; Sarmah, B. J.; Woolins, J. D.; Slawin, A. M.; Fuller, A. L.; Randall, R. A. M. *Eur. J. Inorg. Chem.* **2011**, 835-841.

Ehlers, A. W.; Böhme, M.; Dapprich, S.; Gobbi, A.; Höllwarth, A.; Jonas, V.; Köhler, K. F.; Stegmann, R.; Veldkamp, A.; Frenking, G. *Chem. Phys. Lett.* **1993**, *208*, 111-114.

Endicott, J. F.; Wong, C. L.; Inoue, T.; Natarajan, P. *Inorg. Chem.* **1979**, *18*, 450.

Esteruelas, M. A.; Oro, L. A. *Chem. Rev.* **1998**, *98*, 577-588.

Evrard, D.; Meilleur, D.; Drouin, M.; Mugnier, Y.; Harvey P. D. *Z. Anorg. Allg. Chem.* **2002**, *628*, 2286.

Farrugia, L. J. *J. Appl. Cryst.* **2012**, *45*, 849-854.

Feller, M.; Ben-Ari, E.; Iron, M. A.; Diskin-Posner, Y.; Leitus, G.; Shimon, L. J. W.; Konstantinovski, L.; Milstein, D. *Inorg. Chem.* **2010**, *49*, 1615.

Fornies, J.; Navarro, R.; Sicilia, V.; Martinez, F.; Welch, A. J. *J. Organomet. Chem.* **1991**, *408*, 425.

Frisch, M. J. *et al.*, *Gaussian09*, Revision C.01, Gaussian Inc., Wallingford CT, **2009**.

Fryzuk, M. D.; Lloyd, B. R.; Clentsmith, G. K. B.; Rettig, S. J. *J. Am. Chem. Soc.* ***1991***, *113*, 4332.

Fryzuk, M. D.; Lloyd, B. R.; Clentsmith, G. K. B.; Rettig, S. J. *J. Am. Chem. Soc.* **1994**, *116*, 3804.

Fukui, K. *Acc. Chem. Res.* **1981**, *14*, 363-368.

Fulmer, G. R.; Herndon, A. N.; Kaminsky, W.; Kemp, R. A.; Goldberg, K. I. *J. Am. Chem. Soc.* **2011**, *133*, 17713-17726.

Fulmer, G. R.; Kaminsky, W.; Kemp, R. A.; Goldberg, K. I. *Organometallics* **2011**, *30*, 1627-1636.

Fulmer, G. R.; Muller, R. P.; Kemp, R. A.; Goldberg, K. I. *J. Am. Chem. Soc.* **2009**, *131*, 1346-1347.

Fulmer, G. R. Ph.D. Dissertation, University of Washington, 2010.

Fulton, J. R.; Holland, A. W.; Fox, D. J.; Bergman, R. G. *Acc. Chem. Res.* **2002**, *35*, 44.

Gagliardo, M.; Selander, N.; Mehendale, N. C.; van Koten, G.; Klein G., R. J. M.; Szabó, K. J. *Chem. Eur. J.* **2008**, *14*, 4800-4809.

Gelman, D.; Musa, S. *ACS Catal.* **2012**, *2*, 2456.

Gillard, R. D.; Heaton, B. T.; Vaughan, D. H.; *J. Chem. Soc. A* **1970**, 3126.

Gong, J.-F.; Zhang, Y.-H.; Song, M.-P.; Xu, C. *Organometallics* **2007**, *26*, 6487-6492.

Goto, E.; Begum, R. A.; Zhan, S.; Tanase, T.; Tanigaki, K.; Sakai, K. *Angew. Chem. Int. Ed.* **2004**, *43*, 5029.

Grotjahn, D. B. *Chem. Eur. J.* **2005**, *11*, 7146-7153.

Grotjahn, D. B. *Dalton Trans.* **2008**, 6497-6508.

Grotjahn, D. B.; Larsen, C. R.; Gustafson, J. L.; Nair, R.; Sharma, A. *J. Am. Chem. Soc.* **2007**, *129*, 9592-9593.

Grove, D. M.; van Koten, G.; Ubbels, H. J. C.; Spek, A. L. *J. Am. Chem. Soc.,* **1982**, *104*, 4285-4286.

Gunanathan, C.; Ben-David, Y.; Milstein, D. *Science* **2007**, *317*, 790.

Gunanathan, C.; Milstein, D. *Acc. Chem. Res.* **2011**, *44*, 588.

Gunanathan, C.; Milstein, D. *Top. Organomet. Chem.* **2011**, *37*, 55.

Gnanaprakasam, B.; Milstein, D. *J. Am. Chem. Soc.* **2011**, *133*, 1682-1685.

Haibach, M. C.; Kundu, S.; Brookhart, M.; Goldman, A. S. *Acc. Chem. Res.* **2012**, *45*, 947.

Hao, X.-Q.; Huang, J.-J.; Wang, T.; Lv, J.; Gong, J.-F.; Song, M.-P. *J. Org. Chem.* **2014**, 79, 9512.

Hartshorn, C. M.; Steel, P. J. *Organometallics* **1998**, *17*, 3487-3496.

Hayashi, Y.; Wada, S.; Yamashita, M.; Nozaki, K. *Organometallics* **2012**, *31*, 1073-1081.

Hebden, T. J.; Denney, M. C.; Pons, V.; Piccoli, P. M. B.; Koetzle, T. F.; Schultz, A. J., Kaminsky, W.; Goldberg, K. I.; Heinekey, D. M. *J. Am. Chem. Soc.* **2008**, *130*, 10812.

Hebden, T. J.; St. John, A. J.; Gusev, D. G.; Kaminsky, W.; Goldberg, K. I.; Heinekey, D. M. *Angew. Chem. Int. Ed.* **2011**, *50*, 1873-1876.

Herbert, D. E.; Ozerov, O. V. *Organometallics* **2011**, *30*, 6641-6654.

Höllwarth, A.; Böhme, M.; Dapprich, S.; Ehlers, A. W.; Gobbi, A.; Jonas, V.; Köhler, K. F.; Stegmann, R.; Veldkamp A.; Frenking, G. *Chem. Phys. Lett.* **1993**, *208*, 237-240.

Hornback, J. M.; Organic Chemistry, 2nd ed.; 2006; pp 376-378.

Hou, A.-T.; Liu, Y.-L.; Hao, X.-Q.; Gong, J.-F.; Song, M.-P. *J. Organomet. Chem.* **2011**, *696*, 2857.

IHS Chemical, Propylene Oxide, 2012 report.

Inés, B.; SanMartin, R.; Churruca, F.; Domínguez, E.; Urtiaga M. K.; Arriortua, M. I. *Organometallics*, **2008**, *27*, 2833-2839.

Ito, M.; Ikariya, T. *Chem. Commun.* **2007**, 5134-5142.

Katsuki, T.; Sharpless, K. B. *J. Am. Chem. Soc.* **1980**, *102*, 5974.

Keith, J. M.; Muller, R. P.; Kemp, R. A.; Goldberg, K. I.; Goddard, W. A., III; Oxgaard, J. *Inorg. Chem.* **2006**, *45*, 9631–9633.

Kelley, M. R.; Rohde, J.-U. *Chem. Commun.* **2012**, *48*, 2876-2878.

Kerr, J. A. *Chem. Rev.* **1966**, *66*, 465.

Khake, S. M.; Soni, V.; Gonnade, R. G.; Punji, B. *Dalton Trans.* **2014**, *43*, 16084-16096.

Khouw, C. B.; Dartt, C. B.; Labinger, J. A.; Davis, M. E. *J. Catal.* **1994**, *149*, 195-205.

Khusnutdinova, J. R.; Rath, N. P.; Mirica, L. M. *J. Am. Chem. Soc.* **2012**, *134*, 2414-2422.

Khusnutdinova, J. R.; Zavalij, P. Y.; Vedernikov, A. N. *Organometallics* **2007**, *26*, 2402−2413.

Klein, A.; Dogan, A.; Feth, M.; Bertagnolli, H. *Inorg. Chim. Acta* **2003**, *343*, 189.

Konnick, M. M.; Decharin, N.; Popp, B. V.; Stahl, S. S. *Chem. Sci.* **2011**, *2*, 326.

Konnick, M. M.; Gandhi, B. A.; Guzei, I. A.; Stahl, S. S. *Angew. Chem. Int. Ed.* **2006**, *45*, 2904.

Konnick, M. M.; Stahl, S. S. *J. Am. Chem. Soc.* **2008**, *130*, 5753.

Kundu, S.; Choliy, Y.; Zhuo, G.; Ahuja, R.; Emge, T. J.; Warmuth, R.; Brookhart, M.; Krogh-Jespersen, K.; Goldman, A. S. *Organometallics* **2009**, *28*, 5432-5444.

Jensen, C. M. *Chem. Commun.* **1999**, 2443-2449.

Jessop, P. G.; Ikariya, T.; Noyori, R. *Chem. Rev.* **1995**, *95*, 259-272.

Jessop, P. G.; Morris, R. H. *Coord. Chem. Rev.* **1992**, *121*, 155-284.

Johansson, R.; Öhrström, L.; Wendt, O. F. *Cryst. Growth Des.* **2007**, *7*, 1974.

Johansson, R.; Wendt, O. F. *Organometallics* **2007**, *26*, 2426-2430.

Johnson M. T.; Dzolic, Z.; Cetina, M.; Lahtinen, M.; Ahlquist, M. S. G.; Rissanen, K.; Ohrstrom, L.; Wendt, O. F. *Dalton Trans.* **2013**, *42*, 8484-8491.

Johnson M. T.; Dzolic, Z.; Cetina, M.; Wendt, O. F.; Ohrstrom, L.; Rissanen, K. *Cryst. Growth Des.* **2012**, *12*, 362.

Johnston, L. E.; Page, J. A. *Can. J. Chem.* **1969**, *47*, 4241.

Jonasson, K. J.; Wendt, O. F. *Chem. Eur. J.* **2014**, *20*, 11894-11902.

Joslin, E. E.; Quillian, B.; Gunnoe, T. B.; Cundari, T. R.; Sabat, M.; Myers, W. H. *Inorg. Chem.* **2014**, *53*, 6270-6279.

Lachaize, S.; Essalah, K.; Montiel-Palma, V.; Vendier, L.; Chaudret, B.; Barthelat, J.-C. Sabo-Etienne, S. *Organometallics* **2005**, *24*, 2935.

Lanci, M. P.; Brinkley, D. W.; Stone, K. L.; Smirnov, V. V.; Roth, J. P. *Angew. Chem. Int. Ed.* **2005**, *44*, 7273-7276.

Lane, B. S.; Burgess, K. *Chem. Rev.* **2003**, *103*, 2457.

Lao, D. B.; Owens, A. C. E.; Heinekey, D. M.; Goldberg, K. I. *ACS Catal.* **2013**, *3*, 2391-2396.

Lawson, H. J.; Atwood, J. D. *J. Am. Chem. Soc.* **1989**, *111*, 6223-6227.

Leis, W.; Mayer, H. A.; Kaska, W. C. *Coord. Chem. Rev.* **2008**, *252*, 1787-1797.

Levina, V. A.; Rossin, A.; Belkova, N. V.; Chierotti, M. R.; Epstein, L. M.; Filippov, O. A.; Gobetto, R.; Gonsalvi, L.; Lledòs, A.; Shubina, E. S.; Zanobini, F. and Peruzzini, M. *Angew. Chem. Int. Ed.* **2011**, *50*, 1367-1370.

Li, J.; Siegler, M.; Lutz, M.; Spek, A. L.; Gebbink, R. J. M. K.; van Koten, G. *Adv. Synth. Catal.* **2010**, *352*, 2474-2488.

Linder, R.; van den Bosch, B.; Lutz, M.; Reek, J. N. H.; van der Vlugt, J. I. *Organometallics*, **2011**, *30*, 499-510.

Luconi, L.; Giambastiani, G.; Rossin, A.; Bianchini, C.; Lledós, A. *Inorg. Chem*. **2010**, *49*, 6811-6813.

Luconi, L.; Klosin, J.; Smith, A. J.; Germain, S.; Schulz, E.; Hannedouche, J.; Giambastiani, G. *Dalton Trans.* **2013**, *42*, 16056-16065.

Luconi, L.; Lyubov, D. M.; Bianchini, C.; Rossin, A.; Faggi, C.; Fukin, G. K.; Cherkasov, A. V.; Shavyrin, A. S.; Trifonov, A. A.; Giambastiani, G. *Eur. J. Inorg. Chem.* **2010**, 608.

Luconi, L.; Rossin, A.; Motta, A.; Tuci, G.; Giambastiani, G. *Chem. Eur. J.* **2013**, *19*, 4906-4921.

Luconi, L.; Rossin, A.; Tuci, G.; Germain, S.; Schulz, E.; Hannedouche, J.; Giambastiani, G. *ChemCatChem* **2013**, *5*, 1142.

Luconi, L.; Rossin, A.; Tuci, G.; Tritto, I.; Boggioni, L.; Klosin, J. J.; Theriault, C. N.; Giambastiani, G. *Chem. Eur. J.* **2012**, *18*, 671.

Lynch, B. J.; Zhao Y.; Truhlar, D. G. *J. Phys. Chem. A* **2003**, *107*, 1384-1388.

Lyubov, D. M.; Fukin, G. K.; Cherkasov, A. V.; Shavyrin, A. S.; Trifonov, A. A.; Luconi, L.; Bianchini, C.; Meli, A.; Giambastiani, G. *Organometallics* **2009**, *28*, 1227-1232.

Mackay, S.; Edwards, C.; Henderson, A.; Gilmore, C.; Stewart, N.; Shankland, K.; Donald, A. (**1997**) *MaXus: a computer program for the solution and refinement of crystal structures from diffraction data*. University of Glasgow, Scotland.

Maenaka, Y. Suenobu, T.; Fukuzumi, S. *J. Am. Chem. Soc.* **2012**, *134*, 9417-9427.

Mahoney, W. S.; Brestensky, D. M.; Stryker, J. M. *J. Am. Chem. Soc.* **1988**, *110*, 291-293.

Marenich, A. V.; Cramer C. J.; Truhlar, D. G. *J. Phys. Chem. B* **2009**, *113*, 6378-6396.

Mehendale, N. C.; Sietsma, J. R. A.; de Jong, K. P.; van Walree, C. A.; Klein Gebbink R. J. M. and van Koten, G. *Adv. Synth. Catal.* **2007**, *349*, 2619.

Milstein, D. *Top. Catal.* **2010**, *53*, 915-923.

Mizuno, N.; Yamaguchi, K.; Kamata, K. *Coord. Chem. Rev.* **2005**, *249*, 1944.

Monnier, J. R. *Appl. Catal. A-Gen.* **2001**, *221*, 73-91.

Montag, M. Zhang, J.; Milstein, D. *J. Am. Chem. Soc.* **2012**, *134*, 10325.

Moreno, I.; SanMartin, R.; Inés, B.; Herrero, M. T.; Domínguez, E. *Curr. Org. Chem.* **2009**, *13*, 878.

Motoyama, Y.; Shimozono, K.; Nishiyama, H. *Inorg. Chim. Acta*, **2006**, *359*, 1725.

Moulton, C. J.; Shaw, B. L. *J. Chem. Soc., Dalton Trans.* **1976**, 1020-1024.

Munz, D.; Wang, D.; Moyer, M. M.; Webster-Gardiner, M. S.; Kunal, P.; Watts, D.; Trewyn, B. G.; Vedernikov, A. N.; Gunnoe, T. B. *ACS Catal.* **2016**, *6*, 4584-4593.

Muller, R. P.; Kemp, R. A.; Goldberg, K. I. Unpublished results.

Musaev, D. G. *Inorg. Chem.* **2006**, *45*, 5703-5709.

Myaji, T.; Kujime, M.; Hikichi, S.; Moro-oka, Y.; Akita, M. *Inorg. Chem.* **2002**, *41*, 5286-5295.

Nardelli, M. *Comput. Chem.* **1993**, *7*, 95-98.

Ng, G. K.-Y.; Ziller, J. W.; Borovik, A. S. *Inorg. Chem.* **2011**, *50*, 7922.

Niu, J.-L.; Hao, X.-Q.; Gong, J.-F.; Song, M.-P. *Dalton Trans.* **2011**, *40*, 5135-5150.

Organometallic Pincer Chemistry; Van Koten, G.; Milstein, D., Ed.; Top. Organomet. Chem.; Springer: Heidelberg, 2013; Vol. 40.

Osugi, J.; Kubota, H. *Rev. Phys. Chem. Japan* **1964**, *34*, 19-29.

Oxgaard, J.; Tenn, W. J., III; Nielsen, R. J.; Periana, R. A.; Goddard, W. A., III *Organometallics* **2007**, *26*, 1565.

Özbek, M. O.; van Santen, R. *A. Catal. Lett.* **2013**, *143*, 131.

Pandarus, V.; Zargarian, D. *Chem. Commun.* **2007**, 978-980.

Parkes, M. V.; Bailey, W. D.; Goldberg, K. I.; Kemp, R. A. *J. Organomet. Chem.* **2016**, Submitted.

Parkes, M. V. Ph.D. Dissertation, University of New Mexico, 2012.

Pearlman, W. M. *Tetrahedron Lett.* **1967**, *8*, 1663-1664.

Peterson, R. I.; Himes, R. A.; Kotani, H.; Suenobu, T.; Tian, L.; Siegler, M. A.; Solomon, E. I.; Fukuzumi, S.; Karlin, K. D. *J. Am. Chem. Soc.* **2011**, *133*, 1702.

Petit, A.; Flygare, J.; Miller, A. T.; Winkel, G.; Ess, D. H. *Org. Lett.* **2012**, *14*, 3680.

Pincer and Pincer-Type Complexes: Application in Organic Synthesis and Catalysis; Szabo, K. J., Ed.; Wendt, O. F., Ed; Wiley-VCH: Weinheim, Germany, 2014.

Pizzo, E.; Sgarbossa, P.; Scarso, A.; Michelin, R. A.; Strukul, G. *Organometallics* **2006**, *25*, 3056-3062.

Polukeev, A. V.; Wendt, O. F. *Organometallics* **2015**, *34*, 4262-4271.

Popp, B. V.; Stahl, S. S. *J. Am. Chem. Soc.* **2007**, *129*, 4410.

Portnoy, M.; Frolow, F.; Milstein D. *Organometallics* **1991**, *10*, 3960.

Poverenov, E.; Gandelman, M.; Shimon, L. J. W.; Rozenberg, H.; Ben-David, Y.; Milstein, D. *Organometallics* **2005**, *24*, 1082-1090.

Poverenov, E.; Iron, M. A.; Gandelman, M.; Ben-David, Y.; Milstein, D. *Eur. J. Inorg. Chem.* **2010**, 1991.

Poverenov, E.; Leitus, G.; Shimon, L. J. W.; Milstein, D. *Organometallics* **2005**, *24*, 5937-5944.

Powers, D. C.; Ritter, T. *Nat. Chem.* **2009**, *1*, 302-309.

Prabhakar, R.; Morokuma, K.; Hill, C. L.; Musaev, D. G. *Inorg. Chem.* **2006**, *45*, 5703-5709.

Read, G.; Urgelles, M. *J. Chem. Soc. Dalton Trans.* **1985**, 1591-1596.

Roberts, H. L.; Symes, W. R. *J. Chem. Soc. A* **1968**, 1450.

Roddick, D. M. *Top. Organomet. Chem.* **2013**, *40*, 49-88.

Roesky, H. W.; Singh, S.; Yusuff, K. K. M.; Maguire, J. A.; Hosmane, N. S. *Chem. Rev.* **2006**, *106*, 3813-3843.

Rossin, A.; Bottari, G.; Lozano-Vila, A. M.; Paneque, M.; Peruzzini, M.; Rossi, A. and Zanobini, F. *Dalton Trans.* **2013**, *42*, 3533-3541.

Rossin, A.; Peruzzini, M.; Zanobini, F. *Dalton Trans.* **2011**, *40*, 4447-4452.

Salanouve, E.; Retailleau, P.; Janin, Y. L. *Tetrahedron* **2012**, *68*, 2135.

Scheuermann, M. L.; Goldberg, K. I. *Chem. Eur. J.* **2014**, *20*, 14556-14568.

Schneider, S.; Meiners, J.; Askevold, B; *Eur. J. Inorg. Chem.* **2012**, 412-429.

Schwartsburd, L.; Iron, M. A.; Konstantinovski, L.; Ben-Ari, E.; Milstein, D. *Organometallics* **2011**, *30*, 2721.

Sgarbossa, P.; Scarso, A.; Strukul, G.; Michelin, R. A. *Organometallics* **2012**, *31*, 1257.

Sheldon, R. A. *J. Mol. Catal.* **1980**, *7*, 107.

Sheldrick, G. M. (**1997**) SHELXL-97, Program for the Refinement of Crystal Structures. University of Göttingen, Germany.

SHELL, Ethylene oxide/ethylene glycol (EO/EG) processes, SHELL, 2010.

Shook, R. L.; Peterson, S. M.; Greaves, J.; Moore, C.; Rheingold, A. L.; Borovik, A. S. *J. Am. Chem. Soc.* **2011**, *133*, 5810.

Singleton, J. T. *Tetrahedron* **2003**, *59*, 1837-1857.

Smoll, K. Manuscript in preparation, 2016.

Spek, A. L. *J. Appl. Cryst.* **2003**, *36,* 7.

Stahl, S. S. *Angew. Chem. Int. Ed.* **2004**, *43*, 3400.

Stahl, S. S.; Thorman, J. L.; Nelson, R. C.; Kozee, M. A. *J. Am. Chem. Soc.* **2001**, *123*, 7188-7189.

Stockland Junior, R. A.; Anderson, G. K.; Rath, N. P. *Inorg. Chim. Acta* **1997**, *259*, 173.

Stockland Junior, R. A.; Anderson, G. K.; Rath, N. P. *Inorg. Chim. Acta* **2000**, *300*, 395.

Stockland Junior, R. A.; Anderson, G. K.; Rath, N. P. *J. Am. Chem. Soc.* **1999**, *121*, 7945.

Strukul, G.; Michelin, R. A. *J. Chem. Soc., Chem. Commun.* **1984**, 1538.

Strukul, G.; Michelin, R. A. *J. Am. Chem. Soc.* **1985**, *107*, 7563.

Suh, H.-W.; Schmeier, T. J.; Hazari, N.; Kemp, R. A.; Takase, M. K. *Organometallics* **2012**, *31*, 8225.

Sumitomo Chemical Co., Ltd. Development of New Propylene Oxide Process, vol. 2006-I.

Tanabe, M.; Ishikawa, N.; Chiba, M.; Ide, T.; Osakada, K.; Tanase T. *J. Am. Chem. Soc.* **2011**, *133*, 18598.

"Technology Roadmap: Energy and GHG Reductions in the Chemical Industry via Catalytic Processes" International Energy Agency, 2013.

Timpa, S. D.; Pell, C; Zhou, J.; Ozerov, O. V. *Organometallics* **2014**, *33*, 5254-5262.

Toda, T.; Kuwata, S.; Ikariya, T. *Z. Anorg. Allg. Chem.* **2015**, *641*, 2135-2139.

Umehara, K.; Kuwata, S.; Ikariya, T. *Inorg. Chima. Acta* **2014**, *413*, 136-142.

Umehara, K.; Kuwata, S.; Ikariya, T. *J. Am. Chem. Soc.* **2013**, *135*, 6754-6757.

van der Boom, M. E.; Milstein, D. *Chem. Rev.* **2003**, *103*, 1759-1792.

van der Sluis P.; Spek, A. L. *Acta Crystallogr. A* **1990**, *46*, 194.

Vogt, M.; Nerush, A.; Iron, M. A.; Leitus, G.; Diskin-Posner, Y.; Shimon, L. J.; Ben-David, Y.; Milstein, D. *J. Am. Chem. Soc.* **2013**, *135*, 17004.

Voorhees, V.; Adams, R. *J. Am. Chem. Soc.* **1922**, *44*, 1397-1405.

Vuzman, D.; Poverenov, E.; Shimon, L. J. W.; Diskin-Posner, Y.; Milstein, D. *Organometallics,* **2008**, 27, 2627.

Waasmaier, D.; Kirfel, A. *Acta Cryst. A* **1995**, *51*, 416.

Wang, W.; Wang, S.; Ma, X.; Gong, J. *Chem. Soc. Rev.* **2011**, *40*, 3703-3727.

Wells, D. H.; Joshi, A. M.; Delgass, W. N.; Thomson, K. T. *J. Phys. Chem. B.* **2006**, *110*, 14627-14639.

Wenzel, T. T. *Stud. Surf. Sci. Catal.* **1991**, *66*, 545-554.

Wiley, J. S.; Oldham, Jr., W. J.; Heinekey, D. M. *Organometallics* **2000**, *19*, 1670-1676.

Wilke, G.; Schott, H.; Heimbach, P. *Angew. Chem.* **1967**, *79*, 62.

Yang, L.; Powell, D. R.; Houser, R. P. *Dalton Trans.* **2007**, 955-964.

Yoshinari, A.; Tazawa, A.; Kuwata, S.; Ikariya, T. *Chem. Asian J.* **2012**, *7*, 1417-1425.

Yu, W.-S.; Cheng, C.-C.; Cheng, Y.-M.; Wu, P.-C.; Song, Y.-H.; Chi, Y.; Chou, P.-T. *J. Am. Chem. Soc.* **2003**, *125*, 10800-10801.

Zeng, G.; Guo, Y.; Li, S. *Inorg. Chem.* **2009**, *48*, 10257.

Zhang, J.; Balaraman, E.; Leitus, G.; Milstein, D. *Organometallics* **2011**, *30*, 5716-5724.

Zhang, J.; Gandelman, M.; Herrman, D.; Leitus, G.; Shimon, L. J. W.; Ben-David, Y.; Milstein, D.; *Inorg. Chim. Acta.* 359, **2006**, 1955.

Zhang, W.; Loebach, J. L.; Wilson, S. R.; Jacobsen, E. N. *J. Am. Chem. Soc.* **1990**, *112*, 2801.

Zhang, X.; Suzuki, S.; Kozaki, M.; Okada, K., *J. Am. Chem. Soc.* **2012**, *134*, 17866-17868.

Zhao, Y.; Truhlar, D. G. *Theor. Chem. Account* **2008**, *120*, 215-241.

Zhuravel, M. A.; Moncarz, J. R.; Glueck, D. S.; Lam, K.-C.; Rheingold A. L. *Organometallics* **2000**, *19*, 3447.

Vita

Wilson D. Bailey was born in 1989 to parents Nancy Abens and Scott Bailey. He grew up in Portland, OR where he graduated high school at Ulysses S. Grant High School in 2007. He attended the University of Puget Sound in Tacoma, WA, where he graduated with a Bachelor of Science degree in chemistry in 2011. At Puget Sound, Wilson worked in the research laboratory of Prof. Johanna L. Crane on the synthesis and characterization of multidentate ligands and their lanthanide complexes. Wilson then attended graduate school at the University of Washington in Seattle, WA. There, he worked with Prof. Karen I. Goldberg on late-transition metal pincer complexes and their application to oxidation catalysis. He married Cecily Ferguson in 2015. He obtained a Doctor of Philosophy degree in inorganic chemistry in 2016.